ANALYSIS AND DESIGN OF PLANAR ACTIVE AND PASSIVE QUASI-OPTICAL COMPONENTS USING NEW FDTD TECHNIQUES

Javier Vazquez

A thesis submitted for the degree of
DOCTOR OF PHILOSOPHY

Queen Mary, University of London
Department of Electronic Engineering
Supervisor: Prof. C. G. Parini

5 April 2002

ABSTRACT

New Quasi-optical sensor technology, based on the millimetre and submillimetre band of the electromagnetic spectrum, is actually being implemented for many commercial and scientific applications such as remote sensing, astronomy, collision avoidance radar, etc. These novel devices make use of integrated active and passive structures usually as planar arrays. The electromagnetic design and computer simulation of these new structures requires novel numerical techniques.

The Finite Difference Time Domain method (FDTD) is well suited for the electromagnetic analysis of integrated devices using active non-linear elements, but is difficult to use for large and/or periodic structures. A rigorous revision of this popular numerical technique is performed in order to permit FDTD to model practical quasi-optical devices. The system impulse response or discrete Green's function (DGF) for FDTD is determined as a polynomial then the FDTD technique is reformulated as a convolution sum. This new alternative algorithm avoids Absorbing Boundary Conditions (ABC's) and can save large amounts of memory to model wire or slot structures. Many applications for the DGF can be foreseen, going beyond quasi-optical components. As an example, the exact ABC based on the DGF for FDTD is implemented for a single grid wall is presented.

The problem of time domain analysis of planar periodic structures modelling only one periodic cell is also investigated. Simple Periodic Boundary Conditions (PBC) can be implemented for FDTD, but they can not handle periodic devices (such as phased shift arrays or dichroic screens) which produce fields periodic in a 4D basis (three spatial dimensions plus time). An extended FDTD scheme is presented which uses Lorentz type coordinate transformations to reduce the problem to 3D.

The analysis of non-linear devices using FDTD is also considered in the thesis. In this case, the non linear devices are always model using an equivalent lumped element circuit. These circuits are introduced into the FDTD grid by means of the current density following an iterative implicit algorithm. As a demonstration of the technique a quasi-optically feed slot ring mixer with integral lens is designed for operation at 650 GHz.

GLOSSARY

ABC	Absorbing Boundary Conditions
DGF	Discrete Green's Function
EM	Electromagnetic (field theory)
FD	Finite Differences
FDTD	Finite Difference Time Domain
FEM	Finite Elements Method
FFT	Fast Fourier Transform
FSS	Frequency Selective Surfaces
MM	Mode Matching
MoM	Method of Moments
MRTD	Multi-Resolution in Time Domain
NEC	Numerical Electromagnetic Code
PBC	Periodic Boundary Condition
PBG	Photonic Band Gap structures
PEC	Perfect Electric Conductor
PMC	Perfect Magnetic Conductor
PML	Perfect Matching Layer
PO	Physical Optics
SIS	Superconductor Insulator Superconductor Junctions

TABLE OF CONTENTS

CHAPTER I: INTRODUCTION

1.1 Modelling of Quasi optical devices

1.1.1 The millimetre and submillimetre band.

The millimetre and submillimetre band (30GHz-3THz) is probably the last slice of the electromagnetic spectrum which still remains relatively unexplored in terms of the generation, detection, measurement, radiation and also from the point of view of applications. At these frequencies, RF technology does not often provide suitable solutions because of high losses and propagation effects. At the same time, optical devices and techniques are not possible in many cases because of the low photon energy and long wavelength at these bands.

Nowadays, considerable effort is being applied to the development of these frequency bands. As a consequence, this unexplored gap on the spectrum is being reduced. From the side of infrared optical technology, Lasers based on lead salts are already operating at 10THz and several procedures for generating and imaging beams at a few THz have been developed by using non linear optic mixing [1]. From the microwave side, new solid state devices are reported to operate in the mmW/submmW band, as Gunn diodes (up to 200GHz) and Schottky diodes (up to 1THz). Other special devices have been employed in the detection of these frequencies, such Niobium bolometers and SIS (Superconductor-Insulator Superconductor) junctions [2].

Traditionally, mmW and submmW have been used in scientific instruments for radioastronomy and research on plasmas. New applications are also being identified for these frequency bands, for instance, broadband communications, secure communication links, wireless LAN, vehicle anti collision radars, detection of chemicals in air, food processing, etc.[3]. Space projects have already a large number of applications for mmW/submmW. Earth observation and space scientific missions are increasingly including newer and more sophisticated instruments that operate in these frequency bands. Following this trend, a number of future European Space Agency (ESA) projects on astronomy (i.e. FIRST/PLANCK) and earth observation (i.e. MASTER) will require advanced submmW instrumentation [4].

1.1.2 Devices and systems for the mmW/submmW band

The actual research in mmW/submmW technologies and applications has produced a set of antenna and receiver designs that are quite characteristic of these high frequency bands. These designs are highly conditioned by the special features of the propagation at mmW/submmW and the low manufacturing tolerances associated with very small wavelengths.

One of the most significant constraints on devices operating at mmW/submmW is the large losses in metallic waveguides and transmission lines. For instance, the attenuation of the TE10 on a WR-4 rectangular waveguide at 250GHz is approximately 12 dB/m. In order to avoid these losses the energy is typically guided through free space using a set of mirrors and lenses which is usually referred as a Quasi-Optical waveguide [5](Fig.1.1a). As a consequence, filters and other passive devices have to be implemented Quasi-optically in free space, typically by using passive arrays of metallic patches, the so called dichroic filters [6](Fig 1.1b). These structures have a frequency selective transmission of waves in free space, which is related to the resonant response of the metallic patches.

The high attenuation of transmission lines is also the main reason for using integrated antennas designs in the mmW/submmW bands (Fig.1.1d). In these devices the active or detecting device and associated circuits are directly incorporated into the receiving antenna in order to avoid the transmission line losses from the antenna to the detector or the mixer. The small size of the receiving antennas at these frequencies is also extremely suitable for the integration of semiconductor devices, and the direct use of semiconductor manufacturing techniques for the complete antenna.

Another limitation associated to submmW frequencies is the tiny dimensions of many devices due to the small wavelength. Despite the impressive advance of the micro-machining technology [7], it is still a challenge to manufacture 3D structures to be used as submmW antennas or receivers. Planar technology is quite attractive at these frequencies since it has been extensively developed for the manufacturing of very small components such as semiconductor devices. However, conventional planar technology has a special problem for its application at these bands: the propagation of surface modes due to electrically thick dielectric substrates. However, surface modes can be suppressed by using substrate lenses [8] for the planar structure.

The low power that is provided by solid state devices at these frequencies is a serious limitation for many applications. The power handling of mmW/submmW devices can be increased, by combining the output of solid state devices. This basic idea is used by an emerging technology based on arrays of active/non-linear elements. These structures are quite similar to the dichroic filters but as they include active/non linear elements, they can amplify or mix waves in free space in a Quasi-optical way. These devices can handle high power by combining the scattered wave from each active element in free space [5],[9],[10]. These active/non-linear arrays can be stacked, so they can behave as a sort of active/non-linear media. A fascinating range of devices are possible using this technology, from laser type generators to non-linear artificial crystals (Fig.1.1c) [5],[9],[10],[11].

1.1.3 Modelling of planar structures at mmW/submmW band. The FDTD approach.

Planar structures have an essential role for the quasi-optical systems for mmW/submmW band. Frequency selective surfaces (FSS), mesh grids, and other filtering devices are planar structures, and mixers and detectors at these frequencies can also be implemented as planar structures [12]. The active grids for power generation and amplification of mmW/submmW are based on planar arrays of integrated antennas and active devices [9],[10],[11].

The electromagnetic design of these devices relies on numerical tools, which originally were developed for the analysis of microwave devices. As a consequence, these codes usually are not ready to cover all the requirements of the mmW/submmW planar design [10],[11],[12]. The modelling of planar integrated receivers is an example of this situation, because they require the accurate modelling of both the radiating structures along with the matching circuit, filters and the non-linear detector at the same time. Active arrays for power combining also include active elements and additional circuits such as bias lines that are coupled to the rest of the structure.

The Finite Difference Time Domain (FDTD) algorithm is a general method to solve numerically the electromagnetic equations in the time domain, and has been used extensively to model radiation, scattering, and circuit problems [13],[14]. The potential of this method for application to the modelling of active/non-linear and submmW structures has been pointed out by several authors [10][15]. The main advantages of FDTD for modelling at mmW/submmW band are summarised as follows.

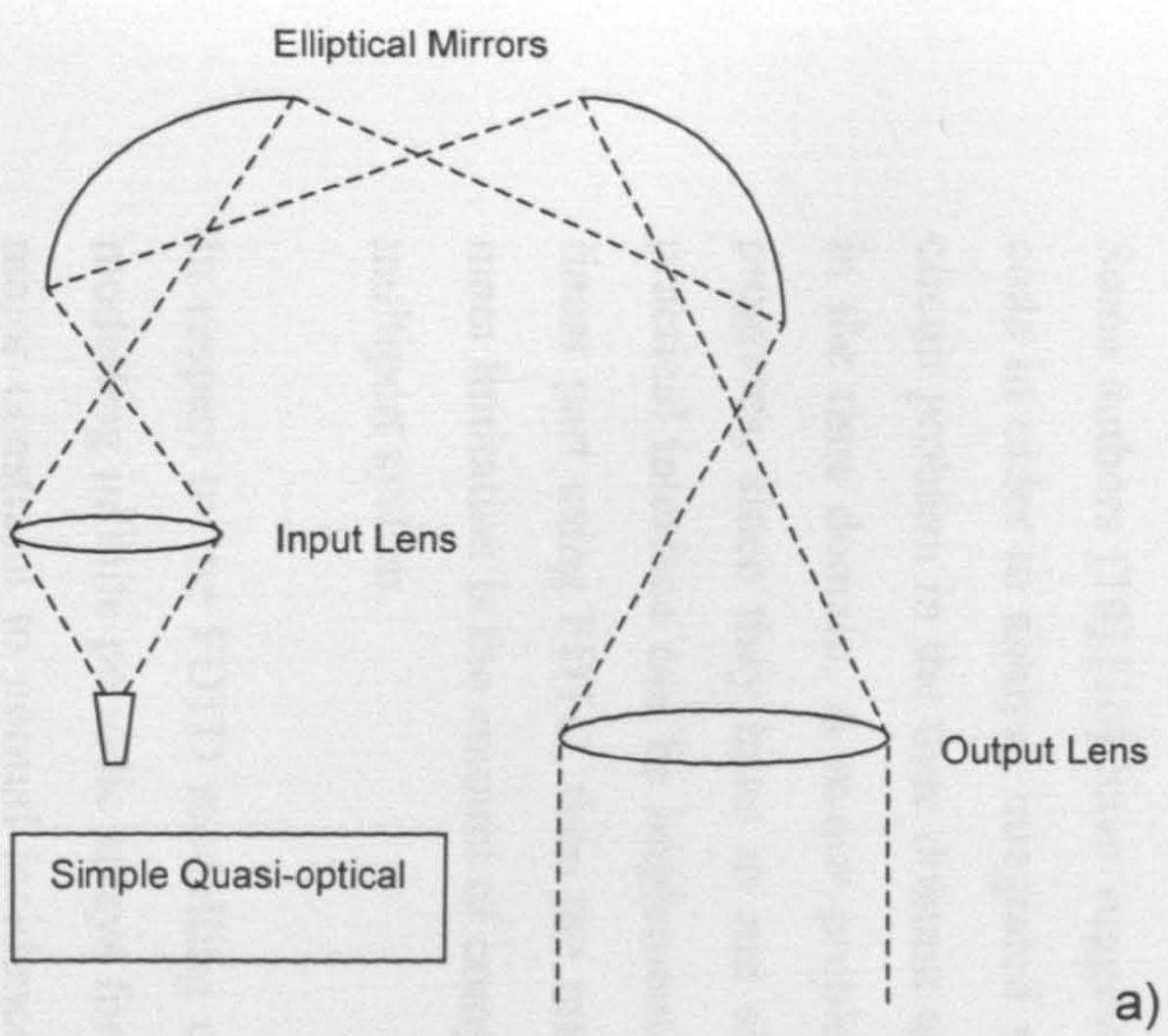

a)

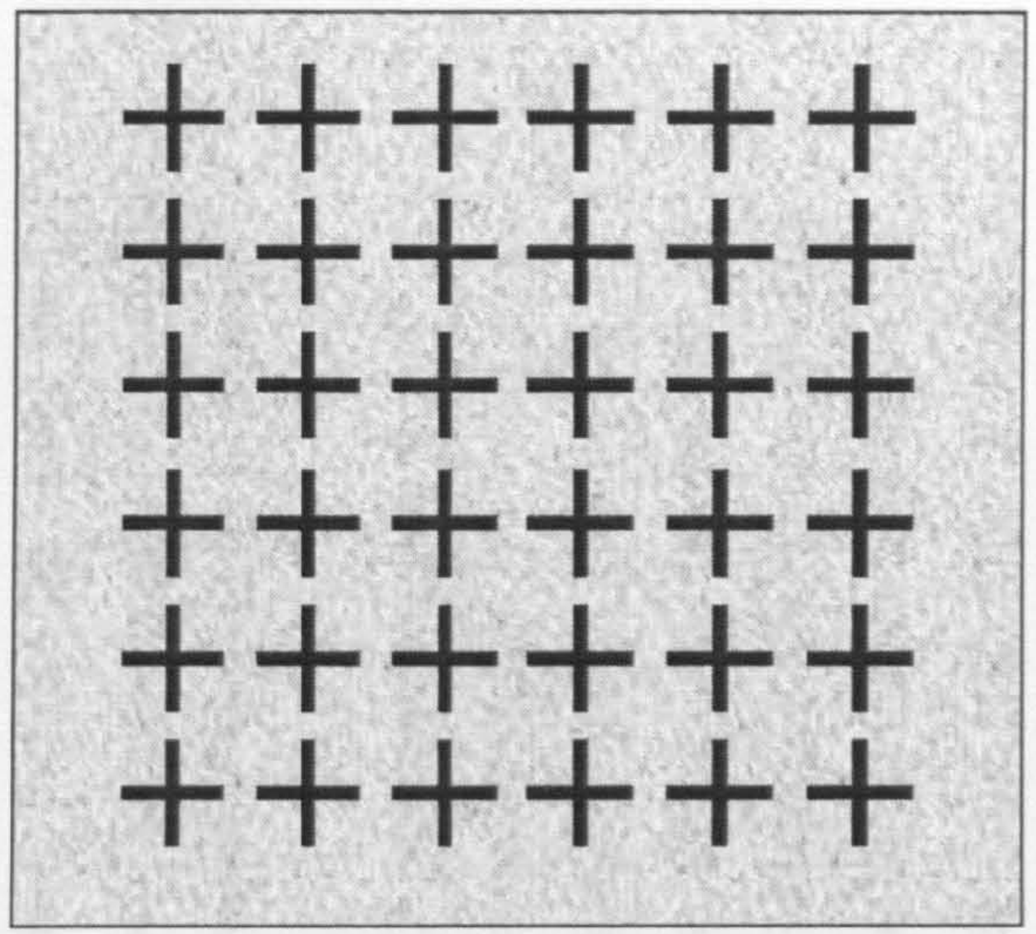

b)

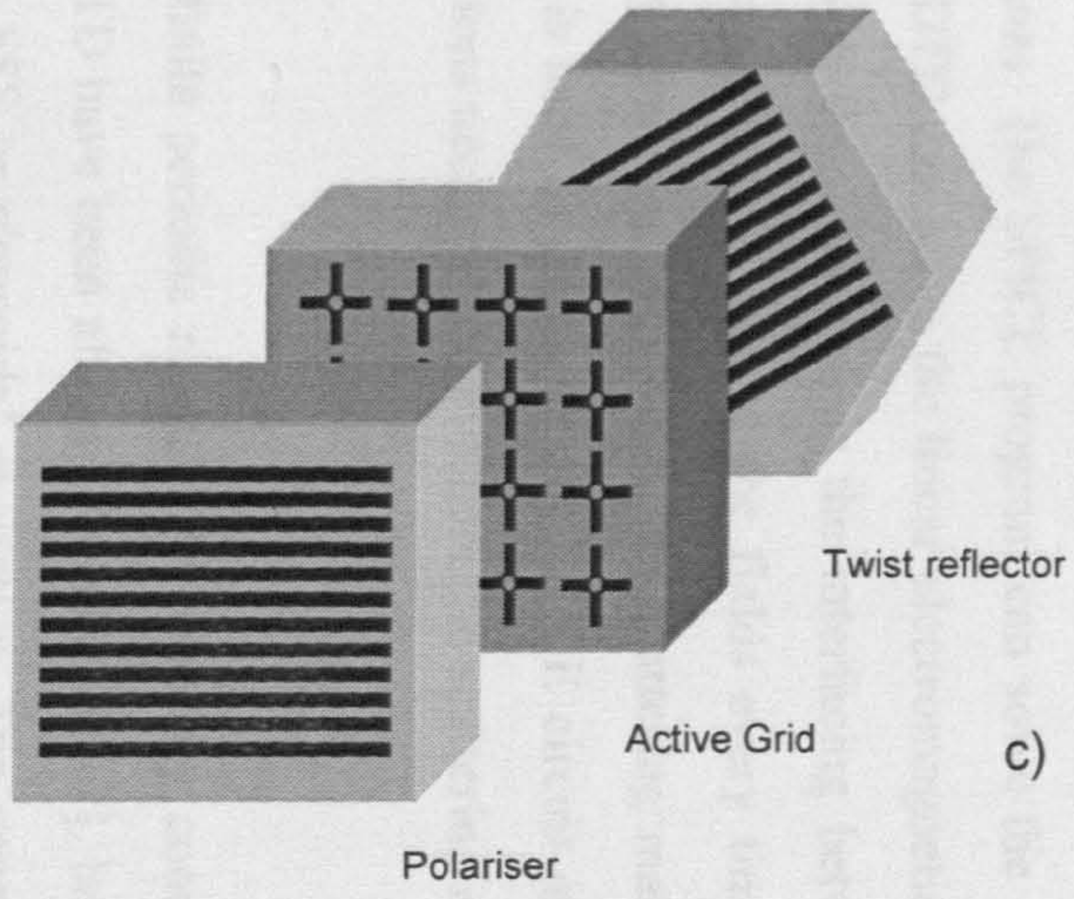

c)

d)

Fig.1.1. mmW and submmW devices: a) Simple Quasi-optical waveguide. b) FSS of cross metallic patches. The structure is highly reflective at the resonance frequency of the crosses. c) Quasi-optical oscillator based on an active grid with HEMT transistors. d) Planar integrated antenna & mixer on coplanar technology for submmW band.

- FDTD is a time domain method, which is able to model non-linear and active media. As a result, integrated and active antennas can be fully analysed in a single model that includes the semiconductor devices and the electromagnetic interaction between passive parts.
- FDTD is a full wave 3D method that is able to model mutual coupling effects in an arbitrarily complex design and for any number of ports in a single run.
- FDTD with periodic boundary conditions can model infinite periodic linear/non-linear and active/passive arrays and FSS. Multilayer designs can also be modelled directly, since mutual coupling between layers is automatically considered.
- FDTD can use pulsed excitations, making possible broadband analysis of the structures. Out of band responses are critical to the design of active antennas

In spite of FDTD being potentially able to model planar integrated antennas and periodic structures, the method has to be extended in order to model these devices. Previous work [15], [16] has shown the required extensions for modelling of active/non linear devices in the FDTD numerical scheme. They introduce lumped element circuit models of devices, which are coupled to the electrical field at the FDTD cells. These methods are the basis for this research on integrated antennas

Some authors [10],[16] have suggested connecting the SPICE circuit simulator to a FDTD code in order to analyse integrated antennas. The SPICE program can solve the non-linear circuit problem in the time domain and FDTD can solve the linear electromagnetic part also in the time domain. A major problem with this approach is the interfacing between both programs, since they have to run simultaneously to update the fields every time step. A practical interface can be implemented by obtaining previously the scattering matrix of the linear part using FDTD, then the matrix is used as input for the SPICE circuit model. The main limitation is the amount of computations necessary to evaluate the scattering matrix in a multiport system.

In respect to the FDTD modelling of infinite periodic media, the boundary conditions for modelling infinite periodic arrays for FDTD have been already developed [17], but with the major constraint to normal incidence for FSS or sinusoidal excitation. The general FDTD analysis of infinite periodic arrays under oblique incidence or with phase shifted generators is still a matter of investigation [18],[19], and it is part of this research. The modelling of infinite

arrays with FDTD is a powerful way of broadband analysis of mutilayer FSS and introduces the unexplored possibility of the full wave analysis of active/non linear arrays.

Small finite arrays can be directly modelled using FDTD [20], but computer resources are a severe limitation for modelling of medium size arrays. On the other hand, Frequency domain methods, as the Conjugate Gradient technique are very efficient in solving passive finite array problems [21], [22]. As a result, only a few works at their early stages are reported dealing with general methods for FDTD modelling of finite array [23]. However, the FDTD method has the possibility of modelling practical active or non-linear finite arrays. This is a novel application that can not be implemented using frequency domain methods in a conventional way.

1.2 Finite Difference Electromagnetics.

The numerical modelling of physical fields requires the description of the field and its fundamental laws by a finite number of parameters. This can be achieved by assuming that the field is described as the linear combination of a finite number of basis functions. Alternatively, it is possible to approximate the fundamental laws of the field using new discrete operators. The Method of Moments (MoM) and Finite Elements (FEM) use the first approach, but Finite Differences techniques (FD) [13] normally are using the second type of approximation.

Both approaches are in fact connected, since the approximation of the field operators can be associated to the use of certain interpolation basis functions. The approximate discrete operator and the continuous one produces the same result for these basis functions (the discrete operator is exact in this case). For instance the approximation of a derivative by a FD assumes that the functions are line segments.

However, the differences between both strategies are not trivial. In the field approximation method, the basis functions can be chosen to fit in a specific geometry, improving the efficiency of the method. In MoM, for instance, the model of circular or ring structures can be optimised using only few cylindrical basis functions. However, the procedure is often not valid for the general case of an arbitrary geometry.

On the other hand, the approximation of field operators by discrete ones provides a quite general and flexible way of numerical simulation, but it can be rather stiff in terms of the modelling of arbitrary shapes. This occurs when the discrete operator is chosen without any consideration about the geometry of the problem. In practice, techniques like MoM and FE use general-purpose basis functions so they can deal with any arbitrary geometry, but allowing some degree of conformal meshing. FD techniques modify the discrete operator introducing variable steps or defining the equations in arbitrary curvilinear coordinates, so they can improve the geometrical modelling of the object.

The numerical methods based on the approximation of the operator (as FD methods) have in addition a quite special feature. If the approximate discrete operator has similar algebraic properties to the continuous one (this is the case for FD's and derivatives), all the equations and theorems valid for the continuous fields can be translated for the discrete operator fields,

just replacing the field operators by discrete ones. For instance, it will be shown in this thesis how the Finite Difference Time Domain method (FDTD) to solve Maxwell's equations satisfies FD second order equations that are closely related to the FD scalar wave equation. These equations are formally similar to continuous equations for electromagnetic field. It will also be shown that FDTD can be alternatively formulated as finite sums in terms of a Discrete Green's Function (DGF), just as in continuous electromagnetic field theory.

As a consequence, these numerical techniques can be considered as 'approximate theories' rather than a numerical approximation of particular field equations. The analogy between the continuous and the discrete theory is limited to the formal similarity of the equations, concepts and theorems. The topology of the discrete space is completely different from the real space. As a consequence, the solutions provided by the discrete and continuous theories are qualitatively quite different, even if the quantitative error between them is very small.

In this thesis the analytical formula of the impulse response or Discrete Green's Function for FDTD is obtained as a polynomial for 1D, 2D and 3D problems. This polynomial function becomes the continuous time Green's function $\delta(r-ct)/r$ when Δt, Δx, Δy, $\Delta z \rightarrow 0$. Mathematically this function has some interesting properties, and it can be seen as a multidimensional generalisation of the Tchebycheff polynomial. However, the full study of its mathematical properties is outside the scope of this thesis

The methodology of this thesis (in particular chapters II and III) with respect to the FDTD modelling of electromagnetic fields is precisely to consider FDTD as an 'approximate EM theory' in a discrete space-time. Equations and theorems are formulated for FDTD independently of the EM theory in the real space. In consequence, the equations and algorithm obtained are exact from the point of view of FDTD and therefore completely compatible with the original FDTD algorithm.

The objective of this methodology is to generalise and obtain alternative formulations of the FD approximation of the EM theory, providing the right theoretical framework for advanced boundary conditions and hybrid modelling techniques. FDTD has a long history since it was devised in 1966 and this thesis presents an alternative view of the method, so it is more involved with new aspects of the technique rather than the compilation of existing developments in the method.

1.3 Objectives of this research. Document organisation

The work presented in this document is intended to develop all the necessary theoretical tools and numerical algorithms for the Finite Difference Time Domain (FDTD) analysis of electromagnetic fields in planar devices. The final application is the analysis of Quasi-optical planar devices used in the millimetre and submillimetre frequency bands, in particular planar integrated/active antennas, Frequency Selective Surfaces (FSS) and Photonic Band Gap Structures (PBG). Besides practical implementations, this research work is also focussed in obtaining a general theoretical framework for finite difference methods to produce advanced boundary conditions and alternative algorithms.

This report is organised into five chapters, including this introduction as chapter I. The second chapter deals with the basic theory of the FDTD method and the application to the modeling of planar structures. A FDTD code for planar structures has been generated and the results are compared to measured data on patch antennas available in the literature. This chapter also presents the basic algorithm to model non-linear elements, and in particular the lumped circuit model for a Schottky diode is presented.

The third chapter is devoted to the theoretical investigation of the FDTD method. The Z transform is used to obtain second order FDTD equations. The relation between the finite difference scalar wave equation and FDTD is determined. FDTD is alternatively formulated in terms of finite sums, which includes the impulse response or discrete Green's function (DGF) of the FDTD method. The analytical formula of the DGF is presented in this chapter. Some application examples of the new FDTD algorithm are also demonstrated, including an example of exact absorbing boundary condition (ABC) for FDTD. Finally this chapter contains a study of higher order algorithms for FDTD to improve the algorithm dispersion and anisotropy of the method.

The fourth chapter is dedicated to the modelling of infinite periodic structures using FDTD. The theoretical basis on which periodic media of infinite extent can be modelled is presented in this chapter. This work includes a novel FDTD algorithm to solve the periodic boundary condition for a planar structure illuminated by a plane wave of arbitrary angle of incidence. This method is verified by comparing results for a Frequency Selective Surface (FSS) with conventional frequency domain methods of calculation.

The fifth chapter is devoted to the design and modelling of an integrated receiver at 650 GHz for a general space-based earth observation mission. This design is intended to demonstrate the possibilities of the FDTD code to produce a state of the art design of a complete submmW device.

The final chapter summarises the work of this thesis and makes recommendations for future work.

1.4 References for the Introduction Chapter

[1] Z.Jiang, G.Sun, X.C.Zhang, "Spatio-temporal Imaging of THz pulses", IEEE Int. Conf. on THz electronics, Sep 1998.

[2] D.B. Rutledge, D.P. Neikirk, D.P.Kasilingam, "Infrared and Millimeter Waves", Volume10 Part II, Chapter I "Integrated circuit antennas" pp.1-63, Academic Press 1983.

[3] H.H.Meinel, "Commercial Applications of Millimeter-Waves History, Present Status, and Future Trends", IEEE MTT Vol 43 pp 1639-1653July 1995.

[4] ESA/ESTEC Annual Report 1997.

[5] P.F.Goldsmith, "Quasi-Optical Systems", IEEE Press, 1997

[6] T.K.Wu, "Frequency Selective Surface and Grid Array", John Wiley, 1995.

[7] C.Mann, "Fabrication Technologies for Terahertz waveguide", IEEE Int. Conf. on THz electronics, Sep 1998.

[8] G.M.Rebeiz, "Millimeter-Wave and Terahertz Integrated circuit Antennas", IEEE Proceedings, Vol 80, pp 1748-1770, November 1992.

[9] Z.B.Popovich, R.M.Weikle, M.Kim ,.D.B.Rutledge ,"a 100 MOSFET planar grid oscillator", IEEE MTT,Feb.1991.

[10] R.A.York, "Quasi-optical power combining techniques", Journal of the Society of Photo-Optical Instrumentation Engineers, 1994.

[11] P.de Lisio, S.W.Duncan, D.W. Tu, S.Weinreb, C.M.Liu, D.B.Rutledge,"44-60GHz Monolithic pHEMT Grid Amplifier",Proceedings of the IEEE APS Int. Symp.1995 pp. 1127-1130.

[12] J.Mees, et al, "Key Advanced Structure Investigations for mm and Submm-wave Integrated Receivers (KASIMIR)". 2nd ESA workshop on Millimetre Wave technology and applications, May 1998.

[13] A.Taflove, "Computational Electrodynamics: The Finite Time Domain Method", Artech House 1995.

[14] K.L.Shlager, J.B.Schneider, "A Selective Survey of the Finite Difference Time Domain Literature", IEEE AP Magazine vol37, pp. 39-56, 1995

[15] B.Toland, J. Lin, T.Itoh, "FDTD Analysis of an Active Antenna". IEEE Microwave and Guided Wave Letters., Vo13, pp. 423-425, November 1993.

[16] P.Ciampolini, P.Mezzanotte, L.Roselli, R.Sorrentino, "Accurate and Efficient Circuit Simulation with Lumped Element FDTD Technique", IEEE MTT Vol 44 pp. 2207-2214, December 1996.

[17] P. H. Harms, R. Mittra, W. Ko, "Implementation of the Periodic Boundary Condition in the Finite-Difference Time-Domain Algorithm for FSS Structures", IEEE APS vol 42, pp.1317-1324, Sep 1994.

[18] J. R. Ren, O. P. Gandhi, L. R. Walker, J. Fraschilla, and C. R. Boerman, ``Floquet-based FDTD analysis of two-dimensional phased array antennas," IEEE Microwave Guided Wave Lett., vol. 4, no. 4, pp. 109--111, 1994.

[19] J.A.Roden, S.D.Gedney, M.P.Kesler, J.G.Maloney, P.H.Harms, "Time Domain Analysis of Periodic Structures at Oblique Incidence Orthogonal and Non-orthogonal Implementation".IEEE MTT,vol. 46, pp.420-427 Apr 1998.

[20] K. Uehara and K. Kagoshima, ``Rigorous analysis of microstrip phased array antennas using a new FDTD method," Electron. Letters., vol. 30, no. 2, pp. 100--101, 1994.

[21] Y.Zhuang, K.L.Wu, C. Wu, and J. Litva, "A combined wave CG-FFT method for rigurous analysis of large microstrip antenna arrays", IEEE APS, Jan.1996.

[22] M.J.Notter, C.G.Parini, "Moments of methods analysis of a finite array of arbitrary shaped microstrip patch radiating elements", Int. Journal of Microwave and mmW Computer-Aided Engineering, Vol 4 pp. 18-30, 1994.

[23] J.Gomez, C.G.Christodoulou, and P.F.Wahid, "Active Impedance and Mutual Coupling Analysis of Phased Array Stacked Microstrip Antennas using FDTD", IEEE APS Int. Symp. Proceedings pp.84-86, June 1998.

CHAPTER II: THE FDTD METHOD FOR PLANAR STRUCTURES

2.1 Introduction to the FDTD method

2.1.1 Central Finite Differences and Notation

Finite differences (FD) are a classical mathematical subject developed in the early days of infinitesimal calculus and before. They have been applied extensively to numerical analysis and statistics. The numerical solution of differential equations has been traditionally closely related to the calculus of finite differences since FD's can be used as approximations to derivatives. Historically, several authors had proposed alternative notations for finite differences. In this chapter, the notation follows the standard used in [1] for FDTD. Following this notation, the integer displacement of a vector field is written as:

$$\vec{P}(x,y,z,t) = P_x(x,y,z,t)\hat{x} + P_y(x,y,z,t)\hat{y} + P_z(x,y,z,t)\hat{z}$$

$$\vec{P}^{\,n}_{i,j,k} = P_x\big|^{n}_{i,j,k}\,\hat{x} + P_x\big|^{n}_{i,j,k}\,\hat{y} + P_z\big|^{n}_{i,j,k}\,\hat{z} = \vec{P}(x + i\Delta x, y + j\Delta y, z + \Delta z, t + n\Delta t)$$

$\Delta x, \Delta y, \Delta z, \Delta t$ are real numbers (intervals or steps) $\quad$ i, j, k, n are integers (indexes)

(Eq.2.1)

The displacement of a half interval is a very important operation for FD theory. The notation for the half displacement is shown in Eq.2.2 for the 'time index' n and for one 'spatial index' i. The symbol ± indicates that the half displacement can be positive or negative.

$$\vec{P}^{\,n\pm 1/2}_{i,j,k} = \vec{P}(x + i\Delta x, y + j\Delta y, z + \Delta z, t + (n \pm 1/2)\,\Delta t)$$

$$\vec{P}^{\,n}_{i\pm 1/2,j,k} = \vec{P}(x + (i \pm 1/2)\Delta x, y + j\Delta y, z + \Delta z, t + n\Delta t)$$

(Eq.2.2)

Similar definitions of half displacements can be done for the j and k indexes. The differences between displacements of a function are the so-called finite differences. The finite difference obtained from half displacements is called central FD. The central FD of a vector field is a good

approximation ($O(h^2)$ precision) of the partial derivative of vector field after an integer displacement. Using the FD operator D_t and D_x, the partial derivatives can be written as:

$$\left.\frac{\partial \vec{P}}{\partial t}\right|_{i,j,k}^{n} = D_t \vec{P}_{i,j,k}^{n} + O(\Delta t^2) \qquad D_t \vec{P}_{i,j,k}^{n} = \frac{\vec{P}_{i,j,k}^{n+1/2} - \vec{P}_{i,j,k}^{n-1/2}}{\Delta t}$$

$$\left.\frac{\partial \vec{P}}{\partial x}\right|_{i,j,k}^{n} = D_x \vec{P}_{i,j,k}^{n} + O(\Delta x^2) \qquad D_x \vec{P}_{i,j,k}^{n} = \frac{\vec{P}_{i+1/2,j,k}^{n} - \vec{P}_{i-1/2,j,k}^{n}}{\Delta x}$$

(Eq.2.3)

This approximation of the derivatives by central FD is the basis to the numerical solution of differential equations that are replaced by analogue FD equations. Despite the fact that the approximation of derivatives by FD can be accurate, it is not sure that the approximation of a whole differential equation by a FD equation is accurate. The FD equation can be unstable or chaotic even if the original differential equation is regular [2]. As a consequence, the use of FD algorithms for the solution of differential equations should be carefully studied, providing full assessment of the stability of the equations as a system.

2 1.2. Basic theory. Yee's Algorithm.

The Finite Difference Time Domain (FDTD) method is an algorithm to solve numerically the time domain Maxwell's equations. The method is based on the approximation of partial derivatives in a regular grid of points by means of central differences. The partial derivatives of the curl Maxwell's equations (Eq.2.4a) can be approached following this scheme: resulting in a set of discrete difference equations. Eq.2.4b shows the discrete equations for the electric field curl equation by direct approximation of the partial derivatives. The magnetic field equations are in Eq.2.4c.

$$\nabla \times \vec{E} = -\mu \frac{\partial \vec{H}}{\partial t} \qquad \nabla \times \vec{H} = \varepsilon \frac{\partial \vec{E}}{\partial t} + \vec{j}$$

$$\nabla \cdot \vec{D} = \rho \qquad \nabla \cdot \vec{B} = 0$$

(Maxwell's equations) (Eq.2.4a)

$$E_x\Big|_{i,j,k}^{n+1} = C_{ijk}^a E_x\Big|_{i,j,k}^{n} + C_{ijk}^b \left[\frac{\left(H_z\Big|_{i,j+1/2,k}^{n+1/2} - H_z\Big|_{i,j-1/2,k}^{n+1/2} \right)}{\Delta y} - \frac{\left(H_y\Big|_{i,j,k+1/2}^{n+1/2} - H_y\Big|_{i,j,k-1/2}^{n+1/2} \right)}{\Delta z} - J_x\Big|_{i,j,k}^{n} \right]$$

$$E_y\Big|_{i,j,k}^{n+1} = C_{ijk}^a E_y\Big|_{i,j,k}^{n} + C_{ijk}^b \left[\frac{\left(H_x\Big|_{i,j,k+1/2}^{n+1/2} - H_x\Big|_{i,j,k-1/2}^{n+1/2} \right)}{\Delta z} - \frac{\left(H_z\Big|_{i+1/2,j,k}^{n+1/2} - H_z\Big|_{i-1/2,j,k}^{n+1/2} \right)}{\Delta x} - J_y\Big|_{i,j,k}^{n} \right]$$

$$E_z\Big|_{i,j,k}^{n+1} = C_{ijk}^a E_z\Big|_{i,j,k}^{n} + C_{ijk}^b \left[\frac{\left(H_y\Big|_{i+1/2,j,k}^{n+1/2} - H_y\Big|_{i-1/2,j,k}^{n+1/2} \right)}{\Delta x} - \frac{\left(H_x\Big|_{i,j+1/2,k}^{n+1/2} - H_x\Big|_{i,j-1/2,k}^{n+1/2} \right)}{\Delta y} - J_z\Big|_{i,j,k}^{n} \right]$$

$$C_{i,j,k}^a = \frac{\left(1 - \frac{\sigma_{i,j,k}}{2\varepsilon_{i,j,k}}\right)}{\left(1 + \frac{\sigma_{i,j,k}}{2\varepsilon_{i,j,k}}\right)} \qquad C_{i,j,k}^b = \frac{\left(\frac{\Delta t}{\varepsilon_{i,j,k}}\right)}{\left(1 + \frac{\sigma_{i,j,k}}{2\varepsilon_{i,j,k}}\right)}$$

(Eq. 2.4b)

$$H_x\Big|_{i,j,k}^{n+1/2} = D_{ijk}^a H_x\Big|_{i,j,k}^{n+1/2} - D_{ijk}^b \left[\frac{\left(E_z\Big|_{i,j+1/2,k}^{n} - E_z\Big|_{i,j-1/2,k}^{n} \right)}{\Delta y} - \frac{\left(E_y\Big|_{i,j,k+1/2}^{n} - E_y\Big|_{i,j,k-1/2}^{n} \right)}{\Delta z} + M_x\Big|_{i,j,k}^{n} \right]$$

$$H_y\Big|_{i,j,k}^{n+1/2} = D_{ijk}^a H_y\Big|_{i,j,k}^{n+1/2} - D_{ijk}^b \left[\frac{\left(E_x\Big|_{i,j,k+1/2}^{n} - E_x\Big|_{i,j,k-1/2}^{n} \right)}{\Delta z} - \frac{\left(E_z\Big|_{i+1/2,j,k}^{n} - E_z\Big|_{i-1/2,j,k}^{n} \right)}{\Delta x} + M_y\Big|_{i,j,k}^{n} \right]$$

$$H_z\Big|_{i,j,k}^{n+1/2} = D_{ijk}^a H_z\Big|_{i,j,k}^{n+1/2} - D_{ijk}^b \left[\frac{\left(E_y\Big|_{i+1/2,j,k}^{n} - E_y\Big|_{i-1/2,j,k}^{n} \right)}{\Delta x} - \frac{\left(E_x\Big|_{i,j+1/2,k}^{n} - E_x\Big|_{i,j-1/2,k}^{n} \right)}{\Delta y} + M_z\Big|_{i,j,k}^{n} \right]$$

$$D_{i,j,k}^a = \frac{\left(1 - \frac{\sigma_{i,j,k}}{2\mu_{i,j,k}}\right)}{\left(1 + \frac{\sigma_{i,j,k}}{2\mu_{i,j,k}}\right)} \qquad D_{i,j,k}^b = \frac{\left(\frac{\Delta t}{\mu_{i,j,k}}\right)}{\left(1 + \frac{\sigma_{i,j,k}}{2\mu_{i,j,k}}\right)}$$

(Eq. 2.4c)

Each field component in the set of finite difference equations is related to field components in a previous time instant. As a result, the equation system can be solved by iteration, provided that the initial conditions for the field are known. At each iteration, the field is updated in a time instant later than the original. This iterative method is known as the Yee's curl algorithm [3]. In principle, this algorithm is just based on the curl Maxwell equations, but the divergence equations are automatically fulfilled by the discrete system [4]. The method presented in this section is

similar to the original formulation, which is based on the linear, isotropic, non-dispersive Maxwell equations in the time domain.

As a consequence of the central difference scheme, the field components have to be located in the middle of other field component in order to compute the central difference. This means that the continuous field has to be sampled alternatively by the proper field component (Fig 2.1). The magnetic and electric field also has to be alternated in time for the same reason. This is the so-called 'leap frog' algorithm.

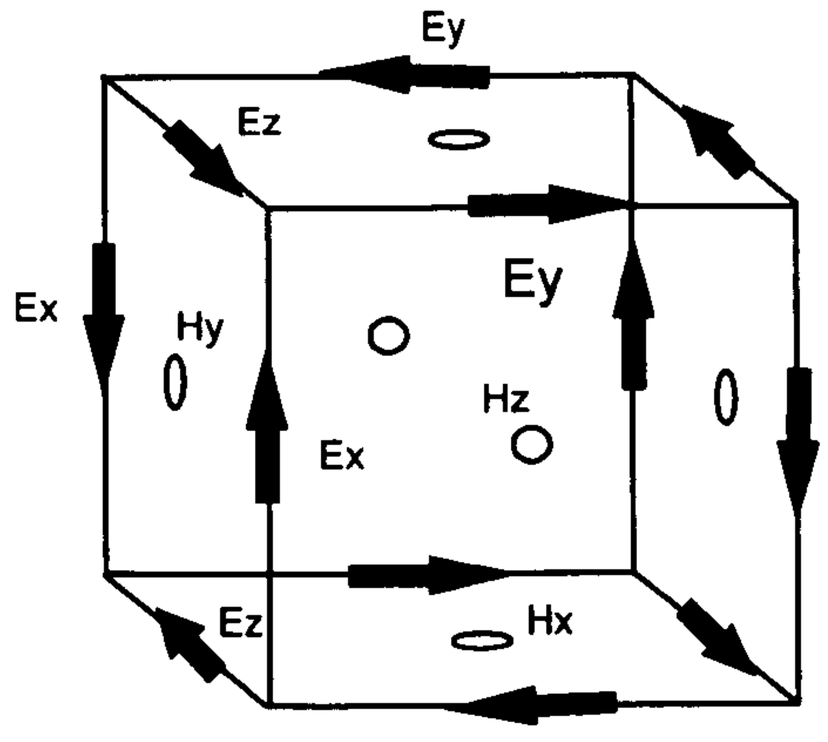

Fig 2.1 Distribution of field components in an elementary FDTD cells.

The algorithm can be extended to handle most known media (Table 2.1). Anisotropic and inhomogeneous media can be modelled with only minor changes on the equations. As the FDTD method works in the time domain, non linear and active media can be fully supported, but the iteration scheme to solve the finite difference equation can be much more complex that the basic one [2], [3] described here.

Table 2.1. Type of Media vs. FDTD

Type of Media	*FDTD support*
Anisotropic	All types of anisotropy supported
Lossy	σ Included in the FDTD.
Dispersive	FDTD + convolution (difficult)
Inhomogeneous	All types for ε, μ, and σ
Non linear/Active	Extended FDTD
Charged particles, Plasma	FDTD coupled to interaction operators

2.1.3 Divergence equation for FDTD.

The Yee's algorithm is based on the FD approximation of Maxwell's curl equations. However the electromagnetic theory also requires some condition on the divergence of the fields. The Yee's algorithm for FDTD must satisfy a divergence FD equation analogue to the Maxwell divergence equation (Eq.2.4a). The central FD approximation of the divergence operator is shown in Eq.2.5.

$$\nabla \cdot \vec{E}\Big|_{i,j,k}^{n} = D_x E_x\Big|_{i,j,k}^{n} + D_y E_y\Big|_{i,j,k}^{n} + D_z E_z\Big|_{i,j,k}^{n} + O(\Delta x^2) + O(\Delta y^2) + O(\Delta z^2)$$

(Eq.2.5)

Using the Yee's algorithm for a homogeneous, non lossy medium, the divergence condition of the FDTD electrical field can be derived. The equation 2.4a can be substituted for the electrical field into the FD divergence (Eq. 2.6).

$$D_x E_x\Big|_{i,j,k}^{n} + D_y E_y\Big|_{i,j,k}^{n} + D_z E_z\Big|_{i,j,k}^{n} =$$

$$\frac{1}{\varepsilon} D_t^{-1}\Big(D_x(D_y H_z\Big|_{i,j,k}^{n} - D_z H_y\Big|_{i,j,k}^{n}) + D_y(D_z H_x\Big|_{i,j,k}^{n} - D_x H_z\Big|_{i,j,k}^{n}) + D_z(D_x H_y\Big|_{i,j,k}^{n} - D_y H_x\Big|_{i,j,k}^{n})\Big)$$

$$-\frac{D_t^{-1}}{\varepsilon}\Big(D_x J_x\Big|_{i,j,k}^{n} + D_y J_y\Big|_{i,j,k}^{n} + D_z J_z\Big|_{i,j,k}^{n}\Big)$$

(Eq.2.6)

The magnetic field components in Eq.2.6 cancel each other, so the FD divergence of the electrical field is only a function of the density of current. The density of current term in Eq.2.6 can be considered as the electrical charge on the cell as a FD version of the law of charge conservation. As a consequence, the divergence condition for FDTD is finally written (Eq.2.7).

$$D_x E_x\Big|_{i,j,k}^{n} + D_y E_y\Big|_{i,j,k}^{n} + D_z E_z\Big|_{i,j,k}^{n} = \frac{\rho_{i,j,k}^{n}}{\varepsilon}$$

$$-D_t \rho_{i,j,k}^{n} = \Big(D_x J_x\Big|_{i,j,k}^{n} + D_y J_y\Big|_{i,j,k}^{n} + D_z J_z\Big|_{i,j,k}^{n}\Big)$$

(Eq.2.7)

A similar expression can be obtained for the magnetic field, just by following the same procedure as used for the electrical field. The Maxwell divergence equations have a counterpart in FD equations. The numerical fields are also divergence free from the FD point of view for all the cells without current density. These relationships will be used in the next chapter to construct second order FD equations.

2.1.4 FDTD Stability, Dispersion and Anisotropy.

The set of difference equations forming the FDTD method is an approximation of Maxwell's equations with a $O(\Delta^2)$ precision. However, it is well known for general finite difference equations that approximation errors can be accumulated at each time step, so the solution to the discrete equation may diverge with respect to the solution of the original continuous differential equation. In that case, the difference equations form an unstable system. The stability of the FDTD method depends on the time and spatial steps used, so this choice is critical.

Stability analysis can be performed by means of the Z transform to calculate the transfer function of the equation system [4], [5]. The stability of the procedure can be easily determined by the zero-pole analysis of the transfer function. The full *Z* transform analysis of the FDTD system is shown in the next chapter. Following this procedure, it is possible to find a stability condition for the FDTD algorithm: The Courant condition (Eq.2.8)

$$\Delta t \leq \frac{1}{c\sqrt{\frac{1}{\Delta x^2}+\frac{1}{\Delta y^2}+\frac{1}{\Delta z^2}}} \qquad \text{(Eq.2.8)}$$

The meaning of the stability limitation is that the discrete grid has to be able to model the flow of energy at light speed inside every cell to verify the law of conservation of energy. This condition holds for linear, isotropic, homogeneous media, but it is usually taken as a reference for other media. In general, non-linear media have different stability criteria [2]. For these media, the condition given in Eq.2.8 is not enough to guarantee stability.

The Z transform analysis of the discrete equations also allows determination of the dispersion relation for the waves represented in the FDTD grid (the full mathematical demonstration also

can be found in the next chapter). The dispersion relation links the wave frequency to the wave numbers (Eq.2.9).

$$\frac{1}{\Delta x^2}\sin^2\left(\frac{k_x\Delta x}{2}\right)+\frac{1}{\Delta y^2}\sin^2\left(\frac{k_y\Delta y}{2}\right)+\frac{1}{\Delta z^2}\sin^2\left(\frac{k_z\Delta z}{2}\right)=\left(\frac{1}{c\Delta t}\right)^2\sin^2\left(\frac{\omega\Delta t}{2}\right)$$

$$\Delta x,\Delta y,\Delta z,\Delta t\to 0 \qquad k_x^{\,2}+k_y^{\,2}+k_z^{\,2}=\left(\frac{\omega}{c}\right)^2$$

(Eq.2.9)

The limit of this equation for zero spatial and time steps is the continuous dispersion relation for plane waves. The discrete dispersion relation is dispersive (phase velocity depends on frequency) and anisotropic (phase velocity depends on direction) (Fig.2.2).

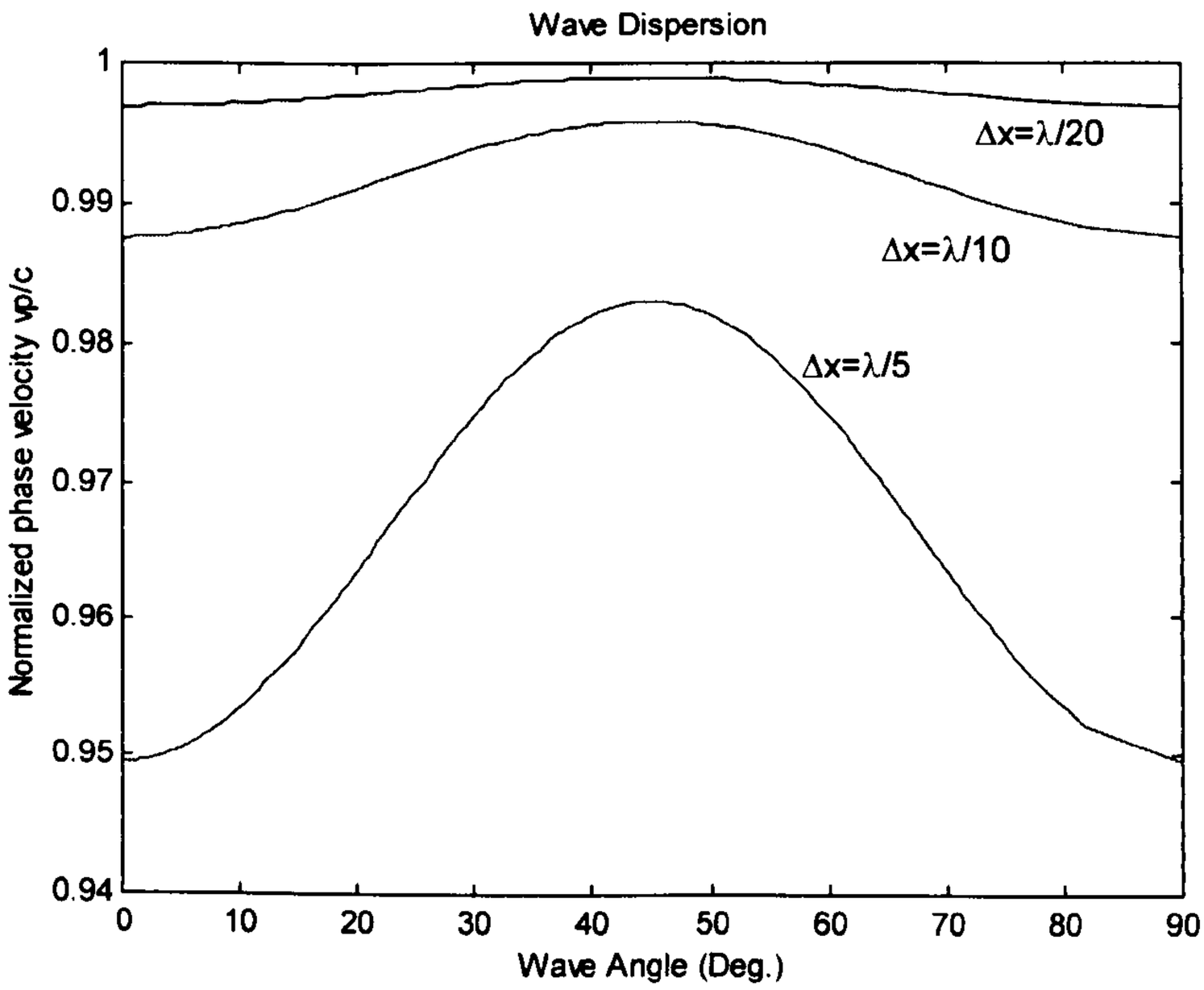

Fig.2.2 Normalised phase velocity for the numerical waves propagating in a FDTD grid. The phase velocity depends on the cell size and the wave direction respect to the FDTD grid.

In Figure 2.2 the FDTD numerical value of the phase velocity is calculated using Eq.2.9 as a function of the angle of propagation with respect to the grid ($\Delta x = \Delta y = 2c\Delta t$) and for several cell sizes. The phase velocity of the numerical waves is smaller than the speed of light. The difference is bigger for waves propagating on the axes (0 and 90 Degrees). This shows the dispersive and anisotropic behaviour of the FDTD grid. The error in the phase velocity is about 1% for a cell size of $\lambda/10$, which is often taken as the minimum cell size recommended for FDTD [2], [3].

However, the modelling of practical devices and circuits often requires cell sizes much smaller than $\lambda/10$. The previous analysis has been done for propagating waves on the FDTD grid, but scattered waves contain a high proportion of evanescent waves. The numerical speed of light for FDTD is shown in Figure 2.3 for the propagating and evanescent waves according to Eq.2.9.

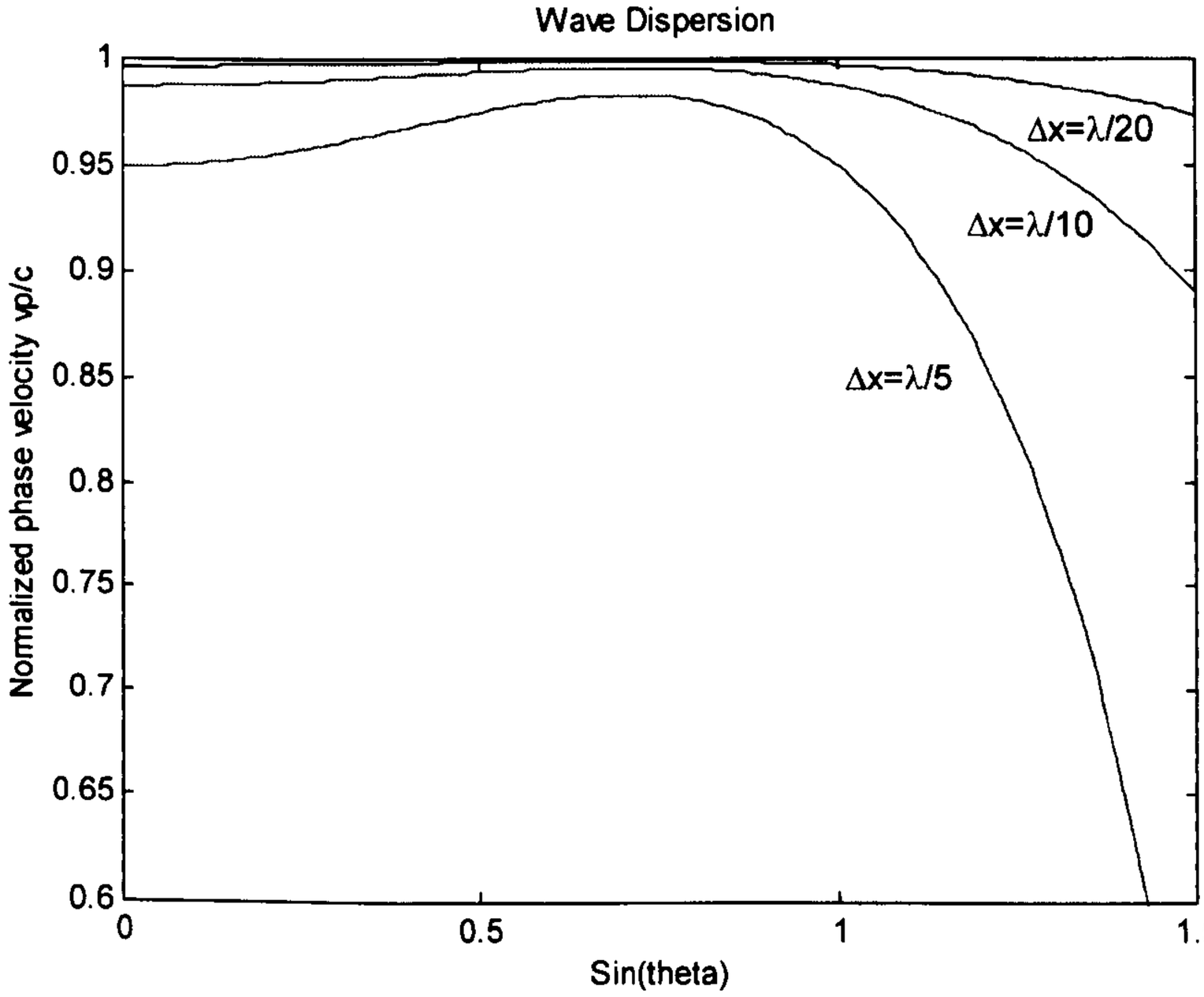

Fig.2.3 Normalised numerical speed of light for the numerical waves propagating in a FDTD grid including evanescent waves ($sin\theta>1$). The numerical speed of light for the evanescent waves degrades more than for the propagating waves.

The percent error of the value of the speed of light is much higher for the evanescent waves ($sin\theta>1$). This result suggest that a smaller cell size would be required to model accurately the evanescent waves since they have faster spatial changes than the propagating ones. As a consequence, scatterers generating a high proportion of evanescent waves (i.e. structures with circular symmetry or sharp edges) will require a cell size down to $\lambda/20$ or $\lambda/40$ to achieve 1% error in the numerical value of the speed of light.

2.1.5 Principle of equivalence for FDTD.

In electromagnetic theory, the principle of equivalence states that the EM solutions can be reproduced exactly outside a volume containing the field sources from an appropriate current distribution (electric and magnetic) on the surface of that volume. This current distribution is directly related to the EM field tangent on the boundary of the volume [6].

This principle is extensively used to solve many electromagnetics problems and is a consequence of the uniqueness theorem and the boundary conditions for the fields at limiting surfaces [7]. The principle of equivalence can be used in FDTD to calculate the far field radiated by a structure from the near field estimated by FDTD in the vicinity of the structure.

However, it still remains the question of finding a true FD principle of equivalence for FDTD. A 'true' FD principle means that the Yee's algorithm can be updated alternatively using the equivalent currents at certain grid nodes where the EM fields are set to zero (or an arbitrary value). This FD principle of equivalence is different from the continuous one since the topology of the discrete space is essentially different from the real one. In the discrete FDTD grid the electrical and magnetic equivalent currents can not be defined at the same surface since they have different positions in the space for electrical and magnetic field.

The first step is to determine how the FDTD algorithm can be updated if a field component is set to an arbitrary value by introducing equivalent currents in other nodes nearby. The equivalence between currents and fields is shown for a single magnetic field components in Eq.2.10 The same idea can be applied to the rest of field components

$$E_y\Big|_{i,j,k}^{n+1} = C_{ijk}^a E_y\Big|_{i,j,k}^{n} + C_{ijk}^b \left[\frac{\left(H_x\Big|_{i,j,k+1/2}^{n+1/2} - H_x\Big|_{i,j,k-1/2}^{n+1/2} \right)}{\Delta z} - \frac{\left(H_z\Big|_{i+1/2,j,k}^{n+1/2} - H_z\Big|_{i-1/2,j,k}^{n+1/2} \right)}{\Delta x} \right]$$

equivalent to

$$\Downarrow$$

$$E_y\Big|_{i,j,k}^{n+1} = C_{ijk}^a E_y\Big|_{i,j,k}^{n} + C_{ijk}^b \left[\frac{\left(H_x\Big|_{i,j,k+1/2}^{n+1/2} - H_x\Big|_{i,j,k-1/2}^{n+1/2} \right)}{\Delta z} - \frac{\left(H_z^0\Big|_{i+1/2,j,k}^{n+1/2} - H_z\Big|_{i-1/2,j,k}^{n+1/2} \right)}{\Delta x} - J_y\Big|_{i,j,k}^{n} \right]$$

$$J_y\Big|_{i,j,k}^{n} = -\frac{\left(H_z\Big|_{i+1/2,j,k}^{n+1/2} - H_z^0\Big|_{i+1/2,j,k}^{n+1/2} \right)}{\Delta x} \qquad J_y\Big|_{i+1,j,k}^{n} = \frac{\left(H_z\Big|_{i+1/2,j,k}^{n+1/2} - H_z^0\Big|_{i+1/2,j,k}^{n+1/2} \right)}{\Delta x}$$

$$J_x\Big|_{i,j,k}^{n} = \frac{\left(H_z\Big|_{i+1/2,j,k}^{n+1/2} - H_z^0\Big|_{i+1/2,j,k}^{n+1/2} \right)}{\Delta y} \qquad J_y\Big|_{i+1,j,k}^{n} = \frac{\left(H_z\Big|_{i+1/2,j,k}^{n+1/2} - H_z^0\Big|_{i+1/2,j,k}^{n+1/2} \right)}{\Delta x}$$

$$M_z\Big|_{i,j,k}^{n} = \frac{D_{ijk}^a H_z^0\Big|_{i,j,k}^{n-1/2} - H_z^0\Big|_{i,j,k}^{n+1/2}}{D_{ijk}^b} - \left[\frac{\left(E_y\Big|_{i+1/2,j,k}^{n} - E_y\Big|_{i-1/2,j,k}^{n} \right)}{\Delta x} - \frac{\left(E_x\Big|_{i,j+1/2,k}^{n} - E_x\Big|_{i,j-1/2,k}^{n} \right)}{\Delta y} \right]$$

(Eq.2.10)

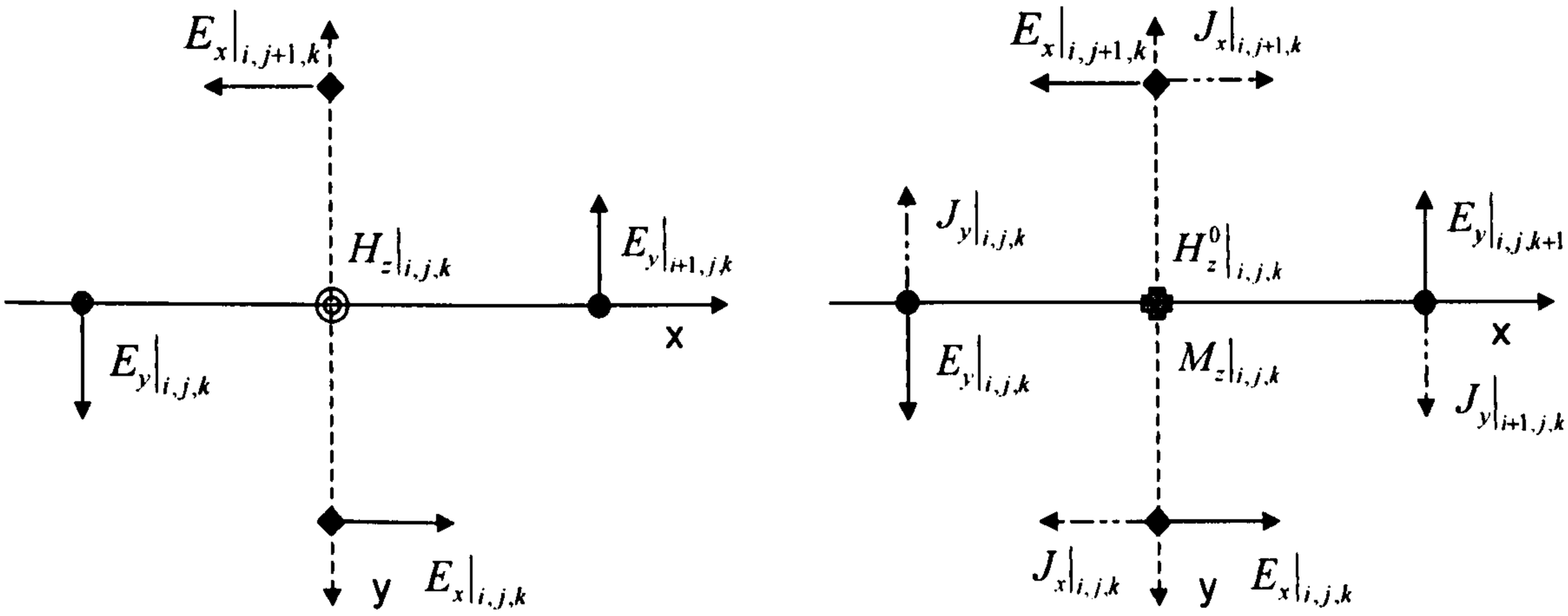

Fig.2.4. The electrical components surrounding $H_z|_{i,j,k}$ (left) can be updated in an alternative way, assuming that an arbitrary value $H_z^0|_{i,j,k}$ for the magnetic field and a distribution of electrical current density (right). The magnetic field is also updated consistently introducing a equivalent magnetic current density.

The field at a node can be replaced by an arbitrary value, using an equivalent way by a distribution of current density (Fig.2.4). This arbitrary value can be chosen to be zero, as if the node was filled by electric or magnetic perfect conductor. This can be considered the principle of equivalence for FDTD applied to a single cell. In order to obtain a general theorem, the single cell equivalence principle has to be extended to a complete subset of the FDTD grid.

The vicinity set of DTD node is defined as the set of FDTD nodes which contributes to the field at that point. For instance, the vicinity of $H_z|_{i,j,k}^{n+1/2}$ is the nodes $H_z|_{i,j,k}^{n-1/2}$, $E_y|_{i,j,k}^{n}$, $E_y|_{i+1,j,k}^{n}$, $E_x|_{i,j,k}^{n}$, $E_x|_{i,j+1,k}^{n}$. The field at the node can be evaluated from the field at the node vicinity.

A region of the FDTD grid, F, is formed by a set of electric and magnetic nodes at any time step n. If a node belongs to F and its vicinity is also included in F, then this node is an inner element. The field at this inner node can be estimated inside F and no nodes from outside F are required to perform that calculation. If the vicinity of a node in F is not included within F, then it is a boundary element (Fig.2.5). It is clear that the calculation of the field require nodes outside F at the boundary. As a result, the field in any finite region F of a FDTD grid can not be calculated just using the nodes of F. The external nodes which are necessary to compute the fields inside F are precisely the boundary nodes of F', the complementary set of F. This can be justified since any element on the boundary of F has one or more elements of its vicinity within F', which must be part of the boundary of F'. As a result, the field in a region F of the FDTD grid free of sources is determined at certain time step in a unique way from the field at previous time instants in F and the boundary of F'.

The principle of equivalence can be applied to a region F. The inner nodes in F' does not contribute to the field in F so they can be set to an arbitrary value, for instance they can be set to zero. At the boundary of F', the equivalence between currents and fields is implemented (Eq.2.10), so the fields can be also set to zero. A distribution of electrical and magnetic currents has to be introduced at the boundaries of F and F'. The currents are set at the vicinity of the boundary nodes of F.

The current distribution is obtained by following the following procedure:

- Determine if the node belongs to the boundary of F'
- If positive then determine which nodes of the vicinity belongs to F
- In these vicinity nodes, introduce currents terms following Eq.2.10
- For the boundary node itself also currents are introduced according to Eq.2.10, but the terms of the vicinity inside F' are assumed to be zero.

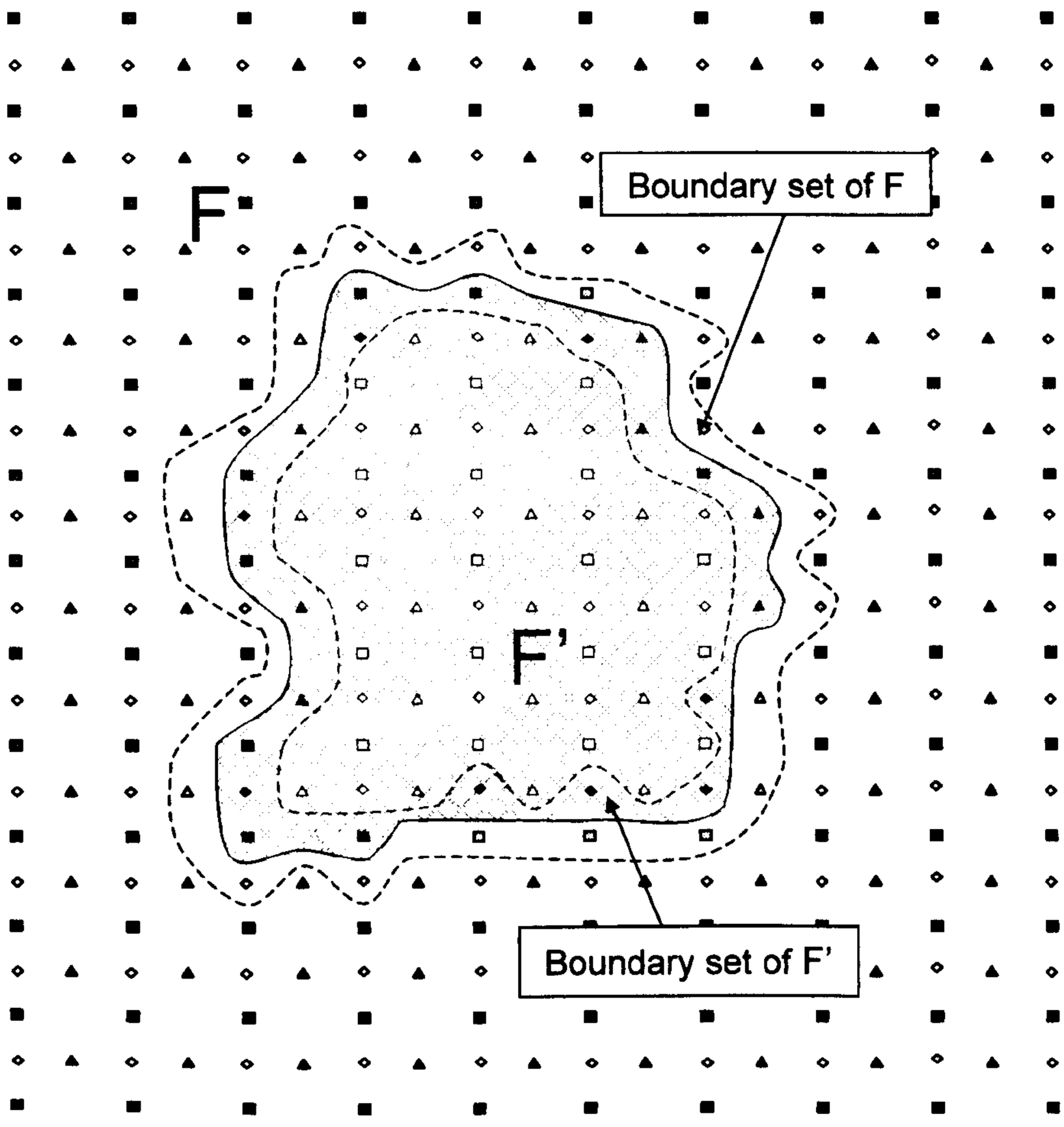

Fig.2.5. Definition of subsets in a 2D TM FDTD grid. F is an open subset and F' is its complementary set. The boundary of F' is necessary to perform the complete field update inside F. The equivalence principle is implemented for F by setting to zero the field in F' and introducing a density of currents in the boundary set of F and F', according to Eq.2.10.

2.1.6 Absorbing boundary condition. Perfect Matching Layer (PML)

A real computer has a limited memory, which is only able to represent a finite subset of the FDTD grid. All the sources and scatter relevant to the problem must be contained into this subset. As shown in the previous section, in order to update the fields inside the subset it is necessary to know the fields at the boundary of the complementary region. In some problems, the field at the boundary is determined (i.e. waveguide, metallic enclosures) or are directly related to the fields inside the subset (i.e. symmetry and periodicity conditions). However in many practical cases, the field at the boundary is not known, for instance to model the field radiated by a structure into an infinite region. In order to solve this problem, it is necessary to introduce a special algorithm (Absorbing Boundary Condition or ABC) to estimate the fields at the external boundary from the fields inside the computer-represented subset (Fig. 2.6).

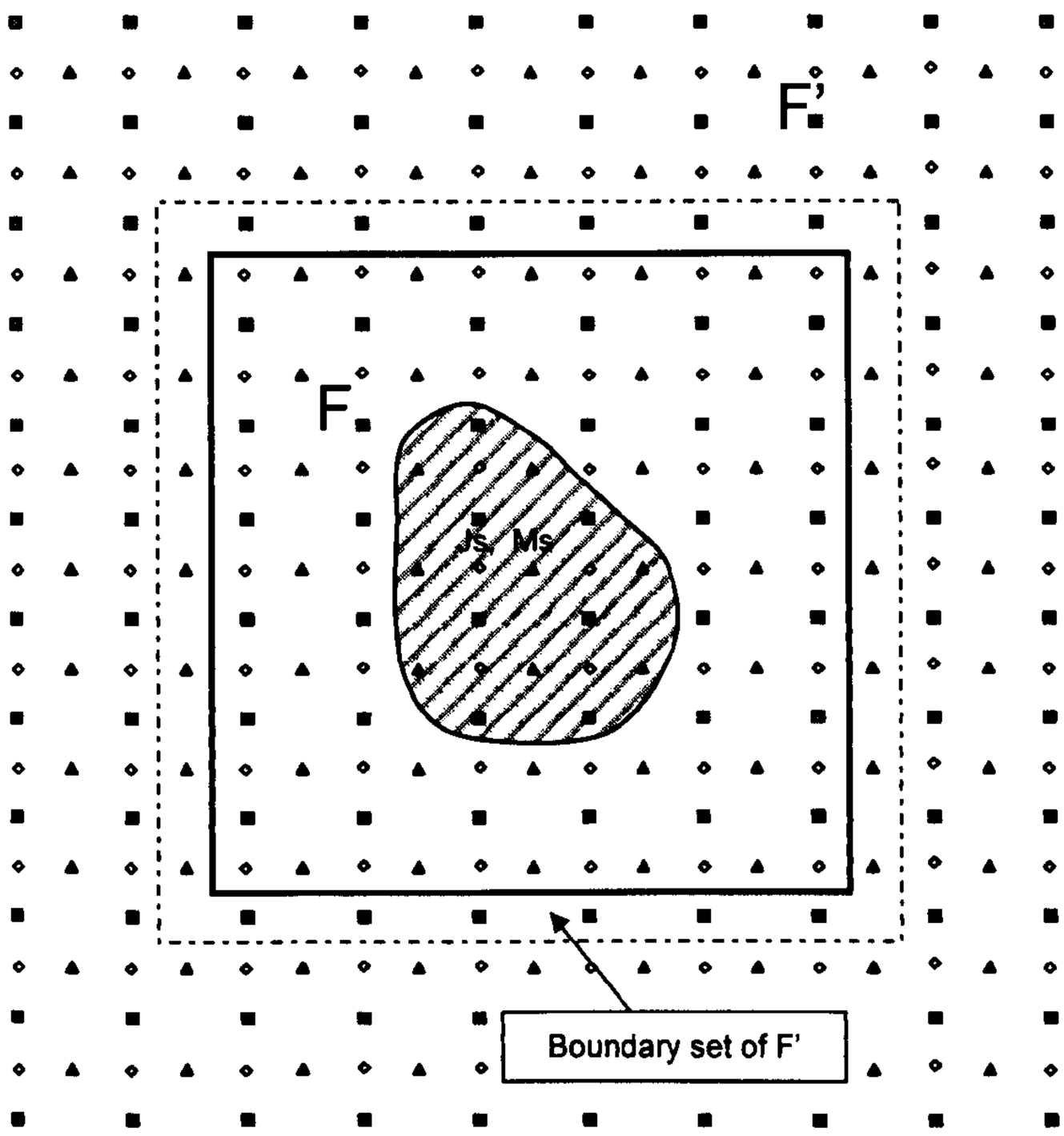

Fig 2.6. The field at the boundary of F' is required to update the field inside F. A special algorithm is necessary to radiate or absorb incoming waves at this boundary (ABC). Otherwise, waves would be 'numerically' reflected back into F.

This problem has been treated extensively by many authors [8], [9], [10], [11]. Absorbing boundary conditions (ABC) were implemented in the 70's and 80's using the theory of the one-way operators [8], [9]. One-way operators only allow wave propagation outward from the grid boundary. These procedures work very well for normally incident waves with respect to the boundaries, but usually they have a poor performance at large incidence angles (more than 45 degrees from normal).

The Mur's ABC is a one way operator technique which became quite popular due to its simplicity. Despite more sophisticated one way operator techniques being developed later on [10], [11], it is reported that the dynamic margin of the FDTD method with these ABC was in the order of –40dB [2]. This relatively small dynamic margin imposes some limitation to the analysis of low reflectivity problems.

The Perfect Matched Layer (PML) is a very low reflectivity ABC that has been more recently developed [12]. This boundary condition is based on the zero-reflection property of special lossy planar media, which satisfy the conditions given in Eq.2.11. This kind of medium is perfectly matched to the air impedance, so no reflection occurs. Once the wave is inside the PML, it is attenuated because of the ohmic losses. The PML is several elementary FDTD cells thick in order to provide good absorption of the outgoing wave. Finally, the FDTD region is terminated setting to zero the fields at the boundary.

$$\frac{\sigma}{\varepsilon} = \frac{\sigma^*}{\mu}$$

$$\sigma(\rho) = \sigma_m \left(\frac{\rho}{\delta}\right)^n \qquad \text{(Eq.2.11)}$$

In order to produce a smooth transition from air cells to the PML cells, the conductivity is gradually increased for each layer, as the boundary becomes closer. The distribution law for the conductivity follows the Eq.2.11, with the parameter n. For n=2 the conductivity profile is parabolic and exhibit the optimum absorption, especially for oblique incidence waves.

In the PML method, the conductivity of the layer is applied only on a sub-component of the fields, so the algorithm is based on PML-modified Maxwell equations. The Cartesian components of the field are split and the resulting PML equations yield a set of 12 equations as follows:

$$\mu_0 \frac{\partial H_{xy}}{\partial t} + \sigma_y^* H_{xy} = -\frac{\partial \left(E_{zx} + E_{zy}\right)}{\partial y}$$

$$\mu_0 \frac{\partial H_{xz}}{\partial t} + \sigma_z^* H_{xz} = \frac{\partial \left(E_{yx} + E_{yz}\right)}{\partial z}$$

$$\mu_0 \frac{\partial H_{yz}}{\partial t} + \sigma_z^* H_{yz} = -\frac{\partial \left(E_{xy} + E_{xz}\right)}{\partial z}$$

$$\mu_0 \frac{\partial H_{yx}}{\partial t} + \sigma_x^* H_{yx} = \frac{\partial \left(E_{zx} + E_{zy}\right)}{\partial x}$$

$$\mu_0 \frac{\partial H_{zx}}{\partial t} + \sigma_x^* H_{zx} = -\frac{\partial \left(E_{yx} + E_{yz}\right)}{\partial x}$$

$$\mu_0 \frac{\partial H_{zy}}{\partial t} + \sigma_y^* H_{zy} = \frac{\partial \left(E_{xy} + E_{xz}\right)}{\partial y}$$

$$\varepsilon_0 \frac{\partial E_{xy}}{\partial t} + \sigma_y E_{xy} = \frac{\partial \left(H_{zx} + H_{zy}\right)}{\partial y}$$

$$\varepsilon_0 \frac{\partial E_{xz}}{\partial t} + \sigma_z E_{xz} = -\frac{\partial \left(H_{yx} + H_{yz}\right)}{\partial z}$$

$$\varepsilon_0 \frac{\partial E_{yz}}{\partial t} + \sigma_z E_{yz} = \frac{\partial \left(H_{xy} + H_{xz}\right)}{\partial z}$$

$$\varepsilon_0 \frac{\partial E_{yx}}{\partial t} + \sigma_x E_{yx} = -\frac{\partial \left(H_{zx} + H_{zy}\right)}{\partial x}$$

$$\varepsilon_0 \frac{\partial E_{xz}}{\partial t} + \sigma_z E_{xz} = -\frac{\partial \left(H_{yx} + H_{yz}\right)}{\partial z}$$

$$\varepsilon_0 \frac{\partial E_{zy}}{\partial t} + \sigma_y E_{zy} = -\frac{\partial \left(H_{xy} + H_{xz}\right)}{\partial y} \qquad \text{(Eq.2.12)}$$

The conductivity is different for each sub-component of the field. The sub-conductivity for the component normal to the PML are set to the value of Eq.2.11 and the others are set to zero. As the PML is based on a set of planar layers, it can only be implemented for a planar boundary. The PML method is applied to rectangular grids implementing a PML for each wall of the FDTD region. At the corners of the grid, the PML's are overlapping with their respective conductivity distributions. The structure of the PML in a two dimensional grid is depicted in figure 2.6

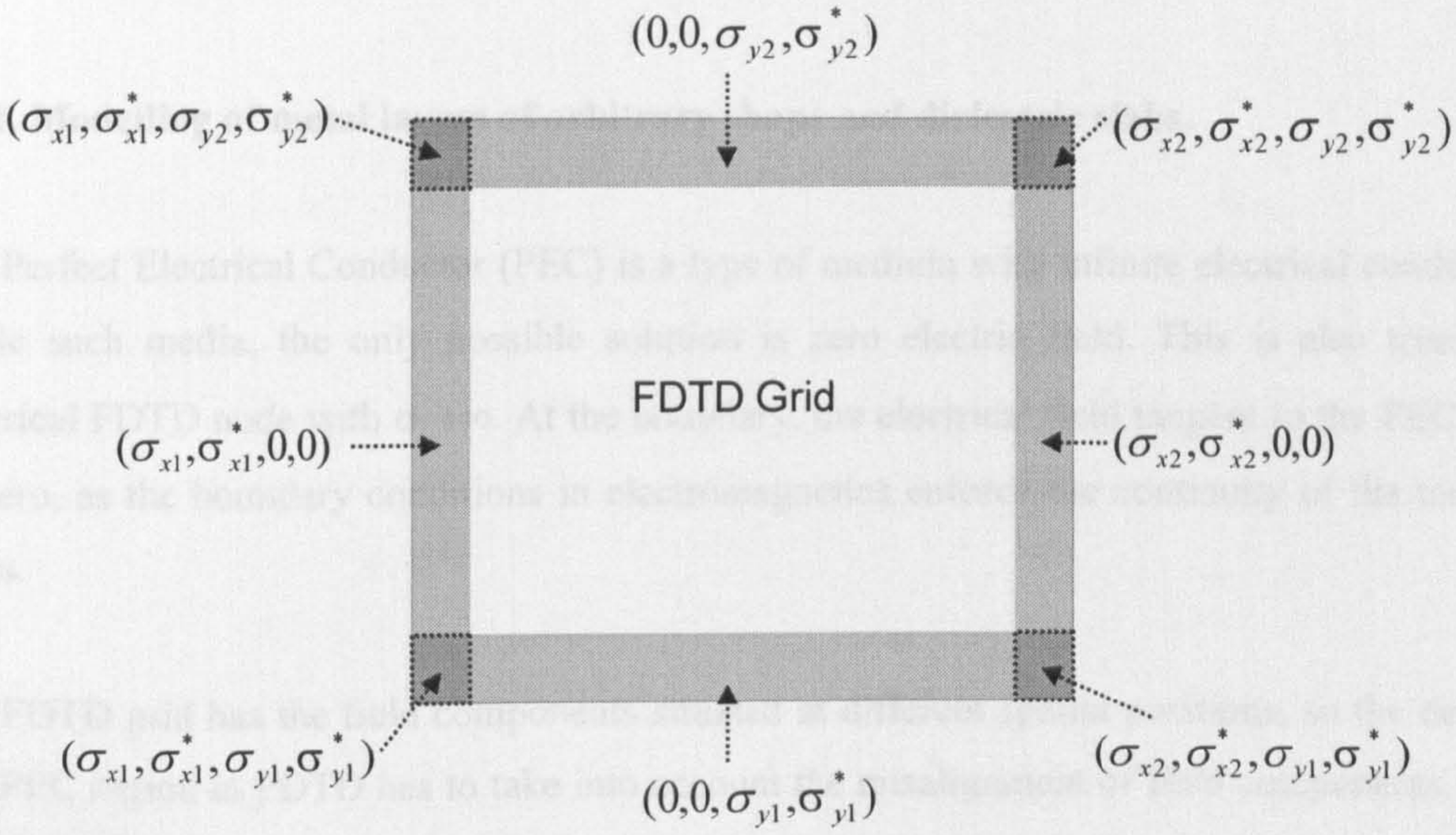

Fig.2.6. Distribution of conductivity in the 2D PML ABC.

The performance of the PML ABC is reported in [1] improving the dynamic margin of the FDTD method up to 70dB, which represent a big advance in respect to the previous existing ABC's. The PML can be placed close (up to 2 cells) to the object being modelled, with very low distortion of the result [13].

The PML ABC requires extra memory in order to implement it, since several layers of FDTD cells are dedicated to the PML. The performance of PML is also greatly reduced for long wavelength waves since the attenuation of the waves inside the PML decreases with frequency. As a result, the number of PML layers has to be increased for small cell sizes and more than 10 layers are required in most practical models.

2.2: FDTD model of planar passive structures

2.2.1. Modelling of metal layers of arbitrary shape and dielectric slabs.

The Perfect Electrical Conductor (PEC) is a type of medium with infinite electrical conductivity. Inside such media, the only possible solution is zero electric field. This is also true for an electrical FDTD node with $\sigma \to \infty$. At the boundary, the electrical field tangent to the PEC should be zero, as the boundary conditions in electromagnetics enforce the continuity of the tangential fields.

The FDTD grid has the field components situated at different spatial positions, so the definition of a PEC region in FDTD has to take into account the misalignment of field components. A PEC in FDTD is a subset of the FDTD grid determined by electric nodes set to zero. The PEC also includes the zero field magnetic nodes, which appear in between zero field electric nodes.

An elegant definition of a PEC in FDTD is based on the vicinity and boundary set concepts given in the previous section: A PEC is a subset of the FDTD grid where the fields associated to each node are set to zero and its boundary set is purely electric. The figure 2.6 shows the PEC definition for a planar case. The boundary set of the PEC consist of nodes of electric field component tangent to the boundary itself. The same definition can be applied for Perfect Magnetic Conductors (PMC), but interchanging electric and magnetic fields.

Planar metal layers can be implemented as a PEC following this definition. In this case, the cartesian nature of the FDTD grid is well suited for modelling planar objects. An infinitely thin planar PEC can be model in a single layer of electric field nodes.

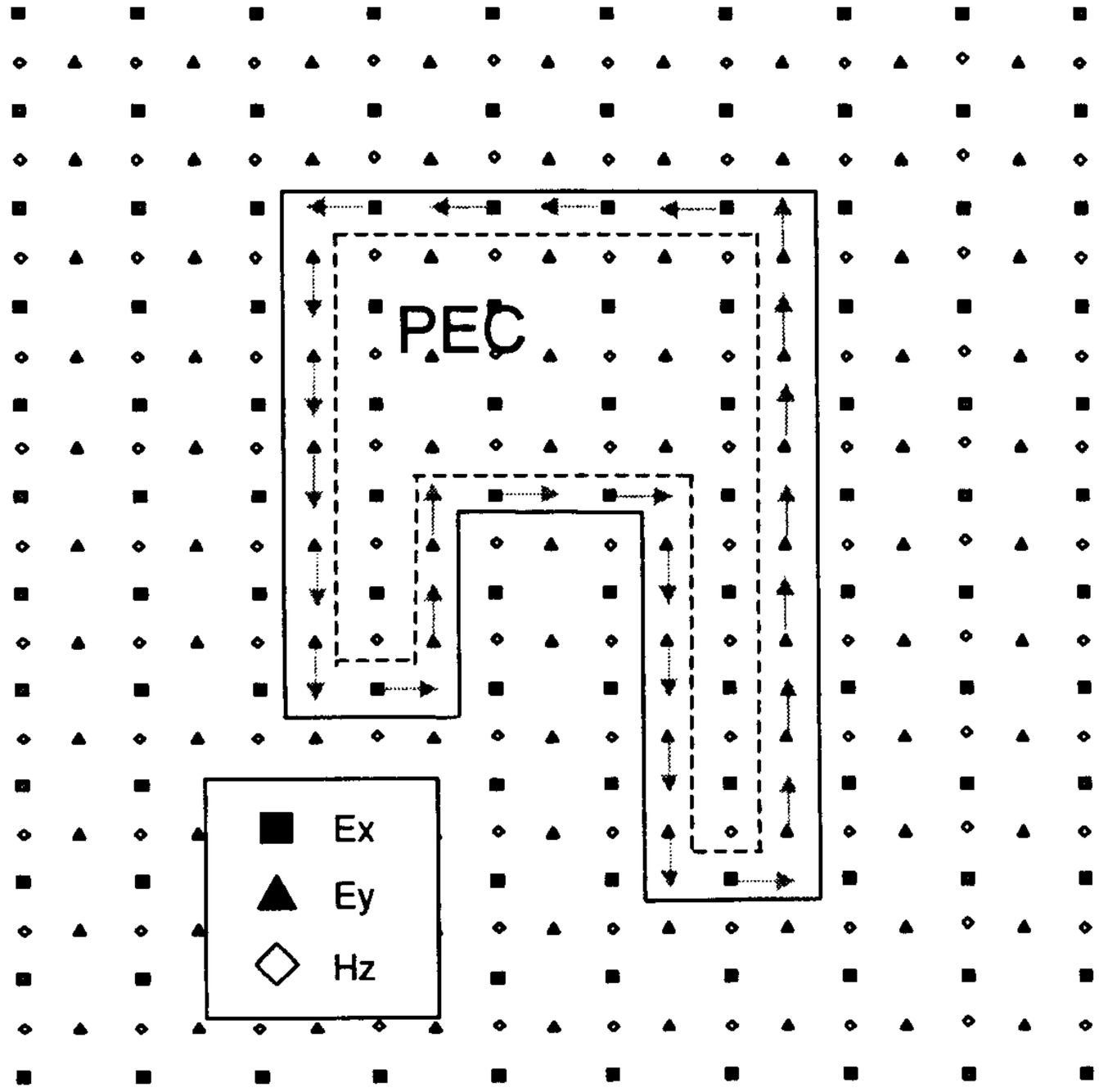

Fig.2.6. PEC in a 2D TM FDTD grid: the electric field is set to zero at the nodes inside the PEC. The boundary set of the PEC must be purely electrical. This definition is also valid for the 3D case.

Dielectric media are defined as a spatial distributions of the electric permitivity $\varepsilon(x,y,z)$. The FDTD equations can implement a different value of ε for each electric node of the grid, similar to the continuous dielectric distribution, but considered at discrete locations. However, the FDTD definition of a finite dielectric object has some essential differences with respect to continuous dielectric media.

The boundary of a dielectric object has to be inserted into a FDTD grid with misalign field component nodes. As a result, the boundary of the dielectric regions is not perfectly symmetrical. Figure 2.7 shows the interface between two regions with different dielectric constants. Inside the medium 1, the first row contains electrical nodes normal to the interface. In the medium 2, the first row contains electrical nodes parallel to the interface. This creates an asymmetric situation at the interface between dielectric media.

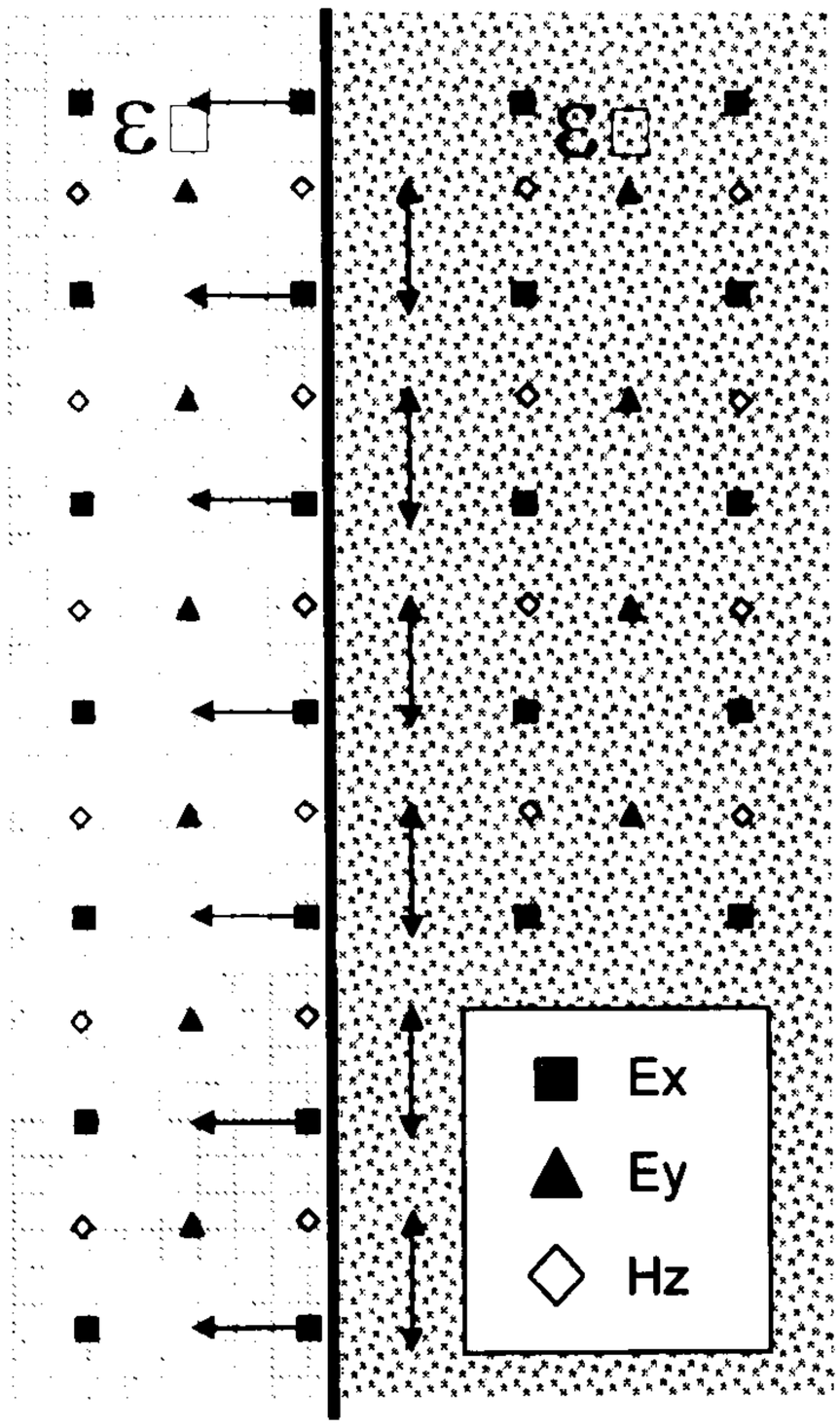

Fig.2.7. The first row of electric field nodes inside the medium 1 is normal to the interface, but is parallel at medium 2, due to the alternate position of field components in the FDTD grid.

The transmission coefficient of planar waves from media 1 to 2 and 2 to 1 is related by the condition $T_{12} = \sqrt{\varepsilon_1/\varepsilon_2}\, T_{21}$, ensuring the symmetry of the dielectric interface from the point of view of power. However as a result of the intrinsic asymmetry of the FDTD dielectric interface, the direct and reverse transmission coefficients are not related by the previous condition Fig.2.8.

There are significant consequences of this asymmetry, the resonant properties of dielectric structures are changed (for instance, the total transmission of a dielectric slab is based on the symmetry of the transmission coefficients). This will lead to inaccuracies on the calculation of resonant frequencies and improper cancel of multiple reflections. The difference between direct and reverse transmission can be about 3% for the interface of air-ε_r=2 and $\Delta x/\lambda_d = 0.1$. This suggests that accurate FDTD calculations on resonant effects involving dielectrics require very small cell sizes $\Delta x/\lambda_d \leq 0.05$.

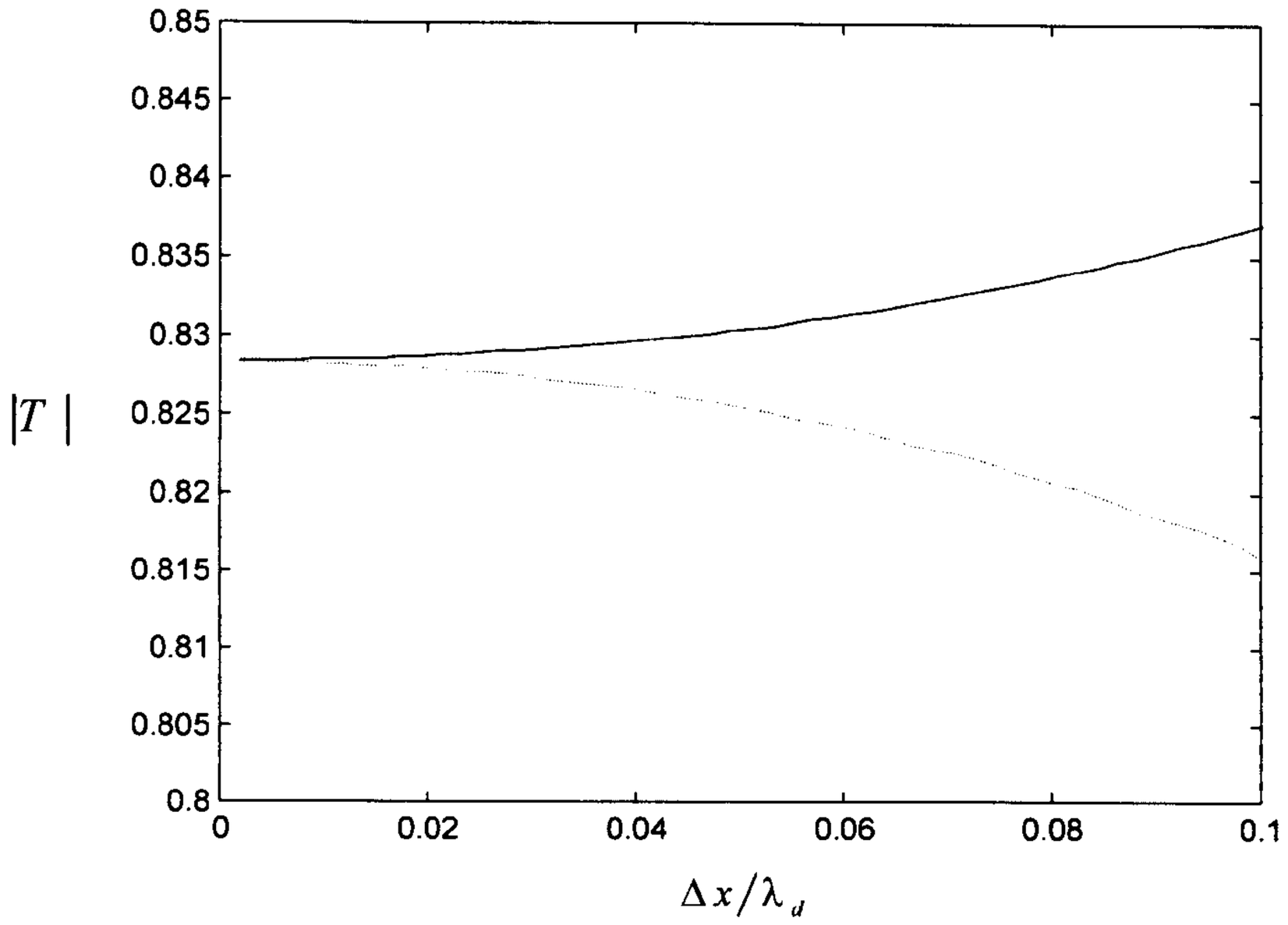

Fig.2.8. Transmission coefficient for a normal incidence on an interface air-dielectric (ε_r=2) estimated using FDTD as a function of the normalized cell size inside the dielectric medium. The theoretical $|T_{air-diel}|$ is 0.8258. ($|T_{air-diel}|$: solid line, $\sqrt{1/\varepsilon_r}\cdot|T_{diel-air}|$: dashed line).

As stated, there is qualitatively different behaviour of the interface between dielectric media in FDTD and the continuous electromagnetics. The FDTD approximation assumes the continuity of the derivatives, but this is not true at the interface of two dielectric media (Eq.2.13). This implies that a boundary node of electric field in FDTD can not belong to two media simultaneously, since it requires more than one derivative for the magnetic/electric field in a single cell.

$$\varepsilon_1 \frac{\partial E_y^{\,1}}{\partial t} = \frac{\partial H_x^{\,1}}{\partial z} - \frac{\partial H_z^{\,1}}{\partial x} \qquad \varepsilon_2 \frac{\partial E_y^{\,2}}{\partial t} = \frac{\partial H_x^{\,2}}{\partial z} - \frac{\partial H_z^{\,2}}{\partial x}$$

Boundary conditions

$$\frac{\partial E_y^{\,1}}{\partial t} = \frac{\partial E_y^{\,2}}{\partial t} \qquad \frac{\partial H_x^{\,1}}{\partial z} = \frac{\partial H_x^{\,2}}{\partial z} \qquad \frac{\partial H_z^{\,1}}{\partial x} \neq \frac{\partial H_z^{\,2}}{\partial x}$$

(Eq.2.13)

A FD approximation for dielectric interfaces is proposed in [15] by averaging the Eq.2.13 in both sides of the interface. Basically, the FD equation is obtained in the same manner than Yee's algorithm with an average permitivity $(\varepsilon_1 + \varepsilon_2)/2$. The average of the magnetic field derivative at each side of the interface is approximated by a central difference (Eq.2.14). The accuracy of the procedure drops to $O(\Delta x)$, but the symmetry of the interface has been restored..

$$\left(\frac{\varepsilon_1 + \varepsilon_2}{2}\right)\frac{\partial E_y}{\partial t} = \frac{\partial H_x}{\partial z} - \frac{1}{2}\left(\frac{\partial H_z^{\,1}}{\partial x} + \frac{\partial H_z^{\,2}}{\partial x}\right)$$

$$\frac{1}{2}\left(\frac{\partial H_z^{\,1}}{\partial x} + \frac{\partial H_z^{\,2}}{\partial x}\right) = \frac{1}{2}\left(\frac{H_z^{\,1} - H_z^{\,12}}{\Delta x/2} + \frac{H_z^{\,12} - H_z^{\,2}}{\Delta x/2} + O(\Delta x)\right) = \frac{H_z^{\,1} - H_z^{\,2}}{\Delta x} + O(\Delta x)$$

(Eq.2.14)

The FDTD procedure described in Eq.2.14 does not seem to improve significantly the estimation of the transmission coefficient. The accuracy of the calculation drops as the cell size increases. It provides a better result for the high-low ε transmission, but it is worse low-high ε transmission (Fig.2.9).

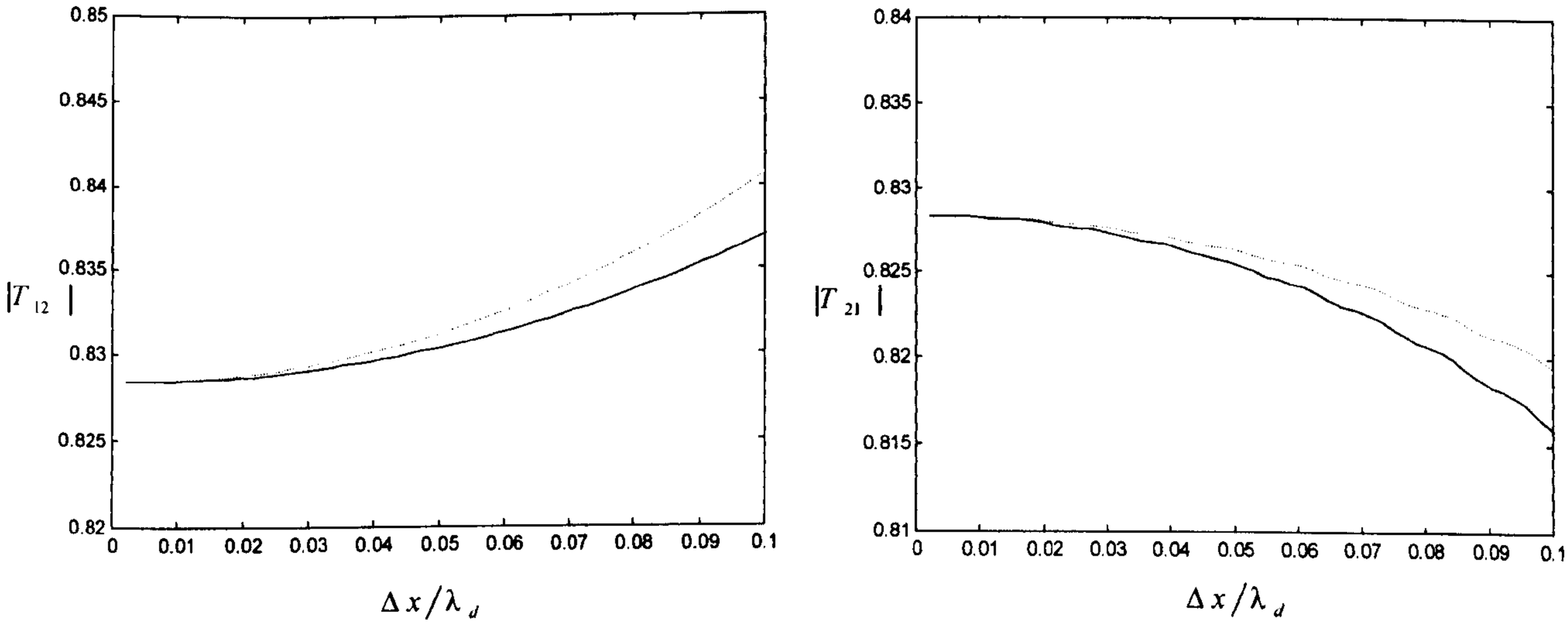

Fig.2.9. Transmission coefficient for a normal incidence on an interface air-dielectric (εr=2) estimated using normal FDTD (solid line) and the procedure of Eq.2.14 (dashed line). The theoretical $|T_{air-diel}|$ is 0.8258. ($|T_{air-diel}|$: right, $\sqrt{1/\varepsilon_r} \cdot |T_{diel-air}|$: left).

2.2.2. Voltage sources, loads and linear passive circuits.

Voltage sources and current sources can be implemented into elementary unit FDTD cells. Intensity can be modelled as external electrical currents using the density of current term *j* into the FDTD field equations. On the other hand, voltage sources also can be implemented by using external magnetic currents in the same way.

A real generator with internal resistance can be modelled by a electrical/magnetic current, but in this case, these currents depends on the electrical or magnetic potential at the generator terminals to take into account the potential at the internal resistance. In some circumstances (quasi-static approach), this potential can be evaluated directly from the electrical field in the FDTD grid (Eq.2.15).

As the FDTD operates in time domain, the voltage source can generate voltage pulses as excitation. These broadband signals can be extracted and analysed via FFT in order to compute the impedance of the system at the generator terminals.

$$E' = grad(v(t) - Rg \cdot i(t)) \qquad v^{n+1/2} = \left(\frac{E^{n+1}(i,j,k) + E^{n}(i,j,k)}{2} \right) \qquad Z(f) = \frac{V(f)}{I(f)} - Rg \qquad \text{(Eq.2.15)}$$

Resistive loads can be implemented as a conductivity distribution in a FDTD cell, but the resistance can also be modelled as a real generator with zero voltage at the source which produces a density of current. Other linear lumped elements, such as capacitors or inductors can be introduced in the same way as resistance, either as density of currents or as distributed electric permitivity or magnetic permeability into the FDTD cell.

2.2.3 Modelling examples

An FDTD code has been implemented in order to show the ability of the method to model planar integrated antennas. The first step was the development of a software package, which could model passive multilayer planar structures of arbitrary shape.

This code uses PML ABC, sinusoidal and pulsed voltage sources, loads, and all the features to model planar structures as described in the previous section. The code is written in standard Fortran 77 in order to keep high portability. The geometry input is based on a Matlab™ front-end program, which is interfaced by a file to the main program. There is an ASCII file to input the parameters for the FDTD method such as grid dimensions, number of cells, type of PML and dielectric constants. The outputs of the code are broadband impedance at the input port, time domain voltages and intensities at specified points, density of currents at the printed circuits and electromagnetic field at given positions.

In order to verify the accuracy of the calculations, several planar antennas have been analysed to determine their impedance (Figs. 2.8-2.11). All these cases are microwave patch antennas whose measured response can be found in the literature [15], [16], [17].

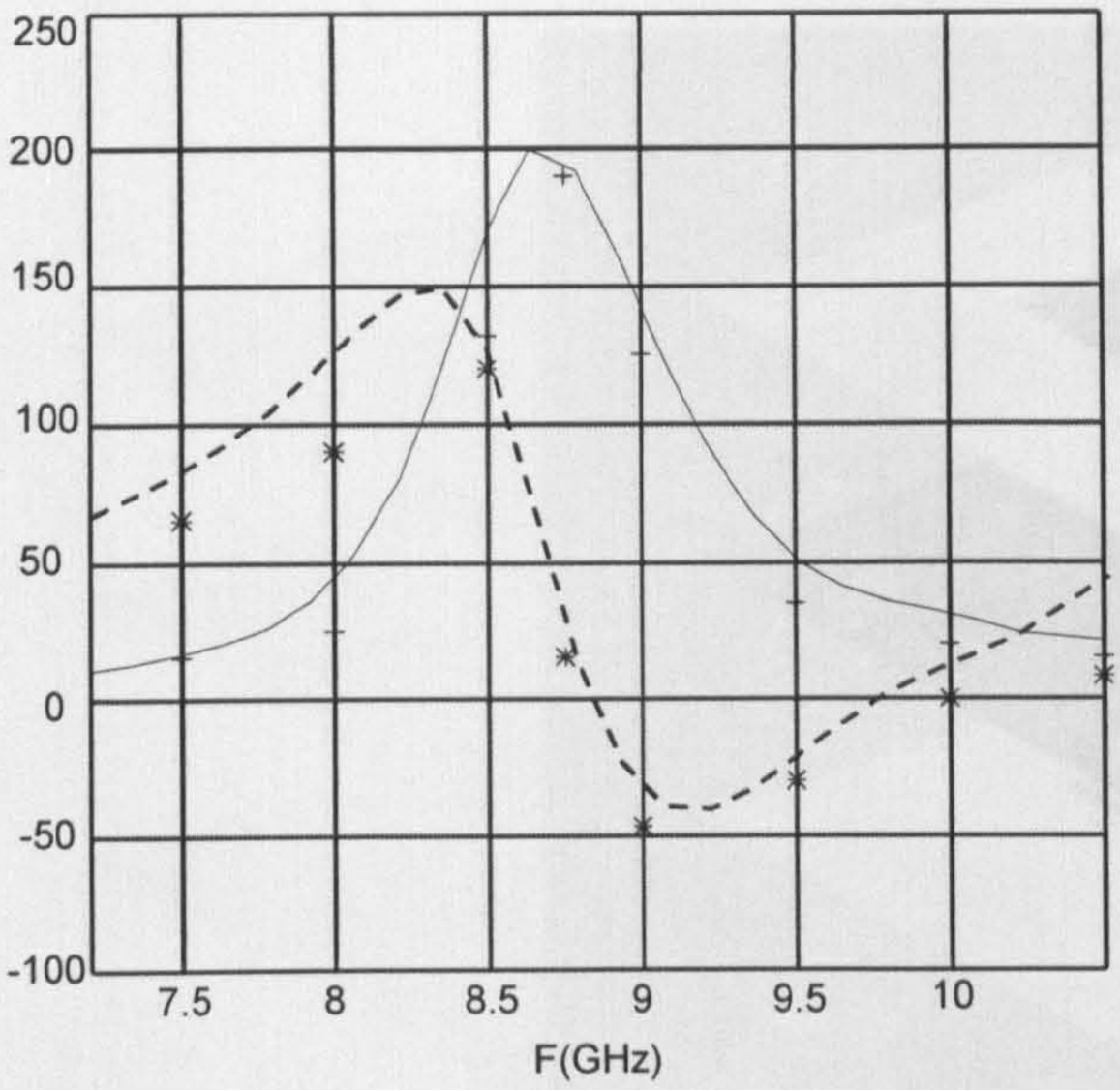

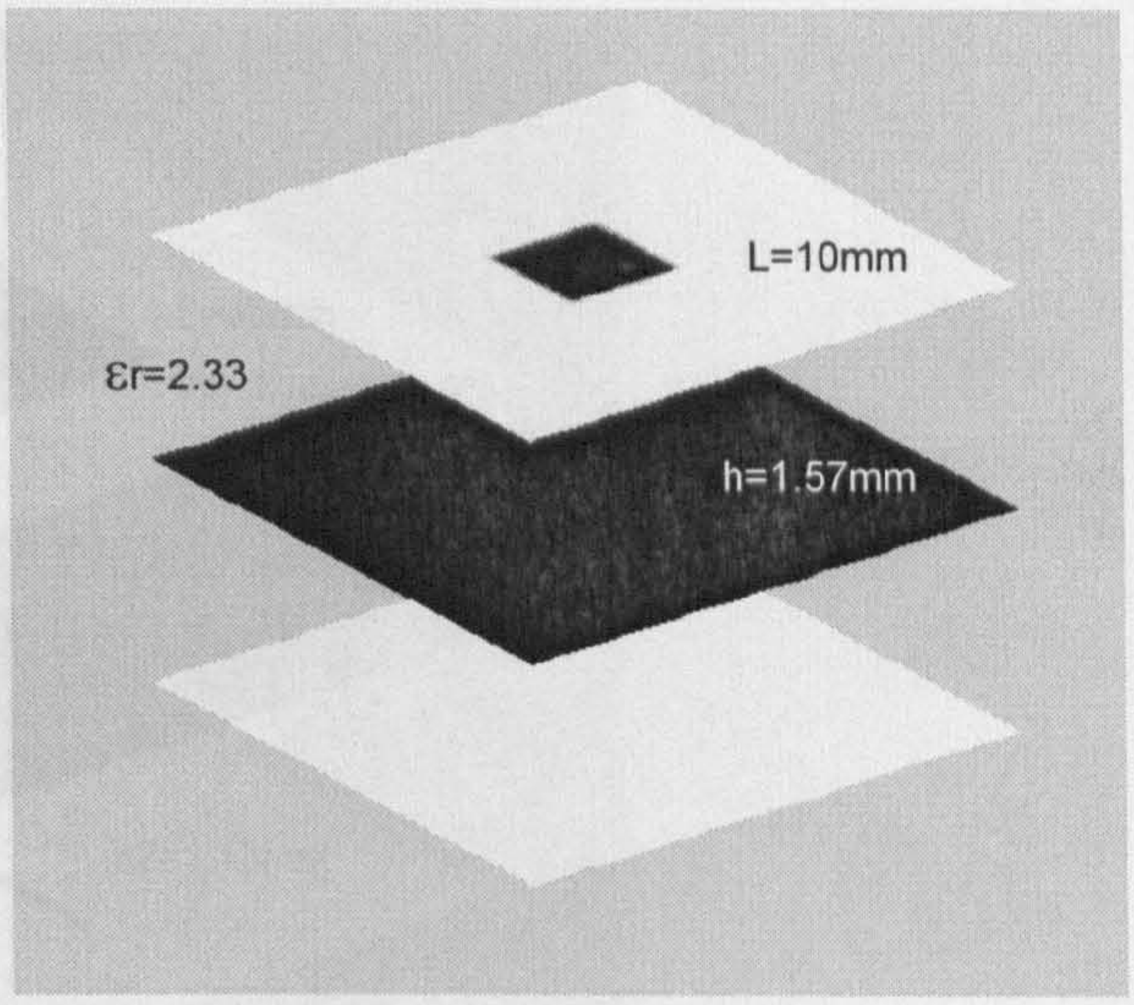

Fig.2.8 Modelling of a square patch antenna .The computed impedance (real part: solid line, imag. part: dashed line) is compared to the measured one [15] (crosses and asterisks). A FDTD grid of 60x60x60 element is used.

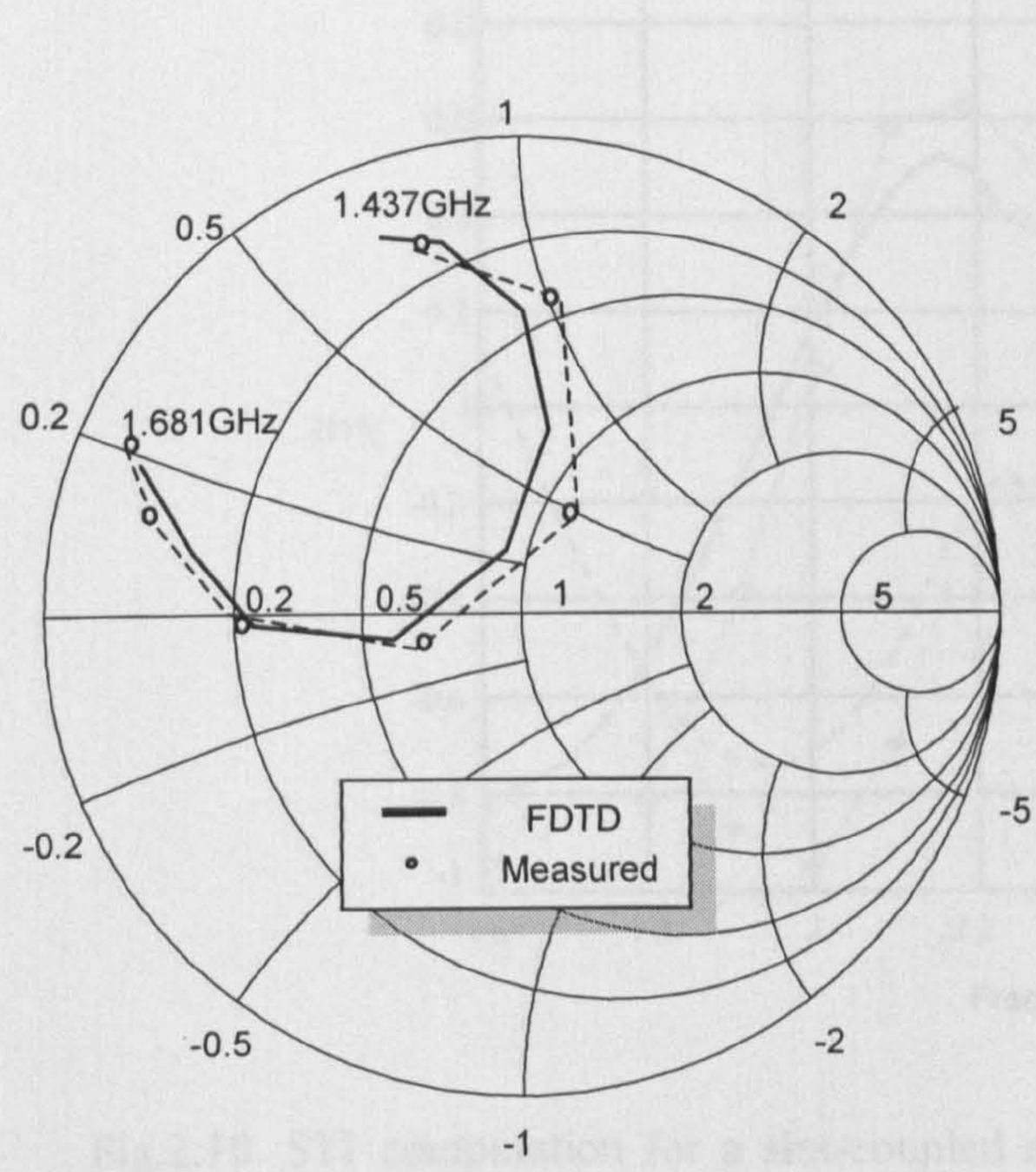

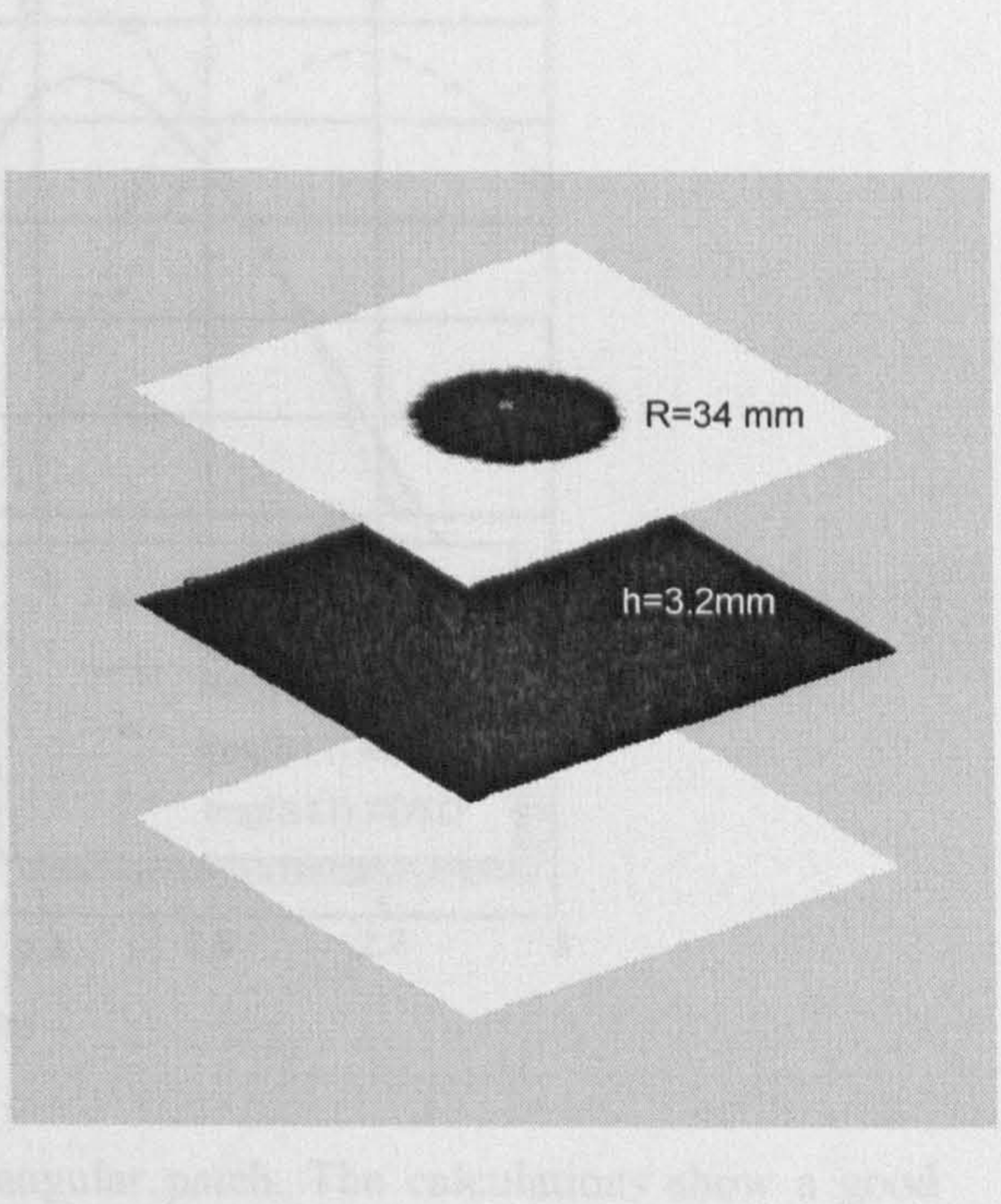

Fig. 2.9 Impedance computation for a circular patch. The FDTD computed impedance is shown in a Smith chart (solid line) and it is compared to the measurements [16] (circles). A FDTD grid of 60x60x60 element is used.

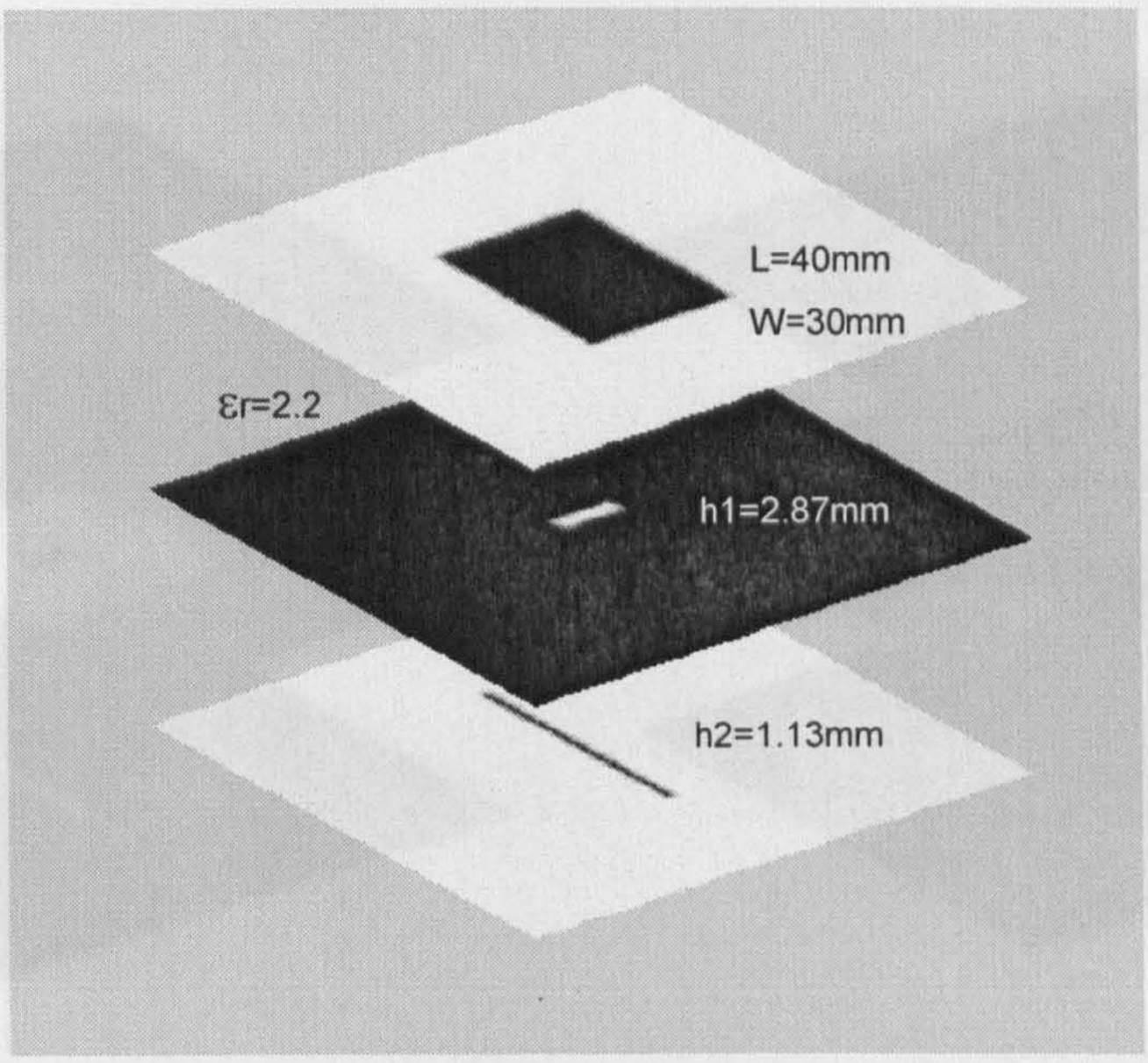

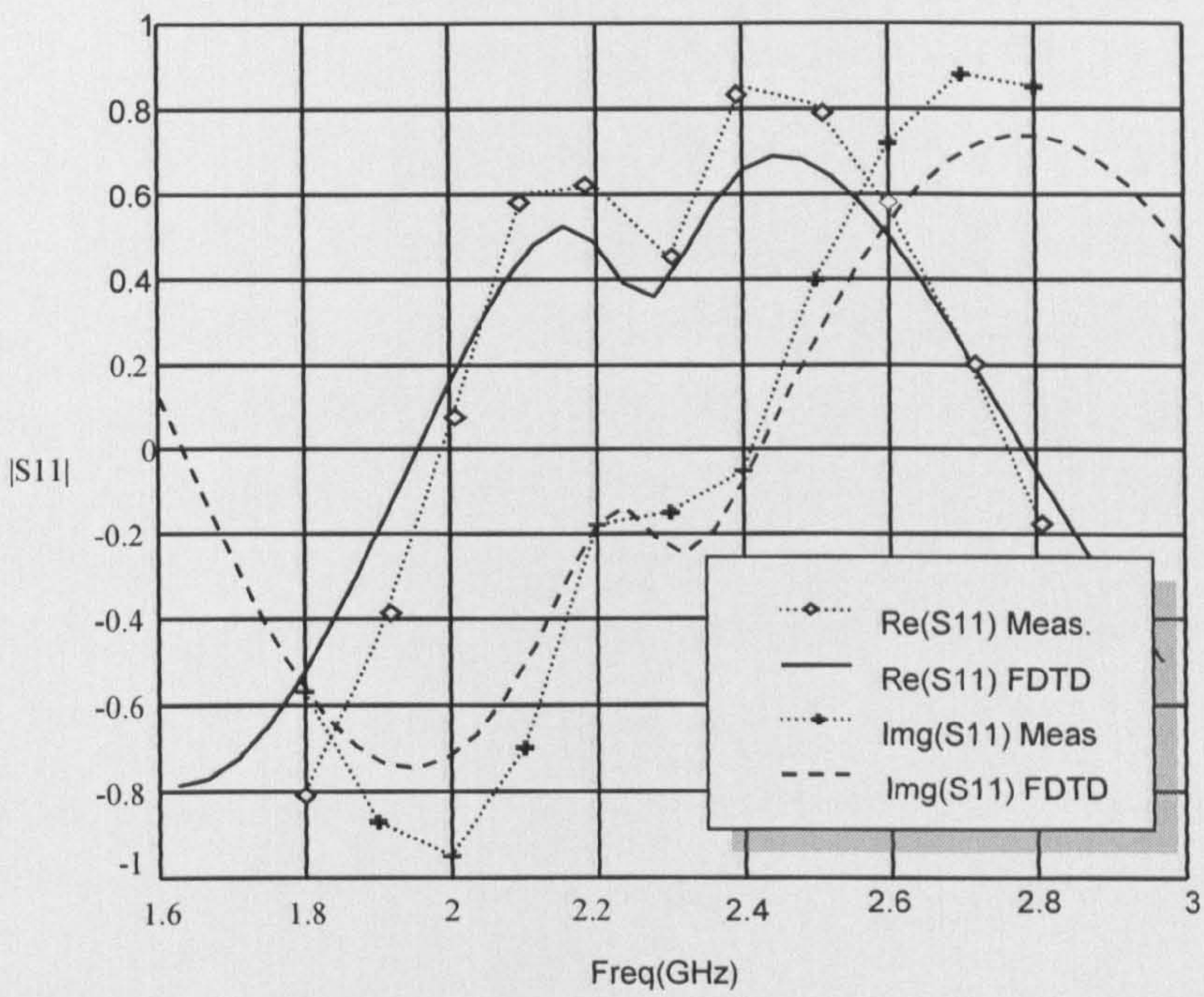

Fig.2.10. S11 computation for a slot-coupled rectangular patch. The calculations show a good agreement at the resonance frequency (2.3GHz) but some differences outside resonance. The FDTD results in [17] show very good agreement with measurements using a high resolution (620 cells, here 240 cells) in order to model the narrow slot.

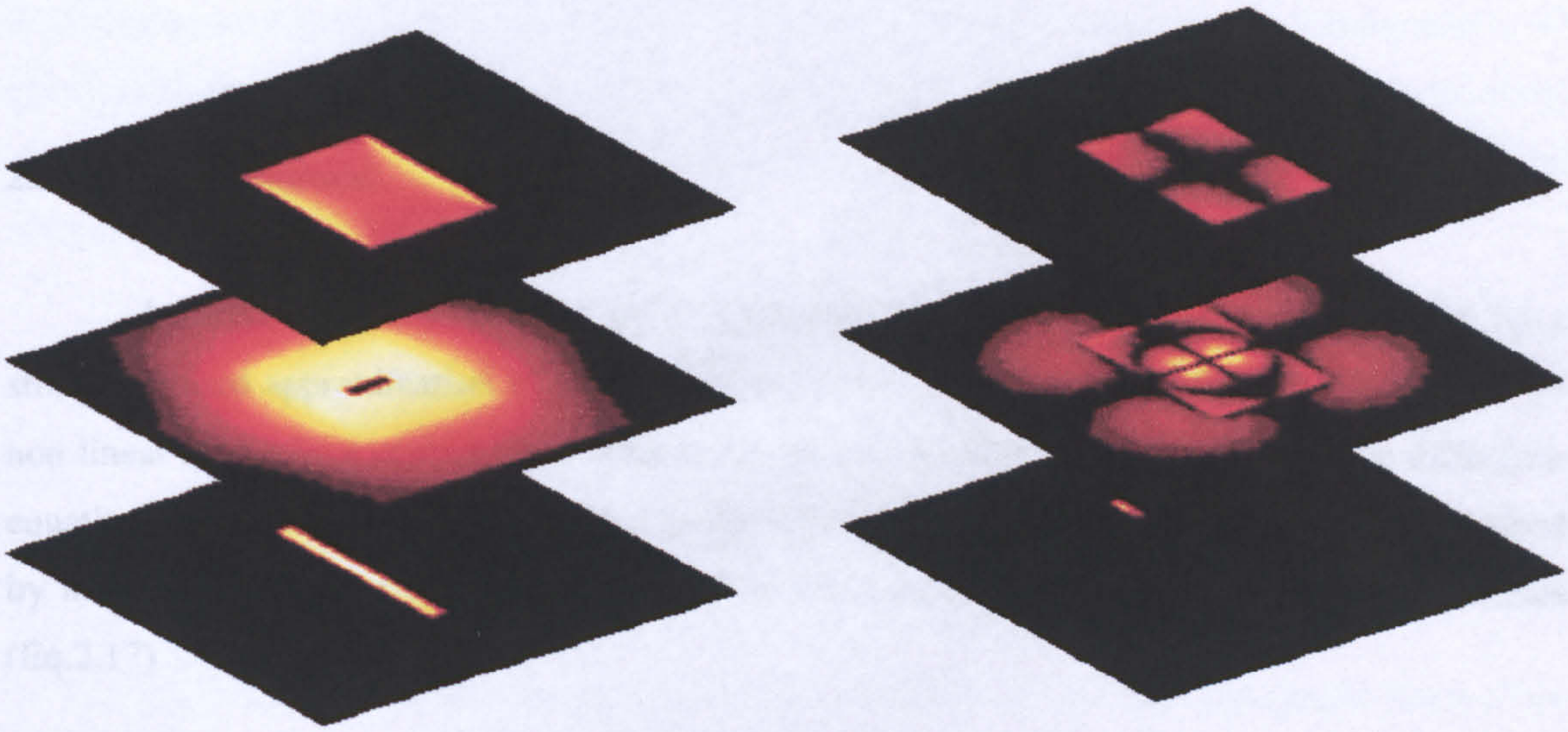

Fig. 2.11. Current density on the metallic parts of the slot-coupled microstrip antenna at the resonance frequency. Copolar currents (Left) and Xpolar currents (Right) are presented.

2.3 FDTD modelling of non linear devices

2.3.1 Basic Equations.

A direct extension of the FDTD method to non-linear media can be obtained by a straightforward approximation of the partial derivatives of the general Maxwell's equations for non linear media by a central finite difference scheme, resulting in a non linear finite difference equations. However, non-linear FDTD can also be implemented from the classical linear method by means of non-linear operator introduced at the equations as some sort of external currents (Eq.2.17)

$$\nabla \times \vec{E} = -\frac{\partial \vec{B}}{\partial t}$$

$$\nabla \times \vec{H} = \frac{\partial D}{\partial t} + \vec{j}_{ex} + J(\vec{E}, \vec{H})$$

$$\vec{B} = \mu * \vec{H} \qquad \vec{D} = \varepsilon * \vec{E}$$

(Eq. 2.17)

In these equations the electrical field E and the displacement vector D are related linearly (the same for B, H), but the symbol J describes an operator on the field vectors E, H that can be non-linear. The symbol $\vec{j}_{ex}$ represents the currents on the system due to an external (non electromagnetic source of energy). So, the non-linear part is modelled in this equation as the result of the interaction of a basic linear electromagnetic field with non-linear induced sources.

The Eq.2.17 presents a general formulation of the non-linear electromagnetic curl equations. This scheme is well suited to implement approximations that can model some particular problems. For instance, this set of equations can be useful to model weak non linear media by means of perturbational procedures [18], since these methods are based in the separation of the linear part of the solution from the non linear part.

Another particular case in which Eq.2.17 can be easily approximated is depicted in Fig 2.11. The non-linearity is strong but it occurs in regions that are electrically small compared to all the wavelengths that exist in the system. In this case the operator J is approximated by the finite sum of terms of currents produced at discrete space points, which are non-linearly related to the electromagnetic field at these points (Eq. 2.18).

$$J(\vec{E},\vec{H}) = \sum_i \sum_l j_{il}(\vec{E}(\vec{r}_l,t),\vec{H}(\vec{r}_l,t)) \cdot \delta(\vec{r}_i) \qquad \text{(Eq.2.18)}$$

The terms j of the sum are non-linear time operators on the electromagnetic fields at the position r. This approximation can be used to model the interaction of the electromagnetic fields in a linear structure with solid state devices. The non-linear part of many detectors is contained in a tiny region surrounding a junction of different materials, as it occurs for solid state diodes.

Two essential problems have to be solved before using Eq.2.17&2.18. First, The equations have to be approximated to a set of discrete equations using a central finite difference scheme. Second, the final form of the j operators has to be determined for each type of device.

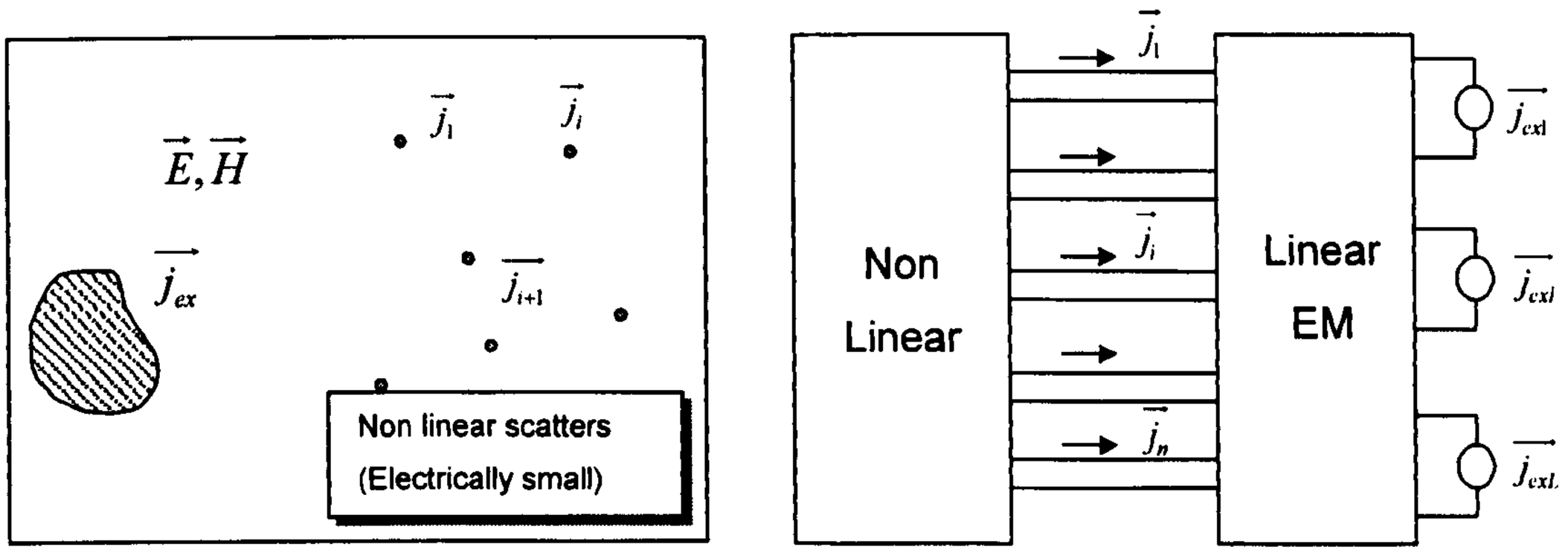

Fig 2.11. A linear system with a finite number of non-linear electrically small scatters (left). In this case the linear part of the equations can be separated from the non-linear part. The link of both parts is obtained by a finite number of ports associated to the induced currents in each scatter (right).

The approximation to a discrete set of equations can be obtained by using the integral form of the equation 2.17 for elementary unit cell. For the sake of simplicity it will be only done for one field component. The integral form can be related to the differential form by means of the integral over each face of the unit cell.

$$\frac{1}{\Delta x \Delta y}\int\left(\nabla \times \vec{H}\right)\cdot dS = \frac{1}{\Delta x \Delta y}\int\left(\frac{\partial \vec{D}}{\partial t} + \vec{j}_{ex} + J(\vec{E},\vec{H})\right)\cdot dS \qquad \text{(Eq.2.19)}$$

Using equation 2.19, the Stokes theorem, and assuming that the r_i point is at the centre of the integration surface, the non-linear part will be assumed to be caused by the electrical field *(J=J(E))*

$$\frac{1}{\Delta x \Delta y}\oint_C \vec{H}\cdot dl = \frac{1}{\Delta x \Delta y}\left[\frac{\partial \int \vec{D}\cdot dS}{\partial t} + \int \vec{j}_{ex}\cdot dS + \sum_l j_{z,l}(\vec{E}_l)\right] \qquad \text{(Eq.2.20)}$$

This equation can be finally approximated to a discrete form, taking into account the elementary grid cell of figure 2.1. The integral on the xy face of the elementary cubic cell can be approximated by:

$$\frac{1}{\Delta x \Delta y}\oint_C \vec{H}\cdot dl = \frac{H_x(i,j-1/2,k)-H_x(i,j+1/2,k)}{\Delta y} + \frac{H_y(i+1/2,j,k)-H_y(i-1/2,j,k)}{\Delta x} + O(\Delta^2)$$

$$\frac{1}{\Delta x \Delta y}\frac{\partial \int \vec{D}\cdot dS}{\partial t} = \frac{\partial D_z(i,j,k)}{\partial t} + O(\Delta^2) \qquad \text{(Eq.2.21)}$$

The Eq.2.21 show the procedure to approximate the spatial part of the curl equation to a set of discrete ones. It has been done here for one co-ordinate, but it can be easily extended for the rest of them. The time domain part of the equation remains continuous, and it has to be approximated by discrete equations. The basic FDTD algorithm uses a central difference scheme for the time domain co-ordinate. However, it can not be done in a straightforward manner for the cells that contains non-linear current elements.

$$\frac{\partial D_z(i,j,k,t)}{\partial t} = L_H(i,j,k,t) + \sum_l j_{zl}(\vec{E}(i_l,j_l,k_l,t)) \qquad \text{(Eq.2.22)}$$

Where L is the contribution of the H field in Eq.2.21. The discrete approximated equation for time domain is obtained by means of central differences on the time domain. In this way for the cells without non-linear contributions the algorithm is exactly the normal FDTD, but in cells with non-linear devices the finite difference scheme has to be changed.

$$\vec{E}^{n+1/2}(i_l,j_l,k_l) = \frac{\vec{E}^{n+1}(i_l,j_l,k_l) + \vec{E}^{n}(i_l,j_l,k_l)}{2} + O(\Delta t^2)$$

$$D_z^{n+1}(i,j,k) = D_z^n(i,j,k) + \Delta t\left(L_H^{h+1/2}(i,j,k) + \sum_l j_{zl}^{n+1/2}(\vec{E}(i_l,j_l,k_l,t)) \right)$$

(Eq.2.23)

Equation 2.23 can not be solved in a direct way since j_l are non-linear operators on the electrical field. In general, these operators can be approximated by a discrete scheme, but the equation 2.23 then become a transcendent equation that remains in an implicit form.

2.3.2 Lumped circuit element model. The Schottky diode.

It is clear from equation 2.23 that the final form of the numerical algorithm depends on the explicit form of the j_l operators. These operators will be related to the type of device that is intended to be model. However, the electrical behaviour of all practical devices can be modelled as a network of elementary circuit elements. This is a good approximation if the following conditions are assumed

- The quasi-stationary approach is possible to model the device.
- The device behaviour can be considered as the linear combination of non-linear effects.

The first point is verified since electrically small scatters are considered. The second is usually verified since the currents at many devices are the result of currents produced by completely different physical sources that are combined in a linear way, although the physical sources can be non-linear (e.g. the recombination mechanism and space-charge capacitance in a diode). The result is that the device model can be handled as typical networks of circuits elements, but now these elements are non-linear.

A major feature of this model is that the device can be split between several elementary FDTD cells. This is possible since contiguous cells can be considered to be series or parallel connected each other. However, it is necessary to verify first that the set of cells used to model a single device, are not too big compared to the wavelength.

2.3.2.1 The Schottky diode circuit element model.

The ability of the lumped circuit element method to model devices can be shown for the Schottky diode (Fig 2.12) whose circuit equivalent is well known. This device is extensively used as a high frequency detector so this model can be used for further investigations. The lumped element model of Schottky diodes is extensively used up to the mmW frequency band (approx. 100GHz). For higher frequencies, there are more sophisticated mathematical models, based on non-linear time domain differential equations. Interfaces between FDTD and these models can be implemented since both are in time domain.

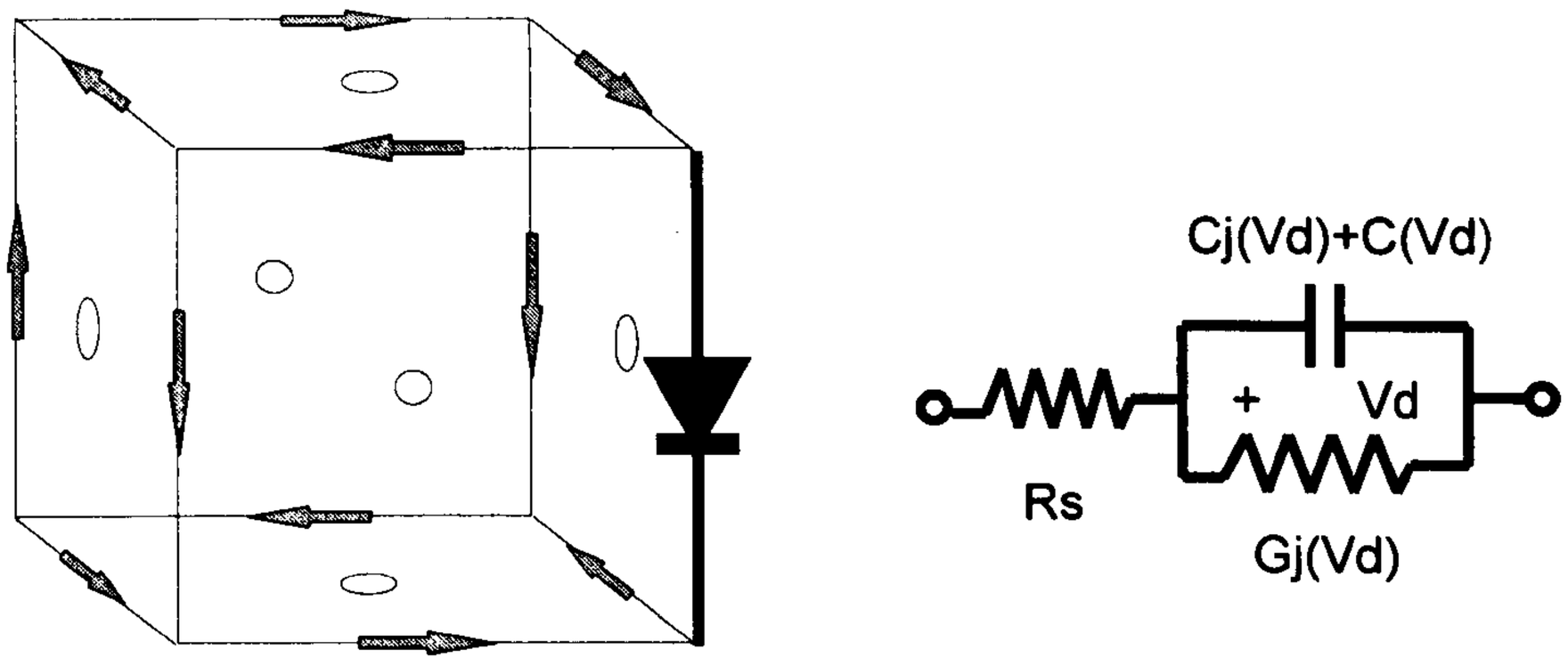

Fig. 2.12. Simple lumped element circuit model for the Schottky diode and its connection to the FDTD grid.

As stated before each circuit element depicted in figure 2.12 can be associated to a physical effect. The series resistance Rs is caused by the resistance of the silicon in intrinsic state connecting the junction to the output terminal. The non-linear capacitance can be considered the sum of two contributions: the junction capacitance due to the space-charge zone being free of holes in reverse mode and the diffusion capacitance due to the distribution of electrons into the semiconductor in forward mode.

$$C_J(V_d) = C_J(0)\left(1 - \frac{V_d}{\Phi_0}\right)^{-m} \qquad V_d < \Phi_o$$

$$C_J(V_d) = \frac{C_J(0)}{cte1}\left(cte2 + \frac{m \cdot V_d}{\Phi_0}\right) \qquad V_d \geq \Phi_o$$

$$C_D(V_d) = \frac{q}{\eta \cdot k \cdot T}\tau_D I_0 e^{q/\eta \cdot k \cdot T) \cdot V_d} \qquad \text{(Eq.2.24)}$$

Cj is the junction capacitance related to the voltage at diode terminals V_d. $C_j(0)$ is the zero bias capacitance and m, cte1,cte2 are suitable constants taking into account the geometry and semiconductor features of the diode. C_d is the diffusion capacitance highly related to the recombination time τ_D of electrons into the semiconductor. $G(V_d)$ is the classical expression for

the conductance of a diode but introducing the parameterη known as the junction emission coefficient to model a real device.

$$G_j(V_d) = I_0 \cdot \left(e^{(q/\eta \cdot k \cdot T)\cdot V_d} - 1\right) \qquad \text{(Eq.2.25)}$$

The currents on the diode can be related to the EM fields in the FDTD cell. The voltage at the diode terminals is estimated from the time average of the electrical field at the cell. In this way, the currents in the device can be solved numerically using the voltage-intensity relation of the device.

$$I_d = G_j(V_d)\cdot V_d + (C_J(V_d) + C_D(V_d))\frac{dV_d}{dt}$$

$$V_d = \frac{E_x\big|_{i+1/2,j,k}^{n+1} + E_x\big|_{i+1/2,j,k}^{n}}{2}\cdot \Delta x - I_d R_s + O(h^2)$$

$$I_d = J_x\big|_{i+1/2,j,k}^{n+1/2}\cdot \Delta y \Delta z + O(h^2)$$

$$\frac{dV_d}{dt} = \frac{E_x\big|_{i+1/2,j,k}^{n+1} - E_x\big|_{i+1/2,j,k}^{n}}{\Delta t}\cdot \Delta x + O(h^2) \qquad \text{(Eq.2.26)}$$

The density of current in the FDTD cell is calculated from I_d and introduced into the FDTD equations to update the electric field component. The algorithm is now implicit since I_d and $E_x\big|_{i+1/2,j,k}^{n+1}$ in Eq.2.26 are non-linear functions depending on themselves. The solution is obtained by iteration, using the currents and fields at the previous time instants as initial guess to estimate the current and field at the actual time. The result is used as initial guess to estimate the current and fields. The algorithm is stable for small values of Δt but no simple stability criterion is given, since for a non-linear system the stability depends also on the initial conditions. For instance, a diode operating deep into the forward region exhibit a low resistance, so in general Δt must be much smaller than the Courant stability condition for FDTD (Eq.2.8).

2.3.2.2 The Bipolar Transistor circuit element model.

Bipolar transistors can be described using an equivalent circuit involving two diodes and current sources (Fig.2.13). The transistor is a two-port device, so at least two FDTD cells are required to

implement the interface. The collector-base current is introduced in one FDTD cell and the base-emitter current in the other.

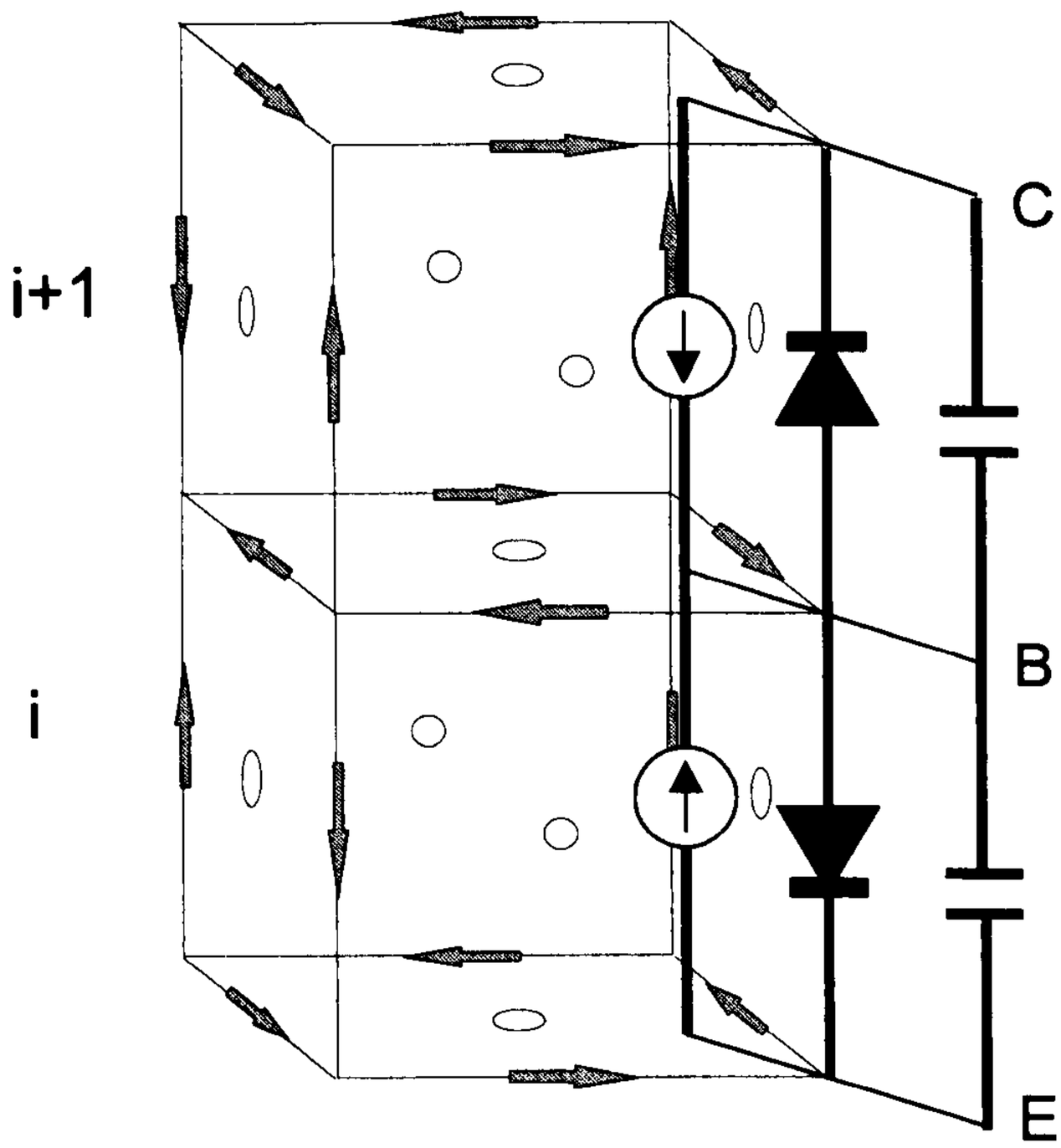

Fig.2.13 Equivalent circuit of a bipolar transistor connected to the FDTD grid. The device is inserted in two FDTD cells

The device equations (Eq.2.27) are consistent with the equivalent circuit using a ideal diode model [19]. As for the diode, The currents and voltages can be associated to the field at some nodes of the FDTD grid.

$$I_C = G_C(V_{BC}) \cdot V_{BC} - \alpha_f G_E(V_{BE}) \cdot V_{BE} + (C_{CJ}(V_{BC}) + C_{CD}(V_{BC})) \frac{dV_{BC}}{dt}$$

$$I_E = G_E(V_{BE}) \cdot V_{BE} - \alpha_r G_C(V_{BC}) \cdot V_{BC} + (C_{EJ}(V_{BE}) + C_{ED}(V_{BE})) \frac{dV_{BE}}{dt}$$

$$V_{BC} = \frac{E_x\big|_{i+1/2,j,k}^{n+1} + E_x\big|_{i+1/2,j,k}^{n}}{2} \cdot \Delta x - I_C R_{sC} + O(h^2)$$

$$I_C = J_x\big|_{i+1/2,j,k}^{n+1/2} \cdot \Delta y \Delta z + O(h^2)$$

$$\frac{dV_{BC}}{dt} = \frac{E_x\big|_{i+1/2,j,k}^{n+1} - E_x\big|_{i+1/2,j,k}^{n}}{\Delta t} \cdot \Delta x + O(h^2)$$

$$V_{BE} = \frac{E_x\big|_{i-1/2,j,k}^{n+1} + E_x\big|_{i-1/2,j,k}^{n}}{2} \cdot \Delta x - I_E R_{sE} + O(h^2)$$

$$I_E = J_x\big|_{i-1/2,j,k}^{n+1/2} \cdot \Delta y \Delta z + O(h^2)$$

$$\frac{dV_{BE}}{dt} = \frac{E_x\big|_{i-1/2,j,k}^{n+1} - E_x\big|_{i-1/2,j,k}^{n}}{\Delta t} \cdot \Delta x + O(h^2) \qquad \text{(Eq.2.27)}$$

The procedure for the time stepping of Eq.2.27 is the same as for the diode Eq.2.26. The algorithm is implicit, but now it forms a system to solve the currents and fields at the emitter and collector.

2.4 Conclusions for Chapter II

The Finite Difference Time Domain (FDTD) method has been presented as an effective numerical solver of the Maxwell's equation in time domain, extensively used to model radiation, scattering and guided wave problems. The requirements of the method are mainly determined by stability and numerical dispersion introduced by the technique. The stability limit is fixed by the Courant condition to determine the maximum stable time step. The numerical dispersion determines the maximum cell size but it is not fixed in an exact way. The condition for travelling waves is commonly accepted as $\lambda/10$ for 1% error in the phase velocity. For evanescent waves, typically at the vicinity of the scatter, the condition can be extended to $\lambda/20$ or $\lambda/40$ depending on the complex propagation constant of the wave. This condition seems to be consistent with the practical experience of FDTD modelling.

Finite differences have similar algebraic properties to derivatives. As a consequence, this thesis chapter shows how FDTD often satisfy similar relations and theorems than Maxwell's equations just exchanging the derivative operator for the central finite difference (this will be seen in detail in the next chapter). However, the topology of the FDTD space defined on the FDTD cell is essentially different of the topology of the continuous space-time since fields components are defined at different spatial and time locations. PEC, dielectric media and the principle of equivalence can be directly implemented in FDTD, but they are defined in a finite set of nodes. As a result, the interface between dielectric media is asymmetrical resulting in a degradation of the model, also, the principle of equivalence is not defined in a surface but in a set of boundary nodes.

FDTD provides all the necessary numerical devices for the modelling of planar structures including metallic and dielectric parts and circuit elements as voltage/current generators and passive loads. FDTD has a natural ability to obtain broadband data, and to handle complicated 3D structures. A FDTD code for the modelling of passive planar structures have been developed. The results of the code for several patch antenna configurations has been compared to measured data obtained from the literature.

FDTD is a time domain method that can be extended to handle non-linear media. This is the basis for the modelling of non-linear/active semiconductor devices inside a FDTD grid. Many devices

can be represented by lumped element circuits, and mathematically described as non-linear systems of time domain differential equations. These equations can be coupled to the FDTD method using the elementary cells as ports. The voltage at the device terminals is related to the electrical field in the FDTD cell and the current at the device determines the density of current in the cell. The combination in a single model of non-linear devices and planar passive structures allows the simulation of new quasi-optical devices like active arrays.

2.5 References for Chapter II.

[1] A.Taflove, "Computational Electrodynamics: The Finite Time Domain Method", Artech House 1995.

[2] K.S.Kunz, R.Luebbers, "Finite Difference Time Domain Method for Electromagnetics" CRC Press, 1993.

[3] K.S. Yee "Numerical Solution of Initial Boundary Value Problems involving Maxwell's Equation in Isotropic Media", IEEE APS vol. 14, pp 302, 1966.

[4] D.M.Sullivan, "Z transform Theory and the FDTD Method", IEEE APS, vol 44 pp 28-34 Jan. 1996.

[5] A.V. Oppenheim, "Discrete time signal processing", Chapter 4 'Z transform' pp. 149. Prentice Hall 1989.

[6] C.A. Balanis, "Advanced Engineering Electromagnetics", pp. 329 John Wiley&Sons, 1989.

[7] J.Stratton, "Electromagnetic Theory", McGraw Hill, NY 1940.

[8] B.Engquist, A.Majda, "Absorbing Boundary Conditions for the Numerical Simulation of Waves", Mathematics of computation, vol 31, pp.629-651, 1977.

[9] G. Mur, "Absorbing Boundary Conditions for the Finite-difference Approximation of Time Domain Electromagnetic Field Equations", IEEE Trans. Elec. Compatibility. Vol. 23, pp.377-382, 1981.

[10] R.L.Higdon, "Numerical Absorbing Boundary Conditions for the wave equation", Mathematics of computation, vol 47, pp.437-459, 1986.

[11] K.K.Mei, J.Fang, "Superabsorption a method to improve absorbing boundary conditions", IEEE APS vol 40, pp 1001-1010, 1992.

[12] J.P.Berenger, "A Perfectly Matched Layer for the Absorption of Electromagnetics Waves", J. Computational Physics, vol 114, pp.185-200, 1994.

[13] J.P.Berenger, "Perfectly Matched Layer for the FDTD solution of Wave-Structure Interaction Problems", IEEE APS, vol.127 pp 363-379, Jan.1996.

[14] D. S. Katz, E. T. Thiele and A. Taflove, 'Validation and extension to three dimensions of the Berenger PML absorbing boundary condition for FDTD meshes', *IEEE Microwave and Guided Wave Letters*,vol 4 Nov.1994, pp.268-270.

[15] A.Reneix, B.Jecko, "Analysis of Microstrip Patch Antennas Using Finite Difference Time Domain Method", IEEE APS vol 37, pp.1361-1369, Nov.1989.

[16] J.F Zurcher, F.Gardiol, "Broadband patch antennas", Artech House, 1995

[17] K.Williams, D.B.Davidson and H.C.Reader, "FDTD Modelling of an Aperture coupled Patch Antenna for use in an Active Array". Private communication to Prof. Parini.

[18] M.Mynskys, "Advanced Mathematics for Engineers", Section 7.6 "Non Linear Integral Equations", pp.592-594. MIR, Moscow,1985

[19] P.Ciampolini, P.Mezzanotte, L.Roselli, R.Sorrentino, "Accurate and Efficient Circuit Simulation with Lumped Element FDTD Technique", IEEE MTT Vol 44 pp. 2207-2217 December 1996.

CHAPTER III: DISCRETE GREEN'S FUNCTION FORMULATION OF THE FDTD METHOD

3.1 Introduction.

The FDTD method is a well-known technique to solve numerically the Maxwell equations in the time domain. As previously described, FDTD has widespread applications in microwave circuit design and antenna modelling mainly because of its ability to represent almost all kind of media and the simplicity by which it can model broadband 3D problems. The classical FDTD formulation (Yee's algorithm), is based on a finite difference approximation of the partial derivatives of Maxwell's equations [1]. The practical implementation of this algorithm requires the computation of free space nodes between scatterers and special termination conditions for the grid when an open radiation problem is investigated (Absorbing Boundary Conditions or ABC) [2].

The FDTD methods is usually demanding in terms of the memory requirements if compared to frequency domain method for electromagnetic modelling. The reasons for the extra storage using FDTD are basically the low order accuracy of the method ($O(h^2)$) and the recursive form of the algorithm. The method's accuracy is given by the linear approximation implicit in the finitte difference aproximation. As a consequence, the cell size required to obtain good results is far away from the real Nyquist sampling rate for the fields. The recursive nature of the classic Yee's algorithm for FDTD implies that all the cells contained in a given volume (including those in the free space without sources) must be computed and the volume must be terminated with an ABC.

As a result of this large memory requirement, the application of FDTD has been limited to the analysis of electrically small regions (usually several wavelengths maximum). The modelling of large or even medium size antennas and scatterers (finite arrays, reflectors, large wire antennas) is impossible for the resources of most computers despite the outstanding improvement of RAM in modern computers.

Much effort has been devoted to improve these features of FDTD. The algorithm's accuracy has been improved largely using wavelet expansions in the so-called multiresolution schemes [3]. Multiresolution techniques still require the computation of free space nodes and the

implementation of ABC specially designed for these algorithms. Other researchers have implemented time domain boundary conditions in order to model several scatter regions avoiding the modelling of the free space volume in between them (Multi-Region FDTD [4]). This technique is very promising for solving problems involving several distant scatters in the time domain, but it does not avoid the modelling of free space nodes in each region and the implementation of ABC.

A different approach to avoid these problems is possible on the grounds that the Yee algorithm is not the only possible formulation of the FDTD method. The classical theory of discrete systems shows that linear and time invariant systems, such as FDTD, can be represented by means of a convolution of the input sequence with the response of the system to an impulse. This is the discrete version of the Green's function technique extensively used in electromagnetics. This formulation does not require ABC or computation of free space nodes, but the analytical formula of the impulse response or discrete Green's function of the FDTD system must be known for a practical implementation of the algorithm

This chapter presents the convolution formulation of FDTD as an alternative algorithm to solve time domain electromagnetic problems. This new algorithm for FDTD produces identical results to the classical Yee algorithm for FDTD, so, they can be combined without interface problems or numerical reflections. The analytical form of the Discrete Green's function for FDTD has been obtained and is presented here as a polynomial function of the spatial and time steps.

Finally, the convolution formulation of FDTD and the Discrete Green Function's formula are demonstrated by solving some canonical problems. The first problem presented is the impedance calculation of a dipole antenna in the presence of a parasitic element without using ABC or computing free space cells, leading to major saving of memory storage. The second problem is the implementation of the exact ABC for FDTD in a wall to produce a virtually reflectionless grid boundary.

3.2 Finite Difference Electromagnetics and the Convolution Formulation of the FDTD method.

3.2.1.Finite Difference Electromagnetics.

Numerical methods in electromagnetics are based on discrete approximation of the field equations. Discrete formulations usually follow a similar development to the continuous equations, so in general, it is possible to redefine physical laws and concepts from the continuous physical world to equivalent discrete laws and entities. Usually the discrete method can be seen as a discrete network of impedance loads and a finite number of ports and nodes operating in continuous world, but it can be also seen as a discrete world with a set of discrete physical laws. This is true for the numerical methods based on finite differences (like FDTD) because finite differences have similar algebraic properties to the partial derivatives [2].

In this section, the formal analogy between the continuous Maxwell's equations, and the discrete set of FDTD equations is exploited to obtain alternative formulations and new aspects of the FDTD method. The first step is the representation of the FDTD system in the spectral domain using the Z transform. Secondly, the second order discrete equations are determined, and the link with the scalar wave equation is established in a similar way to that for continuous electromagnetics. Finally, The FDTD equations are formulated as discrete convolutions with the impulse response or Discrete Green's functions of the FDTD method.

3.2.2. Z transform representation of the FDTD system.

The Z transform is a powerful tool, extensively used to analyse the behaviour of discrete filters and systems (see chapter 4 of [5]). Their properties with respect to discrete systems are similar to the Laplace transform for continuous functions. Using the Z transform the finite difference equations can be reduced to algebraic polynomial expressions, as the Laplace transform does for differential equations.

The definition of the Z transform of a sequence is similar to the expansion as a power series of a function of the complex variable z (Eq.3.1a). The Z transform of a shifted sequence is just the

transform of the non-shifted sequence multiplied by z to the power of the shifted index (Eq.3.1b). This is a remarkable property of great benefit to handle finite difference equation since the transform of finite difference of the sequence can be easily obtained from the original Z transform (Eq.3.1c)

$$X(z) = \sum_{-\infty}^{\infty} x[n] z^{-n}$$

(Eq.3.1a)

$$x[n-m] \rightarrow z^{-m} X(z)$$

(Eq.3.1b)

$$x[n] - x[n-1] \rightarrow (1 - z^{-1}) X(z)$$

(Eq.3.1c)

The FDTD equations can be represented in Z transform terms [6]. In this case there are 4 independent indexes (n,i,j,k), so a Z transform for each of them is required. This means that there are 4 complex variables in the transformed space $(n,i,j,k) \rightarrow (\Omega, X, Y, Z)$. In Eq.3.2 is shown the transform of one of the FDTD equations for the electrical field. The term ½ in the indexes of the magnetic field has been omitted, since from now the treatment will be strictly discrete and the index can take integer values only.

$$E_x^{n+1}(i,j,k) = E_x^n(i,j,k) + \frac{\Delta t}{\varepsilon}\left(\frac{H_z^n(i,j+1,k) - H_z^n(i,j,k)}{\Delta y} - \frac{H_y^n(i,j,k+1) - H_y^n(i,j,k)}{\Delta z} - J_x \right)$$

⇓

Z transform

⇓

$$\varepsilon \frac{\Omega - 1}{\Delta t} E_x(\Omega, X, Y, Z) = \frac{Y - 1}{\Delta y} H_z(\Omega, X, Y, Z) - \frac{Z - 1}{\Delta z} H_y(\Omega, X, Y, Z) - J_x(\Omega, X, Y, Z)$$

(Eq.3.2)

The finite difference operators for each index can be defined in terms of the Z transform as functions of the complex variables Ω, X, Y, Z (Eq.3.3). This can be used to simplify the notation for the rest of the formulas.

$$D_n = \frac{\Omega - 1}{\Delta t} \qquad D_i = \frac{X - 1}{\Delta x}$$

$$D_j = \frac{Y - 1}{\Delta y} \qquad D_k = \frac{Z - 1}{\Delta z}$$

(Eq.3.3)

Using the definition of the finite difference operators in the Z domain the FDTD equations can be written in the transform Z domain in a compact way, by means of vectors and matrices.

$$\vec{\mathrm{H}}(\Omega, X, Y, Z) = \frac{\Omega \cdot D_n^{-1}}{\mu}\left(A_h \cdot \vec{\mathrm{E}}(\Omega, X, Y, Z) - \vec{M}(\Omega, X, Y, Z)\right) \qquad \vec{\mathrm{E}}(\Omega, X, Y, Z) = \frac{D_n^{-1}}{\varepsilon}\left(A_e \cdot \vec{\mathrm{H}}(\Omega, X, Y, Z) - \vec{J}(\Omega, X, Y, Z)\right)$$

$$A_h = \begin{pmatrix} 0 & Z^{-1}D_k & -Y^{-1}D_j \\ -Z^{-1}D_k & 0 & X^{-1}D_i \\ Y^{-1}D_j & -X^{-1}D_i & 0 \end{pmatrix} \qquad A_e = \begin{pmatrix} 0 & -D_k & D_j \\ D_k & 0 & -D_i \\ -D_j & D_i & 0 \end{pmatrix}$$

(Eq.3.4)

3.2.3. Finite difference second order equations

3.2.3.1.Finite difference vector wave equation

The finite difference equations of the FDTD method depend simultaneously on the magnetic and electric fields and contain only first order finite differences. With analogy to the continuous Maxwell's equations, it is possible to obtain second order equations (wave equations) on the electrical or magnetic field separately. The vector wave equations can be obtained by substitution of the electric field equations into the magnetic field equation and vice-versa [7].

The Z transform representation of the FDTD equations is quite appropriate to obtain the finite difference vector wave equation in a direct way. In order to obtain the expression of the finite difference vector equation for the electric field, the Z transform of the magnetic field (Eq.3.4) is substituted into the expression for the electric field, yielding equation.3.5.

$$\left(\frac{\Omega^{-1}D_n^2}{c^2}\cdot\bar{I}-A_e\cdot A_h\right)\cdot\vec{\mathrm{E}}=\Omega^{-1}D_n\mu\cdot\vec{J}+A_e\cdot\vec{M}$$

$$A_e\cdot A_h=\begin{pmatrix}(Y^{-1}D_j^2+Z^{-1}D_k^2) & -Y^{-1}D_iD_j & -Z^{-1}D_iD_k\\ -X^{-1}D_iD_j & (X^{-1}D_i^2+Z^{-1}D_k^2) & -Z^{-1}D_jD_k\\ -X^{-1}D_iD_k & -Y^{-1}D_jD_k & (X^{-1}D_i^2+Y^{-1}D_j^2)\end{pmatrix}$$

(Finite difference vector wave equation) (Eq.3.5a)

$$\nabla\times\nabla\times\vec{E}+\frac{1}{c^2}\frac{\partial^2\vec{E}}{\partial t^2}=\mu\frac{\partial\vec{j}}{\partial t}$$

(Continuous wave vector equation) (Eq.3.5b)

This expression for the discrete vector wave equation (Eq.3.5a) is given in the Z domain but it can be easily translated to the real domain just by taking *D*-terms as finite difference operators. It can be compared to the continuous equation for the vector wave equation (Eq.3.5b). As it can be seen, the discrete and continuous equations are similar if the finite difference operator is replaced by partial derivatives. The solutions to the discrete vector wave equation are fully compatible with the FDTD system since they are deduced from it without any additional consideration.

3.2.3.2 The finite difference scalar wave equation.

The continuous scalar wave equation (Eq.3.6b) has been used to describe physical wave phenomena such as sound waves, waves in fluids or heat propagation. This equation has also a discrete version in terms of second order finite differences (Eq.3.6a). Under some conditions related to the divergence of the fields, the scalar and wave equations can be shown to be equivalent. The Maxwell's divergence equations and the continuity condition of currents link the vector and the scalar equation [7].

$$\left(\Omega^{-1}\frac{D_n^2}{c^2}-(X^{-1}D_i^2+Y^{-1}D_j^2+Z^{-1}D_k^2)\right)\Phi=0$$

Where $\Omega^{-1}\cdot D_n^2=\Omega^{-1}\frac{(\Omega-1)^2}{\Delta t^2}=\frac{\Omega^{-1}-2+\Omega}{\Delta t^2}\xrightarrow{Z^{-1}}\frac{\Phi^{n+1}-2\Phi^n+\Phi^{n-1}}{\Delta t^2}$

(Finite Difference Scalar Wave Equation in Z domain) (Eq.3.6a)

$$\frac{1}{c^2}\frac{\partial^2\phi}{\partial t^2}-\nabla^2\phi=0$$

(Continuous Scalar Wave Equation) (Eq.3.6b)

3.2.3.3 Relationship between vector and scalar wave equations. Dispersion formula.

In order to obtain the relationship between the discrete vector and scalar equation it is also necessary to use the "divergence" equations. These equations are not included within the FDTD method in an explicit way. However, The FDTD equations are "divergence-free" for the elementary FDTD cell in the absence of sources, as demonstrated in the literature [1]. This is essential in order to produce real solutions in source-free regions, which must be divergence free.

The divergence terms provide an additional relationship between the electric field and the currents. This is possible in the continuous case by using Maxwell's divergence equation for the displacement vector and the continuity law for the currents (Eq.3.7b). The equivalent finite difference equation in the Z domain for the divergence equation is defined in Eq.3.7.

$$\varepsilon(X^{-1}\cdot D_i\cdot \mathrm{E}_x+Y^{-1}\cdot D_j\cdot \mathrm{E}_y+Z^{-1}\cdot D_k\cdot \mathrm{E}_z)=-D_n^{-1}(X^{-1}\cdot D_i\cdot J_x+Y^{-1}\cdot D_j\cdot J_y+Z^{-1}\cdot D_k\cdot J_z)$$

(Eq.3.7a)

$$\varepsilon\frac{\partial(\nabla\cdot\vec{E})}{\partial t}=-\nabla\cdot\vec{j}$$

(Eq.3.7b)

The divergence term (Eq.3.7a) can be introduced into the finite difference vector wave equation (Eq.3.5a). The divergence term is used to simplify the non-diagonal parts of the matrix $A_e \cdot A_h$ so it becomes a diagonal matrix. The result is the non homogeneous scalar wave equation on every component of the electric field.

$$\left(\Omega^{-1}\frac{D_n^2}{c^2}-(X^{-1}D_i^2+Y^{-1}D_j^2+Z^{-1}D_k^2)\right)\cdot\vec{\mathrm{E}}=\frac{Z_0}{c}D_n\left(\bar{I}+c^{-2}D_n^{-2}\vec{D}\vec{D}'\cdot\right)\vec{J}+A_e\cdot\vec{M}$$

$$\vec{D}=D_i\hat{x}+D_j\hat{y}+D_k\hat{z}$$

$$\vec{D}'=X^{-1}D_i\hat{x}+Y^{-1}D_j\hat{y}+Z^{-1}D_k\hat{z}$$

(Eq.3.8)

The solution to the equation 3.8 should be exactly the same as the solution of the FDTD system for the electric field. If the excitation currents are zero, the equation 3.8 becomes the homogeneous scalar equation. In that case, a solution is possible only for the values of the complex parameters in the Z domain that cancel the scalar wave operator (Eq.3.9).

$$\Omega^{-1}\frac{D_n^2}{c^2}-(X^{-1}D_i^2+Y^{-1}D_j^2+Z^{-1}D_k^2)=0$$

(Eq.3.9)

This is the dispersion formula for the discrete system. This expression is similar to the formula $k^2-(k_x^2+k_y^2+k_z^2)=0$ in the continuous case. Eq.3.9 shows the relationship for the complete complex plane. In the particular case of the unit circle of the complex plane the formula becomes the normal formula of dispersion (Eq.3.10) as shown in the literature [2].

$$\frac{2}{c^2\Delta t^2}\sin^2\left(\frac{\omega\Delta t}{2}\right)=\frac{2}{\Delta x^2}\sin^2\left(\frac{k_x\Delta x}{2}\right)+\frac{2}{\Delta y^2}\sin^2\left(\frac{k_y\Delta y}{2}\right)+\frac{2}{\Delta z^2}\sin^2\left(\frac{k_z\Delta z}{2}\right)$$

$$\Omega=e^{j\omega\Delta t}\quad X=e^{jk_x\Delta x}\quad Y=e^{jk_y\Delta y}\quad Z=e^{jk_z\Delta z}$$

Dispersion Formula (Eq.3.10)

3.2.4. FDTD as a convolution.

Classical Theory of linear systems shows that any linear invariant system can be completely determined by the response of the system to an impulse (see Chapter 5 of [5]). The FDTD equations can be seen as a linear system whose 'inputs' are the sources J and M and where the 'outputs' are the E and H fields at n, i, j, k (Fig. 3.1). The impulse response of the FDTD equation is defined as a set of 2x2 matrix which represent the E and H discrete fields that are obtained when the field sources J and M are Kronecker delta impulse functions with arbitrary unit vectors $\hat{j}$ and $\hat{m}$ (Eq. 3.11).

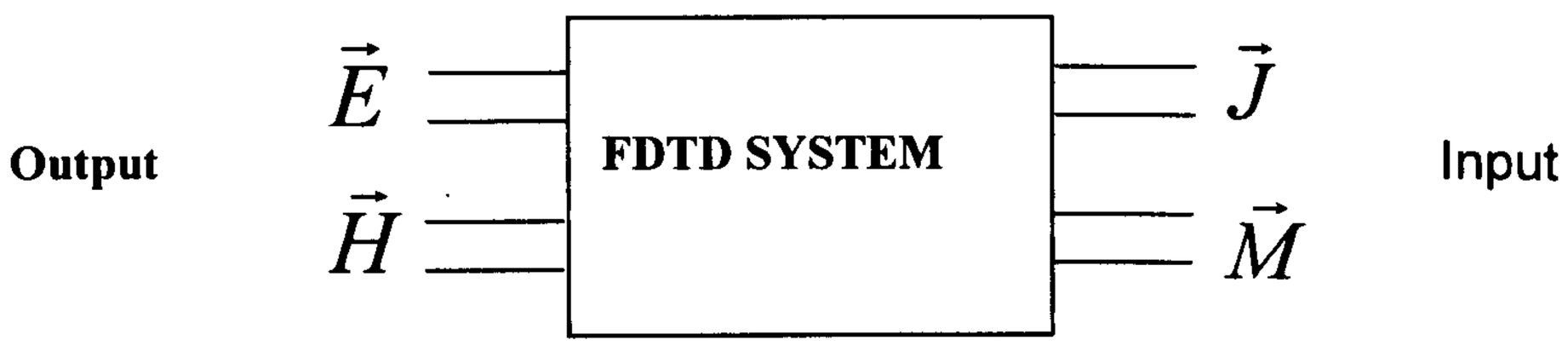

Fig. 3.1. FDTD as a linear system

$$\text{Impulse excitation} \quad \begin{matrix} \vec{J} = \delta^{n}_{ijk}\,\hat{j} \\ \vec{M} = \delta^{n}_{ijk}\,\hat{m} \end{matrix}$$

$$\Rightarrow$$

$$\text{Impulse response} \quad \begin{pmatrix} \vec{E}_{imp} \\ \vec{H}_{imp} \end{pmatrix} = \begin{pmatrix} [G_{ej}]^{n}_{ijk} & [G_{em}]^{n}_{ijk} \\ [G_{hj}]^{n}_{ijk} & [G_{hm}]^{n}_{ijk} \end{pmatrix} \cdot \begin{pmatrix} \hat{j} \\ \hat{m} \end{pmatrix} \qquad \text{(Eq.3.11)}$$

The sources J and M can be expressed in terms of convolution sum with a delta Kronecker function (Eq.3.12). This classical property, which is intrinsic of any discrete sequence, is essential to the actual theory.

$$\vec{J}_{ijk}^{\,n} = \sum_{n'i'j'k'} \delta_{i-i'j-j'k-k'}^{n-n'} \vec{J}_{i'j'k'}^{\,n'}$$
$$\vec{M}_{ijk}^{\,n} = \sum_{n'i'j'k'} \delta_{i-i'j-j'k-k'}^{n-n'} \vec{M}_{i'j'k'}^{\,n'}$$

(Eq.3.12)

The Eq.3.12 and the impulse response of Eq.3.11 can be combined to obtain the field response of the FDTD to an arbitrary excitation. This is possible since FDTD is linear and the response can be considered the superposition of the impulse responses of Eq.3.11.

$$\begin{pmatrix} \vec{E}_{ijk}^{\,n} \\ \vec{H}_{ijk}^{\,n} \end{pmatrix} = \sum_{n'i'j'k'} \begin{pmatrix} [G_{ej}]_{i-i'\,j-j'\,k-k'}^{n-n'} & [G_{em}]_{i-i'\,j-j'\,k-k'}^{n-n'} \\ [G_{hj}]_{i-i'\,j-j'\,k-k'}^{n-n'} & [G_{hm}]_{i-i'\,j-j'\,k-k'}^{n-n'} \end{pmatrix} \cdot \begin{pmatrix} \vec{J}_{i'j'k'}^{\,n'} \\ \vec{M}_{i'j'k'}^{\,n'} \end{pmatrix}$$

(Convolution form of the FDTD method) (Eq.3.13)

The Equation 3.13 is the formulation of the FDTD method as a convolution sum of the sources with the impulse response which assume a matrix form. The impulse response matrix corresponds to the dyadic Green's function concept in continuous electromagnetics and it will be referred to as Discrete Green's Function (DGF) for the FDTD method.

3.3 Discrete Time Domain Green's Function of the FDTD Equations

The FDTD method has been reformulated in terms of a convolution sum of the sources J and M and the impulse response or discrete Green's function of the FDTD system of equations. The analytical form of Discrete Green's Function (DGF) can be obtained as the solution of FDTD to impulse (delta Kronecker) excitations. Numerically, it can be obtained from the Yee algorithm, but this solution has to be calculated and stored for all the indices n, i, j, k in a certain region. The knowledge of the analytical formula of the discrete Green's function will overcome this problem since such a formula allows the calculation of the impulse response at a certain single index position. This is very significant, as it would permit the analytical determination of the exact FDTD response across a homogeneous region without the need to calculate the fields at all intermediate nodes. This analytical formula will depend on the spatial and time steps $\Delta t, \Delta x, \Delta y, \Delta z$ and it will reveal the true dependence of the FDTD method with respect to the step size.

The procedure to find the analytical form of the discrete Green's function, is largely based on the spectral representation of the FDTD system and the second order equations formulated in the previous section. As shown, the electric field solution of the FDTD system also satisfies the scalar wave equation, in that way, the problem of finding the impulse response of the whole FDTD system can be related to the much simpler problem of finding the impulse response to the scalar equation.

3.3.1.The spectral representation of discrete Green's function for the FDTD equations.

3.3.1.1 Impulse response to the scalar equation: Z domain representation

The excitation for the Impulse response analysis can be considered a shifted Kronecker delta in four indexes. Using basic Z transform relations the excitation can be represented in the Z domain in a simple way (Eq.3.14).

$$\delta^{n-n'}_{i-i'j-j'k-k'} = \delta(n-n')\delta(i-i')\delta(j-j')\delta(k-k') \xrightarrow{Z} \Omega^{-n'} X^{-i'} Y^{-j'} Z^{-k'} \tag{Eq.3.14}$$

From the Z domain formula for the scalar equation (Eq.3.8) and Eq.3.14 the Z domain form of the impulse response for the scalar equation can be obtained (Eq.3.15). This formula is just

the ratio between the impulse response in the Z domain and the 'transfer function' of the scalar wave equation.

$$\Gamma = \frac{\Omega^{-n'} X^{-i'} Y^{-j'} Z^{-k'}}{\Omega^{-1} \frac{D_n^2}{c^2} - (X^{-1} D_i^2 + Y^{-1} D_j^2 + Z^{-1} D_k^2)}$$

(Eq.3.15)

The impulse response of the scalar function in the real domain can be obtained by means of the inverse Z transform in the complex domain. This produces the complex plane integral representation of the impulse response of the scalar equation.

$$g_{i-i',j-j',k-k'}^{n-n'} = \frac{1}{(2\pi j)^4} \oint\oint\oint\oint \Gamma \Omega^{n} X^{i} Y^{j} Z^{k} d\Omega \, dX \, dY \, dZ$$

(Eq.3.16)

If the grid is stable (no poles inside the unit circle), the integration path for the inverse transform can be taken as the unit circle in the complex plane for all the Z variables. In this case, the integral is real and quite similar to the integral representation of the Green's function for the continuous case [7] (Eq.3.17).

$$g_{i-i',j-j',k-k'}^{n-n'} = \frac{1}{(2\pi)^4} \int_0^{2\pi/\Delta t} \int_0^{2\pi/\Delta x} \int_0^{2\pi/\Delta y} \int_0^{2\pi/\Delta z} \frac{e^{j(k_x(i-i')\Delta x + k_y(j-j')\Delta y + k_z(k-k')\Delta z + \omega(n-n')\Delta t)}}{s_t^2 - (s_x^2 + s_y^2 + s_z^2)} dk_x dk_y dk_z d\omega$$

$$s_t^2 = \frac{2}{c^2 \Delta t^2} \sin^2\left(\frac{\omega \Delta t}{2}\right) \qquad s_u^2 = \frac{2}{\Delta u^2} \sin^2\left(\frac{k_u \Delta u}{2}\right) \ldots u = x, y, z$$

(Eq.3.17)

3.3.1.2 Impulse response to the vector wave equation: Z domain representation

The vector wave equation can be reduced to the scalar wave equation for the electromagnetic field in the discrete and continuous case. This means that the electrical field must satisfy both the scalar and vector wave equations, simultaneously. However, the excitation term is different for vector and scalar equations. In the case of the vector wave equation, the excitation is directly the density of current as for the FDTD system. For the scalar wave

equation the excitation is an operator applied on the density of current (Eq.3.18). This is true for the continuous and discrete case.

$$\Theta_{scalar} \cdot \vec{E} = \Xi \cdot \vec{J} + \Lambda \cdot \vec{M}$$

$$\Xi \cdot = \frac{Z_0}{c} D_n \left(\bar{I} - c^{-2} D_n^{-2} \vec{D} \vec{D}' \cdot \right)$$

$$\Lambda = \begin{pmatrix} 0 & -D_k & D_j \\ D_k & 0 & -D_i \\ -D_j & D_i & 0 \end{pmatrix}$$

(Eq.3.18)

Using this relation the Green's function for the wave equation can be directly related to the Green's function of the scalar equation by applying the new operator to the current density. The impulse response to the discrete equation in the Z domain can also be determined from the scalar impulse response in the Z domain in a similar way (Eq.3.19).

$$\vec{\Gamma}''_{i,j,k} = (\Xi \cdot \hat{j} + \Lambda \cdot \hat{m}) \Gamma''_{i,j,k}$$

$\vec{\Gamma}''_{i,j,k}$ vector impulse response $\Gamma''_{i,j,k}$ scalar impulse response

$\vec{\delta} = \delta''_{i,j,k} \cdot \hat{j}$ electrical current excitation $\vec{\delta} = \delta''_{i,j,k} \cdot \hat{m}$ magnetic current excitation

(Eq.3.19)

3.3.2. Time Domain Impulse Response (Discrete Green's Function) for the FDTD method.

In continuous electromagnetics the Green's function of the scalar equation can be determined either by inverse transform of the spectral representation or by direct integration of the equation in differential form. The mathematical solution is extremely simplified in the continuous case by using the spherical symmetry of the problem. The Green's function problem can be reduced to a one-dimensional problem in spherical co-ordinates.

However, it is not possible to use the same spherical symmetry conditions in the discrete case. The continuous space-time is isotropic, but the discrete Cartesian grid is essentially

anisotropic [1]. As a consequence, the discrete grid does not support rotationally symmetric solutions and so for the discrete case a much more complicated 4 dimensional approach is required.

3.3.2.1 General solution of the homogeneous scalar wave equation

The discrete scalar wave equation can be solved by separately solving each co-ordinate contribution to the equation. In this method, the homogeneous (homogeneous here implies without excitation) equation is solved for a single index (usually the time index, here equal to n). The remaining operator terms, concerned with the other co-ordinates, are handled as constants (Eq.3.20). This technique is due to G. Boole who, in the 19th century, used it ([8] ,[9]) for solving finite difference equations. This method can be derived using the Z domain for all the spatial components, but operating in the real domain for the time index.

$$\Phi^{n+1} - 2\Phi^{n} + \Phi^{n-1} = K \cdot \Phi^{n}$$

$$\Phi = \Phi^{n}(X,Y,Z) \qquad K = c^2 \Delta t^2 (XD_i^2 + YD_j^2 + ZD_k^2)$$

(Eq.3.20)

The complex exponential sequence can be tested as solution to the equations 3.20, since they are eigenfunctions for any linear system. The parameter of the complex exponential is obtained from direct substitution into Eq.3.21.

$$\mathbf{\Phi^n} = C_1(X,Y,Z)e^{jn\omega\Delta t} + C_2(X,Y,Z)e^{-jn\omega\Delta t}$$

$$\Phi^{n+1} - 2\Phi^{n} + \Phi^{n-1} = K \cdot \Phi^{n} \;\Rightarrow\; \cos(\omega\Delta t)\cdot\mathbf{\Phi^n} = \left(1+\frac{K}{2}\right)\mathbf{\Phi^n}$$

$$\mathbf{\Phi^n} = C_1(X,Y,Z)e^{jn\arccos(\varphi)} + C_2(X,Y,Z)e^{-jn\arccos(\varphi)} \qquad \varphi = 1+\frac{K}{2}$$

(Eq.3.21)

The result can be obtained in terms of Tschebycheff polynomials, which is much more convenient for further manipulation (Eq.3.22). This is the general solution for the scalar wave equation.

$$\mathbf{\Phi^n} = B_1(X,Y,Z)\cdot T_n(\varphi) + B_2(X,Y,Z)\cdot\sqrt{1-\varphi^2}\,U_{n-1}(\varphi)$$

$$B_1 = C_1 + C_2$$
$$B_2 = j(C_1 - C_2)$$

$T_n(\varphi) = \cos(n\arccos(\varphi))$ (Tschebycheff polynomial first order)

$U_n(\varphi) = \dfrac{\sin((n+1)\arccos(\varphi))}{\sqrt{1-\varphi^2}}$ (Tschebycheff polynomial second order)

General solution for the scalar wave equation (Eq.3.22)

3.3.2.2 Green's function for the scalar wave equation

The constants C_1 and C_2 of the general solution for the homogeneous equation are determined by the initial conditions of the problem. In the case of a point source excitation (Kronecker delta), the field is zero for the time instant n=0, and it is 1 for the time instant n=1. (It should be noted that the excitation is 1 for n=0; the excitation happens just one step before the field). The impulse response can now be obtained, but it is still in Z domain for the spatial indexes (Eq.3.23).

$$\Gamma''(X,Y,Z) = U_{n-1}(\varphi) \qquad B_1 = 0 \qquad B_2 = \frac{1}{\sqrt{1-\varphi^2}}$$

(impulse response on index n) (point source excitation)

(Eq.3.23)

The discrete impulse response is in the real domain for the time index and in the Z domain for the spatial indexes. In order to obtain the explicit form of the impulse response for all the indexes in real domain, the Tschebycheff polynomial can be expanded as a power sum [10](Eq.3.23).

$$\Gamma^{n+1}(X,Y,Z) = U_n(\varphi) = \sum_{m=0}^{n/2}(-1)^m\binom{n-m}{m}(2\varphi)^{n-2m}$$

(Eq.3.24)

The inverse Z transform of Eq.3.24 for spatial indexes can be obtained from the inverse transform of all the terms $(2\varphi)^p$

For the 1D case, the problem is considered only for the spatial index i. The 1D solution can be used as starting point for the multidimensional case. For this case, the operator φ has now a simplified form.

$$2\varphi = 2 + K \qquad K = c^2 X D_i^2 \Delta t^2$$

(Eq.3.25)

The function φ can be reduced to a product of X terms expanding the second order polynomial using it two roots (Eq.3.26).

$$2\varphi = \alpha\left(X^{-1} - 2\beta + X\right) \longrightarrow 2\varphi = \alpha X(X^{-1} - R_1)(X^{-1} - R_2)$$

$$\alpha = \frac{c^2 \Delta t^2}{\Delta x^2} \quad \beta = \frac{\alpha - 1}{\alpha} \quad R_1 = \beta + \sqrt{\beta^2 - 1} \quad R_2 = \beta - \sqrt{\beta^2 - 1} \quad R_1 R_2 = 1$$

(Eq.3.26)

The inverse transform of the power terms can be obtained in a direct way by binomial expansion into simple powers of X. Finally, the multiplication of the power terms in Eq.3.24 is transformed into a convolution in the spatial domain (Eq.3.27).

$$(X^{-1} - R_1)^p \xrightarrow{Z^{-1}} \binom{p}{i} \cdot (-R_1)^{p+i}$$

$$(2\varphi)^p = \alpha^p X^p (X^{-1} - R_1)^p (X^{-1} - R_2)^p \xrightarrow{Z^{-1}} \alpha^p \sum_{l=0}^{p-i} \binom{p}{l} \binom{p}{i+l} (-R_2)^{p-l} (-R_1)^{l-i}$$

(Eq.3.27)

The result of the inverse transform is a polynomial that can be identified as orthogonal Jacobi polynomials $J_n^{(\alpha,\beta)}(x)$ on the unit circle [10], multiplied by an extra term (Eq.3.28).

$$(2\varphi)^p \xrightarrow{Z^{-1}} \alpha^p J_{p-i}^{(i,i)}(\xi) \cdot (R_2 - R_1)^{p-i} \qquad \xi = \frac{R_1 + R_2}{R_1 - R_2}$$

(Eq.3.28)

The impulse response of the one-dimensional scalar wave equation can be determined as a polynomial of the grid parameters given in Eq.3.26. This can by achieved by introducing Eq.3.28 into Eq.3.24.This leads to the following formula for the impulse response of the finite difference scalar wave equation in 1D:

$$g_i^{n+1} = \sum_{m=0}^{n/2} (-1)^m \binom{n-m}{m} \alpha^{n-2m} J_{n-i-2m}^{(i,i)}(\xi)(R_2 - R_1)^{n-i-2m}$$

$$\xi = \frac{R_1 + R_2}{R_1 - R_2} \qquad R_1 = \beta + \sqrt{\beta^2 - 1} \quad R_2 = \beta - \sqrt{\beta^2 - 1} \qquad \beta = \frac{\alpha - 1}{\alpha} \quad \alpha = \frac{c^2 \Delta t^2}{\Delta x^2}$$

(Eq.3.29)

The result of this formula can be compared to the impulse response obtained using the simple time stepping algorithm (Eq.3.30) on the scalar wave equation with a Kronecker's delta as excitation of the grid (Fig.3.2).

$$\phi_i^{n+1} = 2\phi_i^n - \phi_i^{n-1} + \frac{\Delta x^2}{c^2 \Delta t^2}(\phi_{i+1}^n - 2\phi_i^n + \phi_{i-1}^n)$$

Time stepping algorithm for the 1D finite difference scalar wave equation (Eq.3.30)

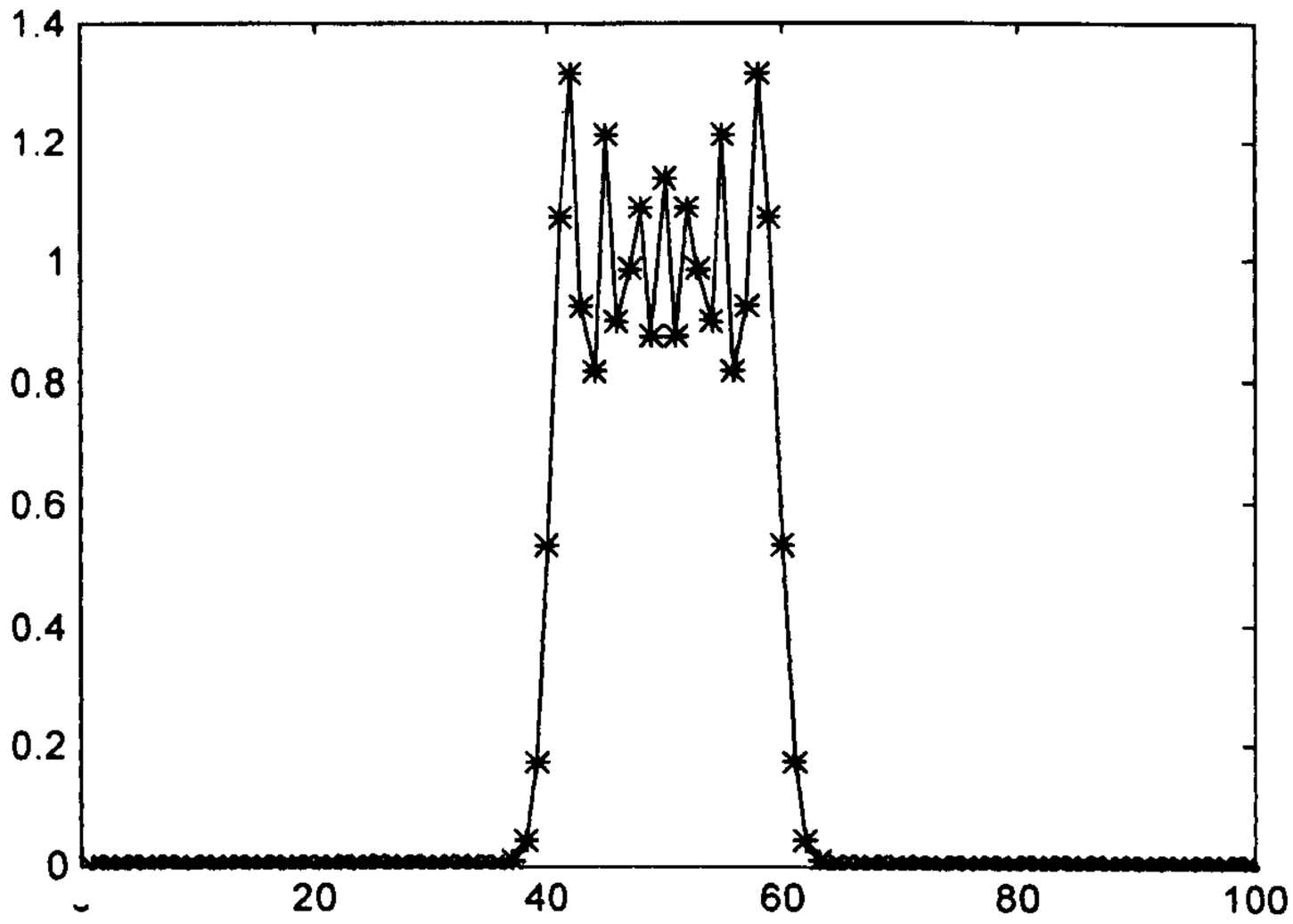

Fig.3.2 One-dimensional Green's function of the finite difference scalar wave equation for n=20 with Δx=1 and $c\Delta t$=0.707. The solid line is the result for the time stepping algorithm (Eq.3.30), the asterisks show the calculations with the Green's function formula of Eq.3.29.

Closer inspection of this result shows that the difference between the numerical and analytical calculation of the DGF lies in the sixth decimal place. This tiny difference is basically due to the finite precision of the floating point representation of real numbers in computers.

The multidimensional impulse response can also be expanded into the power series of Eq.3.24. The spatial dependence is more complicated as it is the sum of three contributions (one per spatial dimension). Eq.3.31 shows the 3D version of the φ operator.

$$2\varphi = 2 + c^2 \Delta t^2 (XD_i^2 + YD_j^2 + ZD_k^2) \qquad \text{(Eq.3.31)}$$

This term of spatial dependence can be related directly to the one-dimensional case in order to perform the inverse Z transform. This can be obtained by using the trinomial power expansion.

$$(2\varphi)^p = (2\varphi_x + 2\varphi_y + 2\varphi_z)^p = \sum (p; p_x, p_y, p_z) \cdot (2\varphi_x)^{p_x} (2\varphi_y)^{p_y} (2\varphi_z)^{p_z}$$

$$(p; p_x, p_y, p_z) = \frac{p!}{p_x!\, p_y!\, p_z!} \qquad p = p_x + p_y + p_z$$

(Eq.3.32)

Using the inverse transform of Eq.3.27 for the one-dimensional case, Eq.3.32 can be inverse transformed to the real domain as a sum of Jacobi polynomials.

$$(2\varphi)^p \xrightarrow{Z^{-1}} \sum (p; p_x, p_y, p_z) \cdot \prod_{\substack{l=i,j,k \\ s=x,y,z}} \alpha_s^{p_s} J_{p_s - l}^{(l,l)}(\xi_l)(R_{2s} - R_{1s})^{p_s} \qquad \text{(Eq.3.33)}$$

The impulse response in the 3D case for the scalar wave equation can be deduced by substitution of the inverse transform of Eq.3.33 into the general solution of Eq.3.24.Leading to the impulse response of the finite difference scalar wave equation 3D (Eq.3.34).

$$g_{i,j,k}^{n+1} = \sum_{m=0}^{n/2} (-1)^m \binom{n-m}{m} \sum (n-2m; p_x, p_y, p_z) \prod_{\substack{l=i,j,k \\ s=x,y,z}} \alpha_s{}^{p_s} J_{p_s-l}^{(l,l)}(\xi_s)(R_{2s} - R_{1s})^{p_s-l}$$

$$\xi_s = \frac{R_{1s} + R_{2s}}{R_{1s} - R_{2s}} \qquad R_{1s} = \beta_s + \sqrt{\beta_s{}^2 - 1} \quad R_{2s} = \beta_s - \sqrt{\beta_s{}^2 - 1}$$

$$\beta_s = \frac{\alpha_s - 1}{\alpha_s} \quad \alpha_s = \frac{c^2 \Delta t^2}{\Delta s^2} \frac{\Delta x^2 + \Delta y^2 + \Delta z^2}{\Delta s^2} \ldots . s = x, y, z$$

$$p_x + p_y + p_z = n - 2m$$

(Eq.3.34)

This expression of the impulse response for the 3D case can be compared to the calculation of the impulse response using a conventional time stepping algorithm. The results are presented for a 2D case in Fig.3.3.

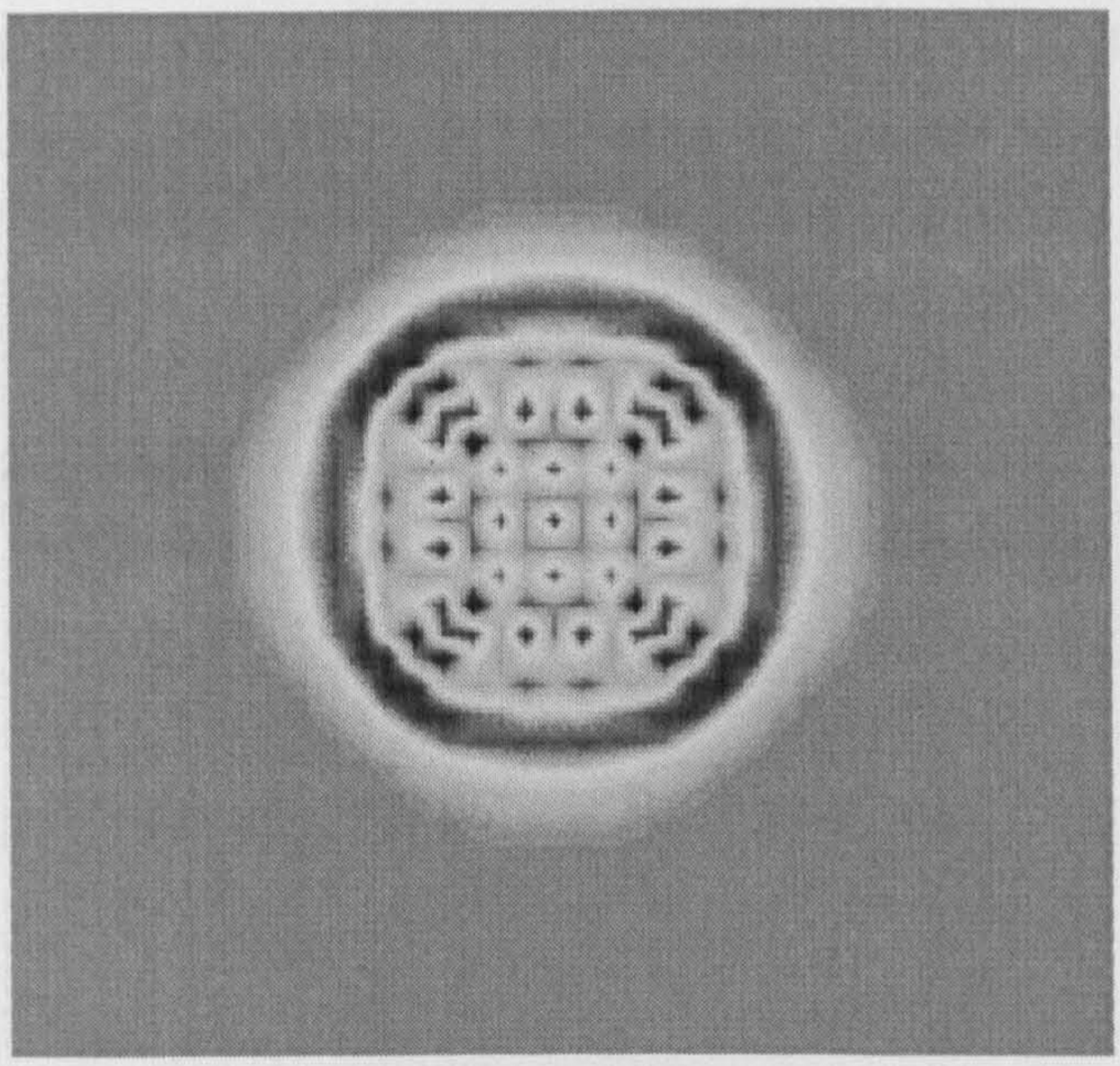

Fig.3.3 Two-dimensional impulse response of the finite difference scalar wave equation for n=20 with Δx=1, Δy=1 and $c\Delta t$=0.632.

The impulse response in the multidimensional case is not simply a discrete version of the Green's function for the continuous equation. The impulse response reflects the basic properties of the discrete grid such as dispersion and anisotropy that do not happen for the continuous co-ordinates. The impulse excitation contains all the frequencies allowed in the discrete grid. For some frequencies Δx is close to $\lambda/2$. In this case, the wave propagation in the numerical FDTD grid shows very strong dispersion.

3.3.2.3. Discrete Green's Function for the FD Vector Wave Equation (FDTD's Green's function)

As shown, the FDTD equations are strongly related to the so called FD scalar wave equation. The spectral representation of the discrete Green's function for the vector wave (FDTD equation) and the scalar wave equation are thus related by the operators Ξ and Λ described in Eq.3.18. These operators can also be used to establish the link between the time domain representations of the Green's function.

Using Eq. 3.18, and the definition of the scalar discrete Green's function Eq.3.34 the FDTD discrete Green's function is obtained (Eq.3.35). The notation used in Eq.3.35 is set according to the convolution formula for FDTD Eq.3.13 where the Green's function assumes matrix form.

$$[G_{ej}]^n_{ijk} = \frac{Z_0 D_n^{-1}}{c}\begin{bmatrix} D_n^2 - D_i^2 & -X^{-1}D_iD_j & -X^{-1}D_iD_k \\ -Y^{-1}D_iD_j & D_n^2 - D_j^2 & -Y^{-1}D_jD_k \\ -Z^{-1}D_iD_k & -Z^{-1}D_jD_k & D_n^2 - D_k^2 \end{bmatrix} g^n_{ijk}$$

$$[G_{em}]^n_{ijk} = \begin{bmatrix} 0 & -D_k & D_j \\ D_k & 0 & -D_i \\ -D_j & D_i & 0 \end{bmatrix} g^n_{ijk}$$

(Eq.3.35)

Where D_n represents finite difference operators and X, Y, Z displacement operators (Eqs.3.1b, 3.3 and 3.36). $g^n_{ijk}(\Delta x, \Delta y, \Delta z, \Delta t)$ is the DGF for the finite difference scalar equation (Eq. 3.34).

$$\Omega^{-1} g_{ijk}^{n} = g_{ijk}^{n-1} \quad X^{-1} g_{ijk}^{n} = g_{i-1jk}^{n} \quad Y^{-1} g_{ijk}^{n} = g_{ij-1k}^{n} \quad Z^{-1} g_{ijk}^{n} = g_{ijk-1}^{n}$$

$$D_n = \frac{\Omega - 1}{\Delta t} \quad D_i = \frac{X - 1}{\Delta x} \quad D_j = \frac{Y - 1}{\Delta y} \quad D_k = \frac{Z - 1}{\Delta z}$$

(Eq.3.36)

The analytical formula from Eq.3.35 can be compared to the numerical computation of the DGF for FDTD using the Yee algorithm. The excitations for the numerical computation are delta Kronecker impulses placed at $i=j=k=0$ and time step $n=1$. The direction and type (electric or magnetic current) of the excitation impulse determines the term of the DGF matrix that is being numerically obtained. Fig 3.4 shows some of the terms of the DGF for the electrical and magnetic currents. The differences between the formula and the numerical calculation (ideally zero) are very low (about -120dB) and are mainly due to the finite precision of floating point numbers in real computers.

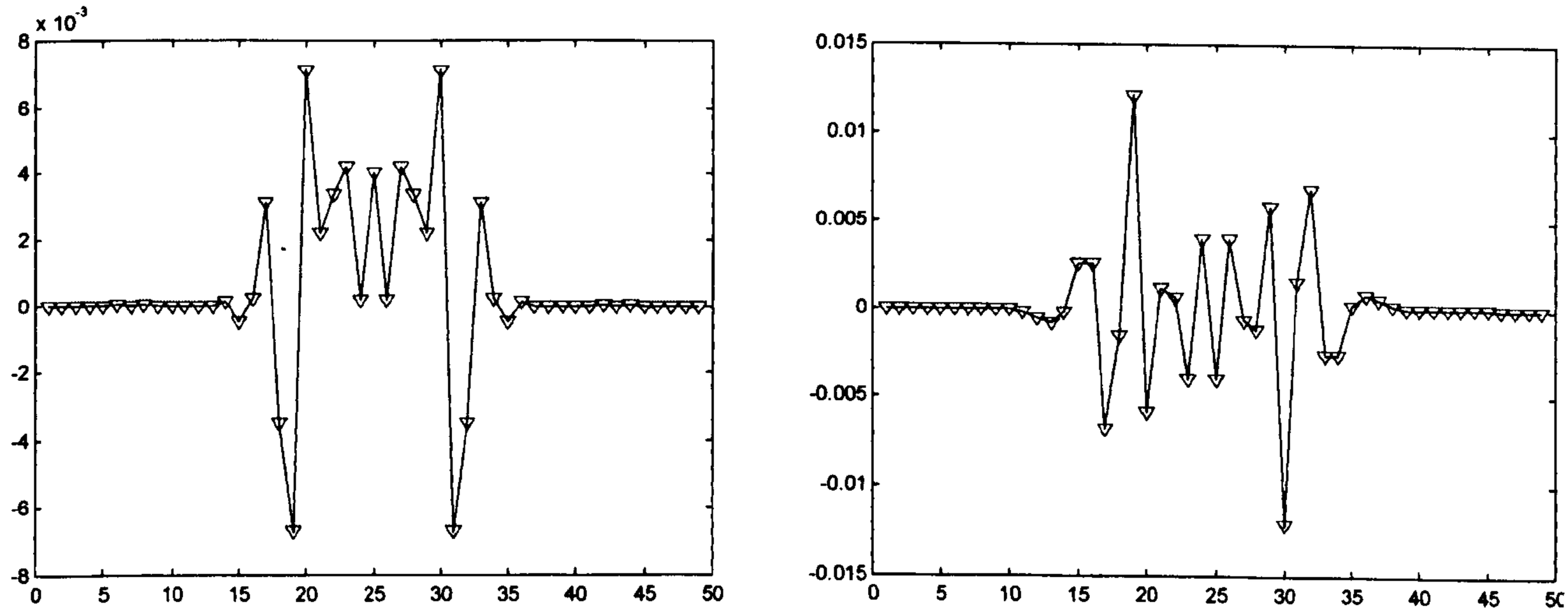

Fig.3.4. Magnetic current Discrete Green's Function (after 20 iterations) G_{em}^{zx} component (left) G_{em}^{yx} component (right) (solid line FDTD, triangles DGF formula) ax=ay=az=0.3.

3.4. Application of the Time Domain Green's Function for FDTD to Electromagnetic Modelling.

For many numerical EM techniques, the primary objective of an electromagnetic simulation is the calculation of the currents induced on a composite structure. These currents are generally produced by an incident field, which is generated by external sources not included within the model. The computed currents on the structure can be used to estimate the electromagnetic properties of the structure such as radiation pattern, RCS, impedance, scattering matrix, etc.

The convolution formula for FDTD of Eq.3.13 describes the electromagnetic fields at discrete locations as a function of the sources J and M. For electromagnetic modelling, this formula has to be inverted to determine the currents on the scatter from the incident field. The inversion result is presented in this section as the scattering equation. This equation resembles the EFIE and MFIE formulas for the continuous electromagnetic field [11]. The scattering equation can be used to solve time domain problems, producing similar results to FDTD but avoiding the need for ABC and the computation of fields at free space nodes.

Another application of the DGF method is to improve the Yee FDTD algorithm's modelling capabilities, rather than to solve the electromagnetic problem by itself. A classical problem of FDTD is the implementation of ABC. Using the equivalence principle for FDTD, the DGF method can provide an exact solution to the ABC problem, which is introduced in this section.

3.4.1 DGF-FDTD Modelling of Scattering Problems

3.4.1.1 Scattering formula for DGF-FDTD

The solution to scattering problems using the convolution form of FDTD is possible if the formula of Eq.3.13 can be inverted, so the currents on an object can be obtained as a function of the incident field. Initially, scattering problems with only electric and magnetic conductors will be considered (Fig.3.5), although the method can be extended to dielectric media in a straightforward manner.

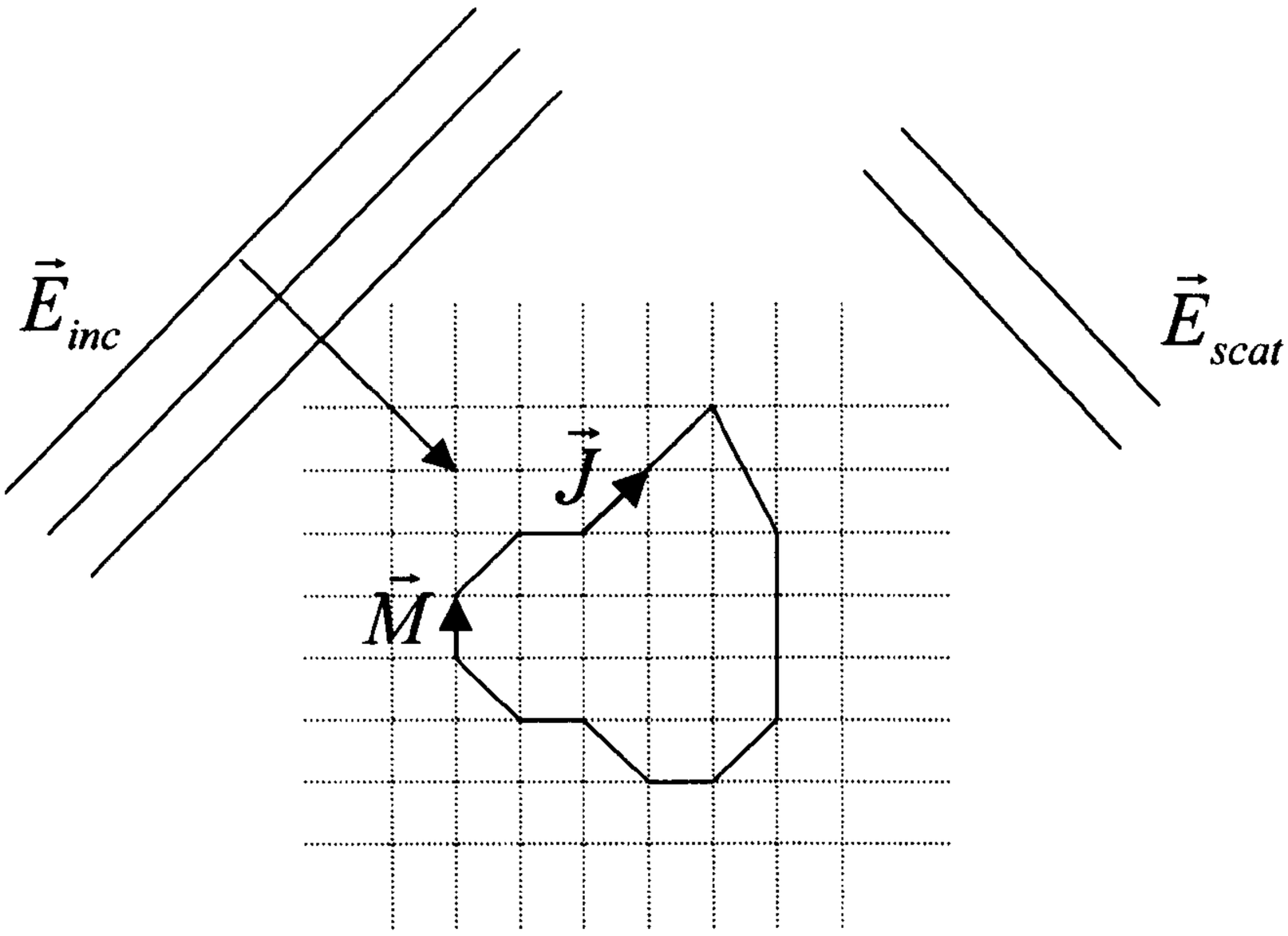

Fig. 3.5. Geometry of a scattering problem involving magnetic and electric conductors in a grid.

The boundary condition at the electric and magnetic conductors in the FDTD grid is enforced by setting to zero the either the total electric or the magnetic field at the nodes which are filled with the electric or magnetic conductors (Eq.3.37).

$$\vec{E}_t = \vec{E}_{inc} + \vec{E}_{scat} = 0 \quad i,j,k \in \text{Electric Conductor}$$

$$\vec{H}_t = \vec{H}_{inc} + \vec{H}_{scat} = 0 \quad i,j,k \in \text{Magnetic Conductor} \qquad \text{(Eq.3.37)}$$

The scattered fields can be determined from the currents induced on the structure using the DGF (Eq.3.13). Using the Eq.3.13 and the boundary condition of Eq.3.37, it is possible to link mathematically the incident field to the currents induced onto the scatter (Eq.3.38)

$$\begin{pmatrix} \vec{E}^{\,n}_{ijk} \\ \vec{H}^{\,n}_{ijk} \end{pmatrix}_{inc} + \sum_{n'i'j'k'} \begin{pmatrix} [G_{ej}]^{n-n'}_{i-i'\,j-j'\,k-k'} & [G_{em}]^{n-n'}_{i-i'\,j-j'\,k-k'} \\ [G_{hj}]^{n-n'}_{i-i'\,j-j'\,k-k'} & [G_{hm}]^{n-n'}_{i-i'\,j-j'\,k-k'} \end{pmatrix} \cdot \begin{pmatrix} \vec{J}^{\,n'}_{i'j'k'} \\ \vec{M}^{\,n'}_{i'j'k'} \end{pmatrix} = 0$$

$$i, j, k, i', j', k' \in Scatterer$$

(Eq.3.38)

In order to solve in a practical way the scattering equation it is possible to use the special properties of the DGF. The DGF for time index n equal to zero is a spatial delta Kronecker for the electrical current–electrical field and zero for magnetic current–electrical field and vice versa for the magnetic field. This property allows one to rewrite the Eq.3.38 as the scattering formula Eq.3.39

$$\begin{pmatrix} \vec{J}^{\,n}_{ijk} \\ \vec{M}^{\,n}_{ijk} \end{pmatrix} = \begin{pmatrix} \varepsilon \vec{E}^{\,n}_{ijk} \\ \mu \vec{H}^{\,n}_{ijk} \end{pmatrix}_{inc} + \sum_{n'}^{n-1} \sum_{i'j'k'} \begin{pmatrix} \varepsilon\,[G_{ej}]^{n-n'}_{i-i'\,j-j'\,k-k'} & \varepsilon\,[G_{em}]^{n-n'}_{i-i'\,j-j'\,k-k'} \\ \mu\,[G_{hj}]^{n-n'}_{i-i'\,j-j'\,k-k'} & \mu\,[G_{hm}]^{n-n'}_{i-i'\,j-j'\,k-k'} \end{pmatrix} \cdot \begin{pmatrix} \vec{J}^{\,n'}_{i'j'k'} \\ \vec{M}^{\,n'}_{i'j'k'} \end{pmatrix}$$

$$i, j, k, i', j', k' \in Scatterer$$

(Scattering algorithm)(Eq.3.39)

In the Equation 3.39, the currents on the scatterer are related to the incident field at the same time instant and to the currents at previous time steps. As a consequence, the induced currents can be solved for each time step from information previously calculated, starting from the index n=0 (before n=0, the incident field and the current are supposed to be zero).

3.4.1.2 Antenna Modelling Using DGF-FDTD algorithm

The Scattering formula Eq.3.39 can be used to model antenna devices since the currents on the antenna can be computed from the incident field. The metallic parts of the antenna will support the electrical induced currents of Eq.3.39. Slots on a ground plane can be considered as induced magnetic currents on Eq.3.39. The relative positions of the electrical and magnetic currents follow the same field distributions as those of the electrical and magnetic field in the Yee algorithm for FDTD (Fig.3.6). The modelling of the structures follows the same staircase pattern as do as the FDTD Yee's models, since the DGF technique is basically a different algorithm for the same FD numerical approximation of Maxwell's equations.

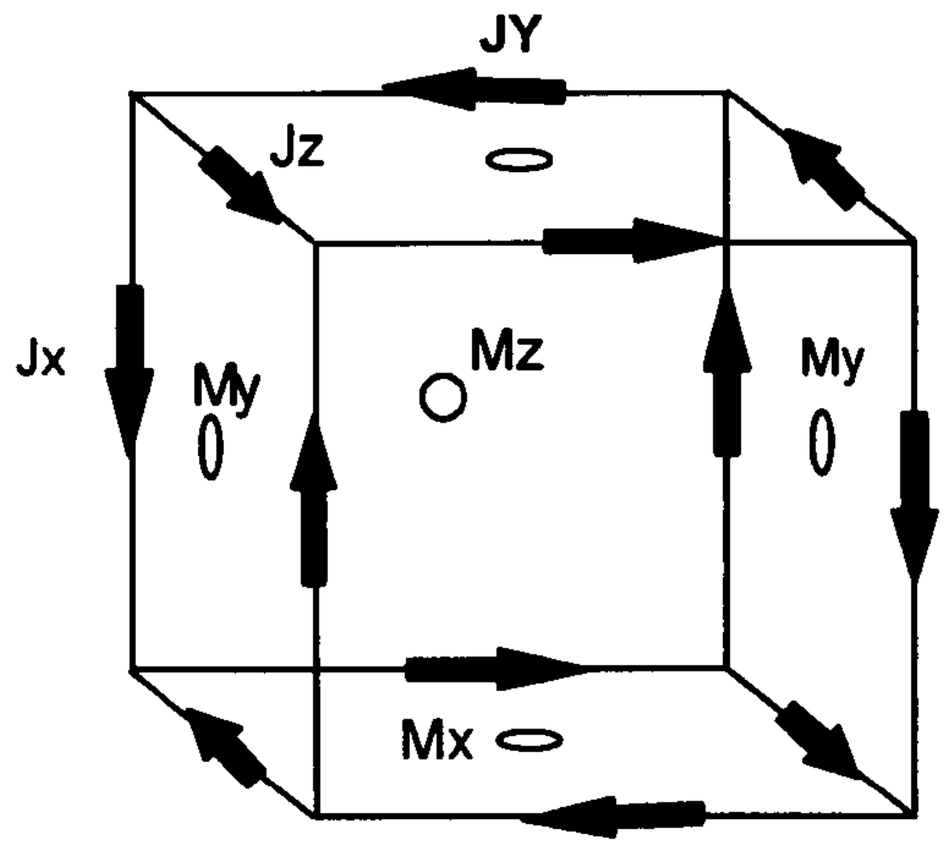

Fig.3.6. Electric and Magnetic currents spatial locations in FDTD.

The antenna ports can be seen as a set of i, j, k nodes where the incident field is applied. Each node is associated to a single antenna port. The currents $\vec{J}^{n}_{ijk}$, $\vec{M}^{n}_{ijk}$ at these nodes define the currents or the voltage at the port terminal. The electric or magnetic incident fields at the port nodes define also the voltage or the currents applied to the antenna port by an external generator. Impedance and scattering matrix parameters for each port can be obtained using basic circuit theory from the currents and voltages calculated for each port. The data computed are time domain, so broadband information can be obtained following standard FDTD procedures [12] (Eq.3.40).

$$Zant(\omega) = \frac{FFT\left(\frac{E_{x\ inc}^{n+1} + E_{x\ inc}^{n}}{2}\Delta x\right)}{FFT\left(J_x^{\,n}\Delta y\Delta z\right)} \qquad E_{x\ inc}^{n} = e^{-\left(\frac{n\Delta t - t_0}{\sigma_t}\right)^2}\delta_{i-i_g,j-j_g,k-k_g} \qquad \text{(Eq.3.40)}$$

Equation 3.13 requires the summation of all previous time instant contributions from n=0, resulting in a very high number of computations and large memory requirements. However in practice, it is not necessary to perform the whole summation, as the DGF is zero for $n < \max(i, j, k)$ (the excitation has not yet arrived). For signals $\frac{\lambda_{min}}{10} > \max(\Delta x, \Delta y, \Delta z)$, the DGF can be truncated since the 'tail' of the function is only contributed by dispersive

frequencies $\frac{\lambda_{min}}{10} << \max(\Delta x, \Delta y, \Delta z)$. This truncation can be performed by appropiate windowing of the DGF. A type of window showing good results is presented in Eq.3.41, but additional research is required to fully asses the impact of the window type on the computations.

$$[WDG] = W(n) \cdot [DG] \qquad W(n) = \begin{cases} 0 & n < n_i, n > n_t \\ 1 & n_i < n < n_0 \\ e^{-\left(\frac{n-n_0}{\sigma_n}\right)^m} & n_t > n > n_0 \end{cases}$$

$n_i = \max(i, j, k)$ and n_t, n_0, σ_n, m are suitable parameters (Eq.3.41)

The DGF-FDTD algorithm is used to compute the impedance of a dipole antenna in order to demonstrate the accuracy of the method in modelling a wire antenna in a full 3D problem. The incident field is a delta source at the dipole terminals, then the density of current on the dipole at time step n is calculated using Eq.3.39 in an iterative form from the dipole currents at previous time steps. The impedance is computed from the density of current obtained from the scattering algorithm Eq.3.39 at the delta source (Eq.3.40). The results are compared to simulations using the well established NEC (Method of Moments) code. The wires are modelled in DGF-FDTD as current elements at the corners of the relevant elementary FDTD cell. In this case, the number of unknowns required to solve the problem in the time domain is relatively small (40 time steps multiplied by 168 nodes) for DGF FDTD compared to (50x50x25 nodes) for conventional FDTD.

This significant reduction occurs since only the scattering nodes (those forming the conducting structure of the dipole) of the grid are considered. The number of calculations to be performed per time step is of the order of $N_t \cdot N_s^2$ where N_s is the number of scatterer nodes, and N_t is the number of elements in the time window. If the number of scatterer nodes is small (i.e. wire antennas) the number of operations is much lower than the required N^3 for Yee's algorithm (where N is the grid's size).

However, it is necessary to include the computation of the DGF at each node, and this adds complexity to the process. This can be avoided by a selective pre-calculation and storage of the DGF, since identical calls to it are repeated for similar relative position between nodes. Figure 3.7 shows the impedance of a single dipole and Figure 3.8 shows the impedance of a

dipole loaded with a parasitic dipole nearby. Agreement with the NEC computations is very good and it is not affected by the windowing of the DGF. The deviation between the two methods in the imaginary part can be explained in terms of the cross-sectional shape of the wire (circular for NEC, square for DGF-FDTD) and the size of the delta gap source used in both methods. For stability the NEC solution for this thick wire dipole uses only 7 elements and so has a wider delta gap source than that used for FDTD (where the dipole is 21 cells long). Since the DGF is an exact solution to the FDTD equations, the results for these dipole examples obtained with a conventional FDTD code, produce identical results (down to the 5th decimal position) for the density of current on the dipole.

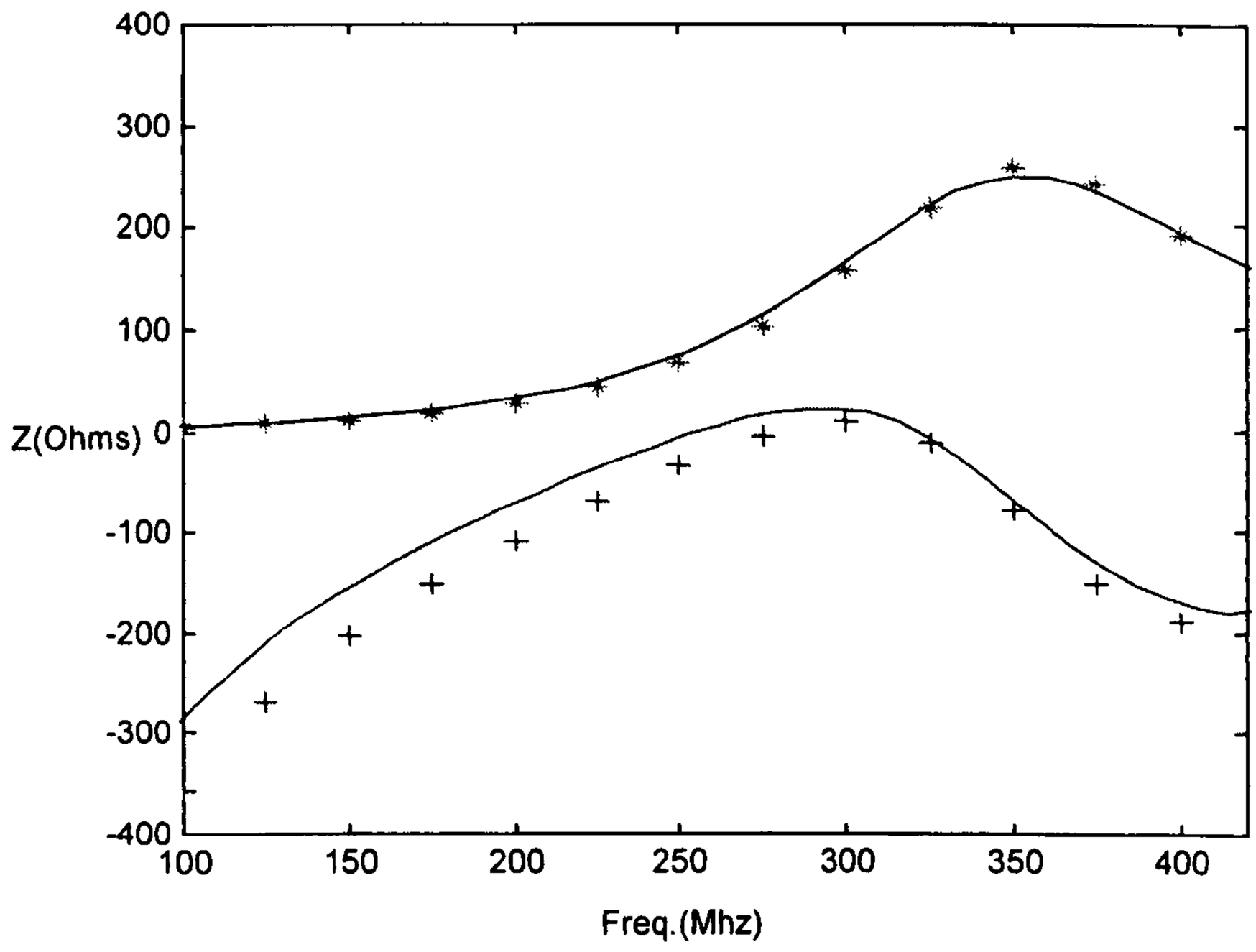

Fig. 3.7. Impedance as function of the frequency for dipole of length 0.5m and wire diameter of 32mm. (* Real part NEC, + Imaginary part NEC. Solid Line DGF-FDTD)

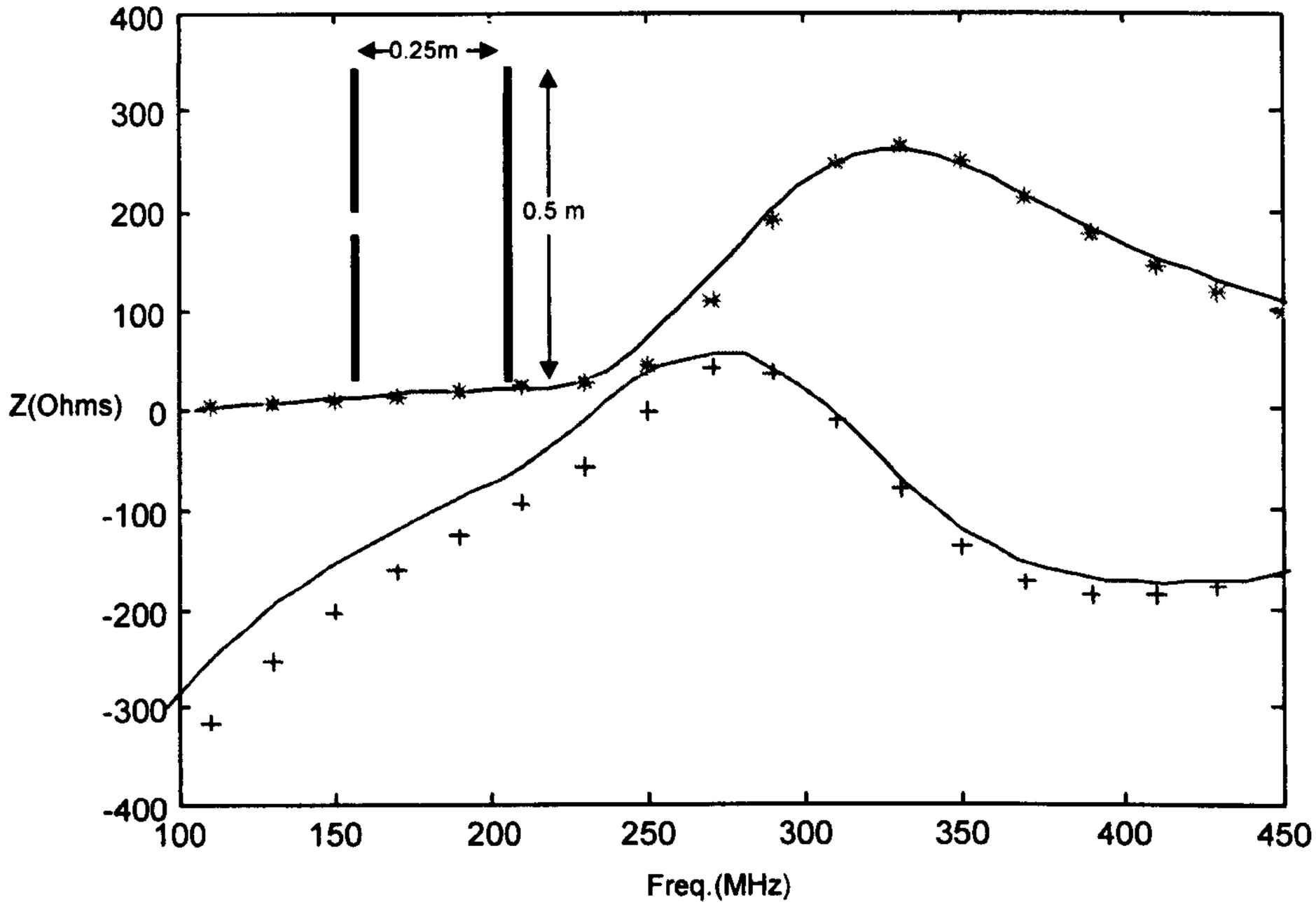

Fig.3.8. Impedance as function of the frequency for dipole as used in Fig.3.7 but in presence of an identical parasitic element located 0.25m away (see inset to figure). (* Real part NEC, + Imaginary part NEC. Solid Line DGF-FDTD)

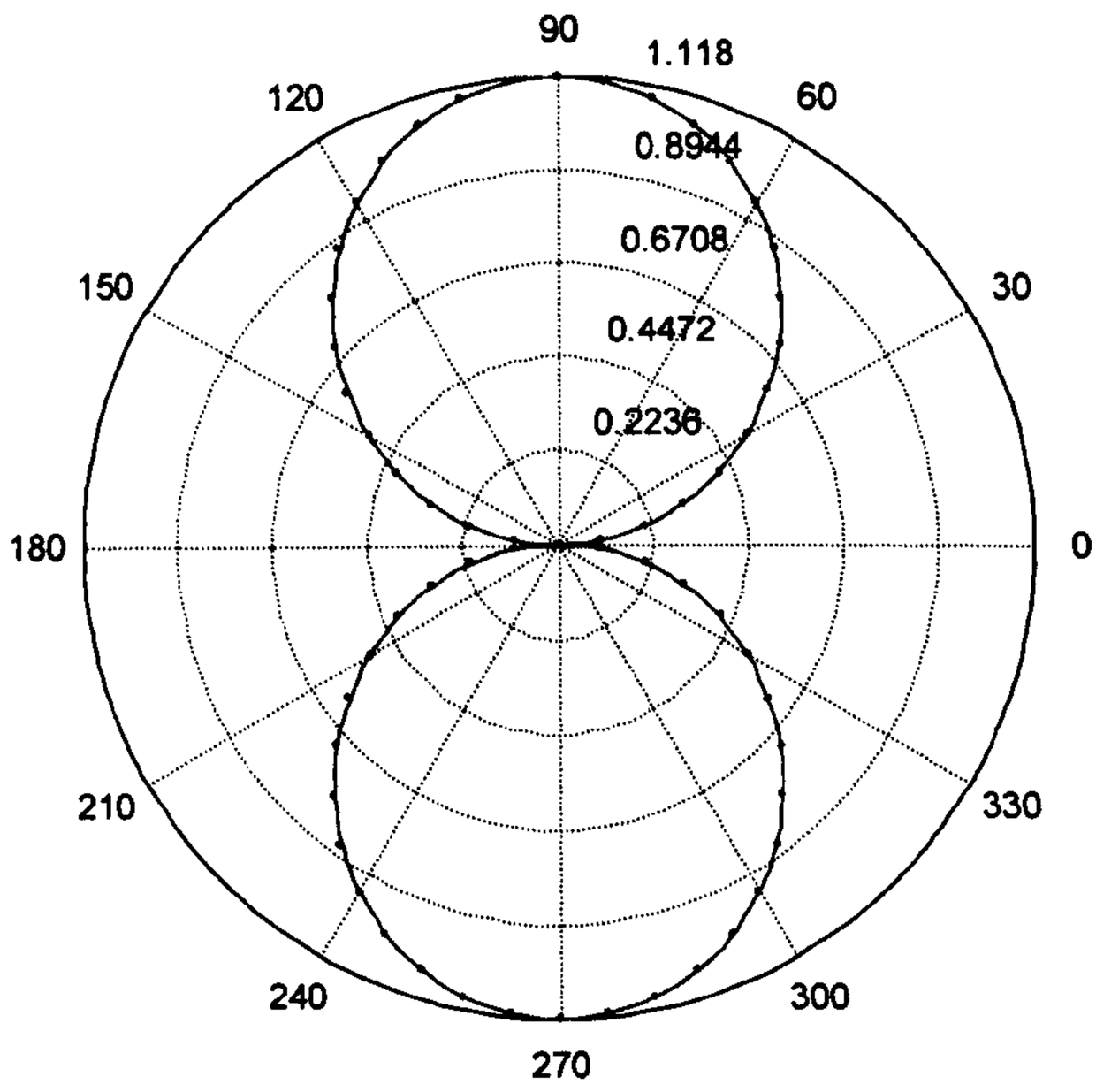

Fig.3.9. Dipole pattern L=0.5m w diam=0.008m at 200 MHz (Dots NEC, Solid Line DGF-FDTD)

3.4.2 Exact Absorbing Boundary Conditions Using the DGF-FDTD algorithm

As stated previously, The DGF method can be combined with the Yee's FDTD algorithm without getting any interfacing problems or numerical errors between them since they are exact algorithms of the same FD problem. On the other hand, The DGF method doesn't require the implementation of ABC's because can determine the field at any point just from the currents without computing the free space nodes in between. This property of the DGF method makes possible to provide an ABC based on the DGF because it can calculate exactly the field at the boundary of the grid from fields inside the grid.

3.4.2.1 Principle of Equivalence and the Exact DGF ABC for the FDTD algorithm

For the calculation of the EM field at the boundary, it is necessary to make use of the rigorous equivalence principle for FDTD in order to represent the EM field just outside the grid boundary in terms of radiation from an equivalent current distribution.

The concept of the DGF boundary condition is illustrated the 2D case. In Fig.3.10 for the TM mode the principle of equivalence in a single wall is shown. The convolution formula for FDTD (Eq.3.13) can be used to predict the electric field outside the boundary, providing a termination value for the FDTD grid. This value is then used by the Yee's algorithm to compute the field inside the boundary as is the case for any ABC.

The DGF ABC for a wall perpendicular to the z-axis can be derived from the convolution formula, substituting the currents by the fields at the grid boundary according to the principle of equivalence (Eq.3.42) (see Chapter II section 2.1.5, equation 2.10 of this thesis).

$$\vec{E}_{ij}^{\,n}\Big|_{wall} = \frac{1}{\Delta z}\sum_{n'}^{n-1}\sum_{i'j'}\left(\hat{z}\times\vec{H}_{i'j'}^{\,n'}\Big|_{wall-1}\right)[G_{ej}]_{i-i'\,j-j'0}^{n-n'} + \left(\hat{z}\times\vec{E}_{i'j'}^{\,n'}\Big|_{wall}\right)[G_{em}]_{i-i'\,j-j'0}^{n-n'}$$

(Eq.3.42)

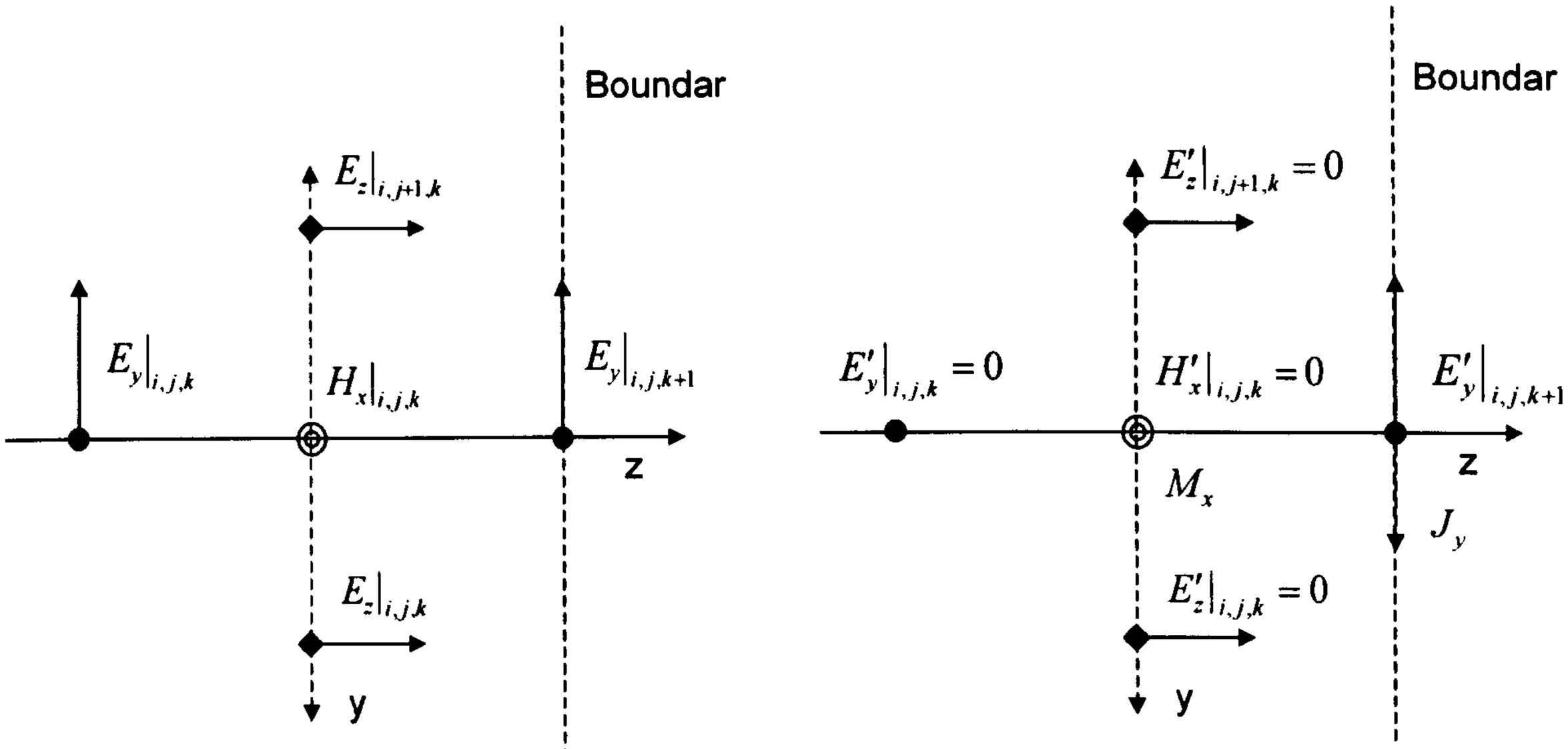

$$E'_y\big|_{i,j,k+1} = E_y\big|_{i,j,k+1}$$

$$M_x = -\frac{E_y|_{i,j,k+1}}{\Delta z} \quad J_y = -\frac{H_x|_{i,j,k}}{\Delta z}$$

Fig.3.10. Principle of equivalence on a wall for a 2D TM FDTD cell. The electrical field at the position k+1 in the normal FDTD grid (left) is consistent (according to FDTD equations) with an equivalent grid (right) which includes magnetic and electric currents. The other field components of the cell are set to zero.

This formula computes the electrical field on the boundary wall at the present time instant from the electrical field on the wall at previous time steps and the magnetic field just before the wall. This value of the electrical field can be used to update the Yee algorithm. It is possible to compare the field at a wall computed using Yee for a large grid with that using the DGF ABC (Eq.3.42). The differences are extremely low mainly due to the finite precision of floating point real number representation in computers. Figure.3.11 shows (in a similar fashion to the PML local error estimation in the classical Taflove's book [2]) the local error of the DGF ABC computation of the field. and these errors are one order of magnitude below the PML ABC in [13].

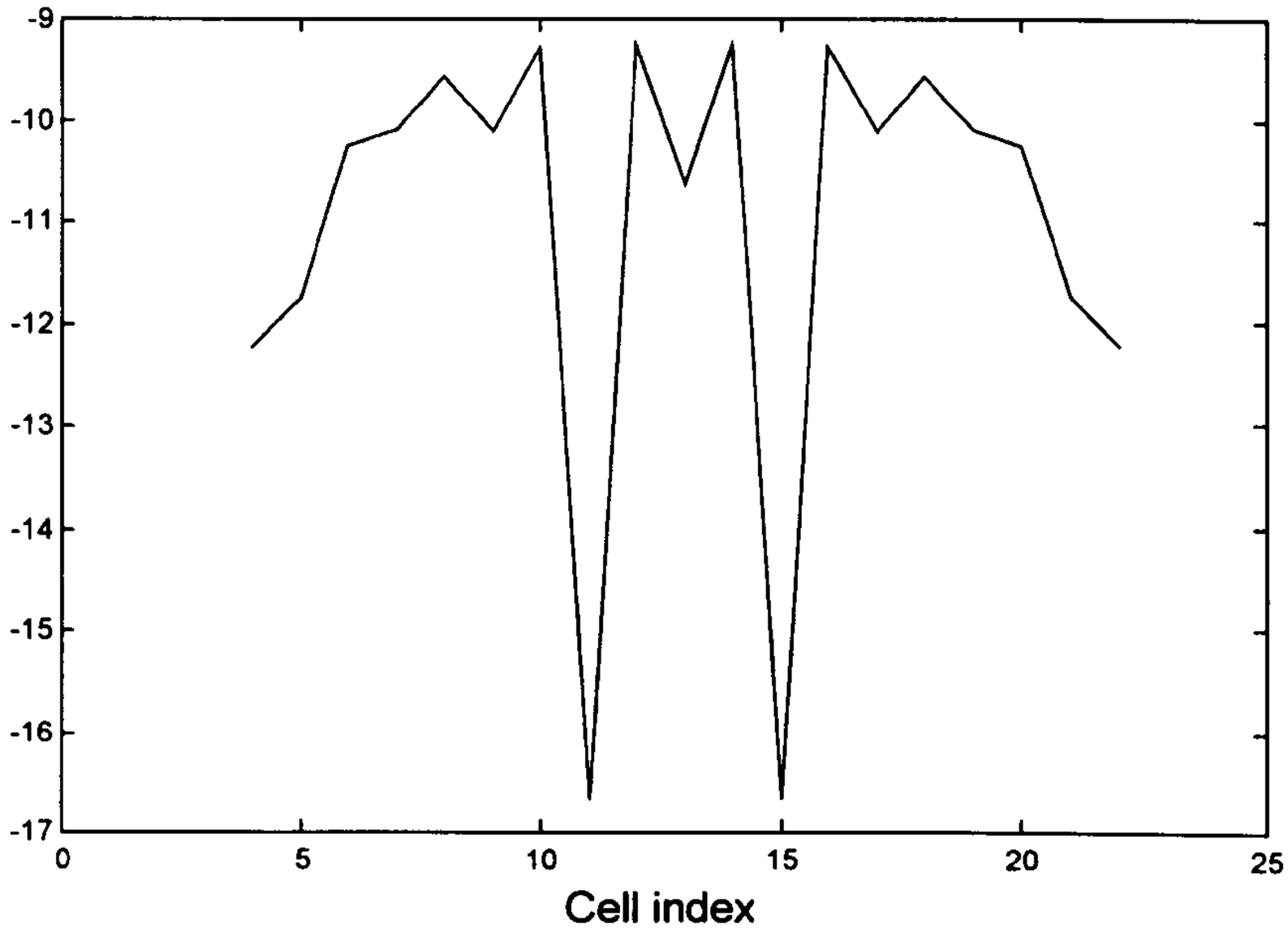

Fig.3.11. Logarithm of the normalised local error $Log\left(\left|\vec{E}_{wallDGF} - \vec{E}_{wallYee}\right|^2\right)$ of the electrical field at a wall (k=constant, 25x25 cells) computed using the DGF ABC of Eq.3.42. The field source is a small dipole situated 10 cells away from the wall.

The computer requirements to apply Eq.3.42 directly are very large. From the point of view of memory requirements, the fields should be stored for each position on the boundary wall for a significant number of time instants. From the point of view of CPU time, each point at the boundary is calculated as the sum of contributions from all the nodes on the boundary wall (including all applicable previous time instants). The result of this is that the order of the number of computations is very high $N_x^2 \cdot N_y^2 \cdot N_t$. As a consequence, the speed of the FDTD is seriously degraded by this direct implementation of the DGF ABC.

3.4.2.2 FFT implementation of the Exact DGF ABC

The performance of the DGF ABC can be dramatically improved using the special properties of the convolution method. The Equation 3.42 is essentially a 2D discrete convolution that can be evaluated using FFT techniques (Eq.3.43). The FFT technique introduces two major improvements. First, the order of the calculations can be reduced from N^2 to $N \cdot \log_2 N$, where N is the number of cells of the model. Secondly, the FDTD nodes separation can be increased to the Nyquist criteria (samples every $\lambda/2$) since the field in FDTD is heavily

oversampled (samples every λ/10) to avoid the dispersion of the FD grid. Once the calculation has been done the nodes in the middle can be obtained by 'zero-padding' FFT interpolation.

$$\vec{E}_{ij}^{\,n}\Big|_{wall} = \frac{1}{\Delta z} FFT^{-1}\left\{ \sum_{n'}^{n-1} FFT\left[\hat{z} \times \vec{H}_{ij}^{\,n'}\Big|_{wall-1}\right]\left[\Gamma_{ej}\right]^{n+n'} + FFT\left[\hat{z} \times \vec{E}_{i'j'}^{\,n'}\Big|_{wall}\right]\left[\Gamma_{em}\right]^{n+n'} \right\} \qquad \text{(Eq.3.43)}$$

This FFT-DGF ABC technique can be used for waveguides or periodic surface problems. It has the advantage that it is exact, and it works for any angle of incidence (providing that the Nyquist criterion is satisfied). The storage requirements are largely reduced by the decimation of nodes. The matrices $[\Gamma_{ej}]^n$ and $[\Gamma_{em}]^n$ are the 2D Fourier transform of the DGF for k=0. These matrices can be pre calculated and stored so the speed of the algorithm is not affected.

3.5 Higher order general algorithms for the FDTD

In EM field theory, the phase velocity of waves in a vacuum is equal to the speed of light for all wavelengths (non dispersive) and propagation direction (isotropic). As stated, FDTD equations are dispersive (wave phase velocity depends on the ratio of the wavelength to cell size) and anisotropic (phase velocity depends on the propagation direction with respect to the FDTD grid). This is because of the fundamental differences between discrete (finite differences) and continuous (derivatives) mathematics. The maximum size of the FDTD cells is limited to $\lambda/10$ or smaller mainly because of the dispersion effect.

The search for higher order algorithms to improve the dispersion of the FDTD method started very early [2] in the 70's. The basic idea is to obtain a more accurate estimation of the derivatives in Maxwell's equations using more field nodes to perform the calculation. Time derivatives are not usually evaluated using higher order formulas since extra field time nodes implies heavy storage requirements. Recently there is renewed interest in high order algorithms [3], Multi resolution (MRTD) techniques are using advanced forms of interpolation to improve the accuracy of the estimation of spatial derivatives in Maxwell's equations.

This section is devoted to showing some of the fundamental limitations of high order methods to achieving dispersion-less algorithms. Instead of using high order interpolation formulas between nodes, an equivalent mathematical device is used. A generalised central finite difference operator is introduced as a series of finite differences. The classical Lagrange formula of derivatives exactly represented by finite differences series is used as the starting point.

From here, two types of low dispersion algorithms are described. First, the spatially low dispersion algorithm and secondly the space-time low dispersion algorithms. The first type is based on the accurate approximation of spatial derivatives in Maxwell's equation. General formulas for the algorithm's coefficients are given for any order of the method. These algorithms minimize the anisotropy of the method. The second type is based on the balance between the dispersion introduced by the time and the spatial finite difference. These algorithms minimize the dispersion of the method in selected directions. It is noted that MRTD algorithms as in [3] belong to the first type so it is believed that the general conclusions for this type of algorithms are applicable to MRD schemes.

3.5.1 Generalisation of the Central Finite Difference Operator in FDTD.

As stated, the FDTD algorithm is based on the approximation of derivatives in Maxwell equations by a discrete operator, D, representing the finite difference of the fields. This operator can be extended to a general form of central finite differences (Eq.3.44). The series only include odd powers of D in order to preserve the 'central' operator type, but there is no restriction on the coefficients for each term.

$$D'_x = \sum_{n=0}^{\infty} a_n X^{n+1/2} D_x^{2n+1} \qquad D'_x E_i = \sum_{n=-\infty}^{\infty} b_n E_{i+n}$$

$$b_n = -b_{-n-1} = \sum_{l=n}^{\infty} (-1)^{l-n} \binom{2l+1}{l-n} \frac{a_l}{\Delta x^{2l+1}}$$

The FDTD finite differences for the spatial indexes are updated using the new FD operator described in Eq.3.44. For the time index, the conventional central FD is used in order to store in memory just the fields at the previous time instant. The generalised FDTD takes a new form, so the vicinity (Chapter 2) of a node contains an infinite set of nodes.Equation 3.45 shows the new FDTD equation for the z component of the magnetic field.

$$H_z\Big|_{i,j,k}^{n+1/2} = H_z\Big|_{i,j,k}^{n+1/2} - \left(\frac{\Delta t}{\mu}\right) \cdot \left[\sum_{l=-\infty}^{\infty} b_{xl} E_y\Big|_{i+1/2+l,j,k}^{n} - \sum_{l=-\infty}^{\infty} b_{yl} E_x\Big|_{i,j+1/2+l,k}^{n} + M_z\Big|_{i,j,k}^{n} \right.$$

(Eq.3.45)

All the relationships obtained for FDTD remain the same but changing the central FD by the generalized operator. As a consequence the dispersion relation for the generalised algorithm can be written directly (Eq.3.46). The new dispersion relation can be controlled by the coefficients of the generalised operator to produce algorithms with specific dispersion properties.

$$\Omega^{-1} \frac{D_n^2}{c^2} - (X^{-1} D_x^2 + Y^{-1} D_y^2 + Z^{-1} D_z^2) = 0$$

(Eq.3.46)

This is the dispersion formula for the discrete system, similar to the formula $k^2-(k_x^2+k_y^2+k_z^2)=0$ in the continuous case. Eq.3.46 shows the relationship for the complete complex plane. The dispersion formula on the unit circle of the complex plane depends on the propagation constants as in the continuous case (Eq.3.47).

$$-\frac{2}{c^2\Delta t^2}\sin^2\left(\frac{\omega\Delta t}{2}\right)=X^{-1}D_i'^2+Y^{-1}D_j'^2+Z^{-1}D_k'^2$$

$$X^{-1/2}D_i'=j\sum_{l=0}^{\infty}(-1)^l\,a_{x\,l}\left(\frac{2}{\Delta x}\sin\left(\frac{k_x\Delta x}{2}\right)\right)^{2l+1}$$

$$Y^{-1/2}D_j'=j\sum_{l=0}^{\infty}(-1)^l\,a_{y\,l}\left(\frac{2}{\Delta y}\sin\left(\frac{k_y\Delta y}{2}\right)\right)^{2l+1}$$

$$Z^{-1/2}D_k'=j\sum_{l=0}^{\infty}(-1)^l\,a_{z\,l}\left(\frac{2}{\Delta z}\sin\left(\frac{k_z\Delta z}{2}\right)\right)^{2l+1}$$

(Eq.3.47)

In the particular case (a_0=1, a_1=a_2=...=0) the Eq. 3.47 becomes the FDTD dispersion formula. The stability of the algorithm depends on the coefficients of the generalised finite difference operator. The algorithm becomes unstable if $\sin^2(\omega\Delta t/2)>1$ since imaginary arguments are required. Let us assume that in the interval $-\pi<k_s\Delta s<\pi$ the odd functions defined in Eq.3.47 are monotonic, so they have the extrema at the interval bounds. In this case, the stability limit can be easily found precisely at the interval limits (Eq.3.48).

$$c\Delta t<\frac{1}{\sqrt{\left(\frac{S_x}{\Delta x}\right)^2+\left(\frac{S_y}{\Delta y}\right)^2+\left(\frac{S_z}{\Delta z}\right)^2}}$$

$$S_x=\sum_{l=0}^{\infty}(-1)^l\,a_{x\,l}\left(\frac{2}{\Delta x}\right)^{2l}\quad S_y=\sum_{l=0}^{\infty}(-1)^l\,a_{y\,l}\left(\frac{2}{\Delta y}\right)^{2l}\quad S_z=\sum_{l=0}^{\infty}(-1)^l\,a_{z\,l}\left(\frac{2}{\Delta z}\right)^{2l}$$

(Eq.3.48)

It is interesting to notice the relationship of the central FD to the operators continuous derivative (Eq.3.49). This symbolic relation is based on the Taylor expansion of a function, so the operator displacement can be represented as an operator exponential function of the

derivative. This notation was introduced by Lagrange [8] (based on Newton's formula) and provides the key to obtaining the symbolic relations between FD and the exact derivatives.

$$XE_i = E(x + i\Delta x + \Delta x) = \sum_{n=0}^{\infty} \frac{\Delta x^n}{n!} \frac{\partial^n E(x + i\Delta x)}{\partial x^n}$$

$$X = \sum_{n=0}^{\infty} \frac{\Delta x^n}{n!} \frac{\partial^n}{\partial x^n} = e^{\Delta x \frac{\partial}{\partial x}}$$

$$X^{1/2} D_x = \frac{X^{1/2} - X^{-1/2}}{\Delta x} = \frac{2}{\Delta x} \sinh\left(\frac{\Delta x}{2} \frac{\partial}{\partial x} \right)$$

(Eq.3.49)

As a consequence the generalised operator can be also considered as an operator function for the exact derivative. This time the relation is in terms of a power series (Eq.3.50)

$$D'_x = \sum_{n=0}^{\infty} a_n \left(\frac{2}{\Delta x} \sinh\left(\frac{\Delta x}{2} \frac{\partial}{\partial x} \right) \right)^{2n+1}$$

(Eq.3.50)

3.5.2. Low dispersion generalised FDTD algorithms.

The coefficients of the generalised operator (Eq.3.44) can be used to synthesise algorithms with low dispersion of the spectral components. In these special algorithms, the phase velocity of the plane waves resulting from Eq.3.47 remains almost constant even for a node size of few cells per wavelength.

A possible strategy to obtain low dispersion algorithms is to improve the accuracy of the approximation of the spatial derivatives. The time derivative is still approximated by a simple central FD to avoid the usage of extra memory. The fourth order FDTD and the so called multiresolution techniques [3] are of this kind. The generalised operator can be selected to improve the dispersion both of spatial and time derivatives approximations. Another possibility reported in the literature [2] is to enforce null dispersion at certain angles of propagation with respect to the grid (Normally 45, 135, 225, 315 Degrees). This has been implemented for the plain FDTD and the fourth order spatial FDTD.

3.5.2.1. Spatially low dispersion algorithms

The objective of these low dispersion algorithms is to improve the approximation of the spatial derivatives in FDTD. The spatially dispersionless algorithm is achieved when the approximation of the derivatives is exact. In this case the algorithm is isotropic and presents the same spatial velocity in all directions. This is possible if the fields are sampled according to the Nyquist criterion (see chapter 3 of [5]). In the case of exact approximation, the dispersion law is described in Eq.3.51.

$$\frac{1}{c^2\Delta t^2}\sin^2\left(\frac{\omega\Delta t}{2}\right) = k_x^2 + k_y^2 + k_z^2$$

$$-\frac{\pi}{\Delta s} < k_s < \frac{\pi}{\Delta s} \qquad \text{(Eq.3.51)}$$

The coefficients of the generalised operator can be determined in order to satisfy the Eq.3.51. From the general form of the dispersion relation, Eq.3.46, it is possible to conclude the condition for the coefficients (Eq.3.52), where only the x component is shown for the sake of simplicity. Multiresolution schemes in [3] use advanced interpolation based on wavelets to achieve the same result: a very accurate estimation of the spatial derivatives.

$$k_x = \sum_{l=0}^{\infty}(-1)^l a_l\left(\frac{2}{\Delta x}\sin\left(\frac{k_x\Delta x}{2}\right)\right)^{2l+1} \qquad \text{(Eq.3.52)}$$

The coefficients can be obtained using the Taylor's expansion of the hyperbolic arcsine (Eq.3.53). These coefficients allow the exact determination of the partial spatial derivative of the fields, provided they are bandlimited and sampled according to the Nyquist criteria. Using the coefficients from Eq.3.53 into Eq.3.50, it is clear that now $D_x' = \partial/\partial x$.

$$\frac{2}{\Delta x}\cdot \arcsin\left(\frac{\kappa_x \Delta x}{2}\right)= \sum_{l=0}^{\infty}(-1)^l\, a_{x\,l}\cdot \kappa_x{}^{2l+1}$$

$$a_{x\,l}=(-1)^l\,\frac{1\cdot 3\cdot \ldots \cdot (2l-1)}{2\cdot 4\cdot \ldots \cdot 2l\cdot (2l+1)}\left(\frac{\Delta x}{2}\right)^{2l}$$

(Eq.3.53)

The coefficients of Eq.3.53 define the convolution sequence b_n to obtain the derivative in the central point for a bandlimited function in an exact way (Eq.3.54).

$$D'_x E_i=\frac{\partial E(x+i\Delta x)}{\partial x}=\sum_{n=-\infty}^{\infty} b_n E_{i+n}$$

$$b_n=-b_{-n-1}=\frac{(-1)^n}{\Delta x}\sum_{l=n}^{\infty}\binom{2l+1}{l-n}\frac{1\cdot 3\cdot \ldots \cdot (2l-1)}{2\cdot 4\cdot \ldots \cdot 2l\cdot (2l+1)}\left(\frac{1}{2}\right)^{2l}$$

(Eq.3.54)

The implementation of the exact derivative operator requires an infinite number of nodes to contribute to the calculation. Practical algorithms using a finite number of nodes can be obtained in a straightforward manner by truncating the coefficients of the generalised operator (a_0, a_1,... a_p, 0, 0...). This produces a similar truncation of the sequence b_n since it depends on coefficients of order n or superior.

The truncated operator using the coefficients of Eq.3.54 provides the exact derivatives for polynomials. The algorithms resulting from the truncation are equivalent to the higher order method using central interpolation polynomials. Table 3.1 shows the sequences b_n for different truncation orders. The truncation in the first coefficients produces the plain FDTD method. The truncation in the second coefficient produces the fourth order FDTD algorithm.

Order of truncation	Coefficients
a_0	$b_0 = 1 \quad b_{-1} = -1$
a_0 , a_1	$b_1 = \frac{1}{24} \quad b_0 = \frac{27}{24} \quad b_{-1} = -\frac{27}{24} \quad b_{-2} = -\frac{1}{24}$
a_0 , a_1 , a_2	$b_2 = \frac{3}{480} \quad b_1 = \frac{35}{480} \quad b_0 = \frac{570}{480} \quad b_{-1} = -\frac{570}{480} \quad b_{-2} = -\frac{35}{480} \quad b_{-3} = -\frac{3}{480}$
$a_0 , a_1 , a_2 , \ldots , a_N$	$b_n = -b_{-n-1} = \frac{(-1)^n}{\Delta x} \sum_{l=n}^{N} \binom{2l+1}{l-n} \cdot \frac{1 \cdot 3 \cdot \ldots \cdot (2l-1)}{2 \cdot 4 \cdot \ldots \cdot 2l \cdot (2l+1)} \cdot \left(\frac{1}{2}\right)^{2l}$

The dispersion law of Eq.3.50 is formally closer than FDTD Eq.3.53 to the real dispersion formula from Maxwell's equations $(\omega/c)^2 = k_x^2 + k_y^2 + k_z^2$. However, this is true only for small values of the time step, $\Delta t < \Delta t_{max}/3$ ($c\Delta t_{max} = \Delta x/\sqrt{3} \quad \Delta x = \Delta y = \Delta z$), Fig.3.12 since the dispersion is due to the error in the estimation of the time derivative. The Multiresolution techniques presented in [3] also belongs to this type of techniques and exhibits the same type of performance.

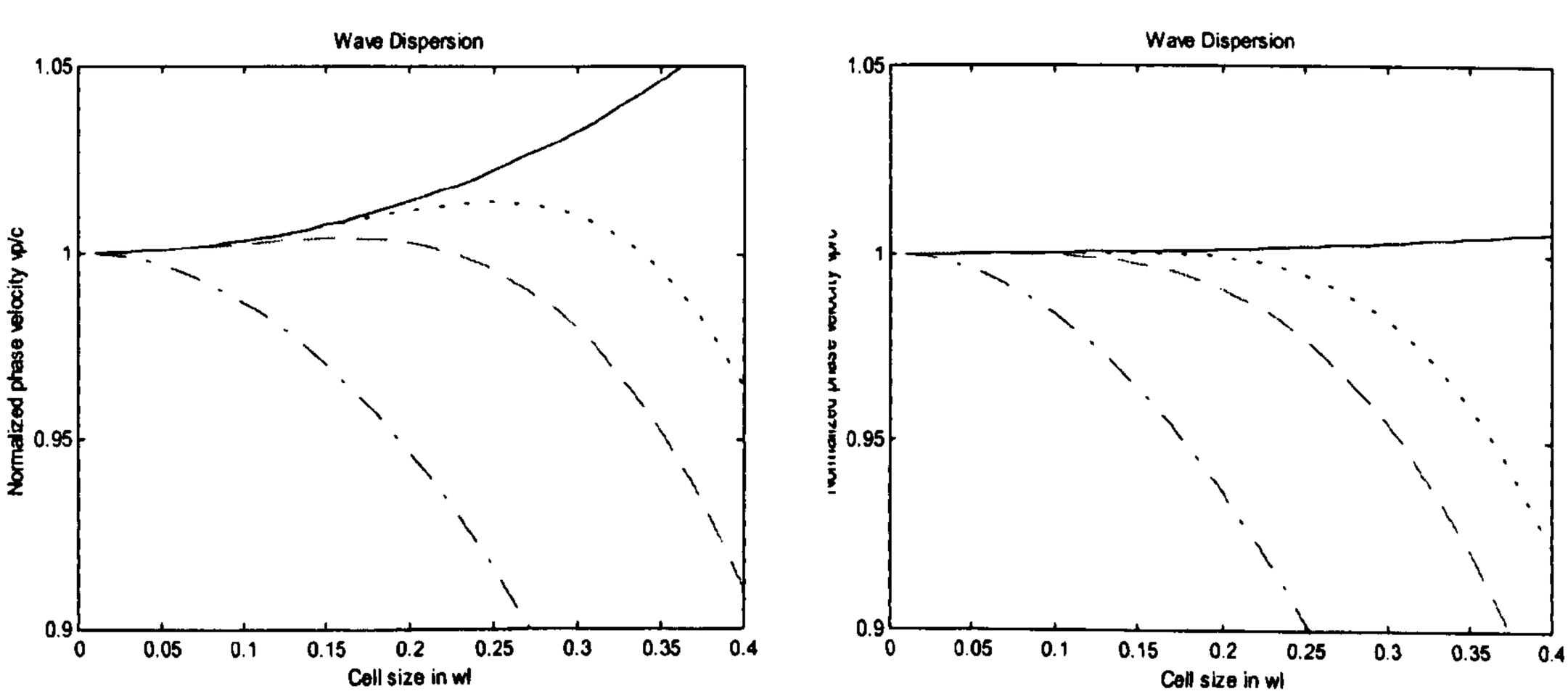

Fig.3.12. Dispersion law for $\Delta t < 0.9\Delta t_{max}$ (Left) and $\Delta t < 0.25\Delta t_{max}$ (Right). The spatial higher order algorithms only improve the dispersion law if the time step is very small compared to the maximum stable time step. (Solid Line: Spatially dispersionless (Eq.3.51), Dot-Dash Line:FDTD, Dot Line: Fourth Order, Dash Line: Sixth Order).

The coefficients of the truncated generalised operator can be optimised to produce minimum spatial dispersion in a specific interval of the cell size axis. In this case, the coefficients are calculated by minimum squares fitting of the arcsine in Eq.3.53. This produces the best fit to the spatially dispersionless law (Eq.3.51) which is isotropic. As a consequence, the best fit algorithm produces also the lowest anisotropic dispersion law. Following standard procedures, the numerical fitting (minimum squares) in the interval $-0.25\lambda < \Delta x < 0.25\lambda$ has been done for two coefficients in order to optimise the fourth order algorithm. The new coefficients are $b_1 = -b_{-2} = 0.0559194$and $b_0 = -b_{-1} = 1.16132$ (standard fourth order $b_1 = -b_{-2} = 0.041666$and $b_0 = b_{-1} = 1.125$) and the resulting dispersion law is shown in Fig.3.13, and the phase velocity versus angle (Fig.3.14).

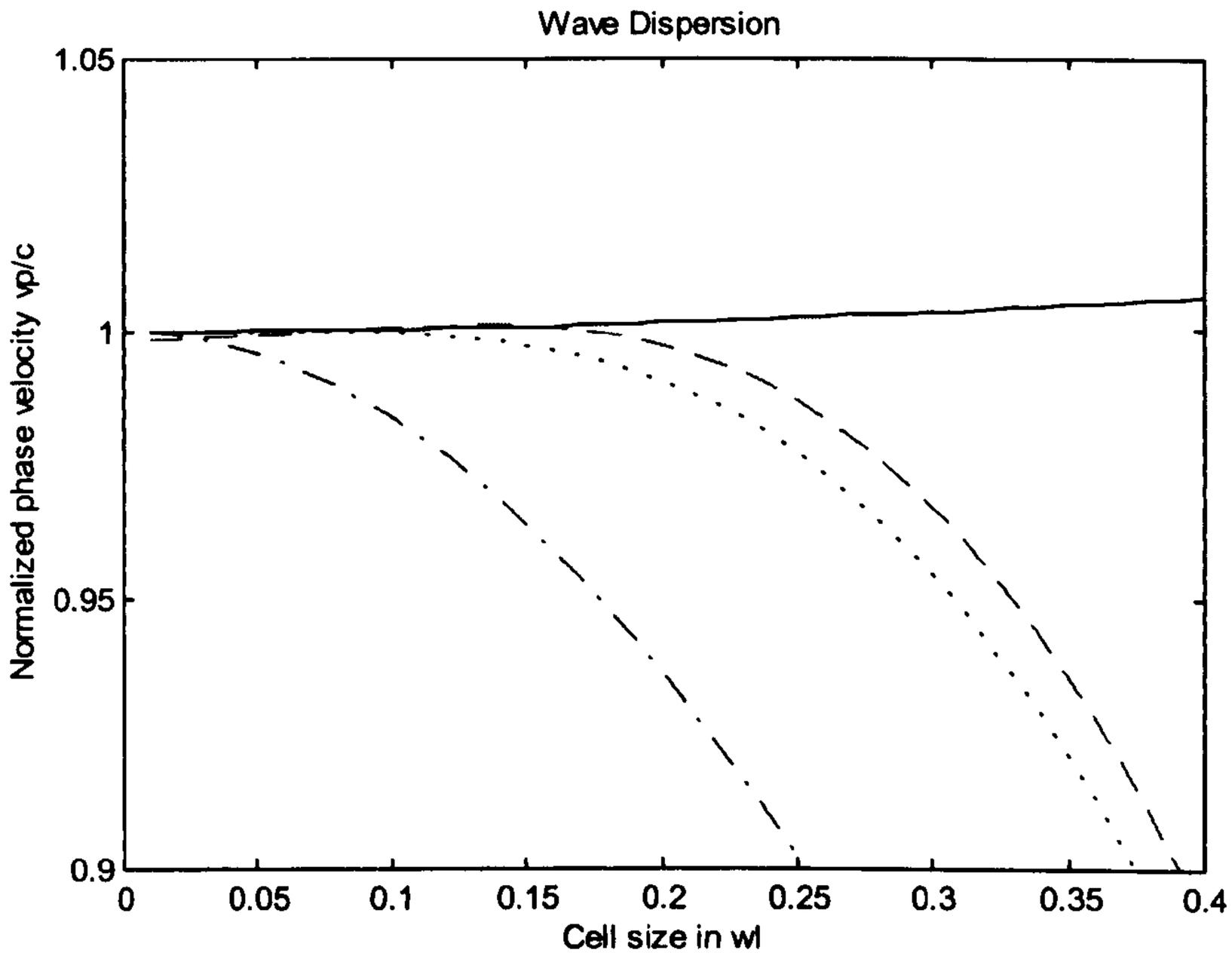

Fig.3.13. Dispersion curve for FDTD (Solid Line: Spatially dispersionless (Eq.3.51), Dot Dashed: FDTD, Dot Line: Fourth Order FDTD (truncated), Dashed Line: Fourth Order FDTD (minimum squares)). The Fourth order FDTD exhibit a dispersion curve more regular (flat) than the minimum squares approach, which has a better performance for large cell sizes.

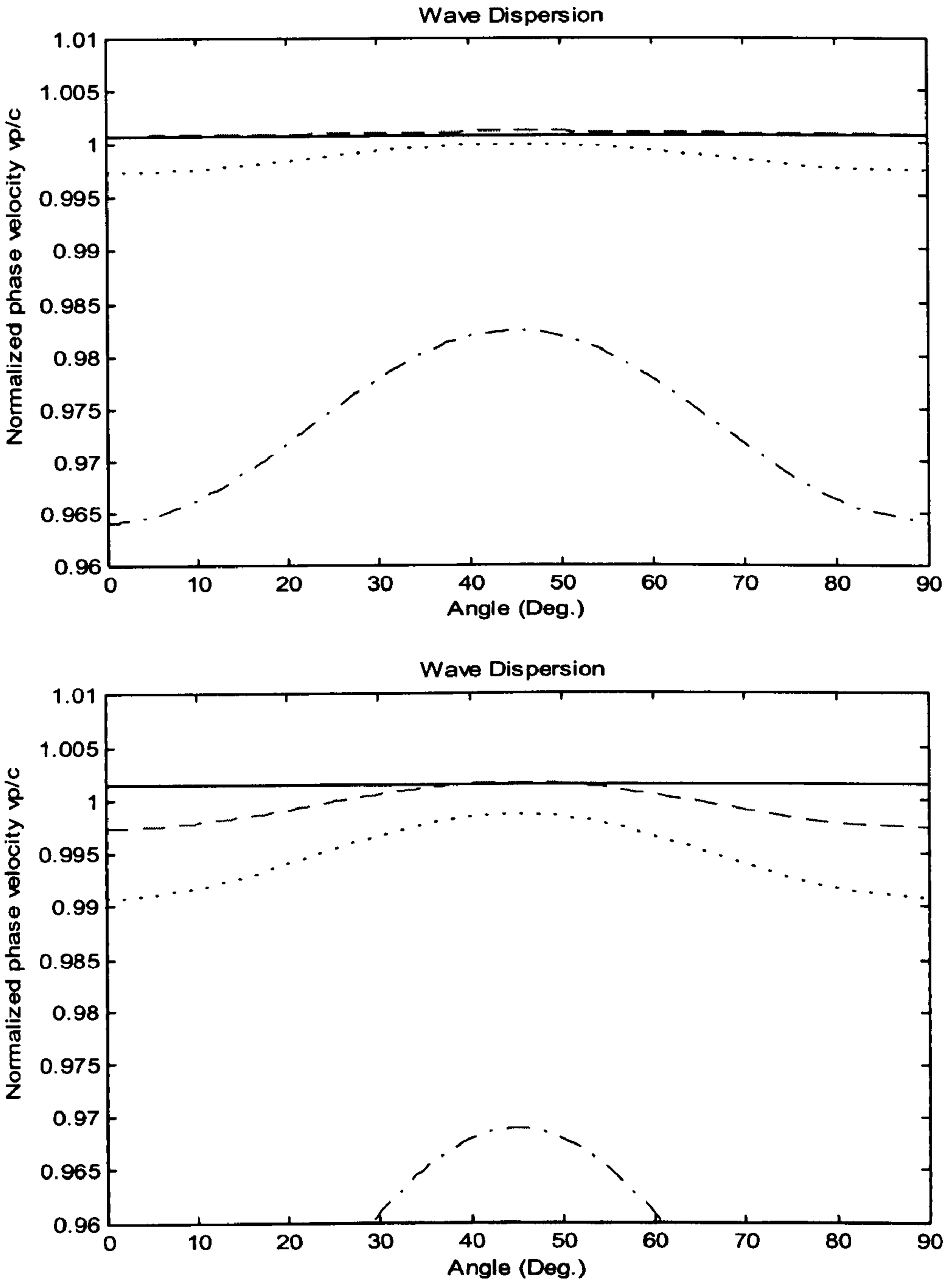

Fig.3.14. Dispersion of the phase velocity vs. angle of the wave propagation with respect to the grid. The cell size is, $\Delta x=\Delta y=0.15\lambda$ (Top) and $\Delta x=\Delta y=0.2\lambda$ (Bottom). (Solid Line: Ideal isotropic (Eq.3.51), Dot Dashed: FDTD, Dot Line: standard 4th Order FDTD, Dashed Line: 4th Order FDTD (minimum squares)). The minimun square approximation is the best fit of a finite order algorithm to the spatially dispersionless case (isotropic), as a result it exhibit the lowest angular dependance for the overall $\Delta x/\lambda$.

3.5.2.2. Space-Time low dispersion algorithms

The approximation of spatial partial derivatives in FDTD using the generalised operator from Eq.3.53 produces an isotropic algorithm, but dispersive with frequency because of the error associated to the central FD approximation of the time derivative. As a consequence, in order to improve the frequency dispersion of plain FDTD, this isotropic algorithm requires time steps smaller than the maximum allowed for stability. The algorithms based on the truncation of the exact generalised operator or on the minimum squares approximation of it also require small time steps. Paradoxically, the higher the order of the approximation, the smaller the value of the time step is required ($\Delta t < 0.5\Delta t_{max}$ fourth order FDTD and $\Delta t < 0.3\Delta t_{max}$ for sixth order FDTD). The multiresolution technique presented in [3] can be seen as a higher order (18^{th} order) approximation to Eq.3.10, so it also requires very small time steps ($\Delta t = 0.2\Delta t_{max}$).

An alternative way to obtain low frequency dispersion without decreasing the time step, is to determine the generalised operator for a frequency dispersionless algorithm at one (or several) angles of propagation. This basic idea is presented in [2] for the fourth order algorithm, adjusting the two coefficients to cancel the error at 0 and 45 step angles, but at a single frequency. A general approach is presented in Eq 3.55, so the coefficients are choosen to minimise the error at several angles and frequencies.

$$-\frac{4}{c^2\Delta t^2}\sin^2\left(\frac{kc\Delta t}{2}\right) = XD_i'^2 + YD_j'^2 + ZD_k'^2$$

$$X^{1/2}\cdot D_i' = j\sum_{l=0}^{\infty}(-1)^l a_{x\,l}\left(\frac{2}{\Delta x}\sin\left(\frac{k\alpha_x\Delta x}{2}\right)\right)^{2l+1}$$

$$Y^{1/2}\cdot D_j' = j\sum_{l=0}^{\infty}(-1)^l a_{y\,l}\left(\frac{2}{\Delta y}\sin\left(\frac{k\alpha_y\Delta y}{2}\right)\right)^{2l+1}$$

$$Z^{1/2}\cdot D_k' = j\sum_{l=0}^{\infty}(-1)^l a_{z\,l}\left(\frac{2}{\Delta z}\sin\left(\frac{k\alpha_z\Delta z}{2}\right)\right)^{2l+1}$$

$$k = \frac{\omega}{c} \quad k_x = k\alpha_x \quad k_y = k\alpha_y \quad k_z = k\alpha_z \qquad \begin{aligned}\alpha_x &= \sin\theta\cdot\cos\phi\\ \alpha_y &= \sin\theta\cdot\sin\phi\\ \alpha_z &= -\cos\theta\end{aligned}$$

(Eq.3.55)

This general formula determines the coefficients of the generalised operator to obtain a dispersionless algorithm at the wave propagation direction defined by the angles θ and ϕ. The

Eq.3.55 can be considered just for the angles (αx=1, αy=0, αz=0) (αx=0, αy=1, αz=0) (αx=0, αy=0, αz=1). In this case, the algorithm is optimized for frequency dispersion rather than for isotropy (Eq.3.56).

$$\frac{2}{c\Delta t}\sin\left(\frac{kc\Delta t}{2}\right) = \sum_{l=0}^{\infty}(-1)^{l}\, a_l\left(\frac{2}{\Delta x}\sin\left(\frac{k\Delta x}{2}\right)\right)^{2l+1} \qquad \text{(Eq.3.56)}$$

The exact coefficients to satisfy Eq.3.56 can be obtained by a change of variable and the Taylor series expansion (Eq.3.57).

$$\frac{2}{c\Delta t}\sin\left(\frac{c\Delta t}{\Delta x}\arcsin\left(\frac{\kappa_x \Delta x}{2}\right)\right) = \sum_{l=0}^{\infty}(-1)^{l}\, a_l \cdot \kappa_x^{\,2l+1}$$

$$a_l = \frac{1}{(2l+1)!}\left(\frac{\Delta x}{2}\right)^{2l}\left[\left(\frac{c\Delta t}{\Delta x}\right)^{2l} + \sum_{l'=1}^{l}(-1)^{l'}\left(\frac{c\Delta t}{\Delta x}\right)^{2(l-l')}\cdot\binom{2l+1}{2l'+1}\cdot(1\cdot 3\cdot\ldots\cdot(2l'-1))^2\right] \qquad \text{(Eq.3.57)}$$

These coefficients for the generalised operator implement the dispersion free exact algorithm for the wave propagation along the cartesian axis. The series can be truncated to obtain a practical algorithm with a finite number of coefficients. The truncated algorithm improves the dispersive behaviour of FDTD using normal time steps $\Delta t \cong \Delta t_{max}$ (maximum time step according to Courant condition) for any order of truncation. This type of algorithm allows one to use high order methods (>4th order) without decreasing the time step, as happens for the spatially low dispersion algorithms such as multiresolution schemes [3]. The new coefficients for the fourth order truncation are $b_1 = -b_{-2} = 0.03125$ and $b_0 = -b_{-1} = 1.09375$ (standard fourth order $b_1 = -b_{-2} = 0.041666$and $b_0 = b_{-1} = 1.125$) and the resulting dispersion law is shown in Fig.3.15.

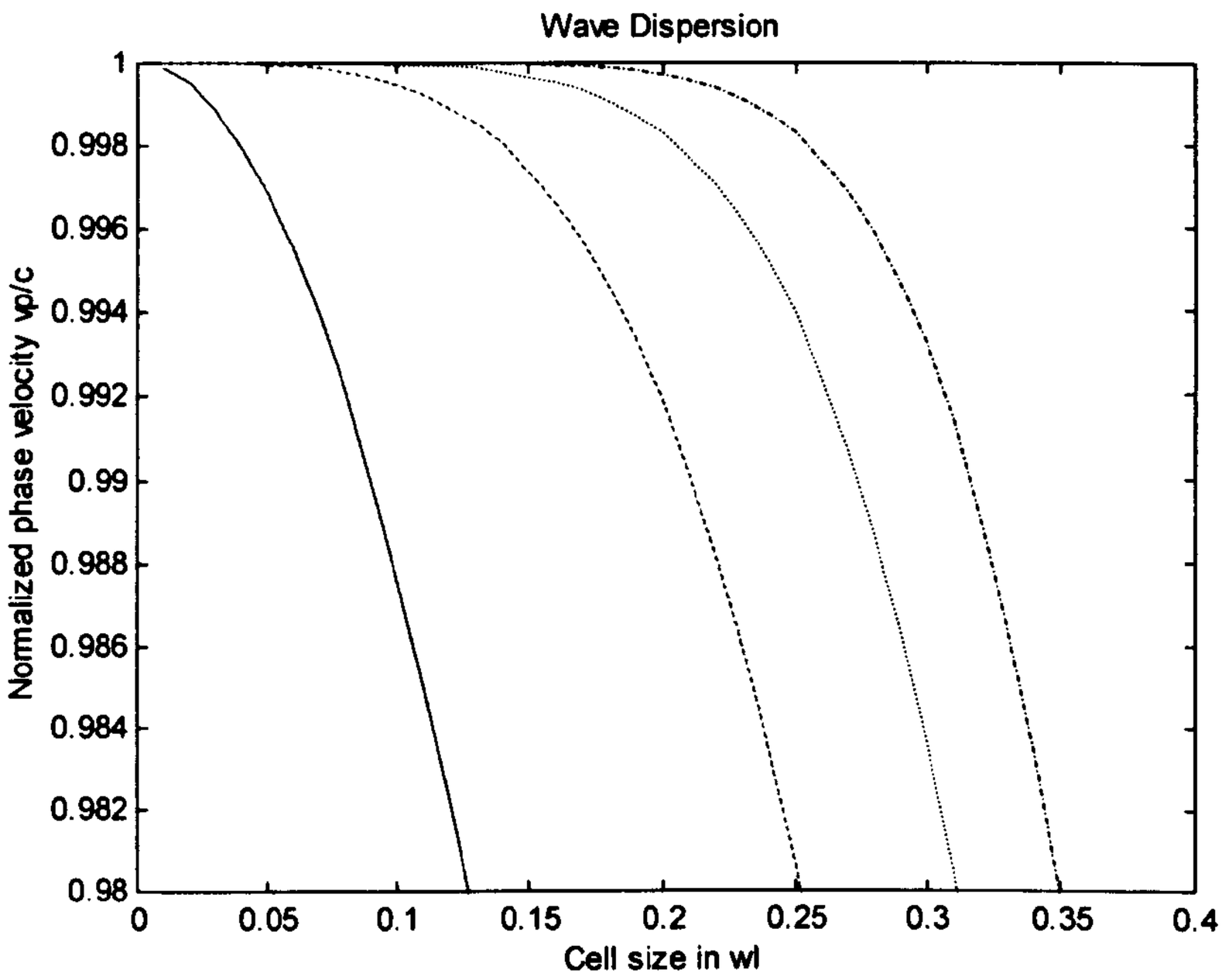

Fig. 3.15. The dispersion curve of the space-time low dispersion algorithm (angle of propagation 0 Deg. $\Delta t=0.5\Delta x$). (Solid Line: FDTD, Dashed Line: Fourth Order, Dot Line: Sixth Order, Dash Dot Line: Eight Order). The high order algorithms decrease dispersion without reduced time steps. For $\Delta t=0.9\Delta t_{max}$, the eight order algorithm is below 0.1% speed of light error for a $\lambda/4$ cell size.

The exact spatially dispersionless algorithm presents no angular dispersion (isotropy) but it is not optimized to compensate the frequency dispersion produced by the approximation of the time derivative. The exact space time dispersionless algorithm presents no frequency dispersion for propagation on the cartesian axis (with coefficients from Eq.3.56), but it is not optimized for isotropy. As a consequence, these generalised operators do not improve the isotropy of the algorithms just by increasing the algorithm's order, unless the time step is reduced.

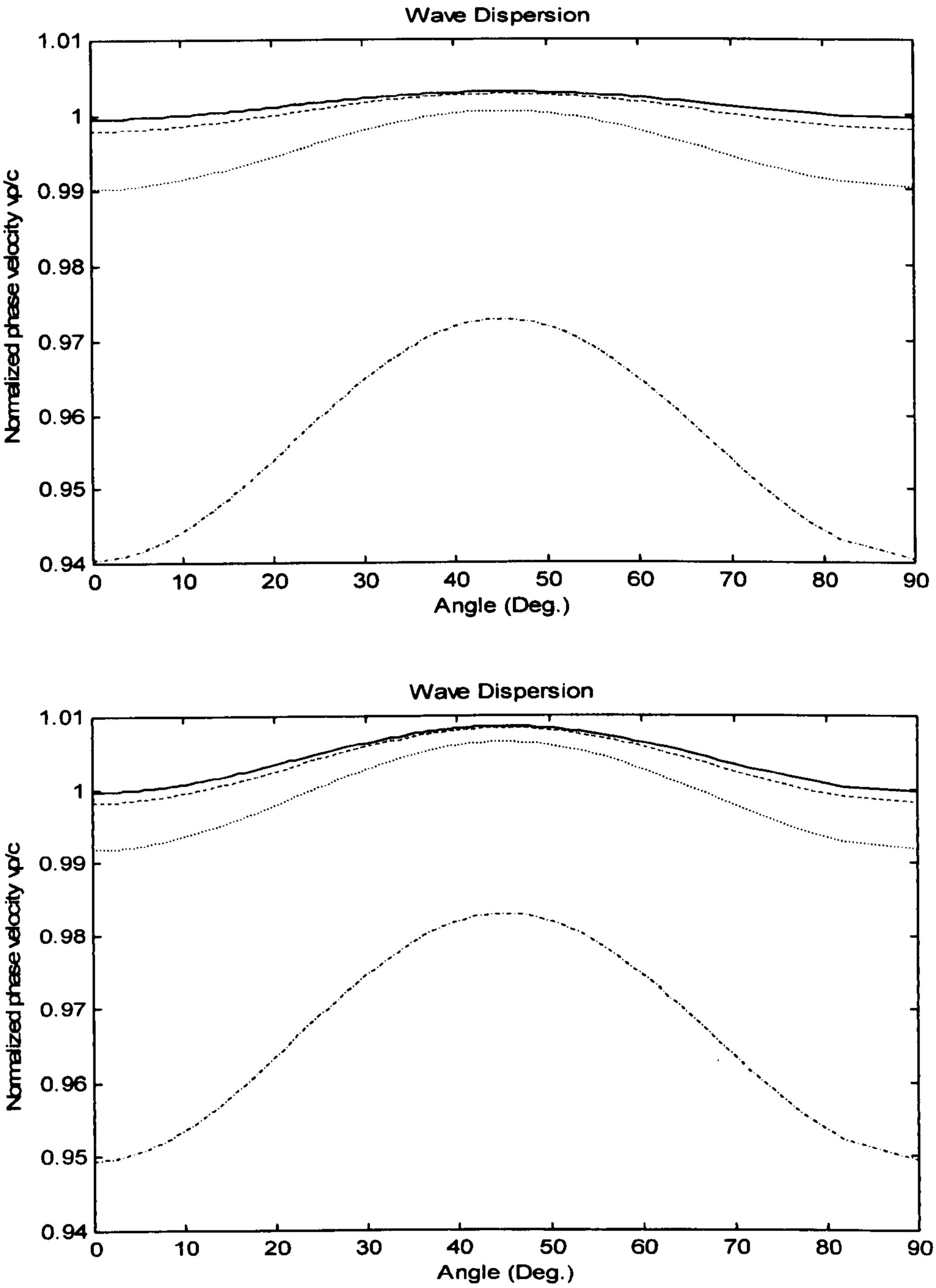

Fig.3.16. Dispersion of the phase velocity vs. angle of the wave propagation with respect to the grid. The cell size is, $\Delta x=\Delta y=0.15\lambda$ (Top) and $\Delta x=\Delta y=0.2\lambda$ (Bottom). (Solid Line: 8^{th} order, Magenta line: 6^{th} order, Black Dot Line: 4th Order FDTD, Red line: FDTD).

3.6 Conclusions of the Chapter III.

This chapter has been devoted to the investigation of new techniques on FDTD electromagnetic analysis, searching for new algorithms in order to avoid some of the limitations of the classical Yee's algorithm, such as the implementation of ABC's, free space nodes calculation, heavy oversampling of the fields, etc. For this a theoretical study of the FDTD discrete equation has been performed, using the classical discrete systems theory both in the real and spectral domain. Higher order FDTD schemes has been also investigated to improve the dispersion of the algorithm. Finally examples on the DGF-FDTD technique have been implemented. The result of this study can be summarized on the following points:

- The FDTD method is described as a system. In a homogeneous and linear region the method can be represented either by finite difference equations or as a discrete convolution of the currents with the impulse response or Discrete Time Domain Green's Function (DGF) for FDTD.
- The FDTD equations use first central differences, but are strongly related to second order finite difference equations, in particular to the finite difference scalar wave equation. The DGF for FDTD and the scalar FD wave equation are directly related.
- The analytical formula of the DGF for the FDTD system is given in Eq.3.35 using the DGF for the scalar wave equation Eq.3.34. The DGF is obtained as a superposition of Jacobi polynomials. The inner structure and all the properties of FDTD are contained in the DGF
- Using the DGF, the FDTD method can be implemented as a discrete convolution sum which produces exactly the same result as that of the Yee algorithm for FDTD based on finite difference equations.
- Although DGF FDTD is equivalent to the Yee algorithm, it does not require ABC. The steps $\Delta x, \Delta y, \Delta z, \Delta t$ are the same as for the Yee algorithm in order to ensure stability and low dispersion of the grid. However the sampling rate of the field and currents can be reduced close to the Nyquist criteria combining FFT or Wavelets analysis along with the DGF FDTD method
- The DGF FDTD method has been demonstrated by solving scattering problems in the time domain and computing any antenna parameters (antenna pattern, impedance). Despite DGF FDTD being equivalent to the Yee algorithm, it does not require ABC and only the currents on the scatterer need to be stored.

- The DGF FDTD can lead to large reductions in memory storage for modelling 1D or thin objects (wires, slots), but implemented in a straightforward manner require a much large number of operations per time steps than conventional FDTD.
- The DGF FDTD can provide an exact ABC condition for the FDTD Yee algorithm, using the principle of equivalence between fields and currents. The concept has been demonstrated for a single wall of an FDTD grid with reflectivities of –110dB on the boundary. The main reason for this reflectivity is the finite precision of floating points in computers which reduces the computed accuracy of the DGF.
- The DGF FDTD can be combined with FFT algorithms to increase its performance. The idea has been applied to the DGF ABC in a wall. This technique produces an exact ABC for FDTD that is also very efficient from the numerical point of view since it uses reduced sampling, but is only useful for waveguide or periodic structure problems.
- General formulas for higher order FDTD algorithms are obtained using the generalised finite difference concept.
- Higher order schemes can be used to improve the accuracy of the spatial derivatives (Spatially low dispersive schemes). However, the wave dispersion is not improved by this type of higher order algorithms, unless the time step is decreased accordingly. The classical fourth order FDTD is a good compromise between accuracy and time step duration. However, higher order algorithms such as the MRD in [3] (equivalent to 18^{th} order) require a time step five to ten times smaller than the Courant limit. These techniques minimise the anisotropy of the method.
- A different approach is to compensate the dispersion of time and spatial finite difference schemes (space time low dispersion algorithms). This technique minimise the wave dispersion at discrete propagation angles. Although dispersion for these schemes are anisotropic, they are a good alternative to the spatially low dispersion schemes since no reduction of the time step size is required.

In general terms, the classic Yee algorithm is based on the estimation of the EM field at certain time instant using the current density as field source [1]. The DGF FDTD scattering algorithm calculates the density of current at a certain time instant using the incident field as source of the induced currents. This is the main reason for the different performance of both algorithms. The density of current only exists in cells where the scatterers are placed, but the EM field exists elsewhere. The DGF method only deals with the cells forming the scatterers. Ideally, Yee's algorithm deals with all the cells where the EM field is not zero. In this way, ABC's can be considered special algorithms, which provide the Yee algorithm with

termination into a finite volume. These considerations are very important to understand the different usage of computer memory (Table 3.1).

Antenna type	DGF FDTD unknowns	FDTD unknowns	Expected Ratio
Wire, Slot	$N_{scatterers}\ N_{time}$	$N_x\ N_y\ N_z$	0.1 to 0.01
Planar, Patch	$N_{xsca}\ N_{ysca}\ N_{time}$	$N_x\ N_y\ N_z$	0.1 to 1
Volume, horn, dielectric antenna	$N_{xsca}\ N_{ysca}\ N_{zsca}\ N_{time}$	$N_x\ N_y\ N_z$	1 to 10

Table 3.1 Number of unknowns for DGF FDTD calculations

Table 3.1 shows the number of unknowns required for the Yee and DGF algorithms. Yee'algorithm always requires a rectangular grid (6 components) able to contain the antenna plus the layers used for ABC and some safety cells between the ABC and the antenna. The DGF algorithm basically requires to store the currents on the antenna for a number of previous time instants. The number of time steps is determined by the time required by the wave to cross the object. For wire and slot antennas that can be represented by a small number of electric/magnetic current cells, thus the DGF requires much less memory storage (expected from 10 to 100 times) than Yee's algorithm (including the ABC). This situation is reversed for modeling volume antennas (e.g. a dielectric rod) since it would be necessary to use a large number of current cells.

On the other hand, the induced current on a cell depends on the rest of the induced currents on the scatterer. For the Yee algorithm the EM field at a cell only depends on the EM fields at the surrounding cells. Using directly equation 3.19, the number of computations per time step is in the order of $N_{scat}^2 \cdot N_{time}$. As a consequence, computations rise very quickly as the number of scatterers increase. So, the direct implementation of equation 3.19 requires larger computation time than normal FDTD even for wire and slot antennas of some complexity. However, under certain conditions the DGF can be implemented using FFT as for the DGF ABC. Wavelets or other discrete wave expansion techniques are also well suited to be combined with Eq. 3.19. These techniques are out of the scope of this work, but an estimation

of the number of computation are given in table 3.2 for a FFT method, including a decimation factor to take into account the reduction of field samples used by this technique.

Method	Number of computations
FDTD	$N_x \cdot N_y \cdot N_z$
DGF FDTD	$N_{scat}^2 \cdot N_{time}$
DGF FDTD & FFT (estimated)	$\frac{N_{scat}}{N_{decim}} \cdot N_{time}$

Table 3.2 Number of unknowns for DGF FDTD calculations

Regarding future work that can be derived from this chapter, the DGF FDTD algorithm has a significant potential to solve time domain EM problems especially when used jointly with the classical FDTD Yee algorithm. The DGF FDTD technique is suitable for combining with FFT, as shown in the single wall DGF ABC, producing high performance algorithms, which are compatible with the Yee algorithm.

Future work on the DGF method must exploit the ability of the technique to be combined with DSP techniques. The convolution algorithm is quite suitable to be implemented using discrete Fourier or Wavelet expansions of the density of current nodes. The result of using these techniques will be the reduction of the number of field and current samples to be stored and computed, since the heavily oversampled FDTD grid can be decimated at a rate close to the Nyquist criteria.

The DGF techniques are quite suitable to implement boundary conditions for the FDTD Yee's algorithm, using the exact principle of equivalence between fields and currents in the FDTD grid. Future work can deal with exact 3D formulations of the ABC, boundary conditions in a multi-region FDTD, and to obtain reflectionless interface problems between subgridded FDTD meshes.

3.7 References of the Chapter III.

[1] K.S. Yee,'Numerical solution of initial boundary problems involving Maxwell's equations in isotropic media', *IEEE Transactions on Antennas and Propagation*, vol 14, 1966, pp 302-307.

[2] A.Taflove, "Computational Electrodynamics: The Finite Time Domain Method", Artech House 1995.

[3] M. Krumpholz, L. P. B. Katehi, 'MRTD: New Time-Domain Schemes Based on Multiresolution Analysis'. *IEEE Transactions on Antennas and Propagation*, vol 44, , pp 555-571,.April 1996

[4] J. M. Johnson and Y. Rahmat-Samii, 'MR/FDTD: Multiple Region Finite Difference Time Domain Method', *Microwave and Optical Technology Letters*, vol 14, pp. 101-105, February 1997.

[5] A.V. Oppenheim, "Discrete Time Signal Processing", Prentice Hall,1989

[6] D. M. Sullivan, "Z transform Theory and the FDTD Method", *IEEE Trans. Antennas and Propagation*. vol 44, pp 28-34, January 1996.

[7] W.W. Chew, "Waves and Fields in Inhomogeneous Media", Chapter 1, pp.1-29, IEEE Press, 1995.

[8] C. Jordan, "Calculus of Finite Differences",Chelsea Publishing Company,NY 1960.

[9] G. Boole, "A Treatise on the Calculus of Finite Differences", Macmillan, London 1880.

[10] M. Abramowitz, I.A. Stegun, "Handbook of Mathematical Functions", Chapter 22, pp.773-785, Dover Publications,NY 1965.

[11] C.A. Balanis, "Advanced Engineering Electromagnetics", Chapter 12, pp. 697-717. John Wiley&Sons, 1989.

[12] A.Taflove, M.E.Brodwin, 'Numerical Solution of steady-state electromagnetic scattering problems using the time dependent Maxwell's equations", *IEEE Trans. Microwave Theory and Techniques*. vol.23,1975 pp 623-630

[13] D. S. Katz, E. T. Thiele and A. Taflove, 'Validation and extension to three dimensions of the Berenger PML absorbing boundary condition for FDTD meshes', *IEEE Microwave and Guided Wave Letters*,vol 4 Nov.1994, pp.268-270.

CHAPTER IV: MODELING OF PERIODIC STRUCTURES WITH FDTD

4.1 Introduction

Periodic structures are being used extensively in antenna and circuit technology in many practical devices as array antennas, transmission line and waveguide filters, corrugated horns, Frequency selective surfaces, etc. Nowadays, periodic structures themselves are being investigated, for instance, to obtain artificial crystals with a complete '*photonic band gap*', a frequency band in which no electromagnetic radiation is allowed to propagate. Other new developments using periodic structures are the arrays of integrated antennas. In this case, active and nonlinear elements are introduced in the array to obtain distributed amplifiers, mixers or oscillators.

FDTD can introduce some advantages to model periodic structure devices. First of all, it is a time domain method, which can handle nonlinear/active devices in the structure in order to model arrays of detectors or amplifiers [1]. FDTD can provide an accurate 3D modeling of the periodic structure including metallic and dielectric parts of arbitrary shape.

The frequency domain modeling of these infinite periodic structures can take advantage of the periodicity properties to reduce the modeling just to one periodic cell of the structure. This can be done using modal expansions of the field [2](the so-called *Bloch mode*), or introducing special boundary conditions that ensure periodicity.

It is possible for FDTD to implement boundary conditions to calculate the complete response of the structure from just one periodic cell. This chapter describes how this boundary condition for periodic media can be obtained for the FDTD algorithm.

There are special difficulties in implementing a periodic boundary condition in time domain. These problems arise when the sources of the field excite each part of the periodic structure at different time instants, and the time domain method computes the field in a causal way (This is the case of FDTD).

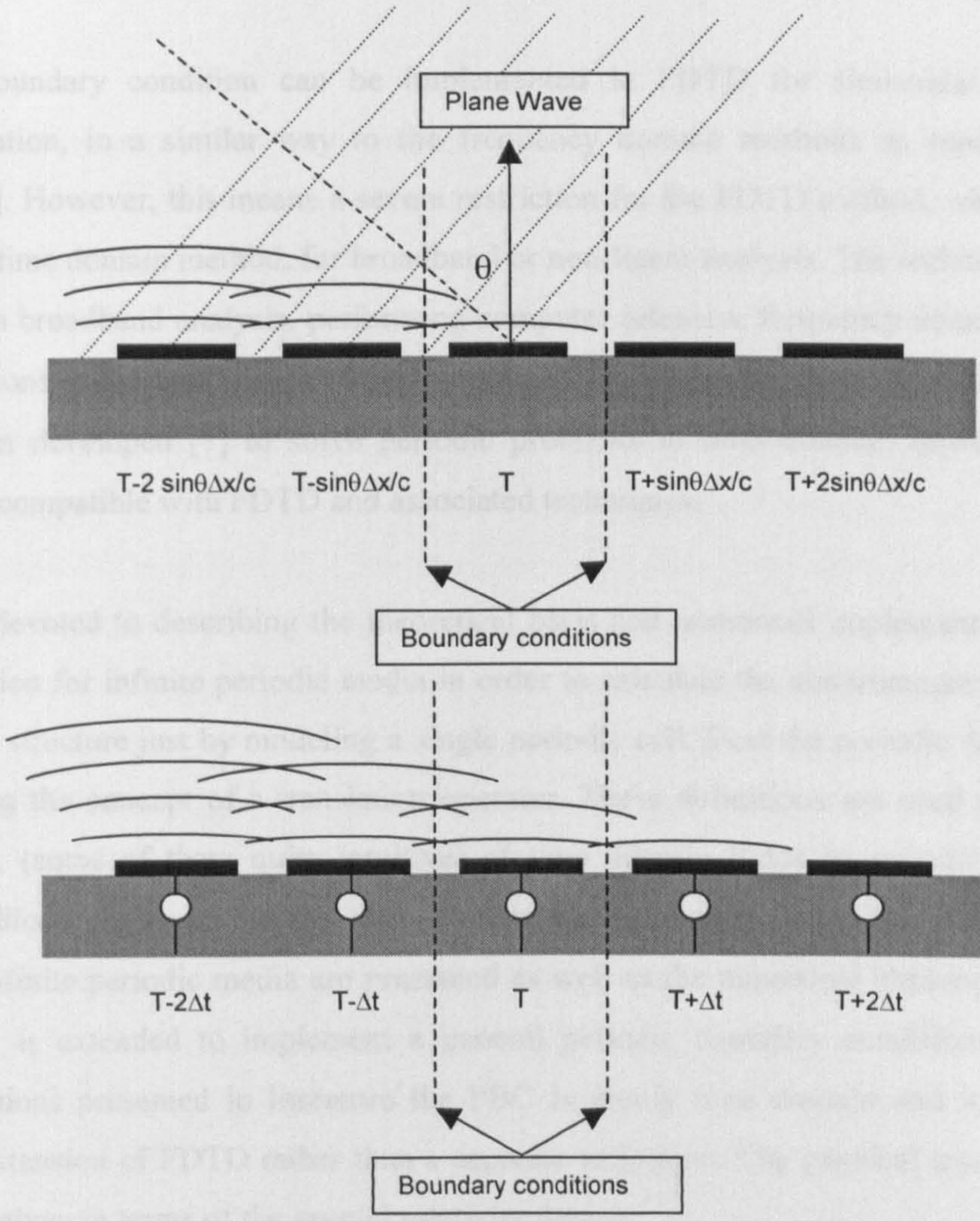

Fig. 4.1. The field at a given periodic cell depends of the scattering at adjacent cells on previous time instants. The boundary condition is not causal since it requires future values of the field as input to estimate the boundary condition at present.

This situation occurs for example, in an infinite phase shift array, the excitation source is applied with a time delay to each element and in an infinite dichroic surface which is scattering a plane wave under oblique incidence (see Fig.4.1). In these cases, the computation of the field from a single periodic cell will require to have knowledge of the field previously scattered by the cells of the neighborhood. As the method is causal, there is no means to predict the fields produced at previous time instants outside the periodic cell which is being modeled. In the frequency domain methods [3], the prediction of fields at a future time instant can be made on the grounds that the fields are sinusoids at a single frequency in steady state, so a time delay can be computed as a phase shift in the sinusoidal behavior.

The periodic boundary condition can be implemented in FDTD for sinusoidal, single frequency excitation, in a similar way to the frequency domain methods as reported in literature [4], [5]. However, this means a severe restriction for the FDTD method, which can not be used as a time domain method, for broadband or non-linear analysis. The technique has been extended to broadband analysis, performing computer intensive frequency domain-time domain conversions at the boundary of the periodic cell [6]. Recently, a specific numerical method has been developed [7] to solve periodic problems in time domain, however the technique is not compatible with FDTD and associated techniques.

This chapter is devoted to describing the theoretical basis and numerical implementation of boundary condition for infinite periodic media in order to calculate the electromagnetic field dispersed by the structure just by modeling a single periodic cell. First the periodic functions are defined using the concept of a translation operator. These definitions are used to show some properties. (some of them quite intuitive) of time domain fields in periodic media, including the '*Bloch theorem*' for the time domain fields. Finally, the FDTD boundary conditions for infinite periodic media are presented as well as the numerical implementation of them. FDTD is extended to implement a general periodic boundary condition (PBC). Unlike the solutions presented in literature the PBC is purely time domain and it can be considered an extension of FDTD rather than a separate technique. The physical meaning of the technique is given in terms of the special relativity theory.

4.2 Electrodynamics on periodic media

4.2.1 The translation operator.

Physical objects and laws have often symmetry properties. Symmetry basically means that these objects and laws remain the same after certain associated transforms (i.e. a geometrical rotation). The symmetry properties can be used to reduce the complexity of a problem, for instance, the problem can be solved for a limited region and the complete solution can be built using the symmetry transformations. In fact, these techniques have been used extensively in electromagnetics (i.e. the image theory), using the basic symmetry properties of the boundary conditions. Finally, the concept of symmetry and invariance is of major importance for modern physics since all valid physical laws have to be invariant to a set of basic transforms and symmetries.

Periodicity can be considered as a special kind of symmetry. In this case, the system is unchanged if everything is translated at certain direction and distance [8]. In a formal way, the translation can be defined as an operator (Eq. 4.1).

$$T_{\overline{X}} \cdot g(\overline{x}) = g(\overline{x} + \overline{X}) \qquad \overline{x} = (x, y, z, t) \qquad \overline{X} = (L_x, L_y, L_z, T) \qquad \text{(Eq 4.1)}$$

$T_{\overline{X}}$ is the translation operator on the four dimensional function $g(\overline{x})$ and the vector $\overline{X}$ represents the displacement of the system in four dimensions (see Fig. 4.2).

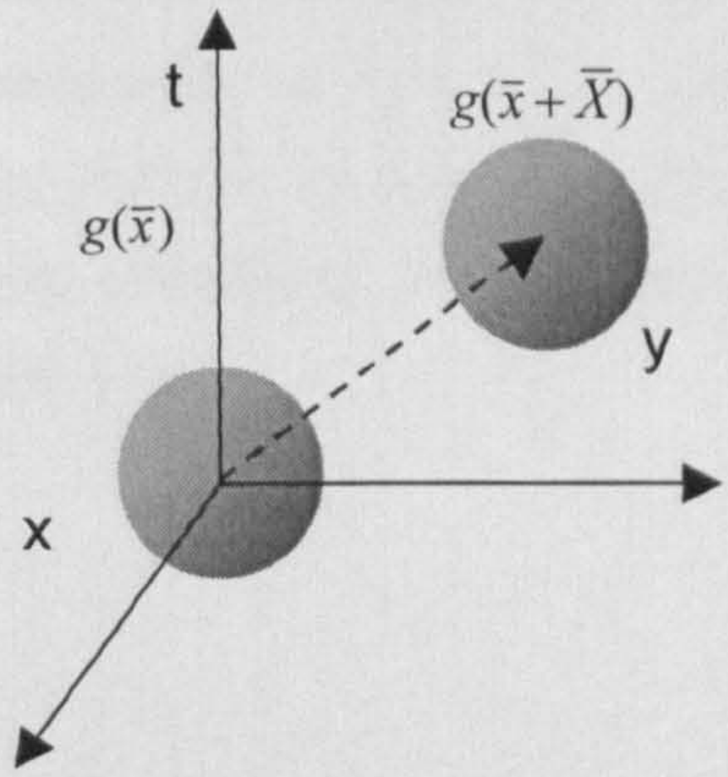

Fig. 4.2 Translation of a distribution g by a vector $\overline{X}$

The translation operator can commute with common operations of functions such as sum or multiplication. It also commutes with any linear, invariant and stable operator (Eq. 4.2)

$$T_{\bar{X}}(g+h) = T_{\bar{X}} \cdot g + T_{\bar{X}} \cdot h$$

$$T_{\bar{X}}(gh) = T_{\bar{X}} g \cdot T_{\bar{X}} h$$

$$T_{\bar{X}}(\lambda g) = \lambda T_{\bar{X}} \cdot g \quad \lambda \text{ constant}$$

$$T_{\bar{X}}(\Theta g) = \Theta(T_{\bar{X}} \cdot g) \quad \Theta \text{ Linear, invariant operator}$$

(Eq.4.2)

4.2.2 Periodic Functions

A Periodic system can be defined as those that remain unchanged after a translation. The translation operator can be used to write this definition in a simple way (Eq. 4.3)

$$T_{\bar{X}} \cdot g(\bar{x}) = g(\bar{x}) \qquad \text{(Eq.4.3)}$$

This is the basic condition for a function to be periodic with period $\bar{X}$. It is easy to show that the condition of Eq.4.3 can be satisfied for period vectors $n\bar{X}$, but the period $\bar{X}$ is defined as the vector with the smallest absolute value in Eq.4.3. The properties of the translation operator (Eq.4.2) can be used to show that the sum and product of periodic functions are also periodic. A periodic function is also obtained by a linear invariant transformation (i.e. a derivative or a Laplacian) of a periodic function.

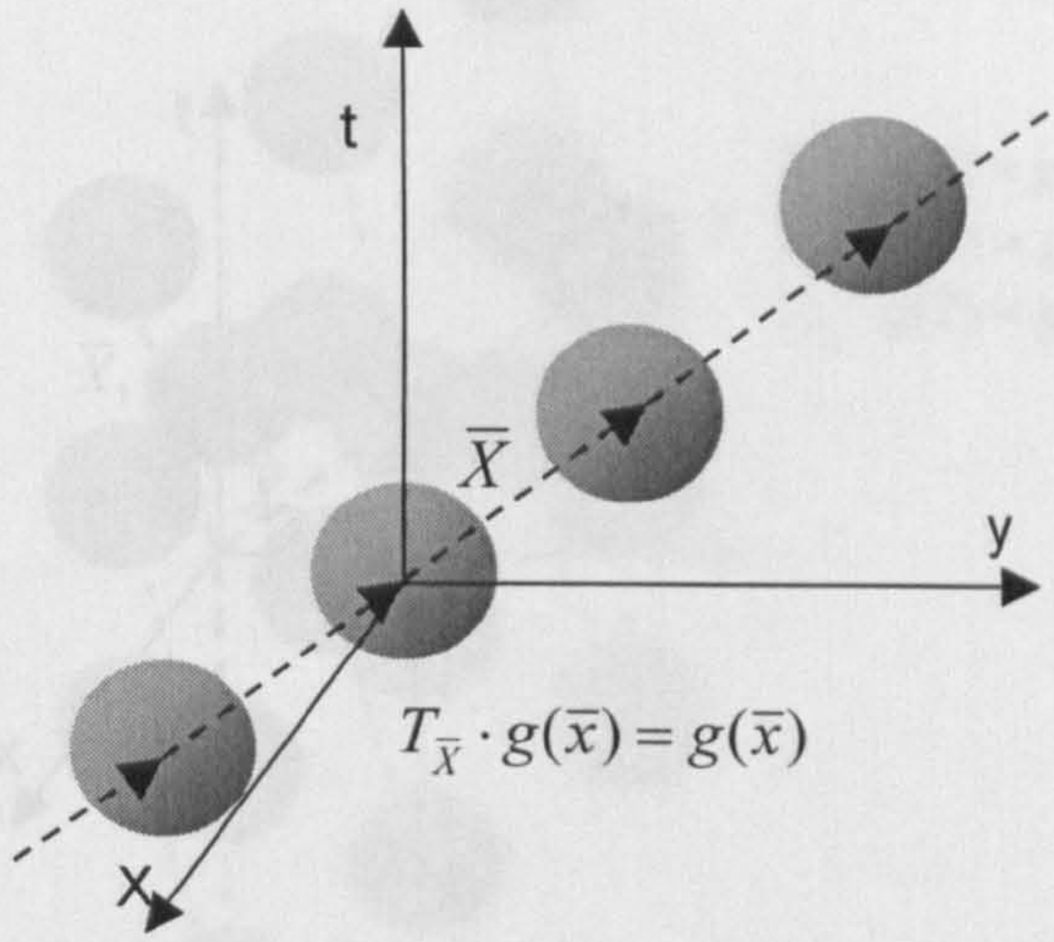

Fig. 4.2 Periodic function with period $\overline{X}$

A function can be simultaneously periodic for several periodic vectors $\overline{X}$ that are linearly independent. This means that in a physical space of four dimensions, the state functions can be periodic in up to four directions in space-time. Each of these vectors will be called a *lattice vector* by analogy with the term used in crystallography.

$$T_{\overline{X}_i} \cdot g(\overline{x}) = g(\overline{x})$$

$$i = 1,2,3,4 \quad \overline{X}_i \text{ linearly independent} \qquad \text{(Eq.4.4)}$$

A function verifying Eq.4.4 is periodic in a multidimensional way (Fig.4.3). The lattice vectors of such functions can be a basis of the domain (so-called lattice basis). The periodic function can be built by repeating the elementary volume defined by the lattice basis.

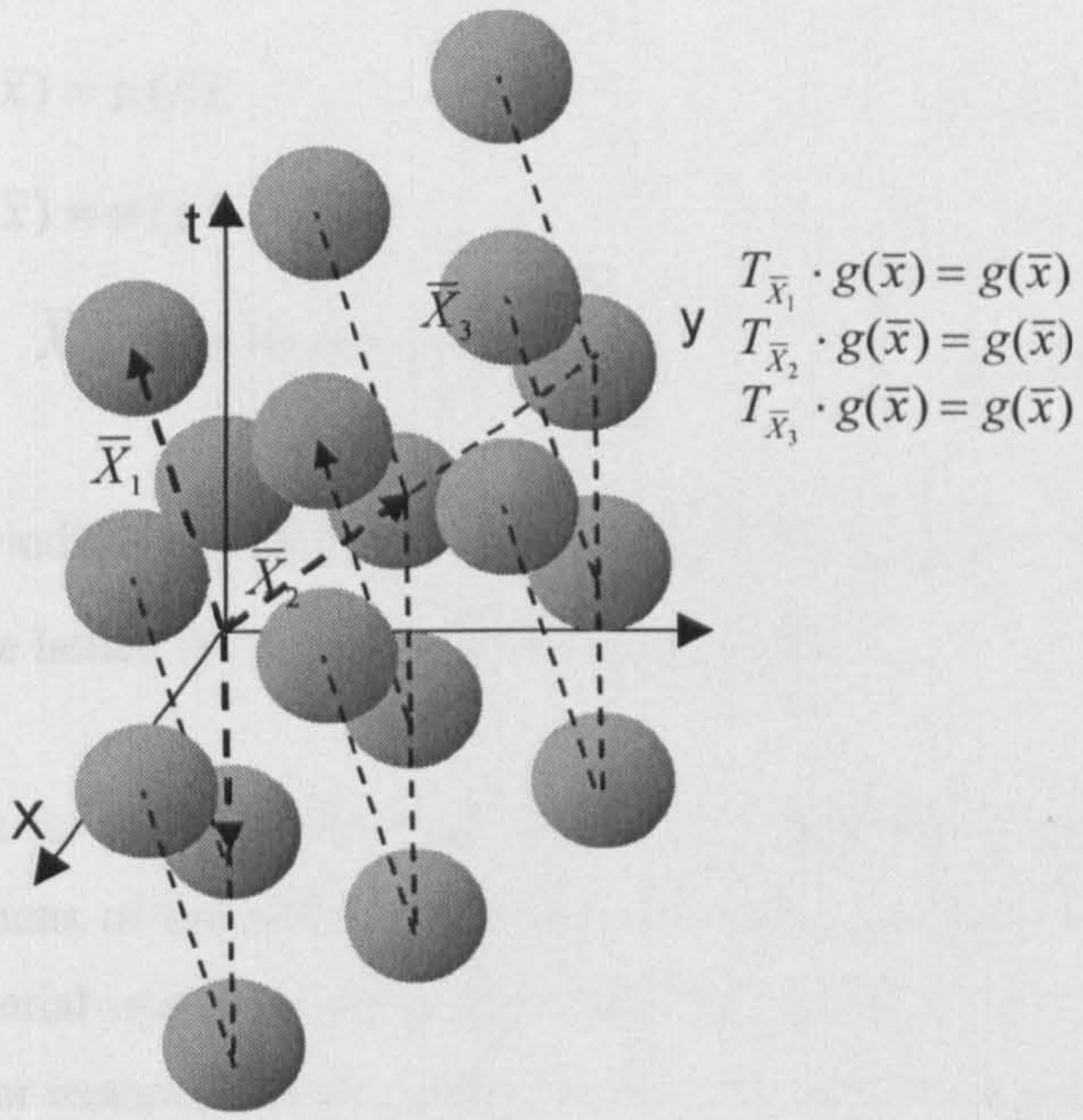

Fig.4.3 Multidimensional periodic function and lattice vectors.

The periodic function can have other kinds of symmetry (i.e. mirror symmetry) apart from discrete translation. In that case the periodic function can be built from a small region into the volume defined by the lattice basis.

Other operators can also be used to extend the definition of periodicity given in Eq.4.3. However the special properties of periodic functions can be limited if those operator can not commute with linear systems.

4.2.3 Time domain electromagnetic field in periodic media.

The interaction of the electromagnetic field with physical media is described by means of the electrical permitivity ε, the magnetic permeability μ, and the conductivity σ. These parameters model the average electrical properties of the media at microscopic level. In general, from the point of view of electromagnetics, a media is periodic when ε, μ, σ are periodic functions with the same lattice vectors $\overline{X}_i$ (Eq.4.5).

$$T_{\bar{X}_i} \cdot \varepsilon(\bar{x}) = \varepsilon(\bar{x}) \qquad \varepsilon(x,y,z,t)$$

$$T_{\bar{X}_i} \cdot \mu(\bar{x}) = \mu(\bar{x}) \qquad \mu(x,y,z,t)$$

$$T_{\bar{X}_i} \cdot \sigma(\bar{x}) = \sigma(\bar{x}) \qquad \sigma(x,y,z,t)$$

$i = 1..n$ $\bar{X}_i$ linearly independent (Eq.4.5)

In this definition of periodicity for electromagnetic media, it is possible for some parameters to be constant or to have lattice vectors of type $n\bar{X}$ (see Fig 4.5).

The Maxwell equations for periodic media are shown in Eq.4.6. The constitutive parameters are now periodic functions of the position and time, so they can not be commuted with the derivatives and differential operators. In general, the field sources are not periodic, but in many practical cases (for instance antenna arrays) the sources can be distributed periodically.

$$\nabla \times \vec{E} = -\frac{\partial\left(\mu(x,y,z,t) \cdot \vec{H}\right)}{\partial t}$$

$$\nabla \times \vec{H} = \frac{\partial\left(\varepsilon(x,y,z,t) \cdot \vec{E}\right)}{\partial t} + \sigma(x,y,z,t) \cdot \vec{E} + \vec{j}_{ext}$$

$$\nabla \cdot \vec{D} = \rho \qquad \nabla \cdot \vec{B} = 0$$

$$\varepsilon(x,y,z,t), \mu(x,y,z,t), \sigma(x,y,z,t) \ \textit{Periodic}$$

(Eq.4.6)

The solutions for the electromagnetic field in Eq.4.6 have a special form due to the periodicity of the media. These properties can be found by applying the translation operator to the Maxwell equations for periodic media. Using the properties of the translation operator (Eq.4.2) it is possible to show that the Eq.4.6 remain invariant to the translation, except for the external current term (Eq.4.7).

$$\nabla \times (T_{\bar{X}} \cdot \vec{E}) = -\frac{\partial\left(\mu(x,y,z,t)(T_{\bar{X}} \cdot \vec{H})\right)}{\partial t}$$

$$\nabla \times (T_{\bar{X}} \cdot \vec{H}) = \frac{\partial\left(\varepsilon(x,y,z,t)(T_{\bar{X}} \cdot \vec{E})\right)}{\partial t} + \sigma(x,y,z,t) \cdot (T_{\bar{X}} \cdot \vec{E}) + T_{\bar{X}} \cdot \vec{j}_{ext}$$

$$\nabla \cdot (T_{\bar{X}} \cdot \vec{D}) = T_{\bar{X}} \cdot \rho \qquad \nabla \cdot (T_{\bar{X}} \cdot \vec{B}) = 0$$

$$\varepsilon(x,y,z,t), \mu(x,y,z,t), \sigma(x,y,z,t) \text{ Periodic}$$

(Eq.4.7)

In the case where the sources of the field are also periodic, the Maxwell's equations after the translation remain the same. This implies that also the field solution must remain invariant to the translation. This shows the intitutive property that the fields must be periodic if the media and the sources are periodic.

$$T_{\bar{X}} \cdot \vec{j} = \vec{j} \;\Rightarrow\; T_{\bar{X}} \cdot \vec{E} = \vec{E} \quad T_{\bar{X}} \cdot \vec{H} = \vec{H} \qquad \text{(Eq.4.8)}$$

In the general case, the sources are not periodic, so the fields are not periodic. On the other hand, an arbitrary distribution of current can be considered as the superposition of harmonic sources using Fourier transform as shown in Eq.4.9. These elementary harmonic functions are not periodic because of a constant term (λ in Eq.4.9).

$$\vec{j}_{ext} = \int \vec{J}(k_x, k_x, k_x, \omega) \cdot e^{j(k_x x + k_y y + k_z z + \omega t)} dk_x dk_y dk_z d\omega$$

$$\vec{j}_{k_x k_y k_z \omega} = e^{j(k_x x + k_y y + k_z z + \omega t)} \qquad T_{\bar{X}} \cdot \vec{j}_{k_x k_y k_z \omega} = \lambda \cdot \vec{j}_{k_x k_y k_z \omega}$$

$$\lambda = e^{j(k_x L_x + k_y L_y + k_z L_z + \omega T)} \qquad \bar{X} = (L_x, L_y, L_z, T) \qquad \text{(Eq.4.9)}$$

This harmonic source can be introduced in Eq.4.7. The result is that the field is also a eigenfunction of the translation operator with a eigenvalue λ. In order to fullfil this condition, the field solutions with the harmonic source have to be periodic function multiplied by a elementary harmonic function. This principle is the *Bloch Theorem* [2],[8] for a 4 dimensional periodic system (Eq.4.10).

$$T_{\bar{X}} \cdot \vec{j}_{k_x k_y k_z \omega} = \lambda \vec{j}_{k_x k_y k_z \omega} \Rightarrow T_{\bar{X}} \cdot \vec{E}_{k_x k_y k_z \omega} = \lambda \vec{E}_{k_x k_y k_z \omega} \text{ where } \lambda = e^{j(k_x l_x + k_y l_y + k_z l_z + \omega T)}$$

Assuming $\vec{E}_{k_x k_y k_z \omega} = \vec{U}_{k_x k_y k_z \omega} \cdot e^{-j(k_x x + k_y y + k_z z + \omega t)}$ where $\vec{U}_{k_x k_y k_z \omega}$ is an arbitrary function

$$T_{\bar{X}} \vec{E}_{k_x k_y k_z \omega} = T_{\bar{X}} (\vec{U}_{k_x k_y k_z \omega}) \lambda e^{-j(k_x x + k_y y + k_z z + \omega t)} = \lambda \vec{E}_{k_x k_y k_z \omega} \Rightarrow T_{\bar{X}} \cdot \vec{U}_{k_x k_y k_z \omega} = \vec{U}_{k_x k_y k_z \omega}$$

$$\Rightarrow \vec{U}_{k_x k_y k_z \omega} \text{ is an periodic function} \qquad \text{(Eq.4.10)}$$

(Bloch Theorem)

The $\vec{U}_{k_x k_y k_z \omega}$ periodic function can be expanded as a Fourier series. Each exponential term of the series multiplied by the exponential harmonic term in Eq.4.10 is the kernel of the *Bloch modes*. As any source can be expanded as a sum of harmonic functions, the total field generated by an arbitrary source can be considered as the superposition of fields of the type shown in Eq.4.10.

4.3 Extended FDTD in Periodic Media.

4.3.1 Periodic boundary conditions

In the previous section it was shown that the electromagnetic field in periodic media with periodically distributed sources can be also described as a periodic function. This result is applicable to many practical situations of periodic media as infinite antenna arrays of dichroic surfaces illuminated by plane waves. This periodical behavior can be used to calculate the fields by solving the problem just for one periodic cell, since the the rest of the fields can be obtained easily by simple translation of the fields on a single cell. This means that the electromagnetic problem can be solved in a finite size volume, but it is necessary to develop a procedure to solve the problem at the boundary of this volume and enforce the periodicity at the same time.

The boundary condition is obtained by assuming that the field solution and its derivatives can be obtained by a translation of the field cell , so the fields outside the periodic cell that are necessary to calculate the fields at the boundary can be simply be estimated by the fields inside the cell by a translation (Fig.4.5). In order to apply this condition it is necessary that the boundary of the region being modeled has to be the same boundary that forms the periodic cell (true for both time and space coordinates).

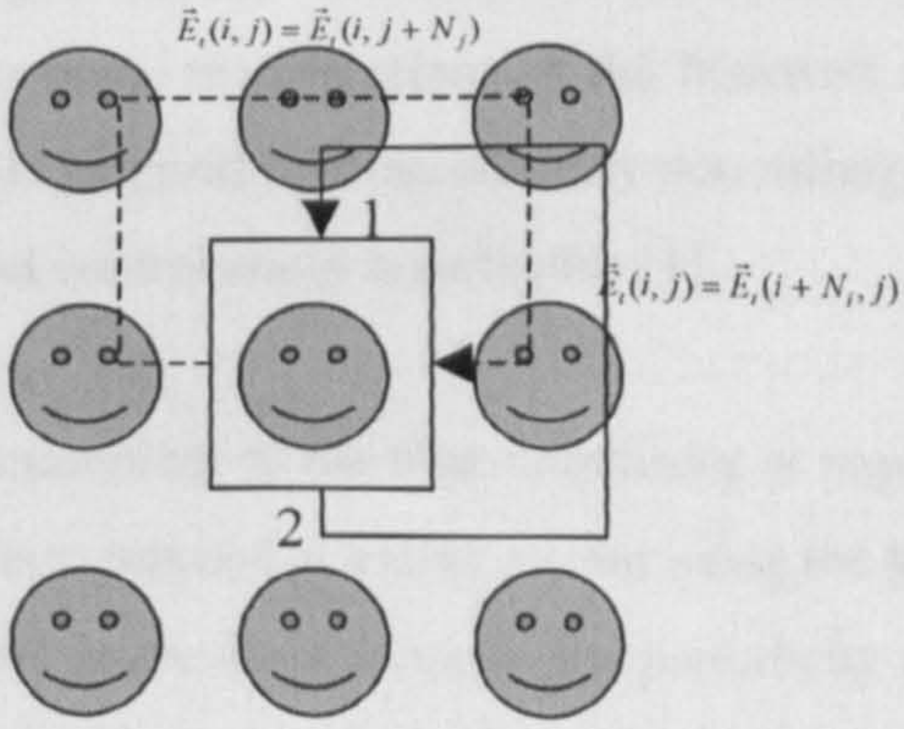

Fig.4.5 The periodic boundary condition: The field outside the boundary in point 1 can be obtained from the field inside the boundary at position 2.

FDTD usually requires a regular grid of points alongside the cartesian axis. As a consequence, if the periodicity does not follow an orthogonal pattern, it is not possible to fit directly the

discrete grid of points defined by the FDTD method into the periodic cell (Fig.4.6). This problem of applying the boundary condition can be solved by interpolation.

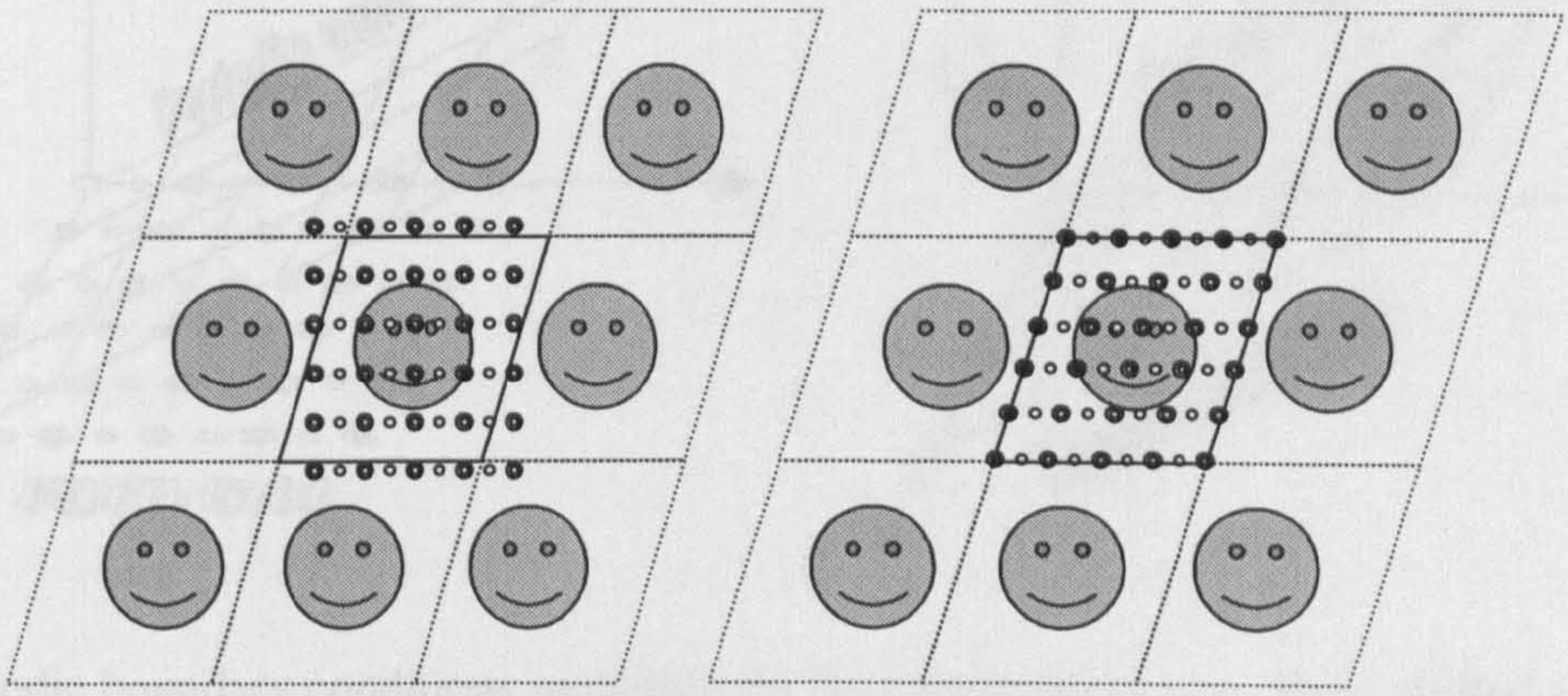

Fig.4.6. The basic FDTD algorithm is defined in a cartesian ortogonal basis. As a consequence, the discrete points for the fields are distributed in a rectangular mesh that is not well suited to apply periodic boundary condition in all cases. The FDTD method can be redefined in the lattice basis.

However, an alternative procedure is obtained by expressing the equations in the lattice basis coordinates, so now the regular grid matches the shape of the boundary of the periodic cell. This basis change only introduce some modifications of the Maxwell equations that can be implemented in FDTD . The FDTD algorithm in an arbitrary non orthogonal basis is obtained using the concept of covariant and contravariant coordinates [1].

The FDTD method also requires sampling of the time coordinate at regular steps, in addition, the method is causal so the field is computed at a time instant using the knowledge of the field at previous time instants. As stated in previous sections, the periodicity of the problem can be essentially four dimensional (for instance the phase shifted array), with field sources that do not act simultaneously in every space periodic cell.

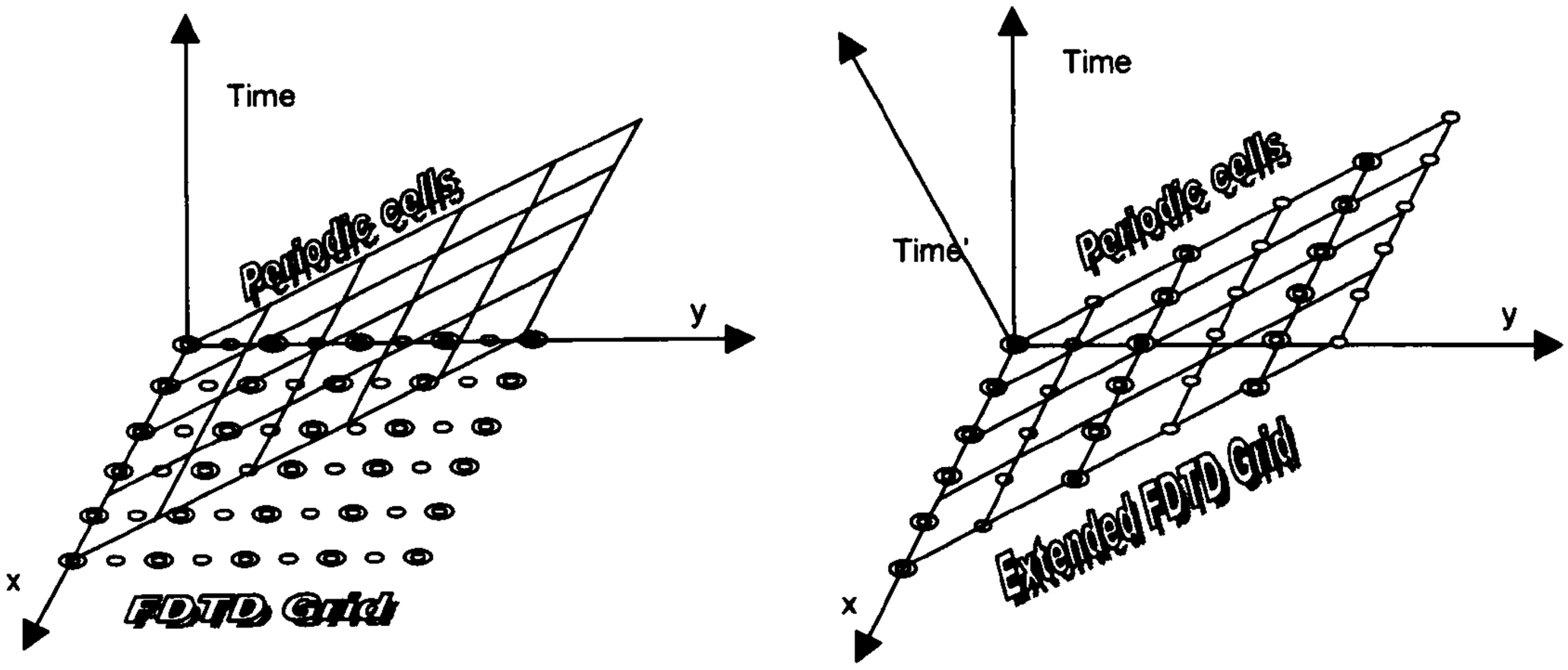

Fig.4.7 Periodic boundary conditions including the time dependance (i.e. phase shifted array) is not well suited for the FDTD grid which represent field at a single time instant.

The typical space-time FDTD grid is not well suited to handle periodic boundary conditions for these situations since the boundaries of the periodic cells are now at different time instants (Fig. 4.7). If the FDTD grid is maintained, an extrapolation procedure is required to predict the fields at future time instants. This is possible for sinusoidal signals in steady state, since the estimation of the field at future time instants can be obtained as a simple phase delay on the sinusoidal response. However, in that case the periodic boundary conditions for the FDTD method is restricted to monocromatic sources and linear media.

For the more general case, the problem can be tackled using a change of basis for the time coordinate. The lattice vectors including its time component are the new coordinate basis to solve the EM fields (Eq.4.11). In this way, the periodic boundary condition can be applied directly in the new time coordinates, but the Maxwell equations in the new basis have extra terms that must be included in the FDTD algorithm.

$$t' = t + \vec{\alpha} \cdot \vec{r} \qquad \overline{X} = (L_x, L_y, L_z, T),\ \vec{\alpha} \cdot \overline{X} = -T \Rightarrow \overline{X}' = (L_x, L_y, L_z, 0) \qquad \text{(Eq.4.11)}$$

Where α is a suitable 3D spatial vector constant with inverse velocity units. In the new basis, the lattice vectors should have no time component. This transformation can be introduced into the Maxwell's equations. New terms are generated for the equations that can be written by using new field functions, $\vec{E}h$ and $\vec{H}e$.

$$\nabla \times \vec{H} = \varepsilon \frac{\partial \vec{E}h}{\partial t'} + \vec{j}' \qquad \nabla \times \vec{E} = -\mu \frac{\partial \vec{H}e}{\partial t'}$$

$$\vec{E}h = \vec{E} + \varepsilon^{-1}\left(\vec{\alpha} \times \vec{H}\right) \qquad \vec{H}e = \vec{H} - \mu^{-1}\left(\vec{\alpha} \times \vec{E}\right)$$

$$\bar{x} = (x, y, z, t') \qquad \text{(Eq.4.12)}$$

A finite difference algorithm has been developed to solve the set of equation (Eq.4.12). The extra terms in the Maxwell equations after the transform, introduce additional memory requirements for the algorithm. In addition, the basic FDTD code has to be modified to take into account these terms, so it is not possible to use an existing FDTD code to implement a time domain code for periodic structures. However, there is a possible way to avoid this problems. Instead of using just the time transform (Eq.4.11) , it is possible to use the Lorentz transform.

Lorentz's Transforms

$$x' = \gamma \cdot (x - vt) \qquad y' = y \qquad z' = z \qquad t' = \gamma \cdot \left(t - \frac{v}{c^2} x\right)$$

$$\gamma = \frac{1}{\sqrt{1 - v^2/c^2}}$$

C velocity of light

V velocity of the observer

(Eq.4.13)

Maxwell equations are invariant to the Lorentz transform. This means that the equations remain formally the same after the transformation, without any additional term, so the basic FDTD algorithm can be used now to solve the problem. The physical meaning of this procedure is clear: Using the Lorentz transform (Eq.4.13), the frame of reference corresponds to a relativistic observer. For this observer, physical laws (including Maxwell equations) remain unchanged, but the perception of an outside static observer can be rather different.

Maxwell curl equation after Lorentz's transform Eq.

$$\nabla \times \vec{H}' = \varepsilon \frac{\partial \vec{E}'}{\partial t} + \vec{j}' \qquad \nabla \times \vec{E}' = -\mu \frac{\partial \vec{H}'}{\partial t}$$

$$\vec{E}' = \bar{\bar{\gamma}} \cdot \vec{E} + Z_0 \cdot \vec{\beta} \times \vec{H} \qquad \vec{H}' = \bar{\bar{\gamma}} \cdot \vec{H} - \vec{\beta} \times \vec{E}/Z_0$$

$$\vec{\beta} = (v_x, 0, 0) \qquad \bar{\bar{\gamma}} = \begin{pmatrix} \gamma^{-1} & 0 & 0 \\ 0 & 1 & 0 \\ 0 & 0 & 1 \end{pmatrix}$$

(Eq.4.14)

For the relativistic observer two simultaneous events can be seen as non simultaneous and viceversa. This strange feature can be used in our problem, for instance an observer moving parallel to a phase shift array can see all the array elements perfectly in phase (without any time delay between them), but a stationary observer will see that each array element has its own phase.

4.3.2 Numerical implementation.

The equations 4.13 have been numerically implemented to demonstrate the ability of the periodic boundary condition and the time transform method to handle a complete 4 dimensional periodic situation. The problem which is intended to be solved is the calculation of the plane wave transmission and reflection coefficients for Frequency Selective Surfaces (FSS) under any angle of incidence.

In this case, the media is essentially periodic in two spatial dimensions. The incident field is a plane wave Gaussian pulse, that propagates at certain angles with respect to the periodic surface. In order to approximate the time derivatives following a central difference scheme, the new field functions $\vec{E}h$ and $\vec{H}e$ defined in Eq.4.13 will be used.

$$\nabla \times \vec{H} = \varepsilon \frac{\partial \vec{E}h}{\partial t'} + \vec{j}' \qquad \vec{H} = A^{-1}(\vec{H}e + \mu^{-1}\vec{\alpha} \times \vec{E}h)$$

$$\nabla \times \vec{E} = -\mu \frac{\partial \vec{H}e}{\partial t'} \qquad \vec{E} = A^{-1}(\vec{E}h + \varepsilon^{-1}\vec{\alpha} \times \vec{H}e)$$

$$A = \begin{pmatrix} 1-c^2(\alpha_y^2+\alpha_z^2) & \alpha_x\alpha_y \cdot c^2 & \alpha_x\alpha_z \cdot c^2 \\ \alpha_x\alpha_y \cdot c^2 & 1-c^2(\alpha_x^2+\alpha_z^2) & \alpha_y\alpha_z \cdot c^2 \\ \alpha_x\alpha_z \cdot c^2 & \alpha_y\alpha_z \cdot c^2 & 1-c^2(\alpha_x^2+\alpha_y^2) \end{pmatrix}$$

(Eq.4.15)

These equations become the normal Maxwell's equations for $\vec{\alpha} = 0$. The structure of the equations are similar to the Maxwell's equations for the new field functions, but the vectors on the each side of the equation are different. In order to be compatible with FDTD, as these equations become the normal Maxwell's equations for $\vec{\alpha} = 0$, the FDTD basic central difference scheme and the alternate gridding of each field component will be maintaned (Fig.4.8).

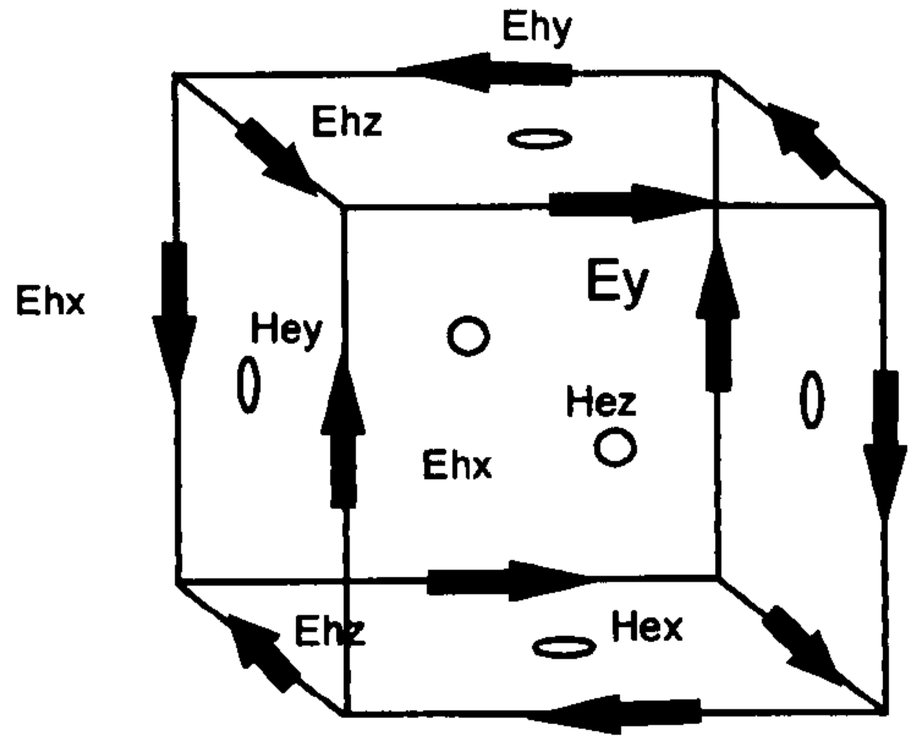

Fig 4.8 The new field components are spatially and temporally alternated, following the FDTD scheme.

However the new system exhibits terms which have time and spatial dependence simultaneously in the same equation. This it is not compatible with a pure central difference scheme of alternated components. The spatial derivatives in that case have to be solved as a second order finite difference. The time finite difference equation it now implicit rather than

explicit since the equations present terms at the same time instant but different spatial positions, so the equation can not be solved in a explicit way.

Implicit schemes can be solved by using an iterative procedure on the equations, by guessing an initial value for the solution at the next time instant and using the new calculation as new initial condition. This procedure makes the algorithm slower and also it requires more memory.

The meaning of the vector α depends on the type of problem proposed. Vector α determines the ratio between spatial period and the time delays between periodic cells. The time delays depends on the incident field. In the case of an incident plane wave these are the time periods needed by the plane wave to cover the lengths of the spatial lattice vectors of the periodic structure. The meaning of vector α for FSS or PBG analysis is now clear as a function of the angles of the incident plane wave (Eq.4.16).

$$\overline{X}_1 = (L_x, 0, 0, T_1), \qquad \vec{\alpha} \cdot \overline{X}_1 = -T_1 \qquad T_1 = \frac{L_x}{c} \sin\theta \cos\phi \Rightarrow \alpha_x = -\frac{\sin\theta \cos\phi}{c}$$

$$\overline{X}_2 = (0, L_y, 0, T_2), \qquad \vec{\alpha} \cdot \overline{X}_2 = -T_2 \qquad T_2 = \frac{L_y}{c} \sin\theta \sin\phi \Rightarrow \alpha_y = -\frac{\sin\theta \sin\phi}{c}$$

(Eq.4.16)

The numerical procedure is similar to the FDTD scheme regarding the terms under the rotational operator and the time derivative. The additonal new term is introduced in the equations in the following way (for the sake of simplicity only one coordinate is shown):

$$He_z^{n+1/2}(i,j,k)^{p)} = He_z^{n-1/2}(i,j,k) + \left(\frac{\Delta t}{\mu}\right) \cdot \left[\frac{E_x^{n(p-1}(i,j,k) - E_x^{n(p-1}(i,j-1,k)}{\Delta y} - \frac{E_y^{n(p-1}(i,j,k) - E_y^{n(p-1}(i-1,j,k)}{\Delta x} \right]$$

$$\vec{E}^{n(p} = A^{-1} \cdot (E\vec{h}^{n(p} + \varepsilon^{-1} \cdot \vec{\alpha} \times (\vec{He}^{n+1/2(p} + \vec{He}^{n-1/2})/2) \quad \text{and} \quad \vec{He}^{n+1/2(0} = \vec{He}^{n-1/2} \qquad \text{(Eq.4.17)}$$

Where p is the index for the iterative algorithm for the implicit equation. A similar expression can be obtained for the Eh field and for the rest of the components. If α_z is set to zero, the algorithm is unstable when the inverse of α is close to the speed of light. This happens for angles of incidence close to 90 degrees to the normal, where there is a singular situation. In principle velocities larger than light speed can be used to analyze the incidence of evanescent waves on the structure.

In this new coordinate system, the boundary condition for the perfect conductor is also changed. The situation is similar to the modification of boundary conditions for a relativistic moving observer. For instance, static surface charge in a media boundary for a stationary observer is observed as surface currents on the conductor for the moving one. In fact, the tangent electric field is zero at the surface of the perfect conductor, but the new field vector Eh is not null since it is also related to the magnetic field. For a layer of perfect conductor on a plane perpendicular to the z axis, the boundary condition can be obtained by setting to zero the Ey and Ex components on Eq.4.12. The final boundary condition is shown in Eq.4.18, introducing the average of field components as they are in different positions.

$$Eh_x = -\frac{Z_0}{c}\alpha_y He_z$$

$$Eh_y = -\frac{Z_0}{c}\alpha_x He_z$$

$$Eh_x^{n+1}(i,j,k) = Eh_x^n(i,j,k) - \frac{Z_0}{c}\alpha_y (He_z^{n+\frac{1}{2}}(i+\tfrac{1}{2},j,k) + He_z^{n+\frac{1}{2}}(i-\tfrac{1}{2},j,k))$$

$$Eh_y^{n+1}(i,j,k) = Eh_y^n(i,j,k) - \frac{Z_0}{c}\alpha_x (He_z^{n+\frac{1}{2}}(i+\tfrac{1}{2},j,k) + He_z^{n+\frac{1}{2}}(i-\tfrac{1}{2},j,k)) \qquad \text{(Eq.4.18)}$$

4.3.3 Test cases.

A computer code has been implemented, in order to demonstrate the method proposed in the previous section. This software calculates the transmission coefficient of a plane wave on a FSS for any angle of incidence and it is capable of modeling thick surfaces and non linear devices in the infinite array. The code simulates the incidence of a plane wave Gaussian pulse on the FSS and it outputs the broadband transmission and reflection of the zero order Floquet mode at the given angle of incidence.

The software is verified using three standard cases of FSS whose transmission coefficient are given in literature [3], [9], [10] for mode matching (MM), method of moment (MoM) and integral equation (IE) computations. The cell dimensions and distribution is depicted in figure 4.8a.

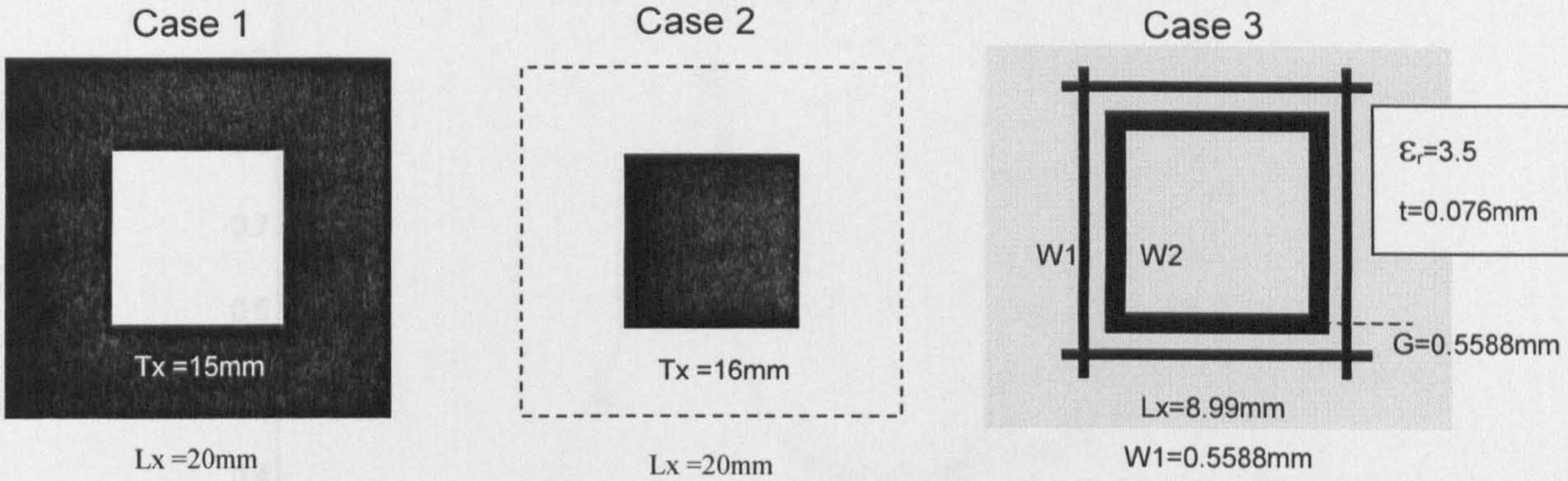

Fig. 4.8a Unit cell for the test cases. Case 1 (Left) mesh of square holes with null thickness. Case 2 (Middle) infinite free standing array of perfectly conducting square patches. Case 3 (Right) Double square loop of metal lines on a thin layer of dielectric (ε_r=3.5, t=0.076mm)

The results show a good agreement of the FDTD calculations with the computations using other methods. Despite there is no measured data, the results of transmission coefficient obtained with Mode Matching are expected to be extremely close to measurements for the simple square geometry. The transmission observed using FDTD match very well in that case for both polarizations. No rigorous criteria for the stability of the method has been developed, but initial analysis suggest that the stability criteria is similar to the courant condition for FDTD but multiplied by $cos\theta$.

The amount of computations required for the oblique incidence case is also bigger than for the normal incidence, due to the extra loop required to solve the implicit equations. The computation time in a PC 300 MHz Pentium, required for the test cases have been about 1h for cases 1&2 (30 Deg. oblique incidence) and 40 min (normal incidence) and 2h (30 deg. oblique incidence) for case 3. The output of the code for the test cases is the transmission and reflection coefficient (TE & TM) at approximately 100 frequency points from 0 to 20GHz. The computer memory required for the test cases is about 6Mb for case3 and 2.5Mb for case 1&2.

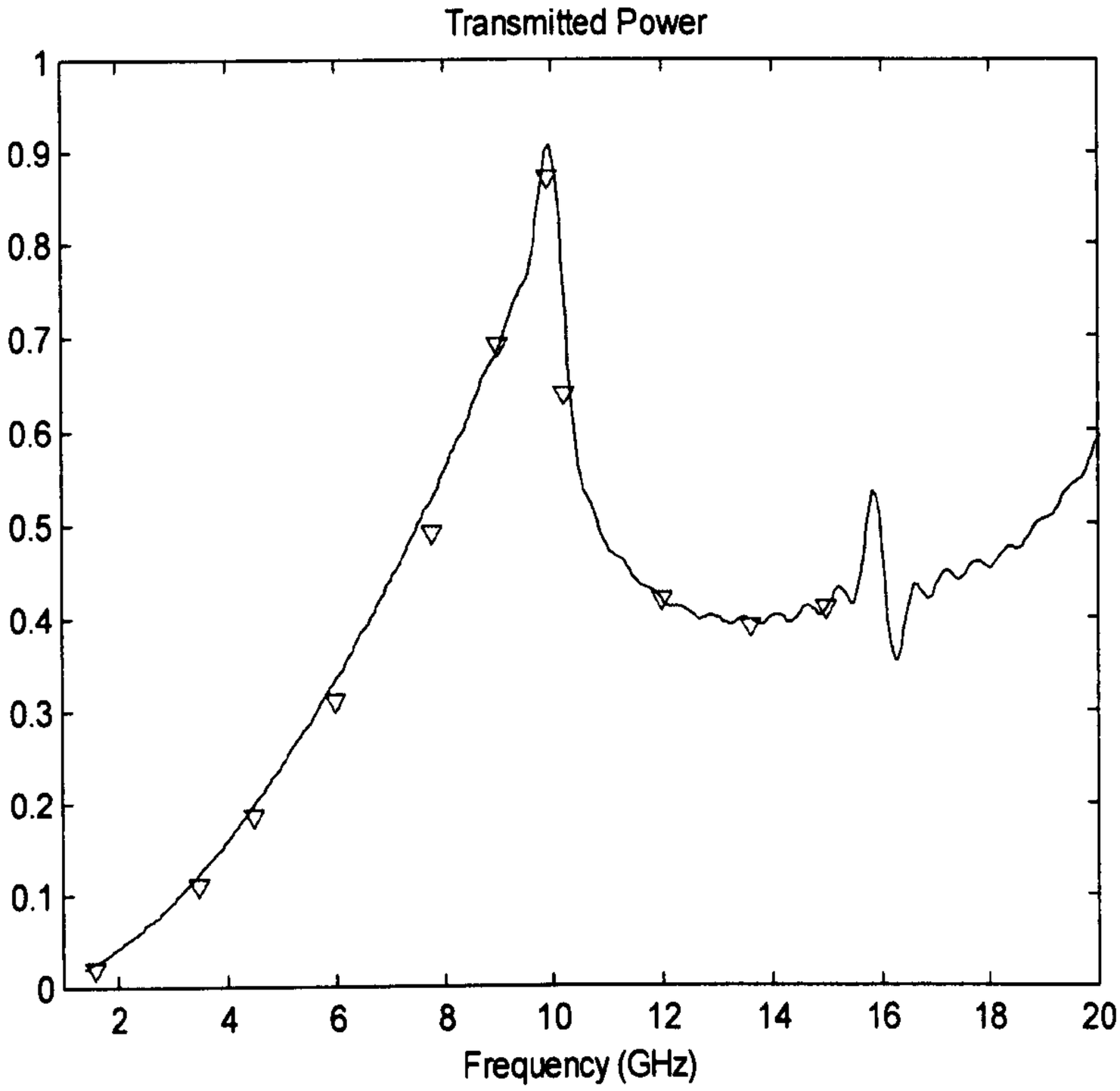

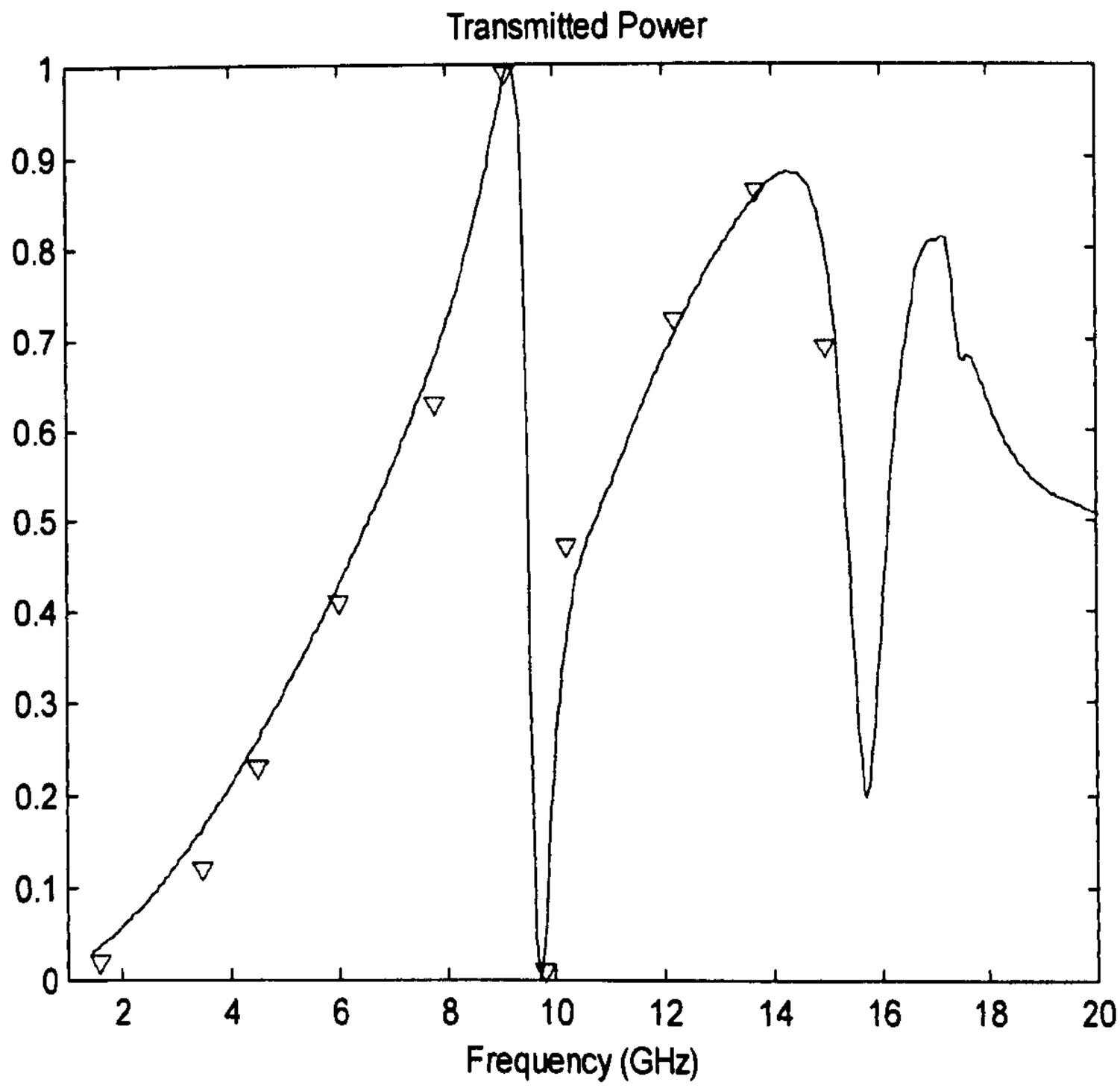

Fig. 4.9 Transmitted power for the case 1 (mesh of square holes) with oblique incidence of 30 degrees for TM (top) and TE (bottom) polarization. The extended FDTD result (solid line) (140x21x21 cells) is compared to Mode Matching (MM) calculations (triangles).

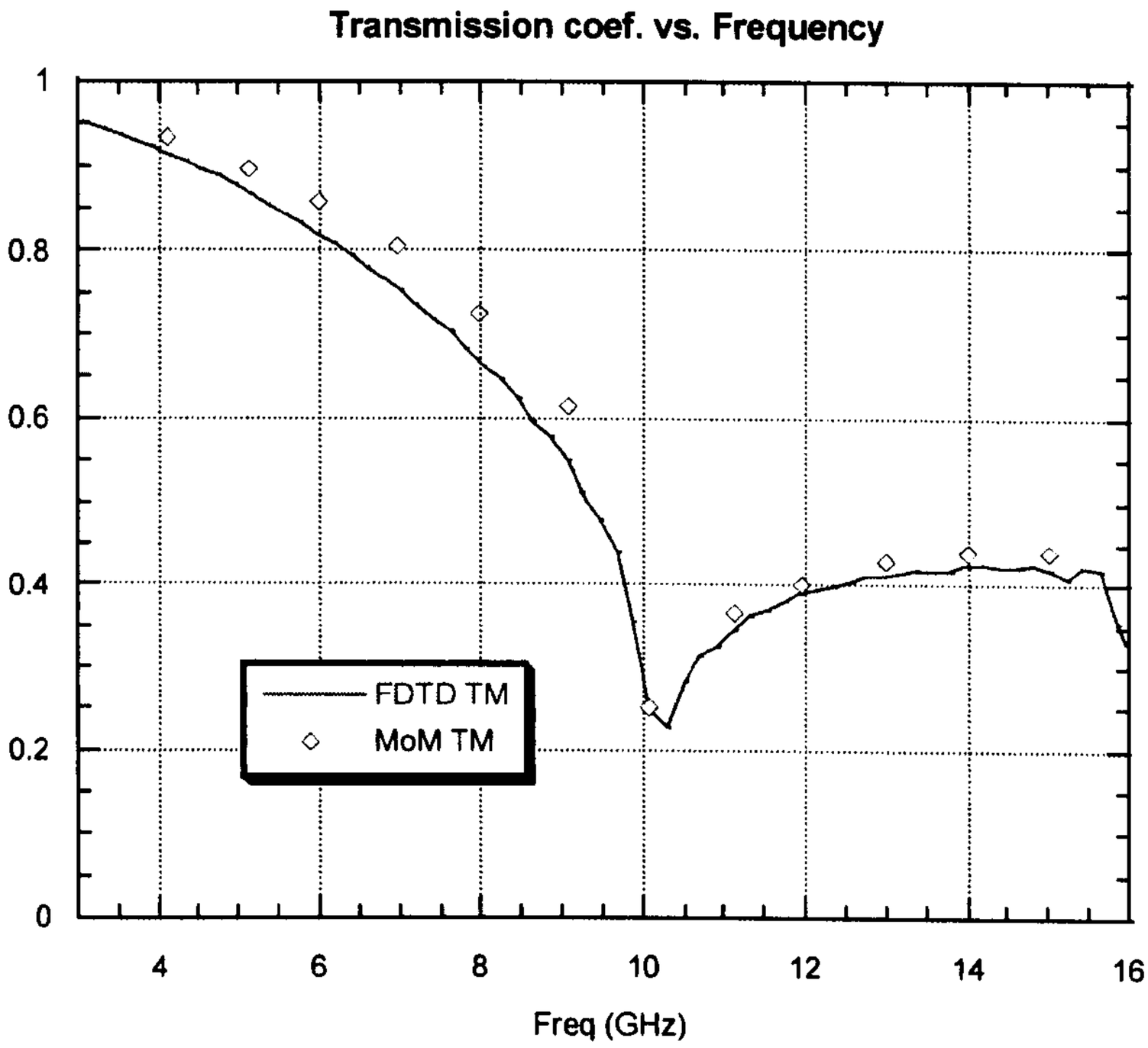

Fig. 4.10.Tranmission coefficient for the case 2 (infinite array of square patches) with oblique incidence of 30 degrees for TE (up) and TM (down) polarization. The extended FDTD result (140x21x21 cells) is compared to Method of Moments (MoM) calculations.

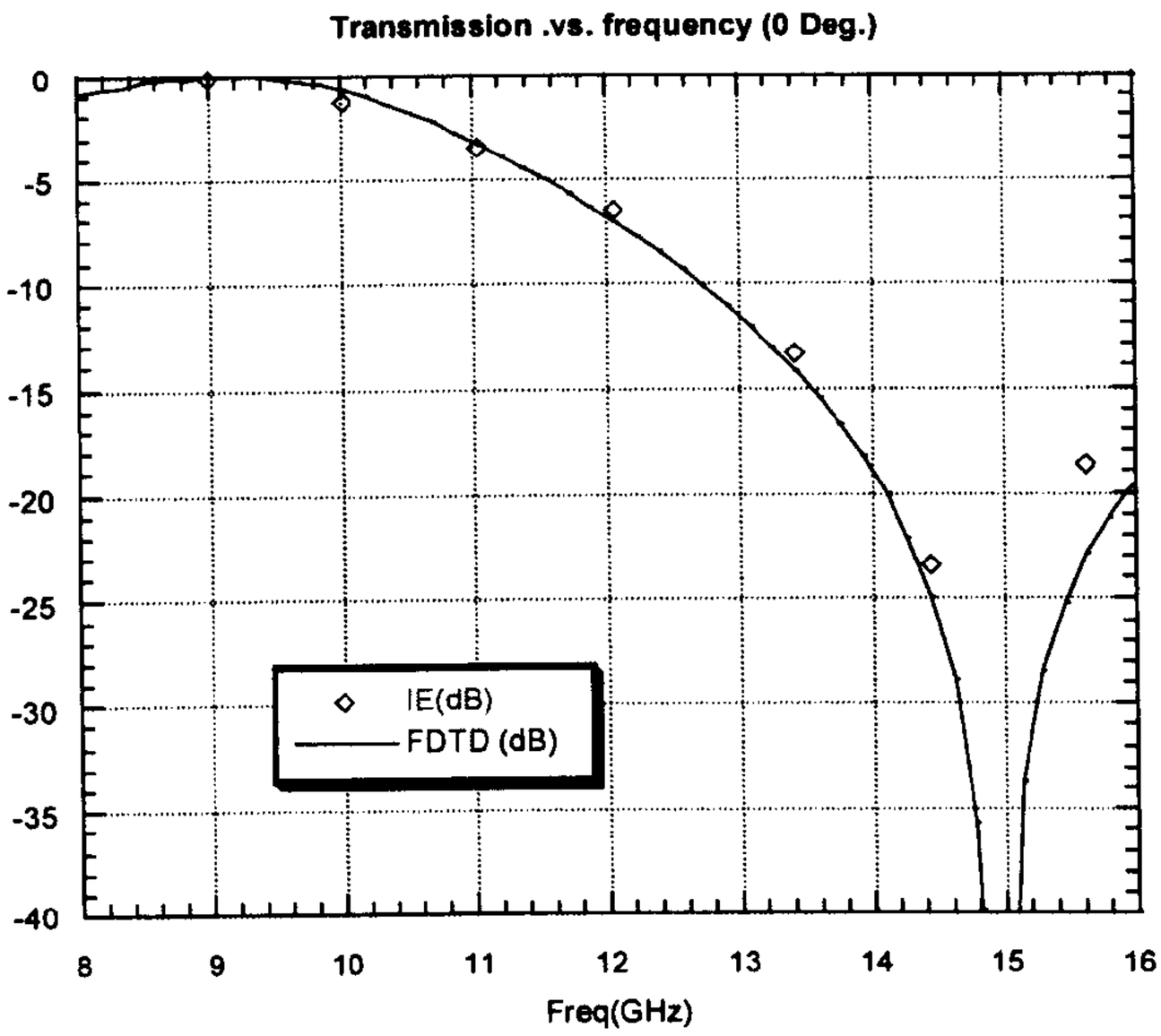

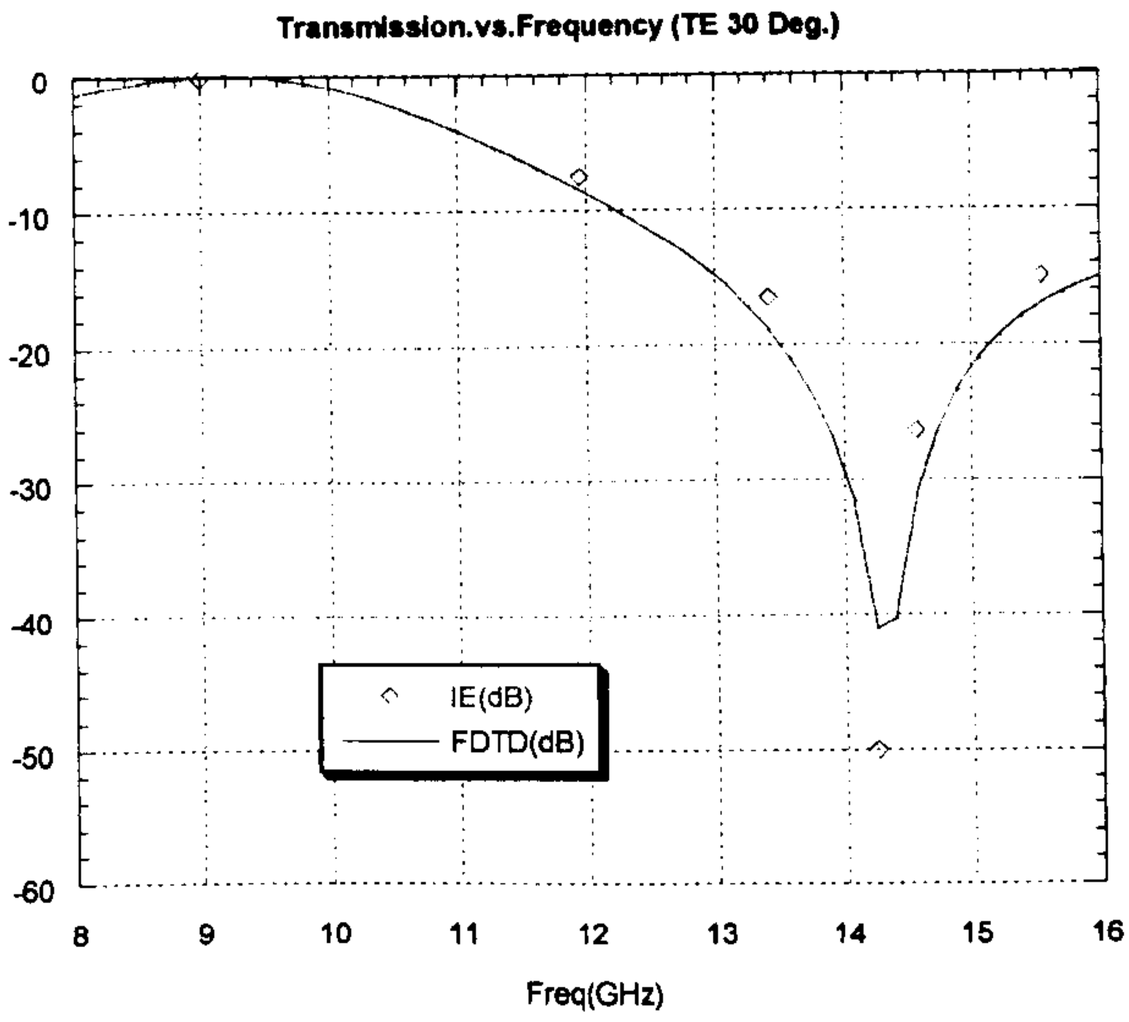

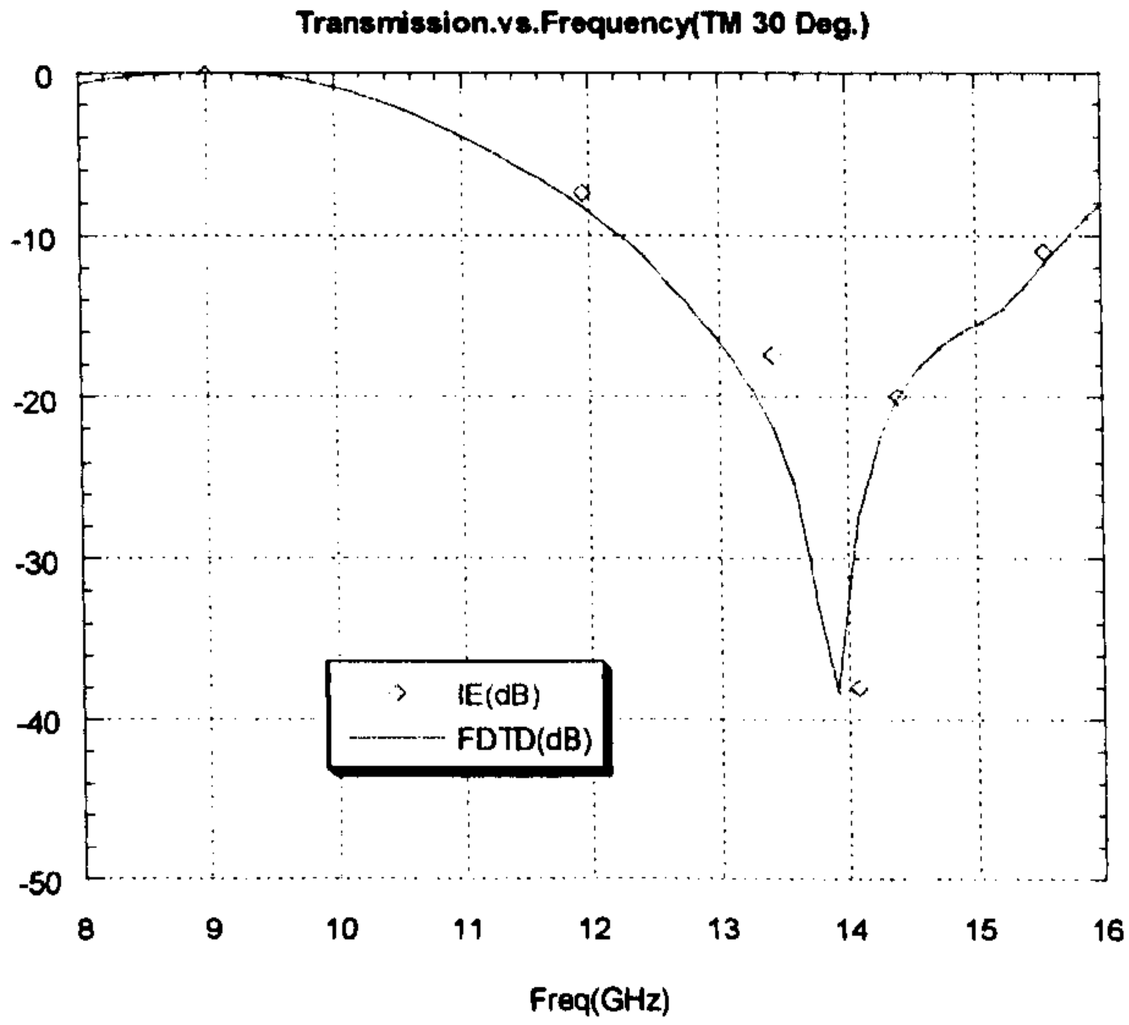

Fig. 4.11.Tranmission coefficient for the case 3 (double square loop on thin dielectric slab) at normal incidence (above) and at oblique incidence of 30 degrees (below) for TE (left) and TM (right) polarization. The extended FDTD result (140x32x32cells) is compared to Integral Equation method (IE) computations

4.4. Electrodynamics in finite periodic media

4.4.1. Mathematical Definition of the Finite Array

The definition of an antenna array is given in [11] as "an assembly of radiation elements in an electrical and geometrical configuration". The mathematical definition of array should match this practical definition in electromagnetics, but in the general context of abstract functions. The "radiation elements" can be described electrically in terms of distributions of conductivity, permitivity and current density, so the array can be defined as a set of associated functions which resembles the electrical properties of each element Eq.4.20. The "geometrical configuration" should be also introduced as a set of points in space, which defines the location of every element.

$$(g_0(\bar{x}), g_1(\bar{x}),..., g_{N-2}(\bar{x}), g_{N-1}(\bar{x}))$$
$$(\bar{x}_0, \bar{x}_1,..., \bar{x}_{N-2}, \bar{x}_{N-1}) \qquad \text{(Eq.4.20)}$$

The mathematical definition of finite array is the sum of the set of associated functions translated to the associated location of each element (Eq.4.21).

$$G(\bar{x}) = \sum_{n=0}^{N-1} g_n(\bar{x} - \bar{x}_n) \qquad \text{(Eq.4.21)}$$

4.4.2 The cyclic translation operator for finite arrays

The complexity of a problem dealing with finite arrays can be reduced if symmetry properties occur. Symmetry is basically the property of a system to remain the same after a transformation (i.e. a rotation) and it is related to the degree of redundancy in the system. Infinite periodic functions are a case of a strong symmetry with respect to a discrete translation. In a Cartesian co-ordinate system, finite arrays can not be invariant to translations and hence they can not be periodic.

The finite periodic arrays are invariant to cyclic translations of the associated positions, as if the elements were distributed in a circle, since all the elements of the finite periodic array are identical. This property is a basic symmetry of the finite periodic array. In order to establish this symmetry, the cyclic translation can be defined as an operator for finite arrays.

$$G(\bar{x}) = \sum_{n=0}^{N-1} g_n(\bar{x} - n\Delta\bar{x}) \qquad T_C{}^m G(\bar{x}) = \sum_{n=0}^{N-1} g_n(\bar{x} - n'\Delta\bar{x}) \qquad n' = MOD\left(\frac{n+m}{N}\right)$$

MOD(n/N)=remainder of n/N

$T_C{}^m$ *is the m-element cyclic translation operator of the finite array G* (Eq.4.22)

For the sake of simplicity the definition only covers the equispaced finite arrays. The cyclic translations (CT) can be composed. The result of the compositions of CT (composition means that two or more CT are applied sequentially) can be considered another CT. The CT set with the composition operation has structure of a commutative group. Other basic operations can be commuted with the CT.

$$T_C{}^m(G+H) = T_C{}^m \cdot G + T_C{}^m \cdot H$$

$$T_C{}^m(\lambda \cdot G) = \lambda \cdot T_C{}^m \cdot G$$

$$T_C{}^m(\Theta G) = \Theta(T_C{}^m \cdot G) \quad \Theta \text{ Linear, invariant}$$

(Eq.4.23)

There is a major difference with respect to the discrete translation operator: the multiplication of functions does not commute with the cyclic translation (Eq.4.24). As a consequence, the solutions to many physical equations, possible with infinite periodic functions, can not be described in terms of finite periodic arrays.

$$T_C{}^m(GH) \neq T_C{}^m G \cdot T_C^m H \qquad \exists G, H \qquad \text{(Eq.4.24)}$$

4.4.3 Finite periodic arrays

A finite periodic array is a truncation of an infinite periodic function to a finite number of periods. The resulting function can be described as a finite array, which is not periodic anymore, but intuitively it still keeps a strong symmetry. The elements of the finite periodic array are equal and this is the basis of his symmetry. Following Fig.4.12 , if a physical law (i.e. gravity) defines an interaction between elements of the finite periodic array, the mutual interaction between elements only depends on the relative index distance between them, for instance the interaction between elements 1 and 3 is the same than for elements 3 and 5. It is significant how the forces are distributed in the finite array of Fig.4.12, being zero at the centre (as for the infinite periodic array) and increasing toward the edges.

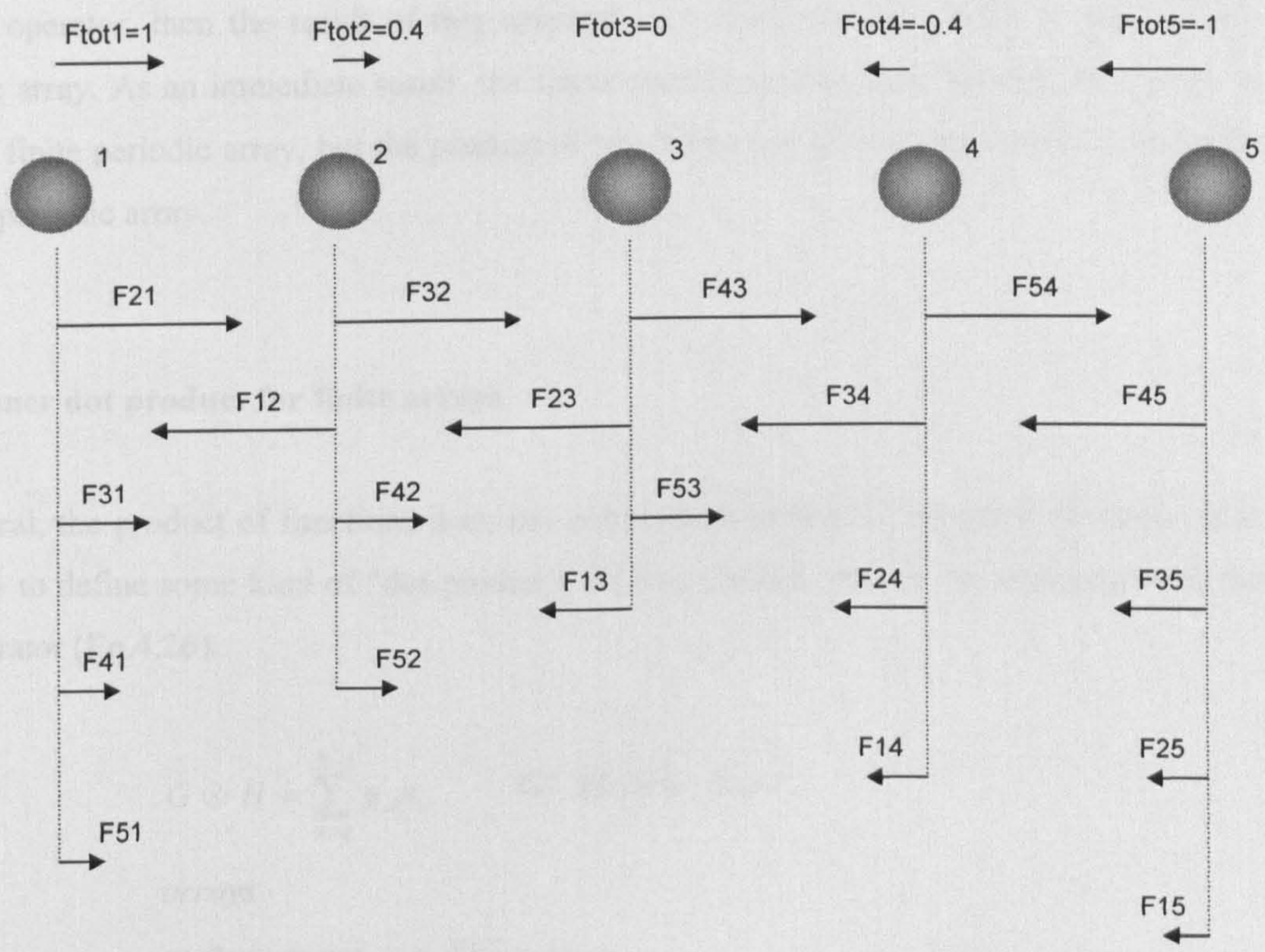

Fig.4.12 Gravitation forces in a finite periodic array of mass spheres. The mutual forces only depend on the relative distance between elements. The mutual forces show the strong imbedded symmetry in the system, rather than the total forces on the system. The total force for the central element is zero as for an infinite periodic array, but the total forces are increasing at the edge elements.

The finite periodic arrays remain invariant under a cyclic translation transformation. This means that finite periodic arrays are eigenfunctions of the cyclic translation operator (Eq.4.25). This property can be used as a mathematical test for finite periodic structures. The CT symmetry does not include any internal symmetry of the array elements. Other types of symmetry can be found simultaneously, or in combination with the CT, but this is not considered here.

$$T_C^{\,m} G = G$$

G is a finite periodic array (Eq.4.25)

The definition of the finite periodic array in terms of the CT operator can be used to obtain some basic features of the finite periodic arrays. For instance, if an operation commute with the CT operator, then the result of this operator on a finite periodic array is also a finite periodic array. As an immediate result, the linear transformation of a finite periodic array is another finite periodic array, but the product of two finite periodic arrays it is not necessarily a finite periodic array.

4.4.4 Inner dot product for finite arrays

In general, the product of functions does not commute with the CT operator. However, it is possible to define some kind of "dot product" for finite arrays, which can commute with the CT operator (Eq.4.26).

$$G \otimes H = \sum_{n=0}^{N-1} g_n h_n \qquad G,\ H \ \textit{are finite arrays}$$

$$T_C^{\,m}(G \otimes H) = T_C^{\,m} G \otimes T_C^{\,m} H \qquad \text{(Eq.4.26)}$$

The normal product between finite arrays can be associated to a matrix for the products of all the array elements. The diagonal of the matrix is precisely the inner product. The terms of the matrix off the diagonal represent the "mutual coupling" terms between the elements of the array.

$$G \cdot H = \sum_{n=0}^{N-1} \sum_{n'=0}^{N-1} g_n h_{n'} \quad G, H \text{ are finite arrays}$$

$$\begin{pmatrix} g_0 h_0 & g_1 h_0 & \cdots & g_{N-1} h_0 \\ g_0 h_1 & g_1 h_1 & \cdots & \cdots \\ \cdots & \cdots & \cdots & \cdots \\ g_0 h_{N-1} & \cdots & \cdots & g_{N-1} h_{N-1} \end{pmatrix}$$

(Eq.4.28)

These mutual coupling terms can be considered as finite arrays using less elements than g and h. They are the result of inner product between finite arrays, which are truncated from the initial arrays g and h. The truncation of the arrays can be defined also as an operation on finite arrays (Eq.4.29).

$$(G)^{+k} = \sum_{n=k}^{N-1} g_n(\bar{x} - n\Delta\bar{x}) = \sum_{n=0}^{N-k-1} g'_n(\bar{x} - n\Delta\bar{x})$$

$$g_n(\bar{x} - (n-k)\Delta\bar{x}) = g'_n(\bar{x} - n\Delta\bar{x})$$

$$(G)^{-k} = \sum_{n=0}^{N-k-1} g_n(\bar{x} - n\Delta\bar{x})$$

Truncation of finite arrays: Left (top) and Right (bottom) truncation of k elements.

(Eq.4.29)

Therefore, the product of functions can be written in terms of inner products and hence as a sum of finite arrays of different lengths (Eq.4.30). As the inner product commutes with the CT, the product of finite periodic arrays can be expressed as a superposition of finite periodic arrays of different length, each of them representing the different mutual interaction terms Fig.4.13.

$$G \cdot H = G \otimes H + \sum_{k=1}^{N-1} (G^{+k} \otimes H^{-k} + G^{-k} \otimes H^{+k})$$

(Eq.4.30)

The terms of Eq.4.30 can be identified in the matrix expression of Eq.4.28. The Eq.4.31 shows the equivalence of the inner dot product terms in the matrix representation.

$$G \cdot H = \begin{pmatrix} G & \cdots & G^{+k} \otimes H^{-k} \\ \cdots & \otimes & \\ G^{-k} \otimes H^{+k} & \cdots & H \end{pmatrix}$$

(Eq.4.31)

For instance, in the case of two finite arrays with only three elements, the finite array product is the following:

$$G = g_0 + g_1 + g_2 \qquad H = h_0 + h_1 + h_2 \Rightarrow G \cdot H = \begin{pmatrix} g_0 h_0 & g_1 h_0 & g_2 h_0 \\ g_1 h_0 & g_1 h_1 & g_1 h_2 \\ g_2 h_0 & g_2 h_1 & g_2 h_2 \end{pmatrix}$$

$$G \cdot H = G \otimes H + G^{+1} \otimes H^{-1} + G^{-1} \otimes H^{+1} + G^{+2} \otimes H^{-2} + G^{-2} \otimes H^{+2}$$

$$G \otimes H = g_0 h_0 + g_1 h_1 + g_2 h_2$$

$$G^{-1} \otimes H^{+1} = g_0 h_1 + g_1 h_2 \qquad G^{+1} \otimes H^{-1} = g_1 h_0 + g_2 h_1$$

$$G^{-2} \otimes H^{+2} = g_0 h_2 \qquad G^{+2} \otimes H^{-2} = g_2 h_0$$

(Eq.4.32)

4.4.5 Time domain electromagnetic field in finite periodic media

The interaction of the electromagnetic field and media is described by means of the electrical permitivity ε, the magnetic permeability μ, and the conductivity σ. These parameters model the average electrical properties of the media at microscopic level. In general, from the point of view of electromagnetic field, a media is a finite periodic array when ε, μ, σ are finite periodic arrays of the same type (Eq.4.32).

$$T_C{}^k \cdot \varepsilon(\bar{x}) = \varepsilon(\bar{x}) \qquad \varepsilon(x, y, z, t)$$

$$T_C{}^k \cdot \mu(\bar{x}) = \mu(\bar{x}) \qquad \mu(x, y, z, t)$$

$$T_C{}^k \cdot \sigma(\bar{x}) = \sigma(\bar{x}) \qquad \sigma(x, y, z, t)$$

(Eq.4.32)

The properties of the electromagnetic field in finite periodic media can be investigated using the CT operator. The CT operator can be applied to Maxwell's equations for the electromagnetic field for different situations. If they commute with the CT operator then the field also has CT symmetry, this means that it is a finite periodic array.

For instance, the Maxwell equations for a homogeneous media, but with a finite periodic array for the density of current commute with the CT operator, so if the density of current is a finite periodic array, then the EM field is also a finite periodic array.

However if the media is a finite periodic array, in general, Maxwell equation do not commute with CT, even if the excitation current j is finite periodic array. This is because the product of functions does not commute with CT (Eq.4.33).

$$\nabla \times (T_C{}^k \cdot \vec{E}) = -\frac{\partial\left(\mu (T_C{}^k \cdot \vec{H})\right)}{\partial t}$$

$$\nabla \times (T_C^k \cdot \vec{H}) = \frac{\partial\left(T_C{}^k (\varepsilon(x,y,z,t)\vec{E})\right)}{\partial t} + T_C{}^k (\sigma(x,y,z,t)\vec{E}) + \vec{j}_{ext}$$

$$\nabla \cdot (T_C{}^k \cdot \vec{D}) = T_C{}^k \cdot \rho \qquad \nabla \cdot (T_C{}^k \cdot \vec{B}) = 0$$

$\varepsilon(x,y,z,t)$, $\sigma(x,y,z,t)$, $\vec{j}_{ext}(x,y,z,t)$ Finite periodic arrays

(Eq.4.33)

The non-commutation of Maxwell's equations and CT is the major difference with respect to the infinite periodic array case where the discrete translation commutes with Maxwell equations. However, EM field can be split into two components, which would verify the following condition

$$\vec{E} = \vec{E}_I + \vec{E}_M$$
$$\vec{H} = \vec{H}_I + \vec{H}_M$$
$$\nabla \times \vec{H}_I = \frac{\partial\left(\varepsilon \otimes \vec{E}_I\right)}{\partial t} + \sigma \otimes \vec{E}_I + \vec{j}_{ext}$$
$$\nabla \times \vec{E}_I = -\frac{\partial\left(\mu \vec{H}_I\right)}{\partial t} \qquad \text{(Eq.4.34)}$$

Since Eq.4.34 commutes with the CT, this means that $\vec{E}_I$ is also a finite periodic array. These equations determine the conditions (Eq.4.35) which have to be verified by $\vec{E}_M$, according to

the composition of the displacement vector and the conductivity, in a sum of inner product terms along the lines of Eq.4.30.

$$\vec{D} = \varepsilon\vec{E} = \varepsilon\vec{E}_I + \varepsilon\vec{E}_M = \varepsilon \otimes \vec{E}_I + \sum_{k=1}^{N-1} (\varepsilon^{+k} \otimes \vec{E}_I{}^{-k} + \varepsilon^{-k} \otimes \vec{E}_I{}^{+k}) + \varepsilon\vec{E}_M$$

$$\sigma\vec{E} = \sigma\vec{E}_I + \sigma\vec{E}_M = \sigma \otimes \vec{E}_I + \sum_{k=1}^{N-1} (\sigma^{+k} \otimes \vec{E}_I{}^{-k} + \sigma^{-k} \otimes \vec{E}_I{}^{+k}) + \sigma\vec{E}_M \qquad \text{(Eq.4.35)}$$

The equations for $\vec{E}_M$ are similar to Maxwell's equations for the complete field, but the equivalent density of current is a sum of truncated finite periodic array distributions.

$$\nabla \times \vec{H}_M = \frac{\partial(\varepsilon\vec{E}_M)}{\partial t} + \sigma\vec{E}_M + \sum_{k=1}^{N-1} (\vec{j}^{+k} + \vec{j}^{-k})$$

$$\vec{j}^{+k} = \frac{\partial(\varepsilon^{+k} \otimes \vec{E}_I{}^{-k})}{\partial t} + \sigma^{+k} \otimes \vec{E}_I{}^{-k}$$

(Induced currents by coupling from $\vec{E}_I$) (Eq.4.36)

The physical meaning of these equations can be described in terms of mutual interactions. The field is decomposed in a non-interacting term, $\vec{E}_I$, which represent the field radiated by the finite array of elements without any mutual coupling. The remaining term $\vec{E}_M$, represent the mutual interactions and is generated by the induced currents in each element.

The field $\vec{E}_M$ can itself be decomposed following a similar procedure of Eq. 4.34-4.36. One part of $\vec{E}_M$,designated $\vec{E}_{II}$, will represent the scattered field by the array elements illuminated by $\vec{E}_I$, a second part represents the remaining mutal coupling field, which is produced by rescattering of this field. If the decomposition is done for each excitation current $\vec{j}^{+k}$, $\vec{j}^{-k}$ the associated fields are finite periodic arrays of the same type as the currents. The total field can be expanded in a series of finite periodic array functions, which represent the scattered and rescattered field from the initial term (the field generated by the array without any mutual coupling effect). This series can be truncated to neglect higher order mutual coupling effects, for instance neglect $\vec{E}_{III}$ and above.

$$\vec{E} = \vec{E}_I + \sum_{k=1}^{N-1}(\vec{E}_{II}{}^{+k} + \vec{E}_{II}{}^{-k}) + \sum_{k=1}^{N-1}\left[\sum_{k'=1}^{k}(\vec{E}_{III}^{+k'} + \vec{E}_{III}^{-k'}) + \sum_{k''=1}^{N-k-1}(\vec{E}_{III}^{+k,+k''} + \vec{E}_{III}^{+k,-k''} + \vec{E}_{III}^{-k,+k''} + \vec{E}_{III}^{-k,-k''})\right] + \ldots.$$

(Eq.4.37)

Fig.4.13 shows the meaning of some of the terms for the Eq.4.37 in terms of interactions between elements of the finite array. A major feature of the expansion formula in Eq.4.37 is that all the field elements are finite periodic arrays and satisfy the modified Maxwell equation formula of Eq.4.34. This property can be used to exploit the symmetry of the structure in order to reduce the amount of computations in a numerical simulation of the finite periodic array. In addition for electrically large array elements where only adjacent element coupling was significant, this means that $\vec{E}_{II}{}^{+k}$ (k>1) could be neglected.

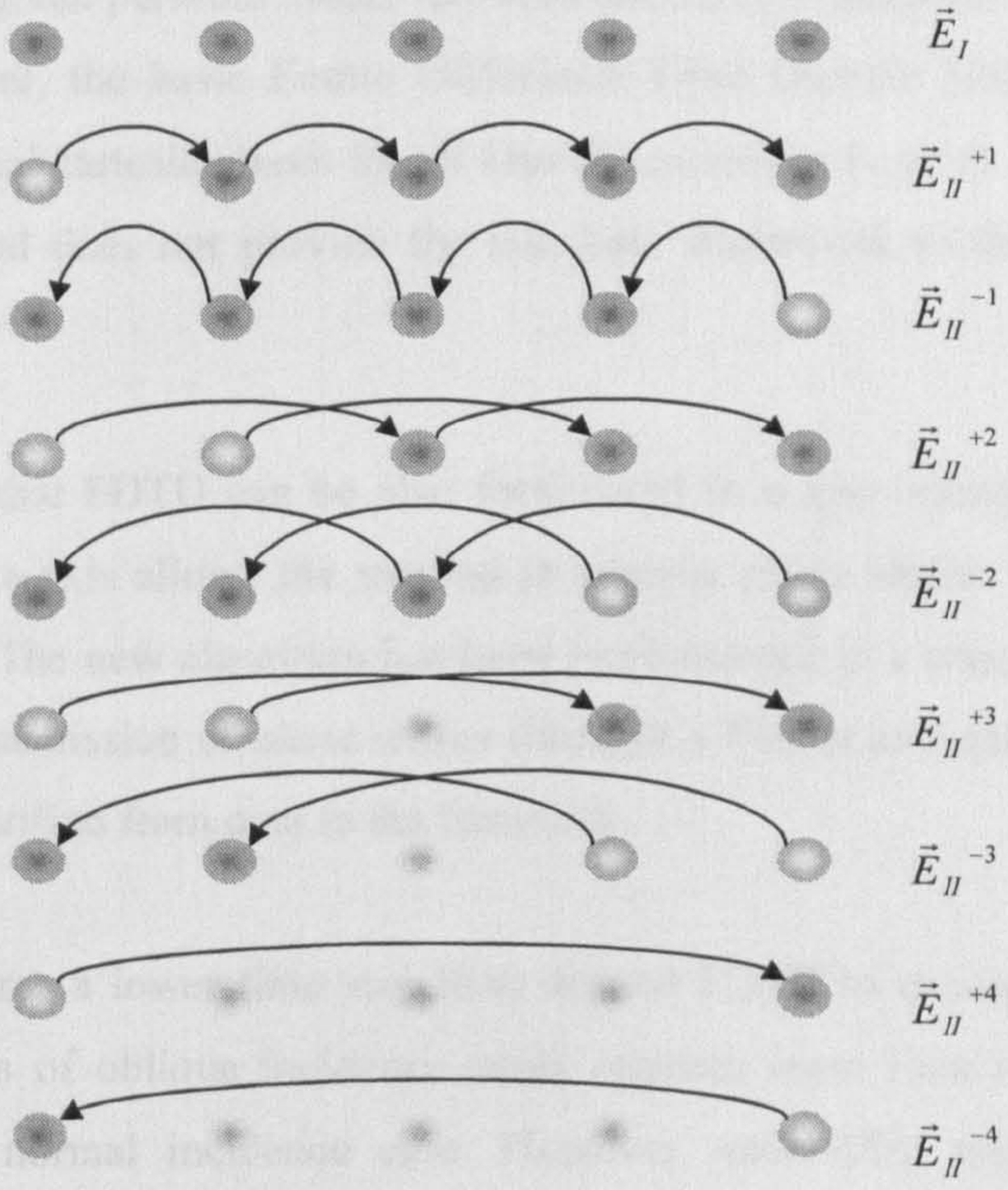

Fig.4.13 The terms of equation 4.37 are related to the mutual scattering between array elements. The figure shows for a 5 element array, which elements are scattering the field (dark balls) for the first order terms of the (Eq.4.37). As all the array elements are similar the $\vec{E}_{II}{}^{\pm k}$ fields are finite periodic arrays with N-k elements.

4.5 Conclusions of the Chapter IV

Periodic media can be considered as a kind of media distribution with discrete translational symmetry. The electromagnetic equations in this periodic media are also invariant with respect to this discrete translational symmetry. As a result, the EM field in periodic media have a special structure, a superposition of harmonic kernels multiplied by a periodic function (Bloch theorem).

The concept of periodicity and translational symmetry can be formulated in a non orthogonal basis in space-time. In fact, as shown in this chapter, non-orthogonal periodicity of the EM field occurs in many practical cases, as in a triangular lattice array or in a FSS under oblique incidence. The non-orthogonal periodic media has been succesfully modeled using frequency domain methods. However, the basic Finitte Difference Time Domain (FDTD) method is formulated in an orthogonal cartesian basis for all four dimmensions (x,y,z,t). This orthogonal formulation of the method does not provide the adequate framework to deal with general periodic media.

Here it has been shown that FDTD can be also formulated in a non orthogonal basis. The transformation of the time axis allows the method to analyse phase shifted arrays and FSS under oblique incidence. The new algorithm has been implemented in a computer code. This code can estimate the transmission of plane waves throught a FSS at any azimuthal angle of incidence and has been verified from data in the literature.

The new algorithm requires a lower time step than normal FDTD to ensure stability. As a consequence, the analysis of oblique incidence cases requires more time to compute than FDTD requires for the normal incidence case. However, such CPU time and memory requirements are perfectly compatible with current PC computers. In fact, the test cases presented here required less than 2h and 6Mb RAM (at the worst case) in a 300MHz Pentium processor.

It has been shown that finite periodic media can be described as a kind of media distribution with cyclic translational symmetry. However in this case, the electromagnetic equations in finite periodic media are not invariant to the cyclic translation (they are only invariant with respect to the field sources). As a result, there is not an equivalent Bloch Theorem for finite periodic media. This means that the fields in finite periodic media and for cases of a finite

periodic excitation the fields are not a finite periodic array, but it can be described as the superposition of finite periodic fields representing the 'mutual coupling' interactions. The main advantage of using mutual coupling terms for modelling is to reduce the problem just to the model of a single element of the finite array in order to evaluate the field radiated by the element and to treat separately the mutual interactions.

It has been shown that each mutual interaction term is a solution of Maxwell's equations with some induced currents. These induced currents are related to the mutual interaction field of a lower order. For the first term (field scatter by the elements without mutual interaction) the currents are related to the incident fields or the currents produced by the sources. In the context of modelling finite arrays using FDTD, this means that each mutual interaction term can be solved using FDTD on a single element, provided that the induced currents from a lower order term has been calculated, starting from the fields scattered by a single array element. A possible practical approach for the calculation of the induced currents is to use PO to estimate the fields beyond the near field region of the array elements (modeled using FDTD). The implementation of this hybrid technique is beyond the scope of this thesis.

4.6 References for Chapter IV.

[1] A.Taflove, "Computational Electrodynamics: The Finite Time Domain Method", Artech House 1995.

[2] L. Brillouin, "Wave propagation in periodic media", Mc Graw Hill 1946

[3] R.Mittra, R. Chan, T. Cwik, "Techniques for analyzing frequency selective surfaces", IEEE Procedings,1988, pp 1593-1615.

[4] J.Tsay, D.Pozar 'Application of the FDTD technique to periodic problems in scattering and radiation'. Microwave and Waveguide Letters. vol 3, pp250-252. Aug. 1993.

[5] P. H. Harms, R. Mittra, W. Ko, "Implementation of the Periodic Boundary Condition in the Finite-Difference Time-Domain Algorithm for FSS Structures", IEEE APS, Vol 42, pp. 1317-1324, Sep 1994.

[6] G.M.Turner, C.Christodoulou, "FDTD analysis of phased array antennas", IEEE Trans. Antennas and Propag. Vol 47 p.661-7, April 1999.

[7] J.A.Roden, S.D.Gedney, M.P.Kesler, J.G.Maloney and P.H.Harms, 'Time-Domain Analysis of Periodic Structures at Oblique Incidence: Orthogonal and Non-orthogonal FDTD Implementations', IEEE MTT Vol 46, pp420-427,April 1998.

[8] Joannopoulos, J.D. "Photonic Band Gap Crystals: Molding the Flow of Light", Princeton University Press 1995.

[9] G. Zarrillo, K Aguiar, "Closed Form Low Frequency Solutions for Electromagnetic Waves Through a FSS", IEEE APS Dec. 1987.

[10] T.K.Wu, W.P. Shilue, "Dichroic Design for the Orbiting VLBI Earth Station Antenna". IEE Proc. Microwave and Antenna Propagation, Vol 141, June 1994.

[11] C.A.Balanis "Antenna Theory", John Wiley 1982.

[12] H. Wakabayasi et al. "Numerical simulations for frequency selective screen with complementary operators". IEE Proc. Microw. Ant. Propag., Vol 141, Dec. 1994.

[13] J.A.Stratton, "Electromagnetic Theory", McGraw Hill NY 1941.

[14] Harrison W.A. "Solid State Theory", Dover,NY 1979.

CHAPTER V: DESIGN OF A SUB-MILLIMETRE PLANAR INTEGRATED RECIEVER USING FDTD

5.1 Introduction

Integrated planar antennas are an attractive and relatively cheap technology for millimetre and sub-millimetre receivers. They can be manufactured using lithography and etching techniques up to a resolution of microns and they can incorporate semiconductor devices that can be mounted directly on the substrate, improving the accessibility of the devices with respect to non-planar systems.

Integrated planar receivers usually consist of a receiving antenna with a solid state detector. In the sub-millimetre region these detectors are usually temperature sensors or bolometers. The temperature of the bolometer is increased because of the ohmic transformation of submmW energy into heat. The change of the bolometer dc resistance with the temperature can be measured with a voltmeter and it is proportional to the amount of submmW power dissipated at the bolometer. Recently, Schottky diodes have became available due to advances in semiconductor technology so coherent detection at these frequencies is also possible.

Integrated receivers have a great relevance in the field of submmW scientific instrumentation [1], [2]. Planar integrated receivers can form imaging arrays of detectors, in an elegant and compact way that non-planar antennas can not imitate. On the same substrate, planar integrated receivers can provide the circuit auxiliary elements and the antenna, simplifying the design and the manufacturing.

Integrated receivers are serious candidates for high-performance scientific instruments applications in space astronomy and earth observation. Future instrumentation for space projects in Europe such as MASTER, and FIRST [3](Far Infrared Space Telescope) have demanding requirements of detectors and imaging arrays with low noise figures.

This chapter presents the design of a submmW integrated receiver. This integrated single element is intended to be part of an imaging array. In fact, the objective of this chapter is to demonstrate a practical model of integrated receiver using FDTD, under realistic requirements. This demonstration exercise is the final step in developing FDTD modelling techniques for planar quasi optical devices.

5.2 Sub-millimetre planar antennas in dielectric substrates

5.2.1 Sub-mmW planar antennas on thin substrates

The initial designs of planar antennas for mmW and submmW antennas were based on substrates much thinner than the wavelength. Several designs of resonant antennas on thin substrates were built and tested in the late 70's, as single dipoles, twin slot arrays, annular slot [1] etc. Microstrip patches were also tested but they show particularly high conduction losses above 100 GHz. Microstrip dipoles and slots have exhibited much better performance than patches and extensive work has been done in this area [1].

At mmW and sub-mmW frequencies, the planar antennas on thin substrates exhibit low gain on the radiation pattern which imposes a severe limitation on the applicability of this kind of antennas. The main causes for this low gain are the losses associated with surface modes, which propagate into the substrate, and limit the power radiated into the air half space Fig.5.1.

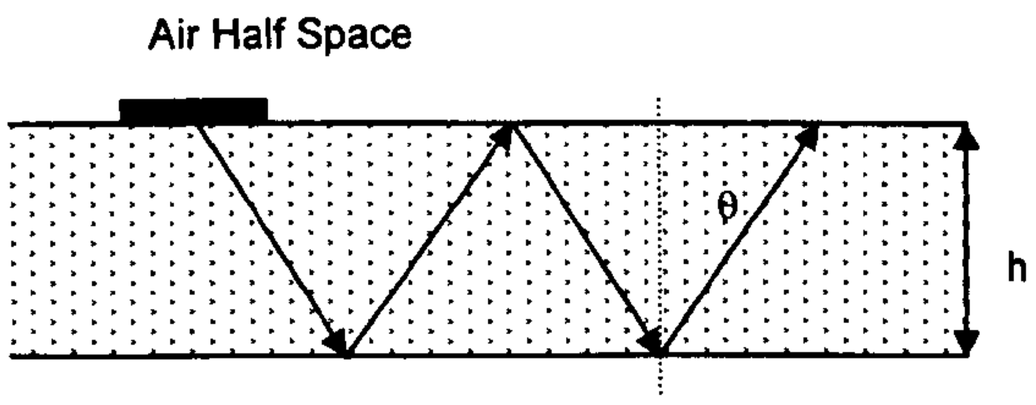

Fig.5.1. Ray optics image of propagation on a dielectric slab wave-guide. The wave is "trapped" inside the dielectric. From the point of view of the antenna, the power is propagating as surface modes, which prevent energy from being radiated into the air.

In respect to the power radiated into the air half space rather than the dielectric substrate, it has been shown [2] that for slots on an infinitely thick substrate, the ratio between power radiated into the dielectric substrate and the air follow Eq.5.1.

$$\frac{P_{substrate}}{P_{air}} = \varepsilon_r^{3/2} \qquad \text{(Eq.5.1)}$$

This formula shows that the power is mostly radiated into the dielectric substrate even for moderate dielectric constants. This result indicates that substrates with high dielectric constants should be used to reduce the losses associated to backward radiation into the air. For

instance, the power radiated into a silicon substrate is 97.5% of the total power radiated by a slot.

However, Eq.5.1 is for an infinitely thick substrate. In case of an electrically thin substrate, it is necessary to take into account the amount of power that could be "trapped" within the dielectric as surface modes. The substrate can be considered as a dielectric slab wave-guide in which modes can propagate. The power of the surface modes generated by a slot on a thin dielectric substrate on a ground plane has been derived in [2] (Eq.5.2). Surface mode losses become null when substrate thickness approaches zero. As the substrate thickness increases, the losses also increase very quickly, following an oscillatory pattern later. As a consequence, the gain of a slot on a thin substrate for a thickness$<<\lambda_d/4$ is slightly higher in the substrate side than in the air half space. The gain raises in the substrate if thickness is increased and it drops (to levels of a tenth of the gain) for thickness above $\lambda_d/4$.

$$P_{TM} = 3\varepsilon_r h_e \lambda_0 / 16 \quad \text{(surface mode TE)}$$

$$P_{TE} = 3\varepsilon_r h_e \lambda_0 \cos^2 \vartheta / 16 \quad \text{(surface mode TM)} \qquad \text{(Eq.5.2)}$$

Unlike the microwave band, planar antennas on thin substrates are difficult to implement at sub-mmW frequencies, since the substrate thickness should face heavy surface mode losses or be extremely thin (<30μm for silicon substrate, <70μm for a quartz substrate at 600GHz). Even if the substrate is thin enough to avoid surface mode propagation, the loss budget can be close to 50% because of strong backward radiation into the air. Despite the bad performance of planar antennas on thin substrates in terms of gain and loss budgets, the radiation pattern of these antennas remains almost unaffected by the substrate. These pattern are capable of a high degree of symmetry, only limited by manufacturing errors and by the parasitic radiation from feed lines and other circuit elements.

5.2.2 Sub-mmW planar antennas on infinite/lens substrates

Surface modes are a major drawback to planar antennas on thin substrates for sub-mmW applications. However, if surface modes can be avoided, for instance in an infinitely thick substrate, planar antennas on high dielectric constant substrate are able to radiate most of the power into the substrate with low backward radiation into the air (Eq.5.1).

An ingenious and simple way of solving the surface mode problem is to mount a lens on the back of the planar antenna [1](Fig.5.2). Lens antennas are able to avoid ray incidence at large angles at which total reflection occurs in the dielectric. Surface mode losses are replaced by reflection losses caused by reflections at the lens air dielectric surface. Reflection losses at near normal incidence are much smaller than surface mode losses, but for substrates with high dielectric constants they can be significantly high (2dB for silicon). These losses can be avoided by using matching layers that can work very well for narrow band [6].

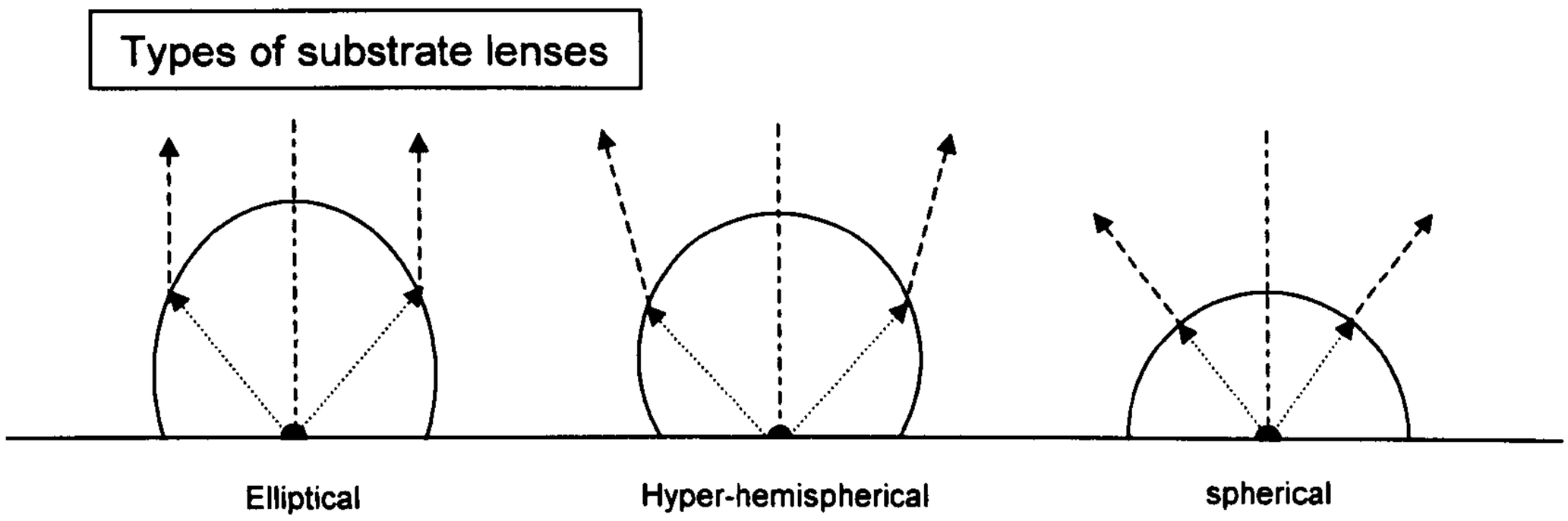

Fig.5.2. Substrate lenses can solve the problem of surface modes for planar antennas on thin dielectric slabs. The planar antenna is placed on the lens focus, so the rays are nearly normal to the lens surface, so total internal reflection is avoided.

There are many types of lenses that can be used for these designs. Elliptical lenses provide a high gain radiation pattern, with a narrow beam (depending on the lens aperture). Hemispherical and Hyper-hemispherical lenses, are aplanatic designs, which are virtually free of spherical aberration or coma [7]. These lenses are quite interesting for imaging arrays or monopulse applications, where array elements are normally placed away from the lens focus, introducing coma aberration if the system does not verify the Abbe sine condition [7]. On the other hand, the hyper-hemispherical lenses require an additional lens (objective lens) or mirrors to focus the plane waves incoming from the far field (Fig 5.3).

The loss budget for planar antennas on lens substrates is outstandingly improved with respect to antennas on thin substrates (Table 5.1). Materials for lens substrates such as Silicon and Galium Arsenide exhibit low losses (loss tangent 0.0001 at 200GHz) in the mmW and submmW band [8], providing the high dielectric constant (11.7 for Si and 13 for GaAs) required to avoid strong backward radiation. Semiconductor materials provide the substrate

for active or non-linear devices that are included in the integrated antenna. The inclusion of a matching layer for the lens reduces the overall losses for the substrate lens to quite acceptable values.

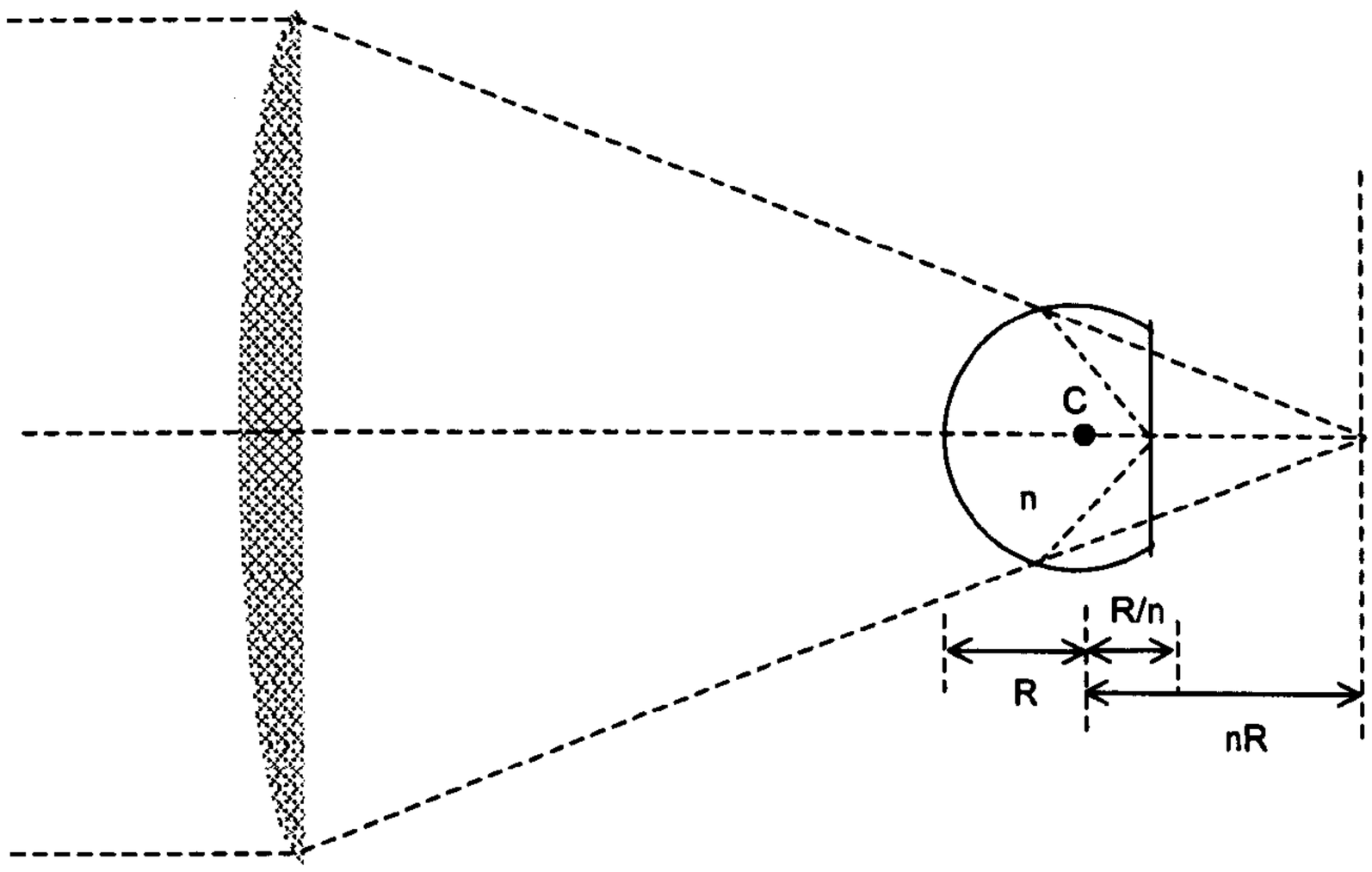

Fig.5.3 Hyper-hemispherical lens with an objective lens. The virtual focus for the objective lens is displaced a distance of *(n-1/n) R* with respect to the real focus into the lens. The system forms a virtual image in its focal plane.

Other types of lenses can be applied as substrate for planar antennas. Fresnel lenses can provide simple and compact geometry for planar lenses with the drawback of reduced aperture efficiency. A simple type of Fresnel lens uses is based on corrugations on a dielectric substrate to compensate the electrical path from the feed at the focus (Figure 4). Metal plate lenses can also do the work and they are easy to manufacture, but they exhibit very low aperture efficiency and do not overcome the surface wave problem.

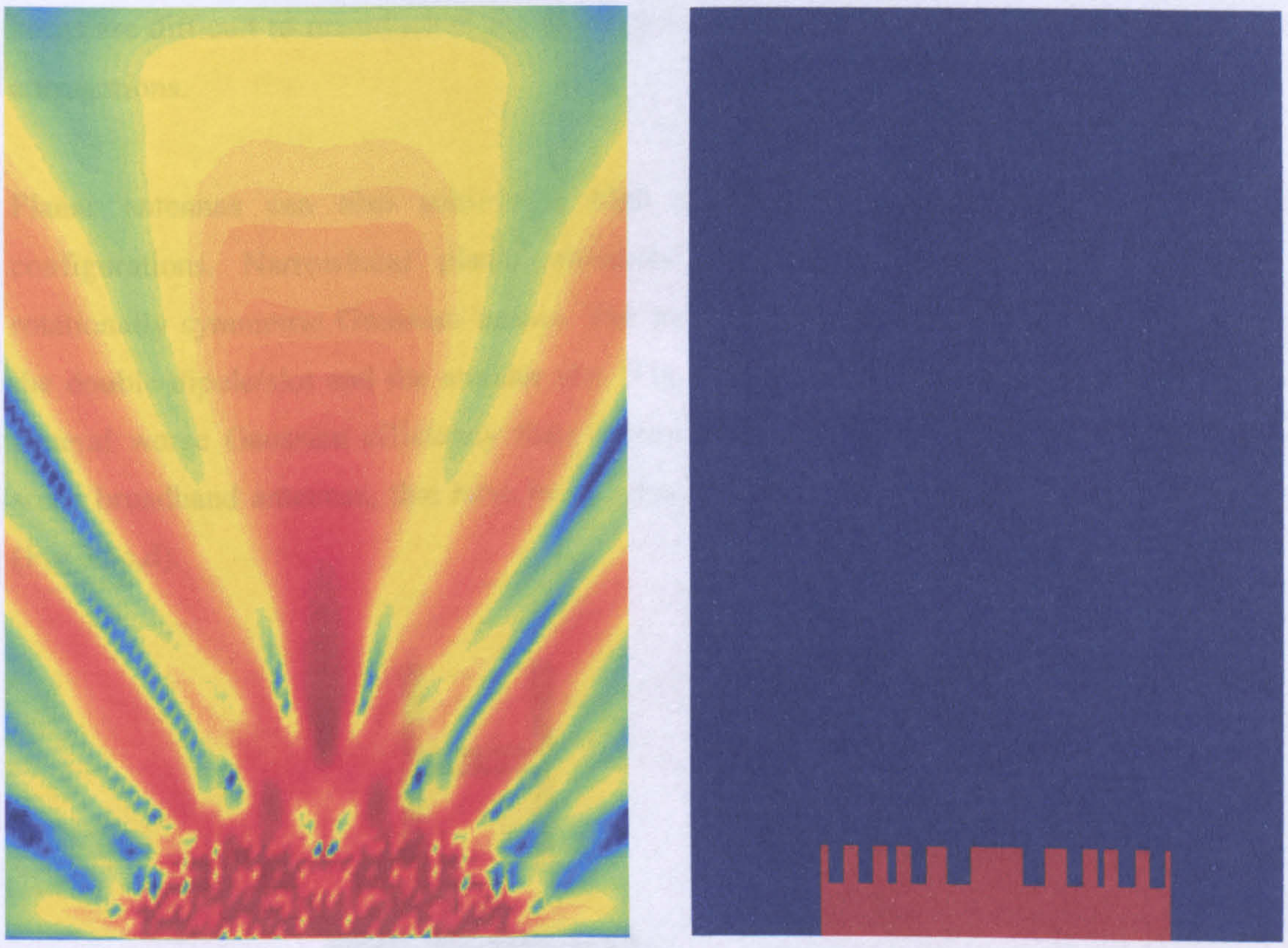

Fig. 5.4. FDTD calculation of the Electrical field radiated at 90 GHz by a Fresnel lens of 18mm radius. The electrical permitivity of the lens material is 3. The figure on the left shows the profile of the lens. the feed is a elementary dipole situated at the bottom.

5.2.3 The annular slot as a submmW antenna

The planar antennas used in mmW and sub-mmW bands usually require a high rotationally symmetry for their patterns in order to form part of a quasi-optical network. Quasi-optical systems are based on the propagation of Gaussian beam modes [9]. These Gaussian beam modes are an approximation of free space electromagnetic solutions that hold for low angles of propagation (paraxial approximation) and perfect symmetry of revolution. As a consequence, the measure of how Gaussian is the radiation pattern of the planar antenna (Gaussian efficiency) is a major figure of merit for the device.

Several types of mmW/sub-mmW antennas have shown high Gaussian efficiency. Of most significance is the corrugated horn, which is able to produce a beam with up to 98% Gaussian efficiency. Despite some impressive micro-manufacturing achievements [10],[11], corrugated horns are difficult to manufacture for sub-mmW operation due to the tiny dimensions of the corrugations.

Planar antennas can also achieve a high degree of Gaussian efficiency for some configurations. Narrowband planar antennas are particulary successful in achieving rotationally symmetric Gaussian beams. The most popular narrowband planar antennas are the double dipole/slot and the annular slot (Fig.5.5a,b). Broadband planar antennas have in general worse Gaussian efficiency than narrowband. Log-Periodic, spiral and bow-tie are some broadband antennas, that have been implemented successfully for submmW operation (Fig 5.5c,d).

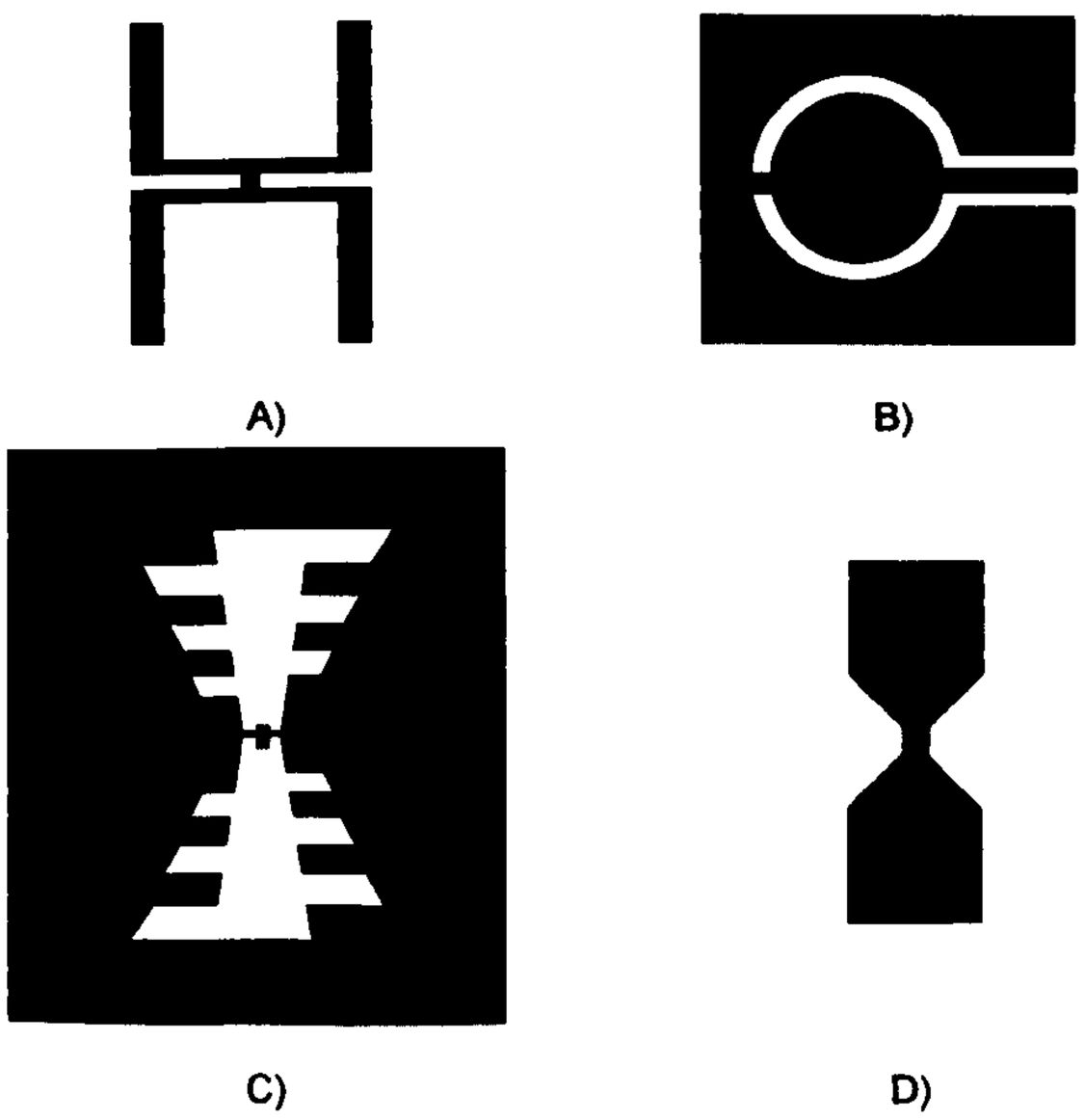

Figure 5.5. mmW/sub-mmW planar antennas. A) twin dipoles. B) annular slot. C) Log-Periodic slot array. D) Bow-tie antenna. The twin and annular slot are used for bandwidths smaller than 5%. The Log-Periodic slot array and the bow tie are broadband antennas, for instance a log-periodic planar antenna has been reported [1] to operate from 26GHz to 220GHz.

The annular slot antenna produces a quite rotationally symmetric pattern at the first resonance mode of the structure ($\lambda=\pi d$) (Fig. 5.6). The electric field in the annular slot for the first

resonant mode is anti-symmetric as shown in the figure 5.7 with two zero field points at opposite sides of the ring. The antenna is smaller than the twin resonant slot and the bandwidth can be controlled by the ring slot width. The impedance of an annular slot depends strongly in the dielectric constant of the substrate, for instance, the impedance of a typical annular slot on silicon at the first resonance is about 100 ohms, but in quartz it can raise to 200 ohms [12]. This impedance is suitable to connect semiconductor devices such as Schottky diodes or FET transistors, although additional matching lines could be needed to adapt the device.

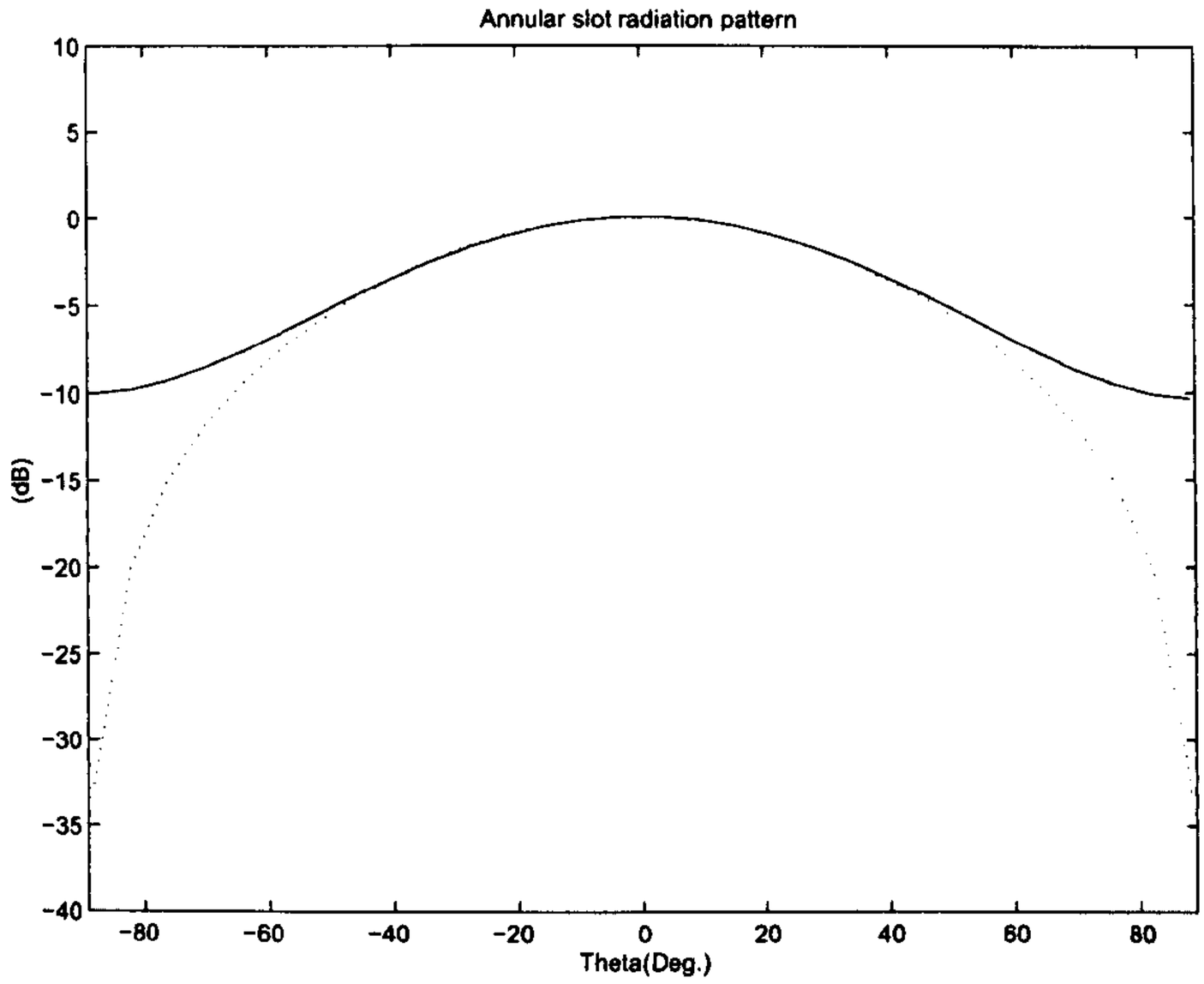

Figure 5.6. Radiation pattern of a free-standing annular slot at the first resonance (*left*).

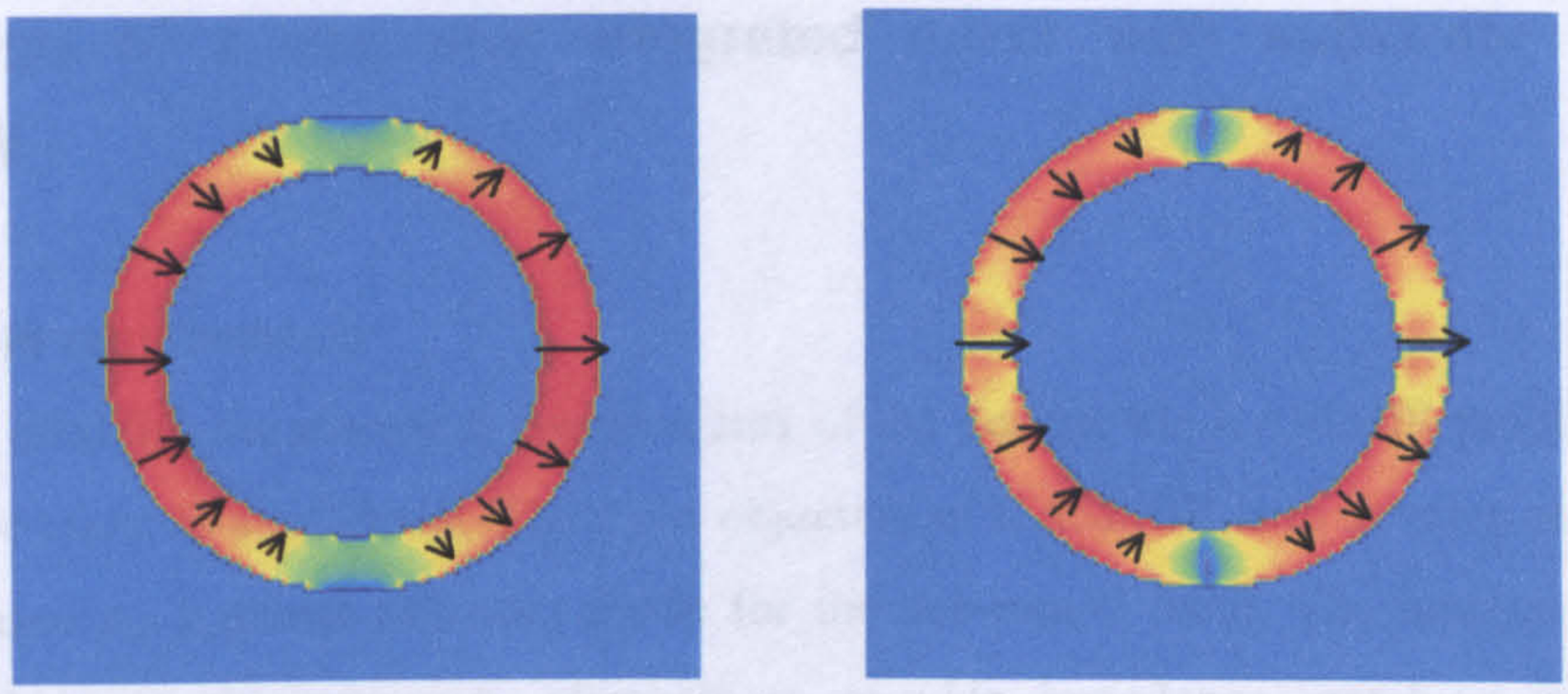

Copolar Xpolar

Figure 5.7 Overview of the electric field distribution in the annular slot at the first resonance. The vectors show the direction of the total E field in the slot. (The electrical field has been computed using FDTD)

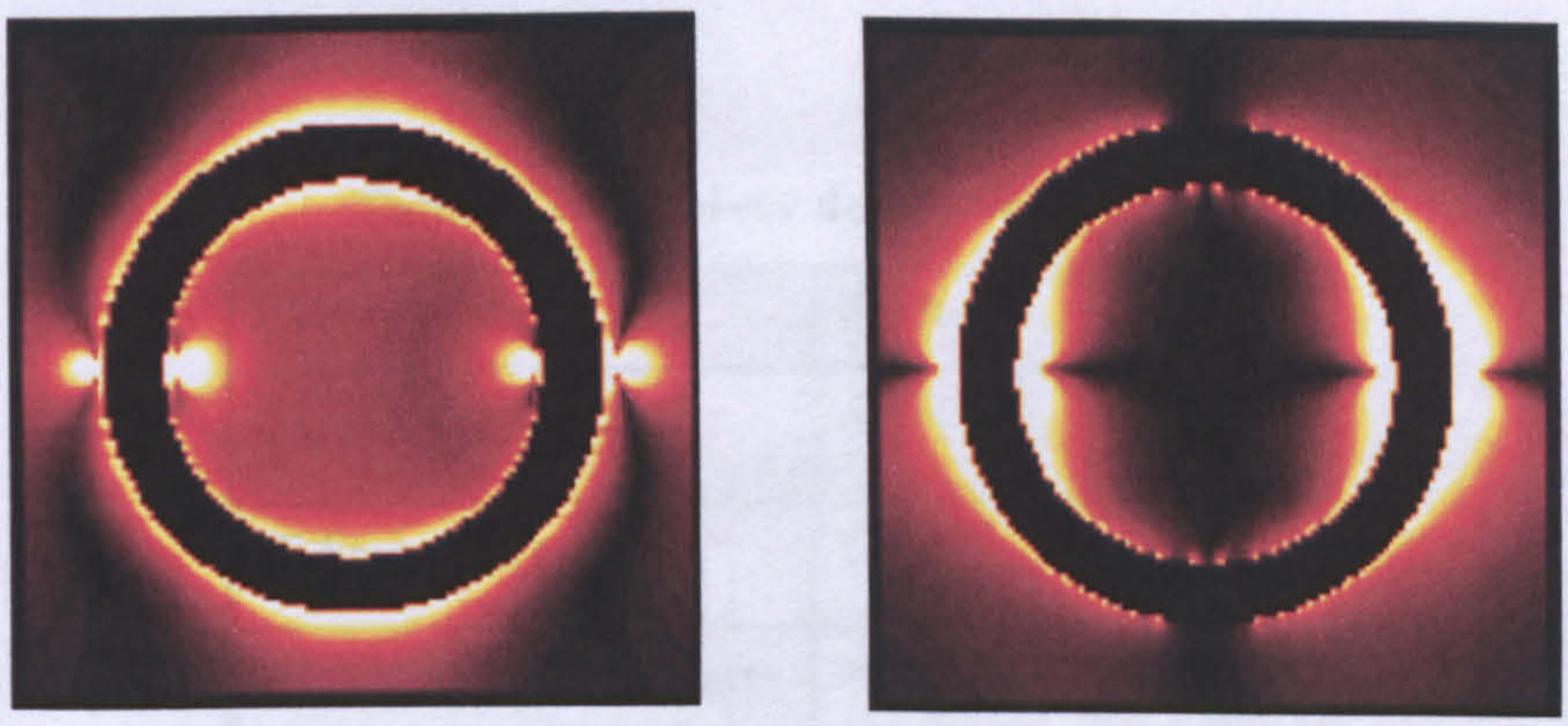

Copolar Jx Xpolar Jy

Figure 5.8 Overview of the current distribution on the ground plane of an annular slot at the first resonance. The four bright spots correspond to the connection point for the voltage sources (Currents computed using FDTD).

5.3 Design of a ring slot integrated mixer with substrate lens for submmW

5.3.1 System requirements

In order to establish the electrical requirements of the design, the KASIMIR project [3] from ESA will be taken as a reference. The main objective of KASIMIR is to develop an integrated receiver based on a planar Schottky diode for the sub-mmW band. The integrated receiver should include all the necessary elements to provide impedance matching between the antenna and the diode, DC return lines and an Intermediate Frequency (IF) port isolated from the Radio-Frequency (RF) and the Local Oscillator (LO) signals. The LO is injected quasi-optically, so, no additional transmission lines are required to drive LO power into the integrated receiver. Image frequency is assumed to be rejected by an external element such a dichroic plate or a Martin-Pupplet interferometer. The receiver specifications are summarised in table 5.2.

Table 5.2: Receiver design objectives

Parameter	**Spec.**
Central Frequency	650 GHz
IF Frequency	10 GHz
RF Rejection at IF port	>-20 dB
Crosspolar Level	<-30 dB
Gaussian efficiency	>94%-98%

The antenna type will be an annular slot planar antenna using coplanar technology. The substrate will be made of silicon or GaAs with a silicon lens placed on top to eliminate surface modes. The diode for the KASIMIR project is mounted in a vertical position with one terminal connected to the antenna port using a 10μm diameter special base of metal alloy. The other terminal is connected by means of a finger (Fig. 5.9).

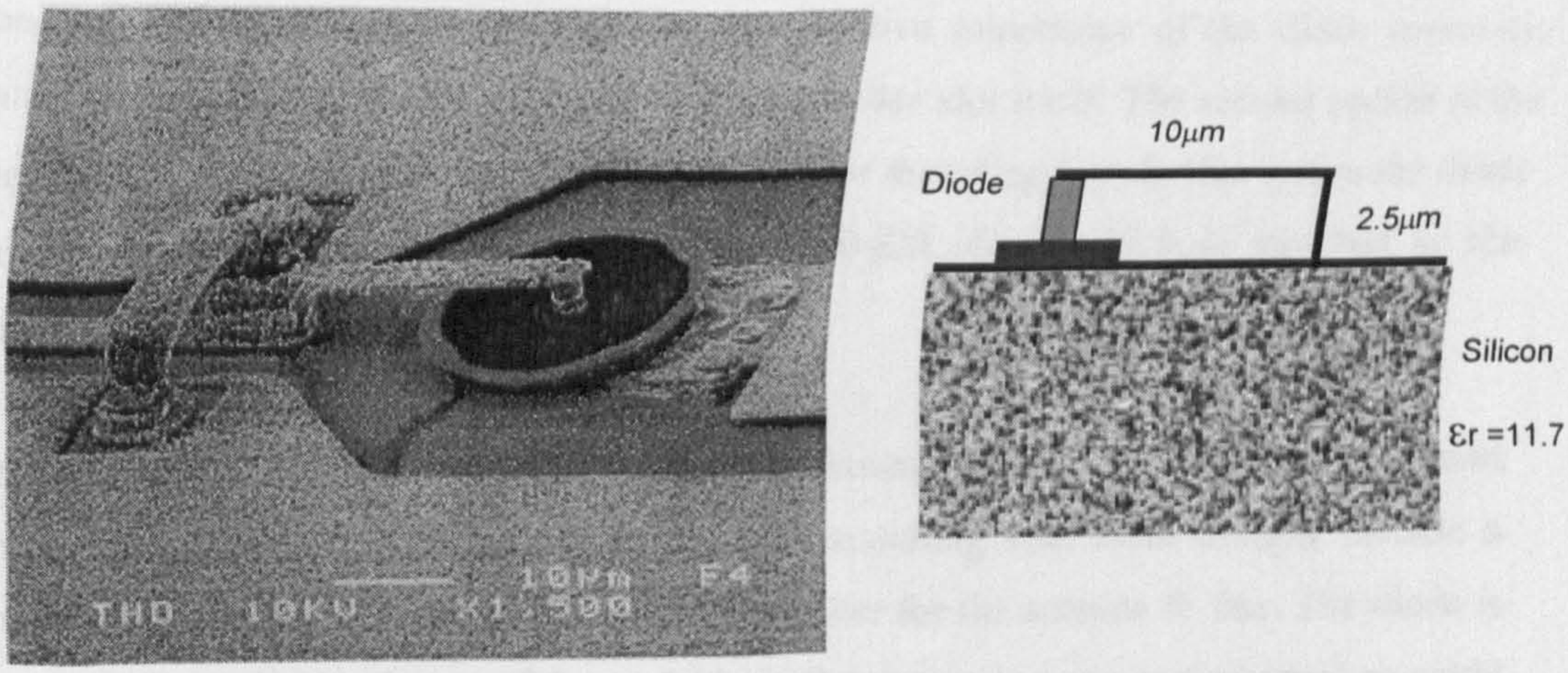

Fig.5.9. Vertical Schottky diode for submmW with finger and special metal base to reduce series resistance. (Photo: European Space Agency from a diode manufactured at the Institut for Hochfrequenztechnik, University of Darmstadt, Darmstadt, Germany)

5.3.2 Design considerations

Additional circuits have to be incorporated to the ring slot basic antennas to fulfil the requirements of the mixing diode. These circuits have to share the ground plane with the annular slot since coplanar technology is requested for the complete receiver. The devices that are included in the integrated antenna sharing the ground plane are summarised in table 5.3.

Table 5.3: Devices in the integrated antenna

Device	Type
Antenna	Annular Slot
IF line	Coplanar line
IF Filter	Stub or $\lambda/4$ Sections
Matching line (optional)	Coplanar
Mixing diode	Vertical Schottky

The matching line is to be defined since the diode impedance at the central frequency is still unknown in the context of the KASIMIR project. In principle, there are two matching options, first is the direct connection of the diode to the ring slot. This option assumes a diode

impedance (real part) close to 100 ohms (approximately the same value as the ring slot at resonance) and controlled by the DC bias, the reactive impedance of the diode (normally negative) is matched by the diode finger and the annular slot itself. The second option is the connection of the diode to the ring slot using a coplanar matching line. In this option the diode impedance is assumed to be low, approximately 20-j20 ohms, which is matched to the antenna by a transmission line.

The designs proposed for the integrated antenna are shown in Fig.5.10 for the design without matching line and in Fig.5.11 for the design with matching line. Both designs include a coplanar stub inside the ring slot, acting as isolation filter for the antenna IF line. The diode is inside the ring slot for the design of figure 5.10, so the design is quite compact and so could be included in an imaging array.

Configuration 1

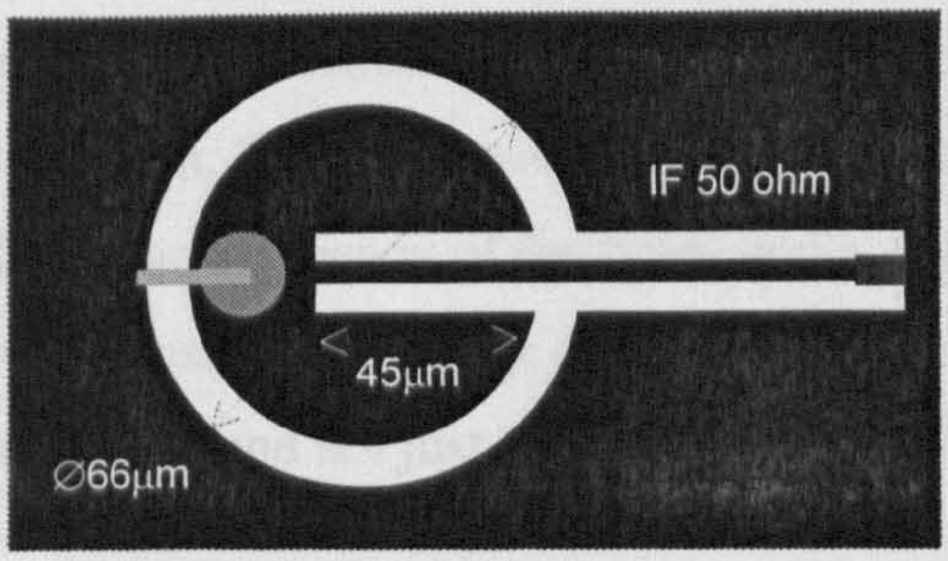

Annular slot width	10μm
IF Line width (inner conductor)	2.5μm
IF Line width (total)	18μm

Fig.5.10. Integrated receiver without matching line. The diode is adapted to the antenna impedance by using the DC bias and the finger.

Configuration 2

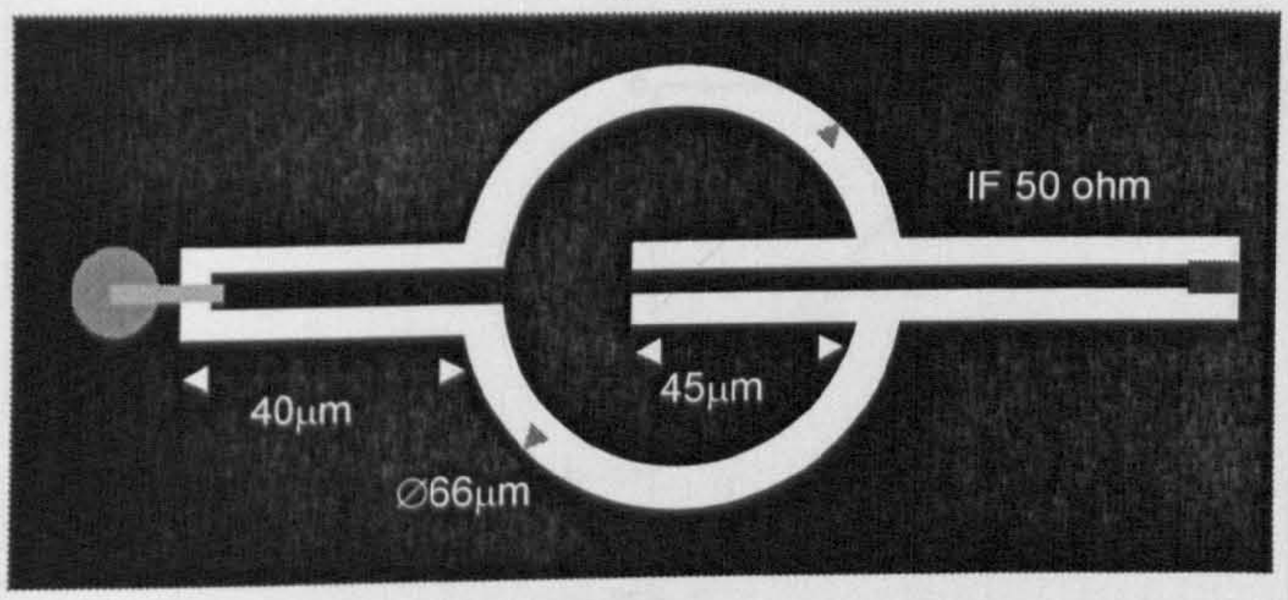

Annular slot width	10μm
IF Line width (Inner conductor)	2.5μm
IF Line width (total)	18μm
Matching Line width (Inner conductor)	7.5μm
Matching Line width (total)	18μm

Fig.5.11. Integrated antenna design with matching line. The antenna impedance is transformed to for matching a low impedance diode.

5.3.3 Imbbeded Radiation Patterns

The imbedded radiation pattern of the planar antenna is the radiation pattern of the antenna within the lens substrate, and so the planar antenna on an infinite dielectric substrate is an approximation. The importance of accurately obtaining the imbedded pattern is the need for high Gaussian efficiency of the beam and a good rotational symmetry. For the overall design, the final Gaussian efficiency of the beam is determined by the complete pattern of lens plus planar antenna and not just by the imbedded pattern of the planar antenna.

The imbedded patterns estimated using FDTD are shown in figure 5.12 for the configuration without matching line and figure 5.13 for the configuration with matching line. The Figure 5.12 show that the pattern symmetry improves if the IF stub in the centre of the antenna is made slightly larger in order to avoid the strong parasitic radiation of the stub at resonance. The symmetry of the pattern is good for both designs up to the –10dB level.

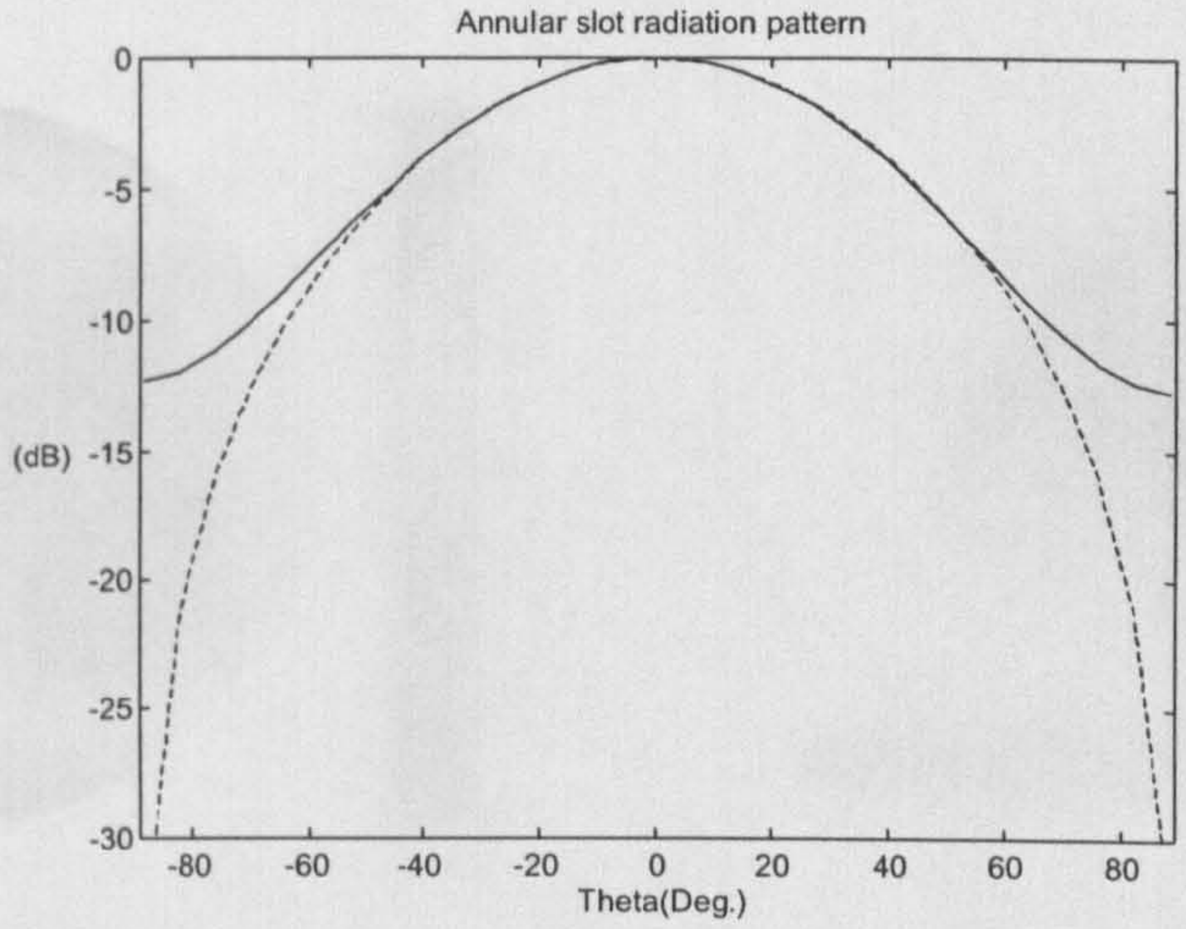

Fig.5.12 Imbedded pattern at 650GHz estimated by FDTD for the integrated antenna in figure 5.10 without matching line. (E plane: solid line, H plane: dashed line).

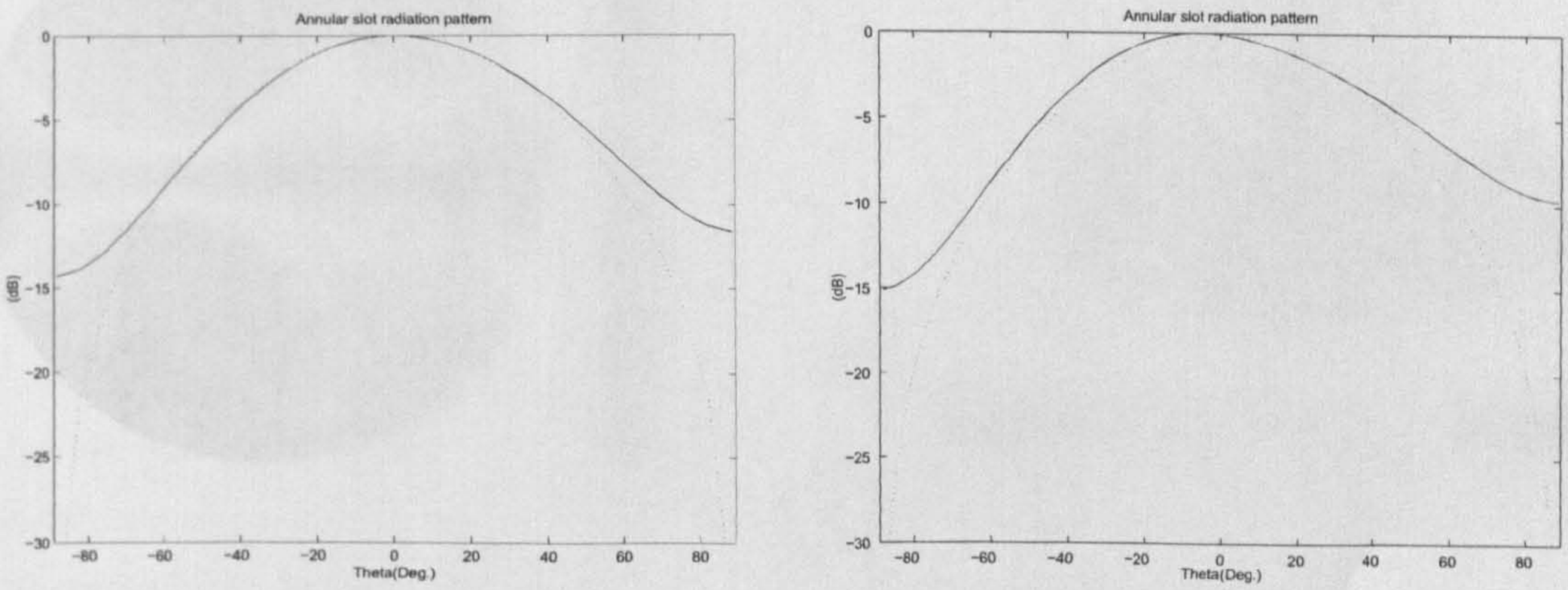

Fig.5.13 Imbedded pattern at 650GHz estimated by FDTD for the integrated antenna in figure 5.11 with matching line. On the left, the pattern with de-tuned IF stub, on the right, the pattern with the IF stub perfectly tuned. (E plane: solid line, H plane: dashed line).

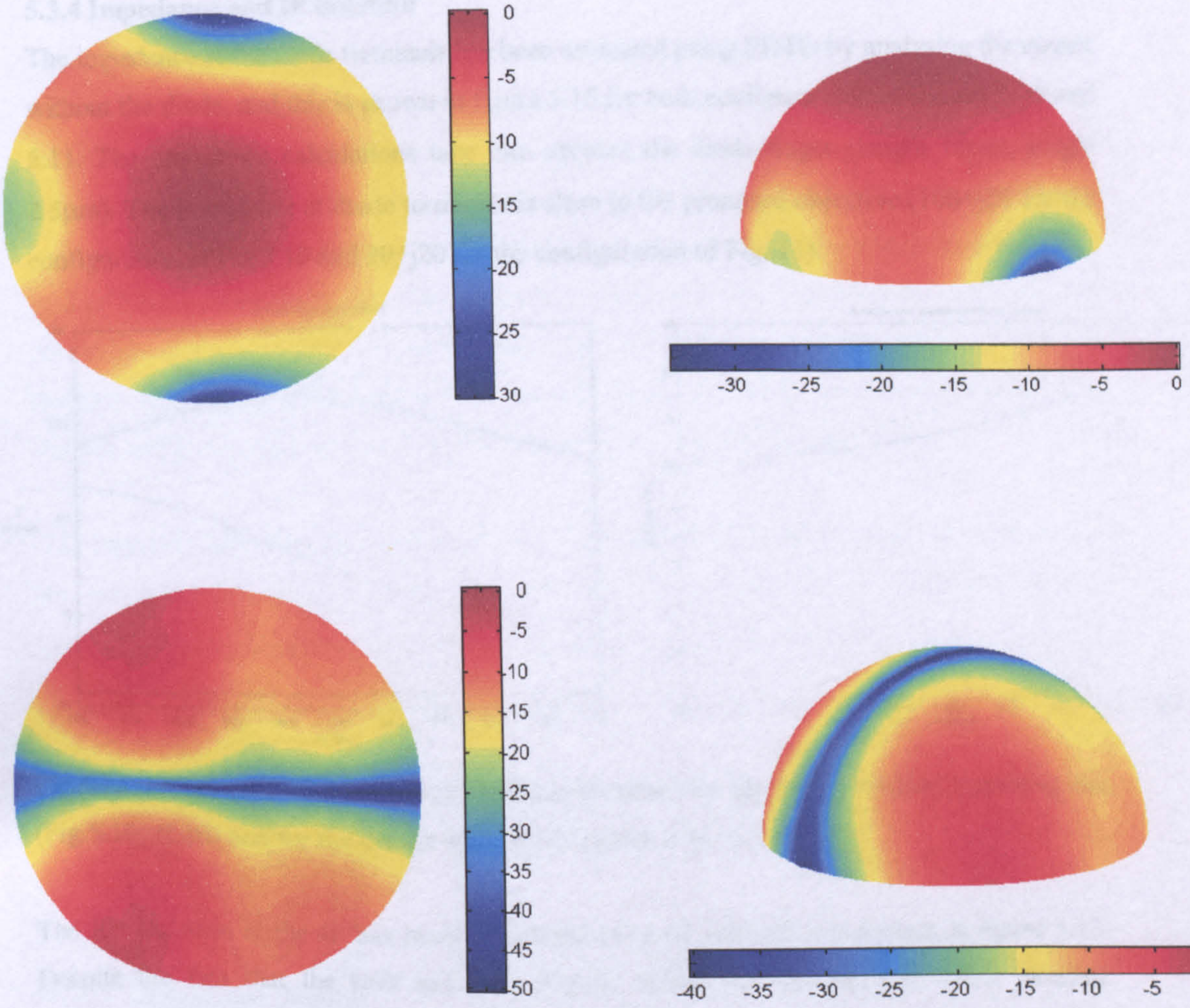

Fig. 5.14.3D plots of the radiation patterns for the integrated antenna (configuration 2). On top the copolar component and the crosspolar component at bottom.

5.3.4 Impedance and IF isolation

The impedance at the diode terminals has been estimated using FDTD by analysing the circuit without the diode, and this is shown in figure 5.15 for both configurations of figures 5.10 and 5.11. The impedance calculations take into account the diode finger (length 10μm, height 2.5μm). The impedance at diode terminals is close to the proposed objective (100+j20 for the configuration of Fig 5.10 and 20+j20 for the configuration of Fig. 11).

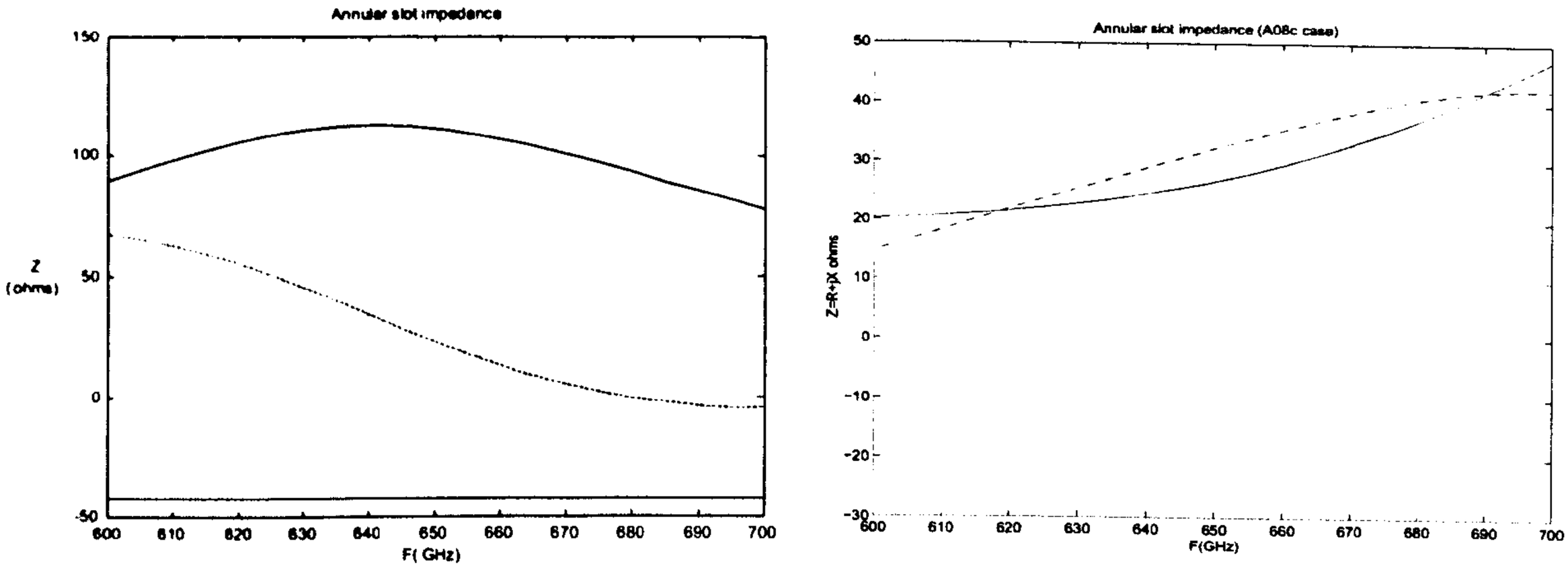

Fig.5.15. FDTD computed impedance at diode terminals for the design without matching line (Fig.5.10) (Left) and for the design with matching line (Fig.5.11) (Right).

The RF isolation at the IF has been calculated using FDTD and it is shown in figure 5.17. Despite the fact that the stub has been slightly drifted off resonance to avoid parasitic radiation, the computed isolation of the IF line is about 20dB with respect to the RF, which meets the design specification.

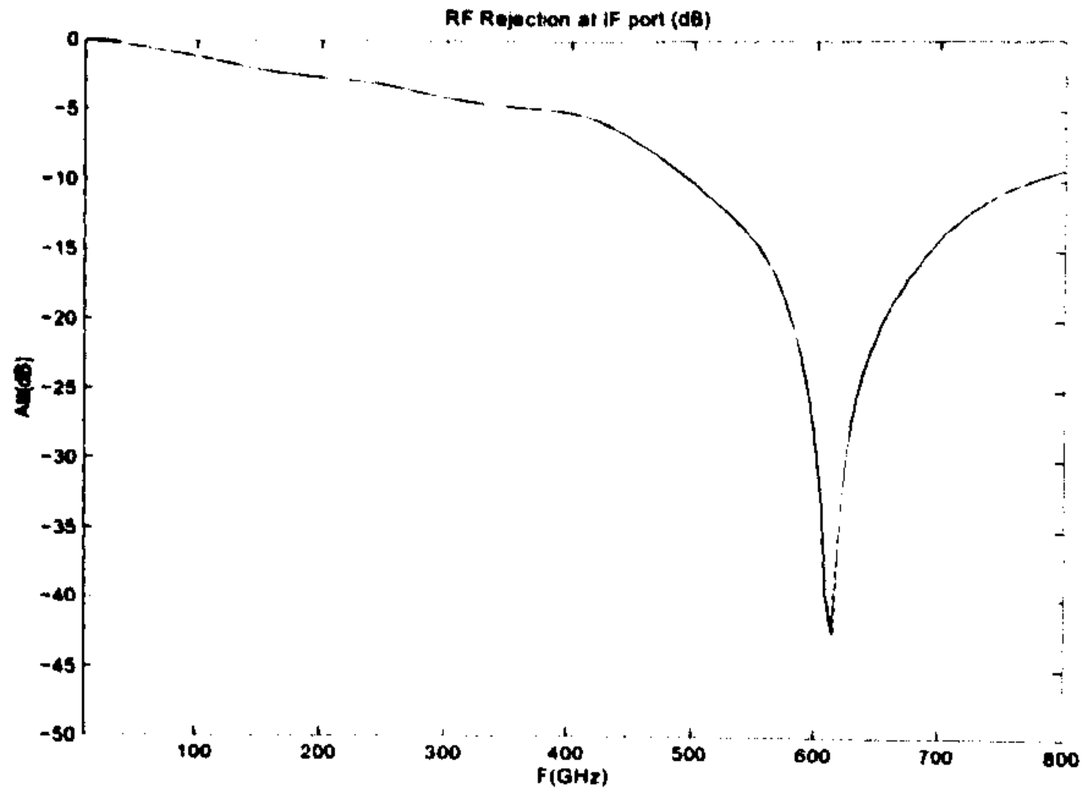

Fig.5.16. Estimated isolation of the IF line calculated using FDTD. The estimated isolation is above 20dB for the central frequency (650GHZ) and it improves for the LO at 640GHz.

5.3.5 Initial modelling for the Mixer

At the present stage, the necessary data for the modelling of the submmW Schottky diode are not available. In order to test the ability of the extended FDTD code to model the integrated mixer, a simple test case is proposed. This simple case consists of an annular slot with an ideal diode on it (Fig. 5.17). The voltage sources for the RF and LO are in series in the same node with the diode, simulating Quasi-Optical excitation. The annular slot is modelled in a grid of 100x100x80 cells with PML boundary conditions. The algorithm has been run for 30000 time steps to ensure the steady state of the mixed signals. Experimentally the stability has been obtained for a 0.2 times the courant limit for the time step, but it has to be noted that stability depends on the amplitude of the source signals and the DC bias (if any)

The spectral analysis of the currents (Fig.5.17) calculated with FDTD shows the signals that are generated by mixing of the RF and LO. The signal can be identified as the intermodulation products at frequencies $nf_{RF} \pm mf_{LO}$ including the IF ($f_{RF} - f_{LO}$) and LO harmonics (mf_{LO}).

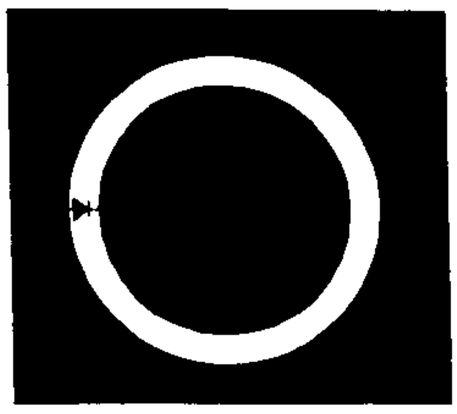

$$G_j(V_d) = I_0 \cdot \left(e^{(q/\eta \cdot k \cdot T) \cdot V_d} - 1\right)$$

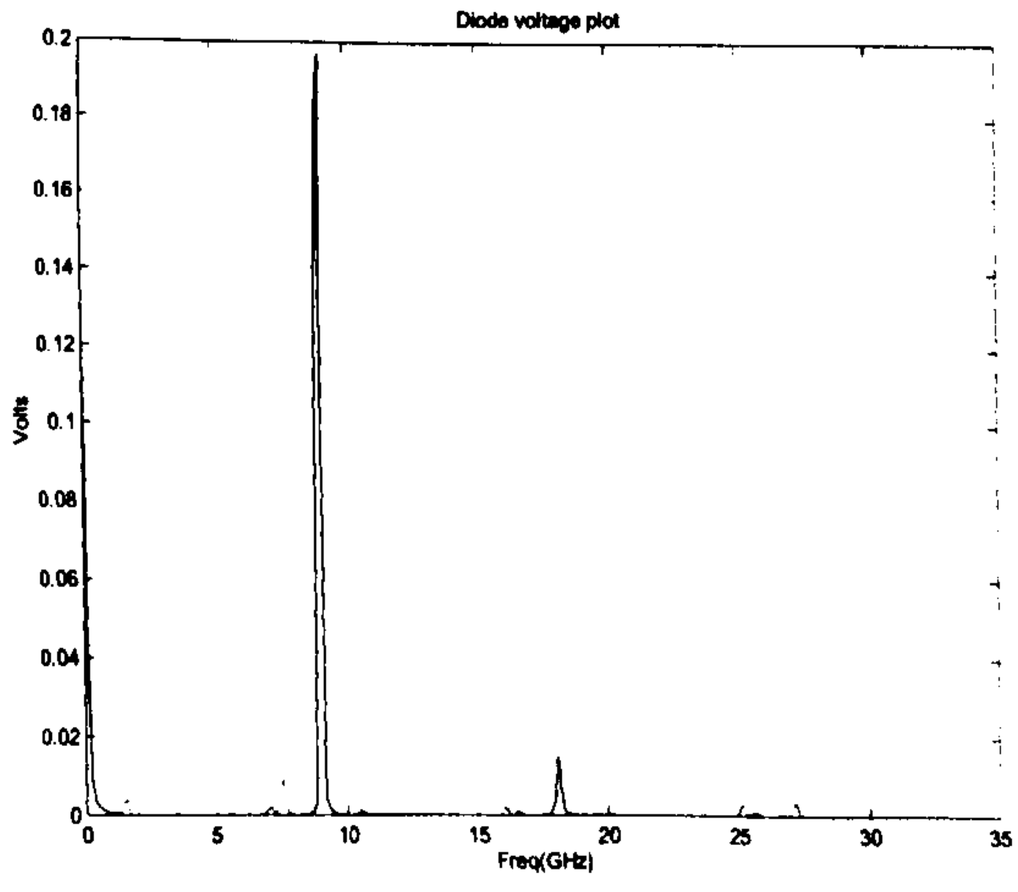

Figure 5.17. FDTD estimation of the currents in the circuit of the figure. For this test case, the OL frequency is 9GHz (big peak) and the RF is at 7.5GHz. The IF ($f_{LO} - f_{RF}$ =1.5GHz) is clearly visible as well as the image frequency ($2f_{LO} - f_{RF}$ =10.5GHz) and the LO harmonic ($2f_{LO}$ =18GHz).

5.4 Conclusions for chapter V.

Planar antennas are an attractive option to implement integrated receivers for mmW/sub-mmW. However, planar antennas mounted on thin dielectric substrates can suffer severe gain loss due to surface mode propagation as showed in previous published work. A simple and effective solution to avoid surface mode propagation can be implemented using substrate lenses.

Using as a reference the requirements for the ESA project KASIMIR on integrated receivers for sub-mmW, two designs of planar antenna, based on an annular slot are produced. These designs are intended to be mounted on a silicon substrate lens. The first design is for a high impedance mixing diode, the second is for a low impedance diode which require a matching line.

Both design are analysed using FDTD and they demonstrate the ability of the designs to match the initial requirements in terms of imbedded radiation pattern inside the lens, impedance at the diode port and IF isolation. In future advanced analysis, FDTD will model the non-linear diode as well, in order to optimise the conversion loss of the receiver. At the time of completing the thesis, the diode data and the manufacture of the proposed design was not undertaken. Therefore, a simple test case with an ideal diode is presented in order to demonstrate how the FDTD can handle all the frequencies involved in the mixing process.

Future work should also consider the use of alternative semiconductor lenses. Planar Fresnel lenses can be highly suitable for integration in a planar substrate using IC techniques for arrays of detectors. This type of lens does not require the accurate machining of the lens surface. The lens is made of air dielectric steps with the proper width, location and thickness. Aperture efficiency and bandwidth are reduced in this type of design for the sake of ease of manufacture.

5.5 References for Chapter V

[1] D.B. Rutledge, D.P. Neikirk, D.P.Kasilingam, "Infrared and Millimeter Waves",Vol 10 Part II ChapterI "Integrated circuit antennas",pp. 1-63, Academic Press 1983.

[2] G.M.Rebeiz, "Millimeter-Wave and Terahertz Integrated circuit Antennas", IEEE Proceedings, vol 80. pp 1748-1170. November 1992.

[3] ESA/ESTEC Annual Report 1997.

[4] J.Mees, et al, "Key Advanced Structure Investigations for mm and Submm-wave Integrated Receivers (KASIMIR)".2nd ESA workshop on Millimetre Wave technology and applications, May 1998.

[5] J.Mosig, P.Otero, "Design and Numerical Modelling of a Class of Mm-wave Planar Integrated Receivers" 2nd ESA workshop on Millimetre Wave technology and applications, May 1998.

[6] D.F.Filipovic, S.S Gearhert, G.M.Rebeiz, "Double slot antennas on extended hemispherical and elliptical dielectric lenses", IEEE MTT p.1738-1749, 1993.

[7] M.Born, E.Wolf, "Principles of Optics", Pergamon Press, 1983.

[8] V.V.Parshin et al, "Silicon as an advanced window material for high power gyrotrons", Journal Infrared Millimeter Waves, May 1995.

[9] P.F.Goldsmith, "Quasi-Optical Systems", IEEE Press, 1997

[10] V.Lubecke, Kmizuno, C.M.Mann "Practical Micromachining Techniques for High Aspect ratio Submillimetre Wave components", 8th Int. Symp. On Space THz technology. JPL March 1998.

[11] M.L.Olfield et al. "Recent Results for a 2.5THz Waveguide Mixer". " 2nd ESA workshop on Millimetre Wave technology and applications, May 1998.

[12] C.E. Tong, R.Blundell, "an Annular Slot Antenna on a Dielectric Half Space", IEEE APS, vol.42, pp.967-974, July 1994.

[13] S.K. Masarweh et al., "Modelling of a Monolithic Slot Ring Quasi-Optical Mixer",IEEE MTT, vol 42, pp.1602-1609, September 1994.

CHAPTER VI: CONCLUSIONS AND FUTURE WORK

This thesis is a contribution to the understanding in depth of the FDTD method to solve electromagnetic problems, in particular those involving planar, periodic or non-linear media and structures. The methodology used here to study this numerical technique relies on the theoretical analysis of FDTD as an independent electromagnetic theory which is defined in a finite universe, rather than consider FDTD as an approximation of Maxwell's equations and its associated continuous electromagnetic theorems.

The similarity of the properties and operations of finite differences and partial derivatives establish a formal analogy between the equations of electromagnetic theory and FDTD. However, the topology of the space where the equations are defined (continuous and discrete) is completely different. The discrete topology of FDTD space-time frame leads to a different treatment of boundary problems. A formal definition of PEC and PMC in FDTD is given in terms of the concepts of vicinity and boundary set and the ambiguity of defining a dielectric interface in FDTD is also addressed. The equivalence principle between currents and fields is also demonstrated for FDTD, but the exact discrete equivalence theorem is intrinsically different of the continuous equivalence principle, since magnetic and electric fields and currents can not be located in the same "surface" in FDTD. The analysis of the FDTD method uses the Z transform as the mathematical tool to represent the discrete sequences in a spectral domain.

The aforementioned similarity between finite difference and continuous electromagnetic equations is demonstrated in this thesis. The finite difference second order equations are obtained in a similar fashion to continuous equations. These equations are the formal link between the finite difference scalar wave equation and the FDTD system. As happens in continuous electromagnetic theory, this relation between scalar and vector waves is fundamental to implementing vector solutions from simpler scalar ones.

However, the main finding obtained in this thesis as a result of the finite electromagnetic approach is the discrete Green's function for FDTD. Under some general conditions, the finite difference equations can be seen as a linear system relating the sources (J and M) and the fields (E and H). As a result, FDTD can be alternatively formulated as a finite sum of fields at discrete locations rather than a finite difference system of equations. FDTD is in fact represented as a convolution of the field sources and a discrete matrix function. Following the classical theory of linear systems, this matrix function describes the impulse response of the

FDTD system. This convolution sum is the discrete equivalent to the Green's function integral of the continuous EM theory. The discrete matrix function is therefore playing the role of the dyadic Green's function in the continuous case.

The formulation of FDTD as finite sums shows that the method does not require ABC's to be solved exactly (numerically speaking) in a finite domain. In fact, the only nodes that are essential to solve the EM fields in FDTD are those where the sources or boundary conditions exist. This type of result was pointed out by diaoptikcs techniques proposed for TLM by researchers some time ago. As for the author is aware, these techniques did not make any attempt to obtain the discrete Green's as an analytical function nor to obtain further theoretical relations out of them.

This thesis presents the analytical form of the discrete Green's function for FDTD. First, the relation between the discrete scalar Green's function and the discrete matrix (dyad) one is obtained. Second, the scalar Green's function for the finite difference scalar wave equation is also obtained for the 1D, 2D and 3D cases. The discrete Green's function is a n degree polynomial of Δt, Δx, Δy, Δz.. This polynomial can be expressed as a superposition of Jacobi polynomials. The formulas of the DGF in the Z transform spectral domain are also obtained as a by-product of the analysis. This function plays a similar role for FDTD to the function $e^{-jwt}/|r-r'|$ for frequency domain EM theory.

Some of the possibilities of this function is shown in this thesis to solve FDTD without ABC's in an integral equation fashion. The possibility of obtaining numerically exact ABC's in conjunction with the equivalence principle for FDTD is also addressed with an example. In this case, the DGF formulation of the FDTD method can obtain an exact FDTD solution at the boundary of the numerical grid, Therefore no numerical reflection are expected at the interface as happens using any other ABC.

The main drawback for the direct numerical solution using this formulation is the formidable amount of computations necessary to evaluate the EM fields. A direct comparison between the Yee's algorithm and the DGF method it is not possible since its performance depends on the size of the object to model. The number of operations required for the DGF technique to compute one time step are in the order of $Nt*N^4$ where N is the number of nodes in the structure.and Nt is the number of previous time instants. Only Nt*N nodes (two components) are required to be stored using the DGF technique. The amount of operations required for the Yee's algorithm to compute one time step is in the order of Nx*Ny*Nz where Nx, Ny, Nz are

the length, width and height of a rectangular grid containing the structure to be model (usually additional nodes are provided for the ABC). Also Nx*Ny*Nz nodes (six components) are stored for the computations. If the structure occupies a small number of nodes N, but it only can be enclosed in a large volume, (i.e. a wire or a plate) the DGF technique will require a moderate number of operations and an amazingly low amount of memory to compute the scattered fields just to produce the exactly the same result as Yee's algorithm. However, as N increases (i.e. for any non planar structure) the amount of computations rise to very high values and even the amount of required memory storage is comparable to the Yee's algorithm.

This large number of computations implies some limitations about using the DGF technique to solve complex EM problems on its own. However, the application of the method to enhance the Yee's algorithm or provide an adequate framework for numerically exact general purpose boundary conditions in FDTD seems perfectly possible.

Future work based on the Green's function has many possibilities. The solution of boundary problems (i.e. between regions with different steps) can be studied using this approach. It has to be noted that boundary problems can be treated by this technique exacting the same solution that the original Yee's algorithm would produce. As a consequence, the technique does not produce numerical reflections at the boundaries. This formulation is well suited to applying higher order interpolation techniques and therefore implement multiresolution and conformal techniques, which are 100% compatibles with FDTD Yee's algorithm.

Another source of future work is the mathematical understanding of the scalar DGF. This function verifies the finite difference scalar wave equation which is a recursive formula on the indexes n, i, j, k and the variables Δt, Δx, Δy, Δz. This recursive formula can be seen as a multidimensional generalisation of the recursive formula for the Tschebycheff polynomials. This suggest the scalar DGF can have in different forms similar properties to these polynomials but in a multidimensional environment. If this can be proven these functions can be used as an improved form of response for multidimensional filters, taper for antenna arrays etc.

Besides the analysis of the FDTD method, this thesis revisits the subject of higher order polynomial approximations for FDTD. The study is carried out using the concept of a generalised finite difference operator, which is described in series form. For certain coefficients of the series and sampling conditions, this operator is exactly a representation of the derivative of a function, as it was demonstrated by Lagrange in the early 19th century.

The introduction of higher order schemes for the time index has not been considered since this implies more time steps are needed and therefore more memory requirements. The study shows two possible strategies to achieve low dispersion higher order algorithms.

The first one only uses higher order approximations of the spatial terms to produce accurate estimations of the spatial derivatives only. This is implemented by using the exact representation of the derivatives as an infinite series of finite differences and truncating this series to certain number of terms (order of the approximation). No matter how accurate is this approximation, it does not provide a better dispersion characteristic of the algorithm, since the dispersion of the time term due to a finite Δt prevails. Dispersion can only be reduced in this case if Δt is also decreased accordingly (in many cases, up to ten times). This is a conclusion that can be applied to any technique (i.e. wavelets etc.) that are intended to improve the FDTD algorithm by a better approximation of the spatial derivatives. The second strategy is based on obtaining a balance of the dispersion of the time and spatial terms. For a given direction it is possible to obtain an operator represented by an infinite series of finite differences which provide zero dispersion. This series is truncated to the order of the algorithm. This approach presents an excellent low dispersion for the selected directions without reducing the time step. However, dispersion increases with angle away from the chosen direction.

This thesis also deals with the modelling of 2D periodic structures using FDTD. The FDTD technique operates in time domain and it is causal with respect to time. The direct formulation of boundary conditions that enforce the periodicity of the scattered fields, according to the Bloch theorem results in non-causal schemes that are not compatible with FDTD. This means that for a general incident field the evaluation of the periodic boundary conditions require the knowledge of EM fields in future and past time instants. In some cases of incident field, for instance, a plane wave normally incident to the 2D periodic structure plane, the periodic condition is causal since it depends only on fields at the present time instant. A solution to non norma l incidence is proposed using coordinate basis transformation including the time axis. In the new basis, the problem is causal with respect to the new time coordinate. As a result a causal finite difference scheme using only EM fields at previous time instants (in the new transformed time) is obtained.

The coordinate transformation can be implemented in different ways. The Lorentz transformations can relate to a new basis where the periodic boundary conditions are causal with respect the transformed time. In this case the transformation has physical meaning since

it can be seen as the scattering problem seen by a relativistic observer moving parallel to the periodic observer. This approach has the advantage that Maxwell equations are invariant with respect the Lorentz's transform. As a result, Maxwell equations are the same for the moving observer and therefore FDTD can be directly applied to solve the problem. The main drawback of this solution is the movement of the structure being analised with respect the observer and the FDTD grid. In the general case, this solution requires the interpolation of the structure across the grid or else to fix the solution at a set of discrete values of the problem parameters (angle of incidence or scan angle).

The solution preferred here is based on a 'static' transformation that avoid the movement of the structure with respect to the observer and grid. No interpolation is required for the structure, but Maxwell's equations are not invariant to the transformation of coordinates in this case. As a consequence, some extra terms are added to Maxwell's equations and FDTD should be extended to account for them.

A possible line of future work is to use the Lorentz transform to develop a method that uses FDTD (without any extension) to solve periodic problems. An interesting possibility is to investigate the FDTD methods invariance with respect to discrete coordinate index transformations. Is it possible to develop a true discrete version of the special relativity? If not, what are the limitations?

The final part of the thesis is devoted to the practical use of FDTD to design a new type of quasi-optical planar receiver at submm wave frequencies. The integrated receiver consists of a coplanar annular slot on a silicon substrate, which feeds an elliptical silicon lens. The receiver should include a mixing diode and IF filters incorporated to the design of the annular slot. The LO power is injected quasi optically via the annular slot antenna. The image frequency rejection filters of the mixer are external to the receiver (i.e. dichroic plates).

Two different designs are considered. The first design places the mixing diode inside the annular slot and a RF/IF isolating slab is also inside the central region of the annular slot. The second design includes a diode matching stub connected to the annular slot. The mixing diode is placed at the end of this stub, but the RF/IF isolating stub is still placed at the central region of the slot. The concept of using the central part of the annular slot for the isolating stub and/or the mixing diode is highly innovative. This design is very compact and highly suitable for coplanar imaging arrays where the integrated receivers should share the same substrate with the beamforming network. However, there is the potential danger of severe distortion of the radiation pattern of the annular slot, because of the undesired radiation from the filtering

stub. The impedance of the combined structure slot+filter should be carefully modelled to evaluate the matching of the passive part of the receiver to the mixing diode.

The FDTD model shows that the pattern from the structure is only slightly distorted by the filtering stub. The calculated isolation and bandwidth of the RF/IF stub is adequate for the mixer in this application (-20dB in a 5% bandwidth). Regarding, the matching for the diode, the configuration with the diode on the central region of the annular slot provide a high impedance at resonance (>100ohms) that is too high for the optimum RF diode impedance (typically about 20 ohms). The configuration with external matching stub can provide a lower impedance by using a quarter wavelength transformer section.

Future work on the modelling of those integrated antennas should aim to determine large and small signal non linear models for the active components, based on experimental characterisation. Experimental verification of this FDTD approach is vital to prove its accuracy and hence provide a CAD design for millimetre and sub millimetrewave active antennas that requires no experimental design iteration. The ultimate objective will be the accurate design of imaging arrays of integrated receivers operating in the submmW region.

Publications Associated to this Thesis

Vasquez, J & Parini, C. G., Antenna modelling using discrete Green's function formulation of FDTD method, *Electronics Letters* 24/06/99 Vol. 35, no. 13 pp 1033-1034

Vasquez, J. & Parini, C. G., Discrete Green's Function Formulation of the FDTD Method for Electromagnetic Modelling, *Electronics Letters* 01/04/99 Vol. 35, no. 7 pp 554-555

Vazquez, J., Parini, C. G. & Pearson, R., Modified finite difference time domain schemes for infinite array and FSS modelling, *AP2000 Conference, Davos, Switzerland* 04/00 session 4A9, paper 0358

Vazquez, J. & Parini, C. G., Discrete Green's function formulation of the FDTD method, *AP2000 Conference, Switzerland* 04/00 session 5A1, paper 0356

Parini, C. G. & Vasquez, J., Active antenna receivers for submillimetre wave operation, *AP2000 Conference, Davos, Switzerland* 04/00 session 4A2, paper 0207

Vazquez, J., Parini., C. G., de Maagt, P. & Clarricoats, P. J. B., Design of Coplanar Integrated SubmmW Receivers by using FDTD Lumped Element Method, *IEEE Antennas and Propagation Society International Symposium. 1999 Digest. Held in conjunction with: USNC/URSI National Radio Science Meeting (Cat. No.99CH37010) Orlando, USA* 06/99 Part vol. 2 pp 1090-1093

Vazquez, J., Parini, C. G. & Clarricoats, P. J. B., The Finite Difference Modelling of Infinite Arrays in the Time Domain, *IEE Conference on Antennas and Propagation, York. (IEE Conf. Publ. No.461).* 1999 pp 209-212

Vazquez, J., de Maagt, P., Parini, C. G., Clarricoats, P. J. B., Modelling of a planar integrated sub millimetrewave receiver by using an extended FDTD method., *PIERS98, Nantes, France* 07/99 pp 1072

Vazquez, J., Parini, C. G., de Maagt, P. & Clarricoats, P. J. B., Full Wave Modelling of Integrated SubMMW Receivers by using the FDTD/Lumped Element Method, *6th IEEE International Conference on Tetrahertz Electronics, Leeds. (Cat. No.98EX171)* 09/98 pp 157-160

Vasquez, J., Parini, C. G. de Maagt, P. & Clarricoats, P. J. B., Modelling of active millimetrewave antennas using an extended FDTD method, *2nd ESA Workshop on Millimetre Wave Technology and Applications, Espoo, Finland* 27-29/05/98 pp 211-216